JYU DISSERTATIONS 553

Henri Jukkala

Quantum Coherence in Relativistic Transport Theory: Applications to Baryogenesis

UNIVERSITY OF JYVÄSKYLÄ
FACULTY OF MATHEMATICS
AND SCIENCE

JYU DISSERTATIONS 553

Henri Jukkala

Quantum Coherence in Relativistic Transport Theory: Applications to Baryogenesis

Esitetään Jyväskylän yliopiston matemaattis-luonnontieteellisen tiedekunnan suostumuksella
julkisesti tarkastettavaksi Ylistönrinteen auditoriossa FYS1
syyskuun 23. päivänä 2022 kello 12.

Academic dissertation to be publicly discussed, by permission of
the Faculty of Mathematics and Science of the University of Jyväskylä,
in Ylistönrinne, auditorium FYS1, on September 23, 2022, at 12 o'clock.

JYVÄSKYLÄN YLIOPISTO
UNIVERSITY OF JYVÄSKYLÄ

JYVÄSKYLÄ 2022

Editors
Ilari Maasilta
Department of Physics, University of Jyväskylä
Päivi Vuorio
Open Science Centre, University of Jyväskylä

ISBN 978-951-39-9190-6 (PDF)
URN:ISBN:978-951-39-9190-6
ISSN 2489-9003

Permanent link to this publication: http://urn.fi/URN:ISBN:978-951-39-9190-6

ABSTRACT

Jukkala, Henri
Quantum coherence in relativistic transport theory: applications to baryogenesis
Jyväskylä: University of Jyväskylä, 2022; 103 p. (+ included articles)
(JYU Dissertations
ISSN 2489-9003; 553)
ISBN 978-951-39-9190-6 (PDF)

We derive field-theoretic local quantum transport equations which can describe quantum coherence. Our methods are based on Kadanoff–Baym equations derived in the Schwinger–Keldysh closed time path formalism of non-equilibrium quantum field theory. We focus on spatially homogeneous and isotropic systems and mixing fermions with a time-dependent mass and a weak coupling to a thermal plasma.

We introduce a new local approximation (LA) method and use it to derive quantum kinetic equations which can describe coherence and also include effects of the spectral width. The method is based on a local ansatz of the collision term. We also improve the earlier coherent quasiparticle approximation (cQPA) by giving a straightforward derivation of the spectral ansatz, a new way of organizing the gradient expansion, and a transparent way to derive the coherence-gradient resummed collision term. In both methods the transport equations can describe flavor coherence and particle–antiparticle coherence, and the related oscillations, of the mixing fermions.

In addition to formulating the local equations we apply them to baryogenesis in the early universe. More specifically, we study the details of CP-asymmetry generation in resonant leptogenesis and the evolution of the axial vector current in electroweak baryogenesis (in a time-dependent analogue). We solve the equations numerically, and perform extensive analysis and compare the results to semiclassical (Boltzmann) equations. The results cover known semiclassical effects. We find that dynamical treatment of local quantum coherence is necessary for an accurate description of CP-asymmetry generation. When these details are known they can then be partially incorporated into simpler (e.g. semiclassical) approaches. However, coherent quantum kinetic equations are needed for accurate results across different scenarios or wide parameter ranges.

TIIVISTELMÄ (ABSTRACT IN FINNISH)

Tässä väitöskirjassa johdetaan kenttäteoreettiset lokaalit kvanttikuljetusyhtälöt, joilla voidaan kuvailla kvanttikoherenssia. Kehittämämme menetelmät pohjautuvat Kadanoffin–Baymin yhtälöihin, jotka on johdettu käyttäen suljettua Schwinger–Keldysh-aikapolkua epätasapainon kvanttikenttäteoriassa. Keskitymme spatiaalisesti homogeeniseen ja isotrooppiseen tapaukseen ja sekoittuviin fermioneihin, joilla on ajasta riippuva massa ja heikko kytkentä termiseen hiukkasplasmaan.

Muotoilemme uuden lokaalin approksimaatiomenetelmän ja johdamme sen avulla kvantti-kineettiset yhtälöt, joilla voidaan kuvailla koherenssia sekä ottaa huomioon spektraalisen leveyden vaikutus. Menetelmä perustuu vuorovaikutustermien lokaaliin yritteeseen. Parannamme myös aiemmin kehitettyä koherenttia kvasihiukkasapproksimaatiota antamalla suoraviivaisen johdon sen spektraaliyritteelle, uuden muotoilun gradienttikehitelmälle ja selkeän tavan johtaa gradienttiresummatut vuorovaikutustermit. Molempien menetelmien kuljetusyhtälöillä voidaan kuvailla sekoittuvien fermionien makutilojen välistä koherenssia ja hiukkas–antihiukkas-koherenssia sekä näihin liittyviä oskillaatioita.

Lokaalien yhtälöiden johtamisen lisäksi sovellamme niitä varhaisen maailmankaikkeuden baryogeneesiin. Tutkimme erityisesti CP-epäsymmetrian synnyn yksityiskohtia resonantissa leptogeneesissä sekä aksiaalivektorivirran kehitystä sähköheikossa baryogeneesissä (analogisessa ajasta riippuvassa tapauksessa). Ratkaisemme yhtälöt numeerisesti, analysoimme tuloksia kattavasti ja vertaamme niitä semiklassisiin (Boltzmannin) yhtälöihin. Tulokset kattavat tunnetut semiklassiset ilmiöt. Lokaalin kvanttikoherenssin dynaaminen tarkastelu on tarpeellista, kun tavoitteena on CP-epäsymmetrian kehittymisen tarkka kuvailu. Kun tämän yksityiskohdat tunnetaan, ne voidaan osittain sisällyttää yksinkertaisempiin (esim. semiklassisiin) menettelytapoihin. Koherentteja kvantti-kineettisiä yhtälöitä kuitenkin tarvitaan tarkkoihin tuloksiin eri skenaarioissa ja laajasti vaihtelevilla parametreilla.

Author

Henri Jukkala
Department of Physics
University of Jyväskylä
Jyväskylä, Finland

Supervisor

Prof. Kimmo Kainulainen
Department of Physics
University of Jyväskylä
Jyväskylä, Finland

Reviewers

Prof. Mikko Laine
Institute for Theoretical Physics
University of Bern
Bern, Switzerland

Prof. Aleksi Vuorinen
Department of Physics
University of Helsinki
Helsinki, Finland

Opponent

Priv.-Doz. Dr. rer. nat. habil. Mathias Garny
Department of Physics
Technical University of Munich
Munich, Germany

PREFACE

The research leading to this thesis was carried out at the Department of Physics in the University of Jyväskylä between the years 2012 and 2022. I gratefully acknowledge the financial support from the Väisälä Fund of the Finnish Academy of Science and Letters, from the Academy of Finland (projects 278722 and 318319), from the University of Jyväskylä, and from the Helsinki Institute of Physics.

There are several people who were integral to this research. First of all, I would like to thank my supervisor Prof. Kimmo Kainulainen for excellent and enduring guidance during all these years. You were always very encouraging. For a long time, during my studies earlier, I could not decide between majoring in physics or mathematics. Under your guidance I finally found my own path between them. It was a priviledge to share a part of your enthusiasm and deep understanding of physics. I would like to warmly thank also Mr. Pyry Rahkila and Mr. Olli Koskivaara for collaboration. I am especially grateful to Pyry for the countless discussions which were indispensable to the research process and also to my understanding of the subject. I would also like to thank Dr. Matti Herranen for early collaboration in one of the research articles. I am grateful to Prof. Mikko Laine and Prof. Aleksi Vuorinen for carefully reviewing the manuscript, and to Dr. Mathias Garny for accepting to be my opponent.

I wish to thank my previous teachers Prof. Jukka Maalampi and Prof. Kimmo Tuominen for giving me the chance to do my graduate and undergraduate theses on particle physics, and Prof. Kari J. Eskola for introducing me to this fascinating subject. Warm thanks belong also to other teachers, councellors and administrative staff at the Department of Physics for their kind help in various tasks and questions. I also thank the CERN Theory Department for hospitality during my brief visit there. I would also like to thank my friends from the university, classmates, colleagues at the office YFL347, and our research group for cheerful atmosphere and company. These thanks belong especially to Pyry Rahkila, Olli Koskivaara, Tommi Alanne and Risto Paatelainen. Special thanks to Risto for helping me out with the access card at CERN.

I would also like to express my gratitude to family and friends for their support. Lopuksi haluan kiittää perhettä ja ystäviä tuesta. Lämpimät kiitokset sekä omille että vaimoni vanhemmille, joilta olemme saaneet lukemattomasti tukea. Suurin kiitos kuuluu vaimolleni Johannalle ja lapsillemme. Kiitos tuesta, kärsivällisyydestä ja kannustuksesta, sekä kaikkein eniten rakkaudesta.

To my wife Johanna and to our "particles": Benjamin, Albin, Adabel and Belinda.

In Muurame, August 2022
Henri Jukkala

LIST OF INCLUDED ARTICLES

This PhD thesis consists of this compilation part and the following articles:

[I] H. Jukkala, K. Kainulainen, and O. Koskivaara, *"Quantum transport and the phase space structure of the Wightman functions"*, J. High Energy Phys. **01**, 012 (2020), DOI: 10.1007/JHEP01(2020)012, [arXiv: 1910.10979 (hep-th)].

[II] H. Jukkala, K. Kainulainen, and P. M. Rahkila, *"Flavour mixing transport theory and resonant leptogenesis"*, J. High Energy Phys. **09**, 119 (2021), DOI: 10.1007/JHEP09(2021)119, [arXiv: 2104.03998 (hep-ph)].

In article [I] the author participated in the calculation of the analytical results and the review of the numerical code. The author also participated critically in the writing and editing of the final draft of the manuscript. In article [II] the author produced all numerical results and plots and participated in their analysis. The author had an essential role in the theoretical work and calculated most of the analytical results in the article. The author also had a leading role in all stages of designing and writing of the final article.

The author also wrote the numerical software package [IIb] which was used in the numerical results of article [II] and in this work.

[IIb] H. Jukkala, *"LeptoGen"*, version 1.1, June 2021, URL: https://doi.org/10.5281/zenodo.5025929.

CONTENTS

1 INTRODUCTION

Coherence is a central feature of quantum physics. In classical physics waves are said to be coherent if they have the same wavelength and frequency but may be displaced in time or space. Coherence is related to the ability of waves to diffract and interfere, and this description carries over to the quantum realm where also particles have wave-like properties [1]. Indeed, according to the wave–particle duality of quantum physics, all matter and radiation have both particle-like and wave-like aspects. This is famously shown in diffraction and interference experiments with electrons and photons, for example [2]. Also, coherence is more generally related to correlation between physical quantities. Correlation functions are a central concept in quantum field theory (QFT), and mixing of quantum fields is the fundamental property which enables the formation of coherence and coherent oscillation of particles [3].

The smaller the considered objects are, the more significant quantum coherence is, generally speaking. It is then no surprise that it is particularly important in elementary particle physics, and by extension, in the very hot and dense state of the early universe which is governed by elementary particle interactions. Known elementary particles and their interactions (excluding gravity) are described by the Standard Model (SM), and the evolution and properties of the observable universe are explained to a large extent by the big bang model of cosmology. These models are immensely successful but they have left several unsolved mysteries such as the neutrino masses or the nature of dark matter and dark energy. The events of the very early universe are also still in the dark: for example, the details of cosmological inflation and the related reheating of the universe as well as the origin of the matter–antimatter asymmetry are unknown.

The universe has been observed to be practically completely devoid of antimatter, while ordinary matter is ubiquitous. This disparity is known as the matter–antimatter asymmetry of the universe. Ordinary matter has a share of approximately 5 % of the total energy density of the present universe [4]. It consists mostly of protons, neutrons and electrons which make up the interstellar gas and astronomical objects

such as stars and planets. A tiny fraction of cosmic rays contains antimatter and minuscule amounts of it have been produced in terrestrial experiments, but there is no evidence of any cosmologically relevant amounts of antiprotons, antineutrons, positrons, or other antimatter particles [5, 6]. This is a problem because the SM lacks a mechanism for producing this asymmetry — the theory is too symmetrical between particles and antiparticles — so it cannot explain how the present universe could have formed from a symmetrical initial state (set by inflation).

There are many ideas and extended models that have been proposed to explain the unsolved problems mentioned above, and coherence often has a central role in them. For example, coherence between different flavor states of neutrinos is behind neutrino oscillations [3, 7], and particle–antiparticle coherence is essential to particle production [8] in the early universe. Coherence can also be important in the generation of particle–antiparticle asymmetries through CP-violating processes, which is relevant to the matter–antimatter problem. Prime examples are coherence between particles reflected and transmitted by phase transition walls in electroweak baryogenesis (EWBG) [9–11] and flavor coherence of heavy Majorana neutrinos in leptogenesis [12, 13].

The use of QFT is required when studying coherent systems in high temperatures and densities of particles. Conventional quantum mechanics is not sufficient for relativistic processes where particle numbers change. Furthermore, evolution of quantum coherence, including its formation and decoherence, is a dynamical process and its description requires a full quantum transport formalism. Non-equilibrium QFT [8] provides a framework of transport equations for correlation functions which describe quantum processes including interactions and (de)coherence. However, the resulting equations are generally very complex and difficult to solve. Approximations such as the Kadanoff–Baym ansatz are conventionally employed to derive simpler kinetic equations, but this reduction usually erases coherence information from the correlation functions.

In this thesis we develop approximation methods for non-equilibrium QFT which include quantum coherence. We apply our methods to the early universe and specifically baryogenesis, which are introduced in chapter 2. Non-equilibrium QFT is reviewed in chapter 3 where general quantum transport equations are presented. In this work we concentrate mainly on fermions in spatially homogeneous and isotropic systems. Our main results, the formulation of a new local approximation method and improvements to the cQPA [14–22] are presented in chapter 4. The derived equations describe both flavor coherence and particle–antiparticle coherence contained in the local two-point correlation function. In chapter 5 we apply our methods to EWBG (in a time-dependent example) and resonant leptogenesis, and we solve and analyze the equations numerically. Finally, in chapter 6 we discuss the results and give the conclusions.

We employ the natural units with $c = \hbar = k_{\mathrm{B}} = 1$ throughout this work.

2 THE EARLY UNIVERSE

Cosmology studies the universe as a whole. Modern physical cosmology [6, 23, 24] rests on three main pillars: (1) observation of the expansion of the universe (i.e. the Hubble expansion), (2) measurement of the primordial light element abundances and explaining their formation via nuclear reactions (BBN, i.e., big bang nucleosynthesis), and (3) detection of the cosmic microwave background (CMB) and measurement of its properties. These findings lead to the practically indisputable conclusion that in the very distant past the universe was in an extremely hot and dense state and has been expanding and cooling ever since [6].

The hot primordial plasma of the early universe is governed by both gravity and elementary particle interactions. The exact timeline of the earlier stages of the universe is still unknown, but there is convincing evidence that before the hot big bang there was a phase of rapid exponential expansion which is called the cosmological inflation [25]. It is also conjectured that even earlier, before the inflationary period, the universe was ruled by the enigmatic quantum gravity (at the Planck scale $\sim 10^{19}$ GeV and above). However, when studying cosmology below such enormous energies it is conventionally assumed that a classical treatment of gravity is sufficient. Gravity can then be described by the Einstein field equations of general relativity, which are the basis for the big bang model. Next we introduce parts of the big bang theory, and baryogenesis, which are necessary for our applications in this work.

2.1 Expanding spatially flat spacetime

The spatial curvature of the universe has been measured to be very close to zero at large scales [4]. Spatial flatness is thus a very good approximation when studying particle cosmology after the inflationary epoch. The curvature of the spacetime then manifests only as the expansion of the universe. The universe may also be assumed to be homogeneous and isotropic at very large scales, as shown by the high uniformity of the CMB, for example. The spacetime of the universe may thus be described by

the spatially flat Friedmann–Lemaître–Robertson–Walker (FLRW) metric, which in conformal coordinates takes the form [8]

$$\mathrm{d}s^2 = g_{\mu\nu}\,\mathrm{d}x^\mu\,\mathrm{d}x^\nu = a(\eta)^2\big(\mathrm{d}\eta^2 - \mathrm{d}\boldsymbol{x}^2\big). \tag{2.1}$$

Here $a(\eta)$ is the dimensionless scale factor and the conformal time η is related to the cosmic time t by $\mathrm{d}t = a(\eta)\,\mathrm{d}\eta$. In the following we denote the cosmic time derivative with a dot and the conformal time derivative with a prime: for example $\dot{a} \equiv \mathrm{d}a/\mathrm{d}t$ and $a' \equiv \mathrm{d}a/\mathrm{d}\eta$. We use the metric signature convention $(+,-,-,-)$, and denote the Minkowski metric tensor by $\eta_{\mu\nu}$ so that $g_{\mu\nu} = a^2\,\eta_{\mu\nu}$ in equation (2.1).

Expansion of the FLRW universe is described by the Friedmann equations. They can be expressed equivalently by the first Friedmann equation and the continuity equation [24], which in the case of zero spatial curvature are given by

$$H^2 = \frac{8\pi G}{3}\rho, \tag{2.2a}$$

$$\dot{\rho} = -3H(\rho + p). \tag{2.2b}$$

Here $H \equiv \dot{a}/a$ is the Hubble parameter, ρ and p are respectively the energy density and pressure of the universe, and G is the gravitational constant. Provided with an equation of state, $p = p(\rho)$, one can solve the time evolution of the scale factor and the energy density from equations (2.2).

After inflation the universe was reheated, resulting in the creation of the primordial plasma consisting of elementary particles in thermal equilibrium, or very close to it. The thermalization process also created an enormous amount of entropy [25]. It can be shown, using basic thermodynamics, that the relativistic particle species (i.e. radiation, with equation of state $p = \rho/3$) dominate the total energy density and pressure of this plasma [6]. Hence, in the early *radiation dominated* epoch it is useful to parametrize the energy density ρ and the entropy density s, given by $s = (\rho + p)/T$, with

$$\rho \equiv \frac{\pi^2}{30} g_*(T) T^4, \tag{2.3a}$$

$$s \equiv \frac{2\pi^2}{45} g_{*s}(T) T^3. \tag{2.3b}$$

Here T is the temperature and $g_*(T)$ counts the effective number of relativistic degrees of freedom of the primordial plasma. Similarly, $g_{*s}(T)$ counts the degrees of freedom for entropy. As long as there are no relativistic particle species which are decoupled from the thermal bath, $g_{*s} = g_*$ [6]. These factors are normalized so that one bosonic and fermionic degree of freedom correspond to $g_* = 1$ and $g_* = 7/8$, respectively. At high temperatures before the electroweak phase transition (EWPT) all SM degrees of freedom contribute, adding up to a total of $g_* = 106.75$ plus possible beyond-the-SM degrees of freedom in extended models.

When solving transport equations for particle numbers in the early universe, it is convenient to compare them to some conserved physical quantity. Often the total entropy $S \propto sa^3$ is used for this purpose, as it is conserved in equilibrium. In this case it is said that the universe *expands adiabatically*, and the entropy density scales as $s \propto a^{-3}$. Also, when there is no net annihilation or production of any particle species taking place, g_* and g_{*s} in equations (2.3) are constants. Using the above adiabatic entropy scaling law we then see from equation (2.3b) that the temperature scales as $T \propto a^{-1}$. Furthermore, when g_* is constant we can use equations (2.2a) and (2.3a) to express the Hubble parameter as a simple quadratic function of T:

$$H(T) = \sqrt{\frac{4\pi^3}{45} g_*} \frac{T^2}{m_{\mathrm{Pl}}}, \tag{2.4}$$

where $m_{\mathrm{Pl}} \equiv 1/\sqrt{G} \approx 1.2209 \times 10^{19}\,\mathrm{GeV}$ [26] is the Planck mass. Using here $T \propto a^{-1}$ and $H = \dot{a}/a$ we can then further solve the time dependence of the scale factor for the radiation dominated universe: $a \propto \eta \propto \sqrt{t}$.

Furthermore, after reheating (i.e. in the beginning of the hot big bang) the total entropy of the universe was so large that often it is a good approximation to treat the expansion of the universe as adiabatic even when it is strictly speaking not so [6]. Then we can continue to use the adiabatic expansion law $s \propto a^{-3}$ and temperature scaling $T \propto a^{-1}$. This incurs only a small error to the description of a given non-equilibrium process in the early universe, granted the process does not produce too much entropy.

2.2 Quantum fields in expanding spacetime

The framework where QFT is studied in the presence of a classical background gravitational field is called *quantum field theory in curved spacetime* [27]. As a relevant example of QFT in a general curved spacetime, we now consider a generic Lagrangian $\mathcal{L}$ with a fermion field ψ, a complex scalar field ϕ and a renormalizable interaction part $\mathcal{L}_{\mathrm{int}}$:

$$\mathcal{L} = \sqrt{-g}\Big[\overline{\psi}(\mathrm{i}\gamma^\mu\nabla_\mu - m_\psi)\psi + (\partial_\mu\phi^\dagger)(\partial^\mu\phi) - (m_\phi^2 + \xi R)\phi^\dagger\phi\Big] + \mathcal{L}_{\mathrm{int}}. \tag{2.5}$$

Here $g \equiv \det(g_{\mu\nu})$ is the determinant of the metric, ∇_μ is the covariant derivative for fermion fields given by the spin connection, m_ψ and m_ϕ are the masses of the fermion and scalar fields, and the constant ξ couples the scalar field to the scalar curvature R [27]. Note that we included here the volume factor $\sqrt{-g}$ which stems from the action integral. The gamma matrices γ^μ are defined by the standard Minkowski space relations $\{\gamma^\mu, \gamma^\nu\} = 2\eta^{\mu\nu}\mathbf{1}$ and $(\gamma^\mu)^\dagger = \gamma^0\gamma^\mu\gamma^0$ [3].

We use the tetrad formalism [23, 27] for the treatment of spinors in general curved spacetime. The covariant derivative for fermion fields in equation (2.5) is

then given by the spin connection

$$\nabla_\alpha = V_\alpha{}^\mu(\partial_\mu + \Gamma_\mu), \tag{2.6}$$

where the tetrads $V_\alpha{}^\mu$ satisfy $g_{\mu\nu} = V^\alpha{}_\mu V^\beta{}_\nu \eta_{\alpha\beta}$ and the spin connection coefficients are given by $\Gamma_\mu = \frac{1}{2}\sigma^{\alpha\beta}V_\alpha{}^\nu V_{\beta\nu;\mu}$ [23]. Here $V_{\beta\nu;\mu} = \partial_\mu V_{\beta\nu} - \Gamma^\lambda{}_{\mu\nu}V_{\beta\lambda}$ is the covariant derivative of the tetrad with the usual Christoffel symbols $\Gamma^\lambda{}_{\mu\nu}$, and $\sigma^{\alpha\beta} = \frac{1}{4}[\gamma^\alpha, \gamma^\beta]$ are the Lorentz transformation generators for Dirac spinors.

Now we restrict to the flat FLRW metric (2.1) with the conformal coordinates. We can then choose the tetrads as $V^\alpha{}_\mu = a(\eta)\delta^\alpha{}_\mu$, whereby $V_\alpha{}^\mu = 1/a(\eta)\delta_\alpha{}^\mu$ and $V_{\alpha\mu} = a(\eta)\eta_{\alpha\mu}$. The results for the spin connection coefficients are

$$\Gamma_0 = 0, \qquad \Gamma_i = \frac{1}{2}\gamma^0\gamma^i\,\frac{a'}{a}, \tag{2.7}$$

where i runs over the spatial indices $1, 2, 3$ only. Using these results we can calculate the contracted covariant derivative:

$$\gamma^\mu\nabla_\mu = \frac{1}{a}\Big(\gamma^\mu\partial_\mu + \frac{3}{2}\frac{a'}{a}\gamma^0\Big). \tag{2.8}$$

We can simplify the Lagrangian further by performing a conformal scaling of the fermion and scalar fields, $\psi \to a^{-3/2}\widetilde{\psi}$ and $\phi \to a^{-1}\widetilde{\phi}$, and by using $\sqrt{-g} = a^4$ [27]. We also do the usual partial integration for the scalar field kinetic term. The resulting scaled Lagrangian is (we now omit the tilde on the fields for clarity)

$$\widetilde{\mathcal{L}} = \overline{\psi}\big(\mathrm{i}\gamma^\mu\partial_\mu - am_\psi\big)\psi + \phi^\dagger\left[-\eta^{\mu\nu}\partial_\mu\partial_\nu - a^2\left(m_\phi^2 + \xi R - \frac{a''}{a^3}\right)\right]\phi + \widetilde{\mathcal{L}}_{\mathrm{int}}. \tag{2.9}$$

This takes the standard form of a Lagrangian in a Minkowski background, except that the masses m_ψ and m_ϕ have been multiplied by the scale factor and there are additional contributions to the scalar mass term from the scalar curvature (now given by $R = 6a''/a^3$ [8]). All renormalizable interaction terms in $\widetilde{\mathcal{L}}_{\mathrm{int}}$ with dimensionless coupling constants also take the usual Minkowski form.[1] This is because the conformal field scalings used the same powers as the length dimensions of the fields, $[\psi] = L^{-3/2}$ and $[\phi] = L^{-1}$, so they always produce a total factor of a^{-4} which cancels the overall a^4 from $\sqrt{-g}$.

To summarize, QFT in expanding flat spacetime is equivalent to QFT in a Minkowski spacetime with time-dependent masses am_i when using the conformal coordinates. Also, the additional contribution to the scalar field mass term vanishes in the radiation dominated universe where $a'' \equiv 0$ (or when using the conformal value $\xi = 1/6$ for the scalar curvature coupling).

[1] With the exception of derivative interaction terms which are not considered here.

2.3 Baryogenesis

In cosmology the asymmetry between matter and antimatter is called the *baryon asymmetry* of the universe (BAU) [28]. The BAU is often quantified with the ratio of the baryon number density $n_B \equiv n_\mathrm{b} - \bar{n}_\mathrm{b}$ to the photon density n_γ (here B denotes the baryon number; $n_\mathrm{b}, \bar{n}_\mathrm{b}$ respectively are the densities of baryons and antibaryons). The present value of this ratio η_B has been measured to be [4, 29]

$$\eta_B \equiv \frac{n_B}{n_\gamma} = (6.129 \pm 0.039) \times 10^{-10}. \tag{2.10}$$

This value can be determined from essentially two independent sources: big bang nucleosynthesis (BBN) and the CMB anisotropy power spectrum. Historically, it was first determined from BBN where η_B is the input parameter which controls the abundances of primordial light elements [6, 29]. Nowadays the CMB measurements are much more precise [26, 29]. The agreement of the results from these two different sources is a remarkable success of big bang cosmology. However, the origin of the BAU is not explained in the big bang model; it is just a parameter.

Baryogenesis [28, 30–32] is the name for the hypothetical process that generated the BAU dynamically from a baryon symmetric initial state [6, 24]. This is still a highly speculative field of particle cosmology as there are many proposed baryogenesis mechanisms and there is not yet strong evidence for any specific one. Strictly speaking it is also not completely ruled out that the observed BAU could have been an initial condition of the universe (or produced by quantum gravitational effects at the Planck scale $\sim 10^{19}$ GeV). The problem with this explanation is that cosmological inflation would have diluted an initial baryon asymmetry to a completely negligible level at the end of reheating [28]. Thus, a dynamical explanation is still likely to be needed for today's observed BAU.

Sakharov conditions. There are three necessary generic requirements for baryogenesis. These are called the *Sakharov conditions* and they are (i) B-violation, (ii) CP- and C-violation, and (iii) deviation from equilibrium [33]. The first condition is obvious: baryon number must not be conserved. The second condition refers to the charge (C) and the combined charge and parity (CP) transformations. In a CP- and C-conserving system the B-violating processes which produce baryons and the related processes which produce antibaryons would have equal rates, meaning that no net baryon number could be generated [6, 30]. The third condition is needed because in thermal (and chemical) equilibrium the B-violating processes and their inverse processes would have equal rates, again implying that no net baryon number could be produced [30]. Another way to understand this is that if the system starts with $B = 0$ and stays in chemical equilibrium, the chemical potential(s) corresponding to the baryon number would be zero and hence the baryon and antibaryon distributions would be identical (ultimately due to CPT-invariance) [6, 24].

It is now known that fulfilling all three Sakharov conditions for successful baryogenesis requires physics beyond the SM, even though all of the ingredients are in some capacity already there [34]. The quark sector of the SM already has CP-violation in the CKM-matrix, but it is widely accepted to be too weak for baryogenesis [30]. The expansion of the universe can provide non-equilibrium conditions, but there are no suitable heavy particles in the SM that would have the required non-equilibrium decays. A strong first order EWPT could also work, but it is known that the EWPT in the SM is only a continuous cross-over with the known value of the Higgs boson mass [35].

One of the Sakharov conditions is still fulfilled already in the SM and that is the B-violation. This seems surprising at first because baryon number is conserved in all perturbative particle interactions in the SM. This is only an accidental global U(1) symmetry [31], however, and the electroweak sector actually breaks B via non-perturbative processes and the axial anomaly [9, 36, 37]. This *electroweak B-violation* in the SM is due to the non-trivial vacuum state structure of the non-Abelian SU(2) gauge field. Under usual conditions in the present universe (zero or low temperature) these B-violating processes are extremely suppressed but at very high temperatures baryon number can be strongly violated.

Some of the most prominent baryogenesis mechanisms are GUT baryogenesis, electroweak baryogenesis and leptogenesis [28, 32]. Historically, after Sakharov's initial work the development of baryogenesis first took off in the context of grand unified theories (GUTs). Most GUTs naturally give rise to baryogenesis because they contain suitable B-violating heavy particles. However, reconciling GUT baryogenesis with inflation is challenging because the reheating temperature is usually below the GUT scale ($\sim 10^{16}$ GeV).[2] Electroweak baryogenesis [9] is an interesting possibility because it only involves electroweak-scale physics and should thus be testable in present and near-future experiments [32]. It makes use of the electroweak B-violation present already in the SM. Leptogenesis [12] also uses the electroweak B-violation, and more specifically, the possibility that a dynamically produced *lepton* number (denoted by L below) may explain the observed BAU [28]. Leptogenesis is a very attractive possibility because it is linked to the see-saw mechanism which may explain the observed light neutrino masses.

2.3.1 Electroweak B-violation

The origin of the electroweak B-violation in the SM is the vacuum state structure of the non-Abelian SU(2) gauge field [11, 30]. The gauge field has multiple vacuum states labelled by an integer: a topological winding number called the Chern–Simons number. The corresponding Chern–Simons current, on the other hand, is coupled to

[2] A higher reheating temperature is problematic in GUTs because of the gravitino-overproduction problem [10, 28]. Most GUTs also rely on supersymmetry which still has not been observed.

the baryon and lepton axial vector currents via the Adler–Bell–Jackiw anomaly [11, 38, 39]. Hence, transitions of the gauge field vacuum state break $B+L$ and transform baryons into antileptons or antibaryons into leptons (and vice versa) so that the quantum numbers change as $\Delta B = \Delta L = \pm 3$ [30, 31].

These gauge vacuum state transitions are negligible in zero temperature as they proceed through instanton configurations (quantum tunneling through the potential barrier) and are extremely suppressed [11, 36]. However, in very high temperatures the suppression is relieved as the transitions can occur classically via macroscopic saddle-point configurations called sphalerons [40–43] and the exponential suppression disappears completely for even higher temperatures in the symmetric electroweak phase [30, 44]. These high temperature $B + L$ violating anomalous processes thus occurred very frequently in the early universe and they were in equilibrium roughly in the temperature range $100\,\mathrm{GeV} \lesssim T \lesssim 10^{12}$–$10^{13}\,\mathrm{GeV}$ [30, 32].[3]

The anomalous electroweak processes still conserve $B - L$, which is non-anomalous in the SM, and they tend to reduce any excess baryon or lepton number so that both $B, L \propto B - L$ in equilibrium [32, 42, 45]. This means that these processes will wash out any baryon asymmetry if $B - L = 0$, and especially they alone cannot generate a baryon asymmetry if initially both B and L vanish. On the other hand, *both* baryon and lepton asymmetries will be generated if $B - L \neq 0$, even if one or the other is zero initially. This is the feature utilized in leptogenesis.

2.3.2 Electroweak baryogenesis

In electroweak baryogenesis [10, 32, 34, 44] the BAU is generated by the anomalous electroweak processes during the EWPT which is required to be strongly first order. In such a transition bubbles of the electroweak broken phase nucleate in the electroweak symmetric plasma. The bubbles expand and eventually fill the universe, and during this transition there are suitable conditions for baryogenesis [34, 44]. First, particles of the plasma scatter with the expanding bubble which results in a chiral asymmetry. A part of this source asymmetry is then converted to a baryon asymmetry by the unsuppressed electroweak processes in the symmetric phase outside the bubble. Finally, some of the generated baryon number is captured by the expanding bubble where it is protected from washout because the sphaleron rate is suppressed. Due to this last point no $B - L$ violation is needed in the process.

Electroweak baryogenesis is a theoretically very interesting process as it involves the non-perturbative effects and vacuum structure of the electroweak gauge sector and bubble nucleation dynamics of the EWPT. It is also attractive due to its potential for experimental testing because it only involves processes at the electroweak scale. Gravitational wave astronomy also provides an interesting new probe for the

[3] These processes are often collectively called "sphaleron processes" even though the sphaleron configuration only exists in the broken state of the electroweak symmetry.

EWPT [32]. As was already touched on above, successful EWBG requires extending the SM in order to get a strong enough CP-violating source and a strong first order EWPT. However, by now the results from the LHC and electron EDM experiments [46] have strongly constrained most popular models, such as the minimal supersymmetric SM, two-Higgs-doublet models and doublet-singlet models [32, 47–50]. For some recent progress in EWBG models see for example [51–54].

2.3.3 Leptogenesis

Leptogenesis [32, 55–57] is a mechanism for baryogenesis in which the BAU is produced from a dynamically generated lepton asymmetry. In leptogenesis the SM is extended with (typically three) heavy singlet neutrino fields N_i with masses m_i (with $i = 1, \ldots$) and they have CP-violating chiral Yukawa interactions and L-violating Majorana mass terms. These Majorana neutrinos mix and their interactions with the SM leptons and Higgs boson produce the lepton asymmetry which is converted to the baryon asymmetry by the anomalous electroweak processes. Leptogenesis is essentially a consequence of the type-I see-saw mechanism (see e.g. [3]) which is a potential explanation for the lightness of the SM neutrinos [57]. The prospect of having the same origin for the light neutrino masses and the baryon asymmetry makes leptogenesis very interesting theoretically.

Leptogenesis has different variants which can be successfully realized at different temperature ranges in the early universe. The most prominent is the original scenario of thermal leptogenesis [12] which can be roughly divided to the unflavored (i.e., one-flavor) and flavored cases [32]. Resonant leptogenesis (RL) [58] is a further special case of thermal leptogenesis with mixing quasidegenerate Majorana neutrinos where the relevant CP-asymmetry is resonantly enhanced. Another notable scenario is the ARS mechanism of leptogenesis [13] where the lepton asymmetry is produced during the production and oscillations of heavy singlet neutrinos close to the sphaleron freeze-out. For other leptogenesis scenarios see for example [32, 55].

In thermal leptogenesis the lepton asymmetry is generated in the non-equilibrium decays of the Majorana neutrinos when they have slight over-abundances compared to equilibrium. The asymmetry then freezes out once the washout processes drop out of equilibrium. Leptogenesis has often been studied in the one-flavor approximation (i.e. the unflavored case) where it is assumed that the asymmetry is generated equally in all lepton flavors and it suffices to consider only one effective SM lepton flavor. Within this approximation and in the case of a hierarchical Majorana neutrino mass spectrum (i.e. in the "vanilla leptogenesis" scenario) successful leptogenesis implies a lower bound of $\sim 10^9$ GeV for the Majorana neutrino mass scale [57, 59]. Strictly speaking the one-flavor approximation is valid only when the SM lepton flavors cannot be distinguished during leptogenesis. This is the case, roughly, if the masses of the Majorana neutrinos are greater than $\sim 10^{12}$ GeV. This corresponds to the

temperature above which all SM lepton Yukawa interactions are still slow enough to be out of equilibrium [32, 55, 57]. On the other hand, if some or all of the SM lepton Yukawa processes are in equilibrium during leptogenesis one needs to take them into account and track the evolution of individual lepton asymmetries.[4] In the flavored case the lower bound for the leptogenesis scale can then be significantly lower when compared to the one-flavor case [32].

The leptogenesis temperature scale can be lowered even more when the Majorana neutrino masses are almost degenerate, as is the case in (thermal) resonant leptogenesis. In RL the lepton asymmetry generation is enhanced for a quasidegenerate mass spectrum and this resonant enhancement is maximal when the mass differences of the Majorana neutrinos are comparable to their decay widths. In this case the CP-violation in the Majorana neutrino decays is dominated by the coherent flavor mixing effects (the so-called self-energy contribution in the semiclassical approach, see below) [55, 56]. In RL the leptogenesis temperature can then be brought down to the TeV-scale or even lower [32, 60]. Low-scale leptogenesis is also possible in the related ARS scenario, which is also called "leptogenesis via oscillations" or "freeze-in leptogenesis" [61, 62]. In fact, both RL and ARS scenarios require at least two quasidegenerate heavy neutrinos and there are resonances and oscillations in both [62]. However, in the ARS mechanism the BAU is frozen in during the production of the heavy neutrinos, in contrast to the standard freeze-out scenario of thermal RL. It has been shown that a unified description of both mechanisms is possible and the parameter regions where they enable successful baryogenesis are merged [62].

Semiclassical transport equations

The non-equilibrium evolution of the lepton asymmetry must be solved from transport equations. Thermal leptogenesis is conventionally studied in a semiclassical approach with Boltzmann equations where the interaction rates are supplied by perturbative vacuum QFT [63–65]. Usually simplified momentum-integrated rate equations are also derived, which requires some additional assumptions such as kinetic equilibrium and Maxwell–Boltzmann statistics. The standard equations in the one-lepton-flavor approximation, with decay and inverse decay processes only, are [32, 57, 65, 66]

$$\frac{\mathrm{d}n_i}{\mathrm{d}t} + 3Hn_i = -\left(\frac{n_i}{n_i^{\mathrm{eq}}} - 1\right)\gamma_i, \tag{2.11a}$$

$$\frac{\mathrm{d}n_L}{\mathrm{d}t} + 3Hn_L = \sum_i \left[\left(\frac{n_i}{n_i^{\mathrm{eq}}} - 1\right)\varepsilon_i^{CP}\gamma_i - \frac{n_L}{2n_\ell^{\mathrm{eq}}}\gamma_i\right]. \tag{2.11b}$$

Here n_i are the number densities of the Majorana neutrinos. The lepton asymmetry density is $n_L \equiv n_\ell - \overline{n}_\ell$ with the lepton and antilepton densities $n_\ell, \overline{n}_\ell$. The corre-

[4] The SM lepton Yukawa interactions are an example of "spectator processes" in leptogenesis, that is, processes which can affect the lepton asymmetry indirectly [32, 55].

sponding equilibrium number densities are $n_i^{\rm eq}$ and $n_\ell^{\rm eq}$ and the reaction density for the decays and inverse decays is denoted by γ_i (explicit formulae are given in [II]). In the standard scenario the lepton asymmetry is generated mainly when $T \lesssim m_1$, where m_1 is the mass of the lightest Majorana neutrino. We have only included the decay and inverse decay processes of the Majorana neutrinos because they give the dominant contributions to Majorana neutrino production and lepton asymmetry washout in this case [32]. Various scattering processes are relevant in higher temperatures $T > m_1$ and also for $T \ll m_1$, and should be accounted for in more complete (or phenomenological) studies.

A crucial part of the semiclassical equations (2.11) is the CP-asymmetry parameter ε_i^{CP} which quantifies the amount of CP-violation in the Majorana neutrino decays. It is defined in the one-lepton-flavor case as

$$\varepsilon_i^{CP} \equiv \frac{\Gamma(N_i \to \ell\phi) - \Gamma(N_i \to \bar{\ell}\bar{\phi})}{\Gamma(N_i \to \ell\phi) + \Gamma(N_i \to \bar{\ell}\bar{\phi})}, \tag{2.12}$$

where $\Gamma(N_i \to \ell\phi)$ is the partial width for the decay of the Majorana neutrino N_i to the SM lepton and Higgs doublets, and $\Gamma(N_i \to \bar{\ell}\bar{\phi})$ is the corresponding partial decay width with antiparticles. The CP-asymmetry vanishes at tree level and its calculation involves the interference of tree level and higher order amplitudes of the decay process. The two main contributions to ε_i^{CP} at one-loop order are the vertex contribution (also called ε'-type or direct CP-violation) which arises from the one-loop correction to the Yukawa interaction vertex and the self-energy contribution (also called ε-type or indirect CP-violation) which is related to the wavefunction renormalization of the mixing Majorana neutrinos [67]. However, the self-energy contribution cannot be calculated correctly in conventional perturbation theory and a straightforward calculation with a one-loop external leg correction (i.e. a non-1PI diagram) gives a diverging result in the limit of degenerate masses. Determining the correct result for ε_i^{CP} in the quasidegenerate case is highly non-trivial because the Majorana neutrinos mix and are unstable [58, 67, 68]. Proper calculations, which usually involve resummations, have been done with different methods in the literature. However, the exact form of ε_i^{CP} is uncertain because different methods yield different results in the maximally resonant region [67, 68] (see also e.g. [69, 70]).

So far we have considered simplified transport equations for calculating the lepton asymmetry. More complete studies should also include the effects of the anomalous electroweak processes which redistribute the generated asymmetry among B and L. A simple way to take this into account is to find the relation between the number densities n_L and n_{B-L}. At very high temperatures when the anomalous processes are slow the relation is trivially $n_L = -n_{B-L}$ (assuming zero initial B). But when the anomalous processes are in equilibrium the relation is non-trivial and depends also on other spectator processes [71–73]. In thermal leptogenesis these processes are conventionally neglected during the generation of the lepton asymmetry

and one continues to use $n_L \simeq -n_{B-L}$ (accurate to within 10 % [74]) [32]. Once n_{B-L} is determined one can then use the standard equilibrium relations [32, 45]

$$n_B = \frac{28}{79} n_{B-L}, \qquad n_L = -\frac{51}{79} n_{B-L} \tag{2.13}$$

to estimate the final redistribution of the asymmetry by the anomalous processes.

CP-asymmetry in resonant leptogenesis

We now concentrate on RL and hence consider the self-energy contribution to ε_i^{CP} as it is the dominant part in this case. We further restrict to the case of two Majorana neutrinos ($i = 1, 2$) which is sufficient in this work. The CP-asymmetry (2.12) in the one-lepton-flavor approximation then takes the generic form [75]

$$\varepsilon_{i,x}^{CP} = \frac{\mathrm{Im}\left[(y_1^* y_2)^2\right]}{|y_1|^2 |y_2|^2} \frac{(m_2^2 - m_1^2) m_i \Gamma_j^{(0)}}{(m_2^2 - m_1^2)^2 + (R_{ij,x})^2}. \qquad (j \neq i) \tag{2.14}$$

Here y_i are the relevant Yukawa couplings and $\Gamma_i^{(0)} = |y_i|^2 m_i/(8\pi)$ is the tree-level total decay width of the Majorana neutrino. The CP-asymmetry (2.14) is resonantly enhanced for small mass differences $\Delta m_{21} \equiv m_2 - m_1$, and the resonance is regulated by the factor $R_{ij,x}$ in the degeneracy limit $\Delta m_{21} \to 0$. Different approaches and approximation methods used in the literature lead to different forms of the regulator, which we have labelled by x. Some of the most relevant ones are

$$R_{ij,\mathrm{mix}} = m_i \Gamma_j^{(0)}, \tag{2.15a}$$

$$R_{ij,\mathrm{diff}} = m_i \Gamma_i^{(0)} - m_j \Gamma_j^{(0)}, \tag{2.15b}$$

$$R_{ij,\mathrm{sum}} = m_i \Gamma_i^{(0)} + m_j \Gamma_j^{(0)}, \tag{2.15c}$$

$$R_{ij,\mathrm{eff}} = (m_i \Gamma_i^{(0)} + m_j \Gamma_j^{(0)}) |\sin\theta_{ij}|, \tag{2.15d}$$

which we call the *mixed* regulator, *difference* regulator, *sum* regulator and *effective* sum regulator, respectively [58, 67, 68, 75, 76]. In the effective regulator (2.15d) the angle θ_{ij} denotes the relative phase of the complex Yukawa couplings y_i and y_j:

$$\sin(\theta_{ij}) \equiv \frac{\mathrm{Im}(y_i^* y_j)}{|y_i||y_j|}, \qquad \cos(\theta_{ij}) \equiv \frac{\mathrm{Re}(y_i^* y_j)}{|y_i||y_j|}. \tag{2.16}$$

In the one-lepton-flavor approximation with two Majorana neutrinos the angle θ_{12} determines the overall strength of the CP-asymmetry. This can be seen by writing the prefactor in equation (2.14) as $\mathrm{Im}[(y_1^* y_2)^2]/(|y_1|^2|y_2|^2) = \sin(2\theta_{12})$.

Finally, it should be noted that some of the regulators lead to spurious enhancements of the CP-asymmetry in certain cases. For example, the difference regulator (2.15b) vanishes when both $|y_2| \to |y_1|$ and $m_2 \to m_1$. Also, the effective regulator (2.15d) overestimates the asymmetry for small θ_{12} [76].

Shortcomings of the semiclassical approach

The application of classical Boltzmann equations to leptogenesis is known to have shortcomings [77]. It is also very non-trivial because the required CP-violation is a purely quantum effect. The source for the lepton asymmetry arises from the interference of a radiatively corrected and a tree level amplitude instead of a purely tree level process. This results in subtle issues, such as the difficulty in determining the exact form of the CP-asymmetry parameter (2.12), as discussed above. Furthermore, the CP-asymmetry generation is fundamentally a dynamical phenomenon and not always adequately captured by a static parameter such as (2.14) [76]. Another fundamental problem is the double counting of real intermediate states (RIS) of the scattering processes. The on-shell part of the s-channel exchange of a Majorana neutrino is included both in the decay and inverse decay contributions and in the $\Delta L = 2$ scattering processes [55, 66, 74]. This results in a spurious CP-violating source (in the decay and inverse decay part) which does not vanish in equilibrium [65, 66]. This is usually resolved by an ad hoc subtraction of the problematic part from the equations, but this is a delicate procedure.

These issues stem from the fact that the semiclassical approach is an ad hoc combination of vacuum QFT calculations and classical transport equations. Another shortcoming of this approach is that the radiative calculations do not include thermal corrections. All of these problems can be avoided by using a different approach where the non-equilibrium and quantum aspects are unified in one dynamical framework, such as the CTP method. The Schwinger–Keldysh CTP method is a first principles approach to non-equilibrium QFT and it has been widely used to study leptogenesis, see for example [75, 76, 78–97] (a more comprehensive list is given in [II]). As a field theoretic and fully-quantum method, it is very well suited to study the delicate features of leptogenesis such as the coherent transitions of the Majorana neutrinos and details of the CP-asymmetry generation. However, full implementation of this method is very difficult and various approximations are usually needed (see e.g. [77–79]). Therefore, some questions about the exact form of the CP-asymmetry, especially in the case of RL, have still not been settled [75, 76, 91, 95, 98]. This shows how non-trivial the CP-violation is in leptogenesis, and it calls for clear and concise treatments of the subject. It is our modest hope that the present work helps to clarify this important issue.

3 NON-EQUILIBRIUM QUANTUM FIELD THEORY

Non-equilibrium quantum field theory is needed to study the time evolution of high-energy thermodynamic systems where quantum effects are essential for the dynamics. Such situations arise in cosmology in the hot and dense early universe and also during the brief existence of the extreme form of matter in high-energy heavy-ion collisions [99, 100]. Ordinary vacuum QFT or the imaginary time formalism of thermal QFT are not sufficient for describing the time evolution of such systems because the boundary conditions are different: vacuum QFT is used to calculate vacuum-to-vacuum transition amplitudes over a large time interval and thermal QFT applies to static systems with no time-dependence.

In thermal equilibrium the quantum density operator of the system takes the form of a time evolution operator with an imaginary time variable. This enables the study of QFTs in finite temperature: thermal expectation values can be formulated as ordinary QFT transition amplitudes over the Euclidean time [101, 102]. This approach, known as the imaginary time QFT formalism, however relies on the specific equilibrium form of the density operator. With general density operators one needs a real time formalism instead. There exist different formulations but common for all of them is that two real time branches are needed in the time-contour, one forward and one backward, and the imaginary part of the contour must be non-increasing [101]. In this work we consider the simplest realization, called the closed time path formalism, which we will turn to next.

3.1 Schwinger–Keldysh formalism

A framework for non-equilibrium QFT is provided by the Schwinger–Keldysh closed time path (CTP) method, which was developed by Schwinger [103], Keldysh [104] and many others [105–110] (see also e.g. [111] and references therein). The CTP method is a rather general idea and it has been applied to various problems in different contexts [111]. In the context of QFT, one way to understand the need

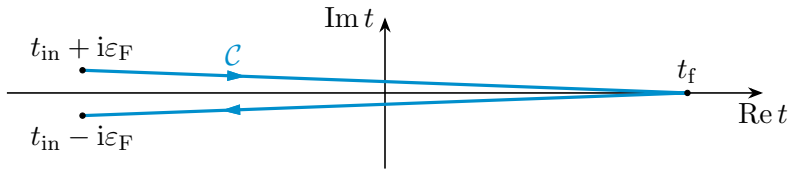

Figure 1. The Schwinger–Keldysh closed time path $\mathcal{C}$ for a considered initial time t_{in} and a final time parameter t_{f}. The arrows on the path show the direction of increasing contour-time. We have also indicated the infinitesimal displacements $\pm\mathrm{i}\varepsilon_{\mathrm{F}}$ required for convergence and correct boundary conditions.

for the closed time path (shown in figure 1) is as follows. Consider for example a two-point correlation function of a real scalar field ϕ in a system with a quantum density operator ρ:

$$\big\langle\hat{\phi}(x_1)\hat{\phi}(x_2)\big\rangle \equiv \mathrm{Tr}\big[\rho\,\hat{\phi}(x_1)\hat{\phi}(x_2)\big]. \tag{3.1}$$

The density operator ρ fully describes the quantum state of the system. The operators $\mathcal{O} = \rho, \hat{\phi}$ in equation (3.1) are written in the Heisenberg picture. In terms of Schrödinger picture operators $\mathcal{O}_{\mathrm{S}}$

$$\big\langle\hat{\phi}(x_1)\hat{\phi}(x_2)\big\rangle = \mathrm{Tr}\Big[\rho\,U(t_1,t_{\mathrm{in}})^\dagger\hat{\phi}_{\mathrm{S}}(\boldsymbol{x}_1)U(t_1,t_{\mathrm{in}})\,U(t_2,t_{\mathrm{in}})^\dagger\hat{\phi}_{\mathrm{S}}(\boldsymbol{x}_2)U(t_2,t_{\mathrm{in}})\Big], \tag{3.2}$$

where t_{in} is the initial time where the density operator $\rho = \rho_{\mathrm{S}}(t_{\mathrm{in}})$ is prepared at, and $U(t_1,t_2)$ is the full unitary time-evolution operator of the Schrödinger states. Now, when the density operator is generic and does not have any specific form (such as $\rho = \mathrm{e}^{-\beta H}$ in the canonical ensemble) the only way to evaluate (3.2) is to use two separate time branches or "histories" [8, 101, 111].

We can understand the need for two time branches by writing equation (3.2) in the functional integral form using standard QFT methods. To do this we use a basis of field eigenstates $|\varphi_a\rangle$ of the Schrödinger field $\hat{\phi}_{\mathrm{S}}$ (i.e. $\hat{\phi}_{\mathrm{S}}(\boldsymbol{x})|\varphi_a\rangle = \varphi_a(\boldsymbol{x})|\varphi_a\rangle$) which is complete and orthonormal: $\int\mathcal{D}\varphi_a\,|\varphi_a\rangle\langle\varphi_a| = 1$ and $\langle\varphi_a|\varphi_b\rangle = \delta[\varphi_a-\varphi_b]$ [112, 113]. We also need the Feynman path integral formulation of the transition amplitude,[5]

$$\big\langle\varphi_b\big|U(t_2,t_1)\big|\varphi_a\big\rangle = \int_{\varphi_a}^{\varphi_b}\mathcal{D}\phi\,\exp\Big(\mathrm{i}S[\phi]_{t_1}^{t_2}\Big). \tag{3.3}$$

[5] We use the following shorthand notation for constrained functional integrals:

$$\int_{\varphi_a}^{\varphi_b}\mathcal{D}\phi\cdots\exp\Big(\mathrm{i}S[\phi]_{t_1}^{t_2}\Big) \equiv \int\mathcal{D}\phi\cdots\exp\Big(\mathrm{i}S[\phi]_{t_1}^{t_2}\Big)\Big|_{\substack{\phi(t_1,\boldsymbol{x})=\varphi_a(\boldsymbol{x}),\\ \phi(t_2,\boldsymbol{x})=\varphi_b(\boldsymbol{x})}}$$

where the action integral is $S[\phi]_{t_1}^{t_2} \equiv \int_{t_1}^{t_2}\mathrm{d}^4x\,\mathcal{L}[\phi(x)]$, and $\int_{t_1}^{t_2}\mathrm{d}^4x \equiv \int_{t_1}^{t_2}\mathrm{d}t\int\mathrm{d}^3\boldsymbol{x}$.

Using these we can express the operator trace in (3.2) as the functional integral

$$\begin{aligned}\big\langle\hat\phi(x_1)\hat\phi(x_2)\big\rangle &= \int \mathcal{D}\varphi_a\mathcal{D}\varphi_b\mathcal{D}\varphi_c\mathcal{D}\varphi_d \,\big\langle\varphi_a\big|\rho\big|\varphi_b\big\rangle\big\langle\varphi_b\big|U(t_1,t_{\text{in}})^\dagger\big|\varphi_c\big\rangle\,\varphi_c(\boldsymbol{x}_1) \\ &\qquad\times \big\langle\varphi_c\big|U(t_1,t_2)\big|\varphi_d\big\rangle\big\langle\varphi_d\big|U(t_2,t_{\text{in}})\big|\varphi_a\big\rangle\,\varphi_d(\boldsymbol{x}_2) \\ &\overset{(t_1\geq t_2)}{=} \int \mathcal{D}\varphi_a\mathcal{D}\varphi_b\mathcal{D}\varphi_c\,\langle\varphi_a|\rho|\varphi_b\rangle\int_{\varphi_b}^{\varphi_c}\mathcal{D}\phi^-\,\phi^-(x_1)\exp\Big(\mathrm{i}S[\phi^-]_{t_{\text{in}}}^{t_1}\Big)^* \\ &\qquad\times\int_{\varphi_a}^{\varphi_c}\mathcal{D}\phi^+\,\phi^+(x_2)\exp\Big(\mathrm{i}S[\phi^+]_{t_{\text{in}}}^{t_1}\Big) \\ &= \int\mathcal{D}\phi^+\mathcal{D}\phi^-\,\langle\phi^+|\rho|\phi^-\rangle\,\phi^-(x_1)\phi^+(x_2) \\ &\qquad\times\exp\Big(\mathrm{i}S[\phi^+]_{t_{\text{in}}}^{t_{\text{f}}}-\mathrm{i}S[\phi^-]_{t_{\text{in}}}^{t_{\text{f}}\,*}\Big)\Big|_{\substack{\phi^+(t_{\text{f}},\boldsymbol{x})\\=\phi^-(t_{\text{f}},\boldsymbol{x})}}\,. \end{aligned}\tag{3.4}$$

The final time parameter t_{f} here must be chosen so that $t_{\text{f}}\geq\max(t_1,t_2)$ but otherwise it is arbitrary. Note that we have written the second equality leading to (3.4) explicitly for the case $t_1>t_2$ but the final result is valid more generally when $t_{\text{in}}<t_i<t_{\text{f}}$ with $i=1,2$. Also, the states $|\phi^\pm\rangle$ in the final result correspond to the field configurations $\phi^\pm(t_{\text{in}},\boldsymbol{x})$.

The result (3.4) for the two-point function indeed contains two time branches: a forward branch for ϕ^+ and a backward branch for ϕ^-. Both functional integrations are independent except for the boundary condition which identifies the fields at the final time. Thus, the result can be interpreted as a single functional integral along the CTP shown in figure 1 *if* we also specify at which branch the fields at x_1 and x_2 are evaluated on [8]. Finally, we note that the form of equation (3.4) with the two time branches and the initial density matrix $\langle\phi^+|\rho|\phi^-\rangle$ is generic to any n-point correlation function, and not only to the two-point function used in this example.

Generating functional

The development of the CTP formalism then proceeds along the lines of conventional QFT where one defines the generating functional of the n-point functions. The generating functional for non-equilibrium systems, also called the in-in generating functional, can be defined as [114]

$$Z[J_\pm;\rho]\equiv\mathrm{Tr}\bigg\{\rho\,\overline{\mathcal{T}}\exp\bigg[-\mathrm{i}\int_{t_{\text{in}}}^{t_{\text{f}}}\mathrm{d}^4x\,J_-(x)\hat\phi(x)\bigg]\,\mathcal{T}\exp\bigg[\mathrm{i}\int_{t_{\text{in}}}^{t_{\text{f}}}\mathrm{d}^4x\,J_+(x)\hat\phi(x)\bigg]\bigg\}.\tag{3.5}$$

There are contributions from both branches of the CTP which have their own external source and time-ordering: the forward branch with J_+ and usual time-ordering $\mathcal{T}$ and the backward branch with J_- and reversed time-ordering $\overline{\mathcal{T}}$.

The generating functional of connected n-point functions is defined as usual as the logarithm

$$W[J_\pm;\rho]\equiv-\mathrm{i}\log Z[J_\pm;\rho].\tag{3.6}$$

The physical n-point functions can be generated from (3.6) by functional differentiation with respect to the sources and taking the limit of vanishing sources in the end, similarly to conventional QFT. However, there are now multiple ways to generate a given n-point function because the amount of sources is doubled. As an example, we show how to generate the one-point function and also the two-point function (3.1) used in the previous example:

$$-\frac{\delta W[J;\rho]}{\delta J_-(x)}\bigg|_{J\to 0} = \frac{\delta W[J;\rho]}{\delta J_+(x)}\bigg|_{J\to 0} = \big\langle \hat{\phi}(x)\big\rangle, \tag{3.7a}$$

$$\mathrm{i}\,\frac{\delta^2 W[J;\rho]}{\delta J_+(x_2)\delta J_-(x_1)}\bigg|_{J\to 0} = \big\langle \hat{\phi}(x_1)\hat{\phi}(x_2)\big\rangle. \tag{3.7b}$$

In the calculation of (3.7) we used the normalization of density operators, $\operatorname{Tr}\rho = 1$ [8], which implies that $Z[0;\rho] = 1$. Note that equation (3.7b) gives just one of four different two-point functions which can be generated from (3.6). Not all of them will be independent functions however, as we will see later on.

The generating functional (3.5) admits a path integral form which can be derived similarly to equation (3.4). The result is [8, 114]

$$\begin{aligned} Z[J_\pm;\rho] &= \int \mathcal{D}\phi^+\mathcal{D}\phi^-\,\langle\phi^+|\rho|\phi^-\rangle \\ &\qquad\times \exp\Big[\mathrm{i}\Big(S[\phi^+]_{t_\mathrm{in}}^{t_\mathrm{f}} + J_+\phi^+\Big) - \mathrm{i}\Big(S[\phi^-]_{t_\mathrm{in}}^{t_\mathrm{f}\,*} + J_-\phi^-\Big)\Big]\Big|_{\substack{\phi^+(t_\mathrm{f},\boldsymbol{x})\\=\phi^-(t_\mathrm{f},\boldsymbol{x})}} \\ &\equiv \int_\mathrm{c}\mathcal{D}\phi^a\,\langle\phi^+|\rho|\phi^-\rangle\,\exp\Big[\mathrm{i}\Big(S_\mathrm{c}[\phi^a]_{t_\mathrm{in}}^{t_\mathrm{f}} + J^a\phi^a\Big)\Big], \end{aligned} \tag{3.8}$$

where we also introduced some often used notation for the CTP components. In this notation $a = \pm$ is the CTP branch index, repeated indices are implicitly summed over, and one defines a "metric" $c^{ab} = c_{ab} \equiv \operatorname{diag}(1,-1)$ using which the indices may be raised or lowered [114]. Furthermore, we suppress the spacetime arguments and integrations where appropriate, so that for example $J_\pm\phi^\pm \equiv \int_{t_\mathrm{in}}^{t_\mathrm{f}} \mathrm{d}^4x\, J_\pm(x)\phi^\pm(x)$. We also defined the shorthand $S_\mathrm{c}[\phi^a]_{t_\mathrm{in}}^{t_\mathrm{f}} \equiv S[\phi^+]_{t_\mathrm{in}}^{t_\mathrm{f}} - S[\phi^-]_{t_\mathrm{in}}^{t_\mathrm{f}\,*}$ for the CTP action, and the subscript 'c' in the integral designates the closure condition $\phi^+(t_\mathrm{f},\boldsymbol{x}) = \phi^-(t_\mathrm{f},\boldsymbol{x})$.

Non-local sources

An important property of the initial density matrix $\langle\phi^+|\rho|\phi^-\rangle$ is that it is a functional of the field configurations $\phi^\pm(t_\mathrm{in},\boldsymbol{x})$. It can then be expanded functionally using the field configurations as [114, 115]

$$\langle\phi^+|\rho|\phi^-\rangle = \exp\Big[\mathrm{i}\big(K + K_a\phi^a + \tfrac{1}{2!}K_{ab}\phi^a\phi^b + \tfrac{1}{3!}K_{abc}\phi^a\phi^b\phi^c + \cdots\big)\Big]. \tag{3.9}$$

The constant K and the infinite sequence of functions K_a, K_{ab}, K_{abc}, ... parametrize the density operator ρ.[6] They have support only at the initial time, and hence they

[6] More precisely: $K_a(x) = \widetilde{K}_a(\boldsymbol{x})\delta(x^0 - t_\mathrm{in})$, $K_{ab}(x,y) = \widetilde{K}_{ab}(\boldsymbol{x},\boldsymbol{y})\delta(x^0 - t_\mathrm{in})\delta(y^0 - t_\mathrm{in})$, etc.

can be viewed as initial-time sources. Note that we used here the notation defined below equation (3.8): repeated CTP indices are implicitly summed over and $K_{ab}\phi^a\phi^b$ denotes $\int_{t_\mathrm{in}}^{t_\mathrm{f}} \mathrm{d}^4x\,\mathrm{d}^4y\,K_{ab}(x,y)\phi^a(x)\phi^b(y)$, for example.

We can now write the original non-equilibrium generating functional (3.5) in a remarkably simple form. By using equation (3.9) in (3.8) and absorbing the constant K to the normalization of the integral measure, we get [114, 116]

$$\begin{aligned} Z[J_\pm;\rho] &= Z[\mathfrak{J}_a, K_{ab}, K_{abc}, \ldots] \\ &\equiv \int_\mathrm{c} \mathcal{D}\phi^a \, \exp\Big[\mathrm{i}\Big(S_\mathrm{c}[\phi^a]_{t_\mathrm{in}}^{t_\mathrm{f}} + \mathfrak{J}_a\phi^a + \tfrac{1}{2}K_{ab}\phi^a\phi^b + \tfrac{1}{3!}K_{abc}\phi^a\phi^b\phi^c + \cdots\Big)\Big], \end{aligned} \tag{3.10}$$

where $\mathfrak{J}_a \equiv J^a + K_a = c^{ab}J_b + K_a$. Equation (3.10) is an exact result and it demonstrates that a general non-equilibrium field theory can be formally described in the CTP formalism by including all possible n-point sources in the generating functional.[7] Of course, the infinite number of initial-time sources is only necessary when describing arbitrary density matrices. For specific situations like a vacuum or a thermal system one can make additional simplifications. For example, in the case of a Gaussian initial state only the sources K_a and K_{ab} are necessary [113].

3.2 Generalized effective actions

Now that we have the non-equilibrium generating functional (3.8) and a path integral representation for the n-point functions we could try to evaluate them in specific theories using the conventional methods of perturbative QFT. Here one runs into problems however. For example, perturbative expansions of the non-equilibrium n-point functions contain so-called secular terms [115] which grow with increasing powers of time at each order, and this ruins the expansion even for small coupling constants [99, 117]. Description of thermalization and late-time universality also generally require non-linear dynamics and conserved charges (e.g. energy conservation) which are usually absent in more conventional approaches [99, 113, 115].

While the secularity problem can be solved by resummation, a more sophisticated and efficient solution is to use a generalized effective action from which equations for the n-point functions can be derived by a variational principle [115, 118, 119]. The non-equilibrium generating functional (3.10) and its logarithm W serve as the starting point for this method. The generalized effective action is defined as the multiple Legendre transform of $W[J_a, K_{ab}, K_{abc}, \ldots]$ with respect to the infinite sequence of sources J_a, K_{ab}, K_{abc}, ... [114]. Stationarity conditions of the effective action then lead to an infinite set of coupled equations of motion for the full n-point functions,

[7] Note that in [99, 113, 115] already the operator representation of Z is given with the non-local sources, in contrast to [114]. We have used the simpler approach in (3.5), leading to (3.10).

which is analogous to the BBGKY hierarchy in classical statistical mechanics [8, 114]. This hierarchy of equations then fully describes the non-equilibrium evolution of the system.

In practice the infinite hierarchy is impossible to solve exactly in realistic interacting theories and one needs to use approximations. First of all, the hierarchy of equations can be truncated by only taking into account the n-point sources up to some finite n when doing the Legendre transformation [8, 114, 115]. This leads to the n-particle irreducible effective action (nPIEA). In classical mechanics and thermodynamics different Legendre transforms lead to different but equivalent descriptions of the same physics. The nPIEAs for different $n \in \mathbb{N}$ are in this sense also equivalent when no other approximations are used [113]. However, further approximations *are* usually needed.

For a given nPIEA one also usually needs some approximative method to calculate the effective action itself. This can be done, for example, by truncating a loop expansion or by using a $1/N$-expansion in theories with N field components [113, 117]. When approximated this way the different nPIEAs are no longer equivalent but form equivalence hierarchies [115, 118]. In practice different nPIEAs have restrictions on what kind of dynamics and initial states they can adequately describe. Which nPIEA to choose then depends largely on the problem at hand and the order of the approximation. Typically the 2PI, the 3PI or the 4PI effective action already provides a complete description of the problem in feasible approximations [115].

Next we turn to the 2PIEA method which is used to derive the non-equilibrium evolution equations used in this work. The 2PIEA method [119] was developed originally for non-relativistic many-body theory in [120–122] and later in the functional formulation for relativistic QFT in [123]. Its adaptation to non-equilibrium QFT using the CTP was given in [111, 114]. We present some details on how the formalism is derived, following mostly [8], culminating in the derivation of the general equation of motion for the two-point function.

3.2.1 2PI effective action on the CTP

The starting point for the CTP 2PIEA method [8] is the generating functional

$$Z[J_a, K_{ab}] \equiv \int_{\mathrm{c}} \mathcal{D}\phi^a \exp\Big[\mathrm{i}\Big(S_{\mathrm{c}}[\phi^a]_{t_{\mathrm{in}}}^{t_{\mathrm{f}}} + J_a\phi^a + \tfrac{1}{2}K_{ab}\phi^a\phi^b\Big)\Big], \tag{3.11}$$

which is a truncation of the general non-equilibrium case (3.10). The notation was defined below equation (3.8). As in the previous section, we continue to use real scalar field theory as an example on the development of the formalism. The generating functional (3.11) is equivalent to the full $Z[J_\pm; \rho]$ only for Gaussian initial density matrices or a vacuum initial state, and otherwise it must be considered an approximation. The effects of non-trivial initial correlations tend to be short-lived

however [124], so this should be a sound approximation when the focus is on the dynamical evolution rather than the intricacies of the initial conditions.

The connected generating functional $W[J_a, K_{ab}] \equiv -\mathrm{i}\log Z[J_a, K_{ab}]$ is defined like in equation (3.6), but there is now a difference when the physical n-point functions are calculated from W. When taking the limit of vanishing sources also the initial density matrix gets discarded in the process, which is also reflected in that $Z[0,0] \neq 1$. But because the initial density matrix (3.9) has support only at $t = t_{\mathrm{in}}$ one can compensate for this loss of information by adjusting the initial conditions of the n-point functions suitably [115]. Hence, the physical n-point functions can still be calculated by the standard method where the sources are removed in the end.

To formulate the 2PIEA we still need to keep the sources, of course. We first define the mean field $\bar{\phi}^a(x)$ and the fluctuation propagator $G^{ab}(x,y)$ by

$$\bar{\phi}^a(x) \equiv \frac{\delta W[J,K]}{\delta J_a(x)}, \tag{3.12a}$$

$$G^{ab}(x,y) \equiv 2\frac{\delta W[J,K]}{\delta K_{ab}(x,y)} - \bar{\phi}^a(x)\bar{\phi}^b(y). \tag{3.12b}$$

In the limit $J, K \to 0$ both of the mean fields $\bar{\phi}^{\pm}$ reduce to the physical one-point function. The function G^{ab} describes the propagation of the field fluctuations around the mean value. It thus reduces to the physical two-point function when both the mean field and the sources vanish. The 2PIEA is defined as the double Legendre transform

$$\begin{aligned}\Gamma_{\mathrm{2PI}}\big[\bar{\phi}^a, G^{ab}\big] &\equiv W[J_a, K_{ab}] - J_a\frac{\delta W}{\delta J_a} - K_{ab}\frac{\delta W}{\delta K_{ab}} \\ &= W[J_a, K_{ab}] - J_a\bar{\phi}^a - \frac{1}{2}K_{ab}\Big(G^{ab} + \bar{\phi}^a\bar{\phi}^b\Big).\end{aligned} \tag{3.13}$$

The meaning of the Legendre transform here is that we switch from the functional W and its independent variables (functions) J, K to the effective action Γ_{2PI} and $\bar{\phi}, G$. The inverse relations of (3.12) are then given by

$$\frac{\delta\Gamma_{\mathrm{2PI}}}{\delta\bar{\phi}^a} = -J_a - K_{ab}\bar{\phi}^b, \tag{3.14a}$$

$$\frac{\delta\Gamma_{\mathrm{2PI}}}{\delta G^{ab}} = -\frac{1}{2}K_{ab}. \tag{3.14b}$$

In the first equation we also used that for a real scalar field the two-point source is symmetric: $K_{ab}(x,y) = K_{ba}(y,x)$. This follows from the corresponding property of the propagator $G^{ab}(x,y)$.

Equations (3.14) give the stationarity conditions of the effective action in the limit of vanishing sources. That is, eventually they yield the equations of motion for the full one- and two-point functions. To this end, we need to eliminate the sources

J, K from Γ_{2PI}. Exponentiating equation (3.13), using (3.11) and (3.14) and shifting the functional integral variable to the fluctuation field $\varphi^a \equiv \phi^a - \bar{\phi}^a$ leads to the compact equation

$$\mathrm{e}^{\mathrm{i}\Gamma_{\text{2PI}}} = \int_{\mathrm{c}} \mathcal{D}\varphi^a \exp\left[\mathrm{i}\left(S_{\mathrm{c}}\left[\bar{\phi}^a + \varphi^a\right]_{t_{\text{in}}}^{t_{\mathrm{f}}} - \frac{\delta\Gamma_{\text{2PI}}}{\delta\bar{\phi}^a}\varphi^a - \frac{\delta\Gamma_{\text{2PI}}}{\delta G^{ab}}\left(\varphi^a\varphi^b - G^{ab}\right)\right)\right]. \quad (3.15)$$

Equation (3.15) gives an exact self-contained formula for Γ_{2PI} in terms of $\bar{\phi}, G$ only. If we could solve Γ_{2PI} from it we could then calculate the variations on the left-hand sides of equations (3.14) and take the limit $J, K \to 0$ to get the equations of motion. This is of course not possible to do exactly for realistic interacting theories so some approximative method is needed.

Expansion of the 2PIEA

We will now use a loop expansion to calculate Γ_{2PI}.[8] To proceed from equation (3.15) we must extract the lowest order parts of Γ_{2PI}. This can be done by using the background field method [8] where the shifted action $S_{\mathrm{c}}[\bar{\phi}^a + \varphi^a]_{t_{\text{in}}}^{t_{\mathrm{f}}}$ is functionally expanded around the mean field:

$$S_{\mathrm{c}}\left[\bar{\phi}^a + \varphi^a\right] = S_{\mathrm{c}}\left[\bar{\phi}^a\right] + \frac{\delta S_{\mathrm{c}}[\bar{\phi}^a]}{\delta\bar{\phi}^b}\varphi^b + \frac{1}{2!}\frac{\delta^2 S_{\mathrm{c}}[\bar{\phi}^a]}{\delta\bar{\phi}^b\delta\bar{\phi}^c}\varphi^b\varphi^c + S_2\left[\varphi^a; \bar{\phi}^a\right]. \quad (3.16)$$

Here $S_2[\varphi^a; \bar{\phi}^a]$ is defined as the rest of the terms which are *cubic* or higher order in the fluctuation field φ; the reason for this notation will become clear below. Next we define the function [115]

$$\mathrm{i}G^{-1}_{0,ab}(x, y) \equiv \frac{\delta^2 S_{\mathrm{c}}[\bar{\phi}^c]_{t_{\text{in}}}^{t_{\mathrm{f}}}}{\delta\bar{\phi}^a(x)\delta\bar{\phi}^b(y)}, \quad (3.17)$$

which is a generalization of the inverse free propagator in the presence of the mean field. The quadratic term in equation (3.16) can then be written as $\frac{\mathrm{i}}{2}G^{-1}_{0,ab}\varphi^a\varphi^b$.

As an effective quantum action, Γ_{2PI} should contain the classical CTP action plus quantum corrections: $\Gamma_{\text{2PI}} = S_{\mathrm{c}}[\bar{\phi}^a] + \mathcal{O}(\hbar)$ [8]. We can already verify the classical part by using equation (3.16) in (3.15); the term $S_{\mathrm{c}}[\bar{\phi}^a]$ can be factored out of the functional integral. We will now construct the rest of the terms. The first quantum correction is the "one-loop part", that is, the Gaussian functional integral which corresponds to the functional determinant of the propagator:

$$\int_{\mathrm{c}} \mathcal{D}\varphi^a \exp\left(-\tfrac{1}{2}G^{-1}_{ab}\varphi^a\varphi^b\right) \propto \left(\operatorname{Det} G^{-1}\right)^{-\frac{1}{2}}. \quad (3.18)$$

To get this contribution to the right-hand side of equation (3.15) we need to add a term to Γ_{2PI} which yields $-\frac{\mathrm{i}}{2}G^{-1}_{ab}$ from the variation $\delta\Gamma_{\text{2PI}}/\delta G^{ab}$. The correct

[8] The expansion parameter, number of loops, technically corresponds to powers of $\hbar$ [123].

term is given by the functional identity $\delta \operatorname{Tr}[\log G^{-1}]/\delta G^{ab} = -G^{-1}_{ab}$, which leads to $\Gamma_{\text{2PI}} = S_{\text{c}}[\bar{\phi}^a] + \frac{\mathrm{i}}{2}\operatorname{Tr}[\log G^{-1}] + \text{const.} + \mathcal{O}(\hbar^2)$. The addition of the one-loop term also introduces an infinite constant $-\frac{\mathrm{i}}{2}\operatorname{Tr}\mathbf{1} \equiv -\frac{\mathrm{i}}{2}G^{-1}_{ab}G^{ab} = -\mathrm{i}\int_{t_{\text{in}}}^{t_{\text{f}}} \mathrm{d}^4x\, \delta^{(4)}(0)$ which, however, does not affect the stationarity conditions [8]. Lastly, we also add an extra term to Γ_{2PI} to cancel the quadratic part of equation (3.16) in (3.15). The term is $\frac{\mathrm{i}}{2}\operatorname{Tr}[G_0^{-1}G] = \frac{\mathrm{i}}{2}G^{-1}_{0,ab}G^{ab}$ and it is required for the stationarity conditions to eventually produce the correct Schwinger–Dyson equation for the propagator.

The final parametrization of the 2PIEA is then [8, 115, 123]

$$\Gamma_{\text{2PI}}\big[\bar{\phi}^a, G^{ab}\big] = S_{\text{c}}\big[\bar{\phi}^a\big]_{t_{\text{in}}}^{t_{\text{f}}} + \tfrac{\mathrm{i}}{2}\operatorname{Tr}\big[G_0^{-1}G\big] + \tfrac{\mathrm{i}}{2}\operatorname{Tr}\big[\log G^{-1}\big] + \Gamma_2\big[\bar{\phi}^a, G^{ab}\big] + \text{const.} \tag{3.19}$$

Equation (3.19) is essentially a definition for the non-trivial part Γ_2, that is, the higher-order quantum corrections. Due to the construction we expect it to consist of diagrams with two or more loops. To derive an equation for Γ_2 we first calculate the variations

$$\frac{\delta\Gamma_{\text{2PI}}}{\delta\bar{\phi}^a} = \frac{\delta S_{\text{c}}[\bar{\phi}]}{\delta\bar{\phi}^a} + \frac{1}{2}\frac{\delta^3 S_{\text{c}}[\bar{\phi}]}{\delta\bar{\phi}^a\delta\bar{\phi}^b\delta\bar{\phi}^c}G^{bc} + \frac{\delta\Gamma_2}{\delta\bar{\phi}^a}, \tag{3.20a}$$

$$\frac{\delta\Gamma_{\text{2PI}}}{\delta G^{ab}} = \frac{\mathrm{i}}{2}G^{-1}_{0,ab} - \frac{\mathrm{i}}{2}G^{-1}_{ab} + \frac{\delta\Gamma_2}{\delta G^{ab}}. \tag{3.20b}$$

By using equations (3.16), (3.19) and (3.20) (and the identity $\log[\operatorname{Det} G^{-1}] = \operatorname{Tr}[\log G^{-1}]$) in (3.15) we can then derive the result

$$\mathrm{e}^{\mathrm{i}\Gamma_2} = (\operatorname{Det} G^{-1})^{\frac{1}{2}}\int_{\text{c}}\mathcal{D}\varphi^a \exp\Bigg[\mathrm{i}\Bigg(\tfrac{\mathrm{i}}{2}G^{-1}_{ab}\varphi^a\varphi^b + S_2\big[\varphi^a;\bar{\phi}^a\big] - \widetilde{J}_a\varphi^a - \widetilde{K}_{ab}\big(\varphi^a\varphi^b - G^{ab}\big)\Bigg)\Bigg], \tag{3.21a}$$

where

$$\widetilde{J}_a \equiv \frac{\delta\Gamma_2}{\delta\bar{\phi}^a} + \frac{1}{2}\frac{\delta^3 S_{\text{c}}[\bar{\phi}]}{\delta\bar{\phi}^a\delta\bar{\phi}^b\delta\bar{\phi}^c}G^{bc}, \qquad \widetilde{K}_{ab} \equiv \frac{\delta\Gamma_2}{\delta G^{ab}}. \tag{3.21b}$$

This is a self-contained equation for Γ_2 in terms of $\bar{\phi}, G$. At first glance it seems even more cryptic than equation (3.15), but it actually has a very specific meaning.

It turns out that $\mathrm{i}\Gamma_2$ consists of the *2PI vacuum diagrams* where the propagator lines correspond to G, that is, the *full* propagator of the original theory, and the interaction vertices are given by $S_2[\varphi^a;\bar{\phi}^a]$ [8, 115, 123]. This is a consequence of the constraining sources $\widetilde{J}_a$ and $\widetilde{K}_{ab}$ in equation (3.21a). To understand this, consider a system with a generating functional corresponding to the functional integral in (3.21a). The form of the sources is precisely such that the exact connected propagator in this system is fixed to G and the exact one-point function vanishes [123, 125]. This can be shown from the invertibility of the Legendre transformation by taking variations of Γ_2 with respect to $\bar{\phi}$ and G [8]. Furthermore, because the one-loop part was already extracted, the diagrams contained in Γ_2 have two or more loops, as expected.[9]

[9] The $\operatorname{Det} G$-factor in equation (3.21a) cancels to lowest order due to (3.18).

Physical equations of motion

We can now finally obtain the equations of motion for the (full) physical one- and two-point functions. Combining equations (3.20) and (3.14) and taking the limit $J, K \to 0$ results in coupled non-linear equations for $\bar{\phi}^a$ and G^{ab} in terms of the actions $S_c[\bar{\phi}^a]$ and $\Gamma_2[\bar{\phi}^a, G^{ab}]$. We are mainly interested in the propagator equation which can be written as

$$G^{-1}_{ab}(x,y) = G^{-1}_{0,ab}(x,y) - \Pi_{ab}(x,y), \tag{3.22}$$

with

$$\Pi_{ab}(x,y) \equiv 2\mathrm{i}\frac{\delta\Gamma_2[\bar{\phi}, G]}{\delta G^{ab}(x,y)}. \tag{3.23}$$

Note that equation (3.22) is generally a very complicated non-linear equation for G because of the dependence on Γ_2.

Now, we know that G is the full connected propagator because of its definition (3.12b). This means that equation (3.22) is nothing else but its Schwinger–Dyson equation. Therefore Π_{ab}, given by (3.23), must also be equal to the proper 1PI self-energy (i.e. it does not contain propagator insertions) [123]. There are thus two different perspectives for Π_{ab}: it is the (whole) perturbative series of proper 1PI self-energy diagrams (with internal lines corresponding to G_0) and, on the other hand, it can be calculated from Γ_2 (in terms of the full G).[10] This is one of the main points of the 2PIEA method: a large class of diagrams is automatically resummed in Γ_2. The 2PIEA method is however more than just a resummation scheme as the equations of motion are derived *self-consistently* from a variational principle [119]. The method is consistent with global symmetries of the theory and it provides an efficient and systematic way to derive approximations [118].

The main 2PIEA results which we use in this work are equation (3.22) and the method to calculate the self-energy (3.23) from the 2PI loop expansion. Although equation (3.22) has the form of the usual Schwinger–Dyson equation, the viewpoint is now very different compared to the standard perturbative approach: equation (3.22) is a non-linear equation of motion for the full propagator.

Generalization to other types of fields

So far we have considered only a real scalar field theory when we introduced the CTP and the 2PIEA and derived the equations of motion in this chapter. Already the derivation of the path integral form of the propagator, given by equation (3.4), is much more complicated for other types of fields. The formulation of the 2PIEA method is also considerably more complicated in more realistic situations, such as in gauge theories [126, 127]. Furthermore, in an interacting theory with different

[10] This provides another way to see that Γ_2 can only contain 2PI diagrams (with internal lines corresponding to G) as otherwise Π_{ab} would contain propagator insertions [115, 123].

types of fields (e.g. quantum electrodynamics) one generally has to consider in the intermediate steps also all mixed propagators (like e.g. a photon-fermion propagator) and all mixed non-local sources to get the correct equations of motion [126].

In these more realistic cases the final *physical* equations of motion are luckily not so complicated and they are mostly analogous to the real scalar field case. The main differences are that the 2PIEA parametrization (3.19) contains additional one-loop and inverse free propagator terms for each degree of freedom separately, the functional determinant has a different numerical coefficient depending on the type of field (like in standard QFT), and the propagators and self-energies have more complicated symmetry properties in the spacetime-arguments and CTP indices [123, 126, 128, 129]. We will not give these results explicitly but from now on just quote the relevant parts when needed. As a final remark we point out that in these more general situations the non-trivial part Γ_2 of the 2PIEA is still calculated as the sum of all 2PI vacuum diagrams but it is then a functional of all physical propagators and mean fields of the system. Also, when all mean fields of the system vanish, the action S_2 (used for calculating Γ_2) consists of the same interaction vertices as the classical CTP action of the theory.

3.3 Non-equilibrium evolution equations

In this section we present the non-equilibrium evolution equations based on the Schwinger–Dyson equation (3.22) derived in the CTP 2PIEA formalism. From now on we are working with vanishing mean fields in which case the non-equilibrium evolution of the system is completely described by the propagators. We first give the definitions of the CTP propagators, one of which was already used as an example in equations (3.1) and (3.7b). Then we present the general evolution equations which are written in the form of Kadanoff–Baym equations [130, 131].

3.3.1 Closed time path propagators

The CTP propagators with real time arguments can be conveniently packaged into one object by using contour-ordered (complex) time arguments on the CTP [101, 129]. Using this "contour notation", we define the propagators of a fermion field ψ and a complex scalar boson field ϕ as [129]

$$\mathrm{i}S(u,v) \equiv \big\langle \mathcal{T}_\mathcal{C}\big[\psi(u)\overline{\psi}(v)\big]\big\rangle, \tag{3.24a}$$

$$\mathrm{i}\Delta(u,v) \equiv \big\langle \mathcal{T}_\mathcal{C}\big[\phi(u)\phi^\dagger(v)\big]\big\rangle, \tag{3.24b}$$

where u^0, v^0 lie on the CTP and $\mathcal{T}_\mathcal{C}$ denotes the contour-ordering (indicated in figure 1).[11] Also, $\overline{\psi} \equiv \psi^\dagger\gamma^0$ denotes the usual conjugated fermion field, and we now

[11] We use an explicit imaginary unit in the definitions (3.24). This is different from the convention used for G in section 3.2.1 which is what is usually used in the 2PIEA-literature.

suppress the hats on the operators. The expectation values are taken with respect to the non-equilibrium density operator of the system as in equation (3.1). In the definitions (3.24) the ordering of any discrete indices of the fields, such as flavor or spinor indices, follows the ordering of the spacetime arguments. For example, the fermion propagator (3.24a) reads $\mathrm{i}S_{\alpha\beta}(u,v) = \langle \mathcal{T}_\mathcal{C}[\psi_\alpha(u)\overline{\psi}_\beta(v)]\rangle$ when written explicitly with the Dirac spinor indices.

The component propagators with the CTP branch indices $a, b = \pm$ and real time arguments can be found by evaluating the time-ordering in equations (3.24) for the different cases. There are four of these real-time propagators and we denote them as

$$S^< \equiv -S^{+-}, \qquad \mathrm{i}S^{+-}_{\alpha\beta}(u,v) \equiv -\big\langle \overline{\psi}_\beta(v)\psi_\alpha(u)\big\rangle, \tag{3.25a}$$
$$S^> \equiv S^{-+}, \qquad \mathrm{i}S^{-+}_{\alpha\beta}(u,v) \equiv \big\langle \psi_\alpha(u)\overline{\psi}_\beta(v)\big\rangle, \tag{3.25b}$$
$$S^\mathrm{T} \equiv S^{++}, \qquad \mathrm{i}S^{++}_{\alpha\beta}(u,v) \equiv \big\langle \mathcal{T}\big[\psi_\alpha(u)\overline{\psi}_\beta(v)\big]\big\rangle, \tag{3.25c}$$
$$S^{\overline{\mathrm{T}}} \equiv S^{--}, \qquad \mathrm{i}S^{--}_{\alpha\beta}(u,v) \equiv \big\langle \overline{\mathcal{T}}\big[\psi_\alpha(u)\overline{\psi}_\beta(v)\big]\big\rangle, \tag{3.25d}$$

for the fermion and

$$\Delta^< \equiv \Delta^{+-}, \qquad \mathrm{i}\Delta^{+-}(u,v) \equiv \big\langle \phi^\dagger(v)\phi(u)\big\rangle, \tag{3.26a}$$
$$\Delta^> \equiv \Delta^{-+}, \qquad \mathrm{i}\Delta^{-+}(u,v) \equiv \big\langle \phi(u)\phi^\dagger(v)\big\rangle, \tag{3.26b}$$
$$\Delta^\mathrm{T} \equiv \Delta^{++}, \qquad \mathrm{i}\Delta^{++}(u,v) \equiv \big\langle \mathcal{T}\big[\phi(u)\phi^\dagger(v)\big]\big\rangle, \tag{3.26c}$$
$$\Delta^{\overline{\mathrm{T}}} \equiv \Delta^{--}, \qquad \mathrm{i}\Delta^{--}(u,v) \equiv \big\langle \overline{\mathcal{T}}\big[\phi(u)\phi^\dagger(v)\big]\big\rangle, \tag{3.26d}$$

for the scalar [8, 129]. The symbols $\mathcal{T}$ and $\overline{\mathcal{T}}$ denote the usual time-ordering and reversed time-ordering metaoperators, and the minus sign in the definition of S^{+-} is due to the fermionic time-ordering. The functions $S^{<,>}$ and $\Delta^{<,>}$ are called the *Wightman functions*, and we use the convention where the fermionic function $S^<$ is defined without the sign: $\mathrm{i}S^<_{\alpha\beta}(u,v) = \big\langle \overline{\psi}_\beta(v)\psi_\alpha(u)\big\rangle$ (cf. [129]).

The different propagators in equations (3.25) and in (3.26) are not independent, as we briefly mentioned already below equations (3.7). Writing the time-orderings explicitly we get directly

$$S^\mathrm{T}(u,v) = \quad \theta(u^0 - v^0)S^>(u,v) - \theta(v^0 - u^0)S^<(u,v), \tag{3.27a}$$
$$S^{\overline{\mathrm{T}}}(u,v) = -\theta(v^0 - u^0)S^<(u,v) + \theta(v^0 - u^0)S^>(u,v), \tag{3.27b}$$

and similarly for the scalar propagators. Here it is evident that only two of the propagators, say $S^>$ and $S^<$, are independent. It is a general feature that two independent propagators (per field) are needed to describe non-equilibrium systems [111, 115]. However, the functions we have given so far are not optimal for arranging and solving the equations of motion and often various other combinations of the propagators are introduced. Next we give these for the fermion field; the bosonic case is similar and can be obtained by replacing first $S^< \to -S^<$ and then $S \to \Delta$.

Profusion of propagators

An often used pair of independent propagators are the statistical propagator S^{F} and the spectral function $S^{\mathcal{A}}$ [115], which we define as

$$S^{\mathrm{F}} \equiv \frac{1}{2}\big(S^{>} - S^{<}\big), \qquad S^{\mathcal{A}} \equiv \frac{\mathrm{i}}{2}\big(S^{>} + S^{<}\big). \tag{3.28}$$

Statistical observables of the system, such as occupation numbers or current densities, can be extracted from S^{F}. The spectral function $S^{\mathcal{A}}$ describes the spectrum of the system and it is constrained by the canonical equal-time (anti)commutation relations. It does not contain direct information on the state [8, 115].

The spectral function $S^{\mathcal{A}}$ can be used to further define the retarded and advanced pole propagators

$$\mathrm{i}S^{r}(u,v) \equiv \quad 2\theta(u^0 - v^0)S^{\mathcal{A}}(u,v), \tag{3.29a}$$
$$\mathrm{i}S^{a}(u,v) \equiv -2\theta(v^0 - u^0)S^{\mathcal{A}}(u,v). \tag{3.29b}$$

They are useful for deriving kinetic equations in the limit $t_{\mathrm{in}} \to -\infty$ of the CTP. In this context it is also convenient to define the "Hermitian part" S^{H} of the pole propagators which satisfies $S^{r,a} \equiv S^{\mathrm{H}} \mp \mathrm{i}S^{\mathcal{A}}$ where the minus (plus) sign corresponds to S^{r} (S^{a}). Using the relations (3.27) and the definitions of the different propagators we can then derive the following general identities:

$$S^{\mathrm{H}} = \frac{1}{2}\big(S^{r} + S^{a}\big) \ = \frac{1}{2}\big(S^{\mathrm{T}} - S^{\overline{\mathrm{T}}}\big), \tag{3.30a}$$
$$S^{\mathcal{A}} = \frac{\mathrm{i}}{2}\big(S^{r} - S^{a}\big) \ = \frac{\mathrm{i}}{2}\big(S^{>} + S^{<}\big), \tag{3.30b}$$
$$S^{\mathrm{F}} = \frac{1}{2}\big(S^{\mathrm{T}} + S^{\overline{\mathrm{T}}}\big) = \frac{1}{2}\big(S^{>} - S^{<}\big). \tag{3.30c}$$

These relations are useful for converting between different formulations of the equations and in practical calculations of the self-energies.[12]

We also make frequent use of the Hermiticity conditions of the various propagators, which follow directly from the definitions. For the fermion these are

$$\overline{S}^{<,>}(u,v)^{\dagger} = \overline{S}^{<,>}(v,u), \tag{3.31a}$$
$$\overline{S}^{\mathrm{H},\mathcal{A}}(u,v)^{\dagger} = \overline{S}^{\mathrm{H},\mathcal{A}}(v,u), \tag{3.31b}$$
$$\overline{S}^{r,a}(u,v)^{\dagger} = \overline{S}^{a,r}(v,u), \tag{3.31c}$$

where we also defined the barred propagators $\overline{S}^{<,>} \equiv \mathrm{i}S^{<,>}\gamma^0$, $\overline{S}^{r,a} \equiv S^{r,a}\gamma^0$ and $\overline{S}^{\mathrm{H},\mathcal{A}} \equiv S^{\mathrm{H},\mathcal{A}}\gamma^0$. Note that the pole propagators $S^{r,a}$ are swapped under Hermitian conjugation in equation (3.31c). The scalar propagators satisfy similar Hermiticity relations with the matrix γ^0 omitted.

[12] Also, the *spectral relation* $S^{\mathrm{H}}(u,v) = -\mathrm{i}\,\mathrm{sgn}(u^0 - v^0)S^{\mathcal{A}}(u,v)$ follows directly from (3.29).

3.3.2 General CTP equations of motion

The generalizations of the 2PI equation of motion (3.22) for the fermion and complex scalar boson are [126, 128, 129]

$$S_{ab}^{-1}(x,y) = S_{0,ab}^{-1}(x,y) - \Sigma_{ab}(x,y), \tag{3.32a}$$
$$\Delta_{ab}^{-1}(x,y) = \Delta_{0,ab}^{-1}(x,y) - \Pi_{ab}(x,y), \tag{3.32b}$$

with the self-energies

$$\Sigma_{ab}(x,y) \equiv -\mathrm{i}\frac{\delta\Gamma_2}{\delta S^{ba}(y,x)}, \tag{3.33a}$$
$$\Pi_{ab}(x,y) \equiv \mathrm{i}\frac{\delta\Gamma_2}{\delta \Delta^{ba}(y,x)}. \tag{3.33b}$$

The different numerical factors in the definitions (3.33) compared to the real scalar case (3.23) reflect the different scalings of the Gaussian path integrals in the fermionic and complex scalar cases. In the case of vanishing mean fields we can write the inverse free propagators explicitly as [113, 129]

$$S_{0,ab}^{-1}(x,y) \equiv \big(\mathrm{i}\partial\!\!\!/_x - m_\psi\big)\delta^{(4)}(x-y)\, c_{ab}, \tag{3.34a}$$
$$\Delta_{0,ab}^{-1}(x,y) \equiv \big(-\partial_x^2 - m_\phi^2\big)\delta^{(4)}(x-y)\, c_{ab}, \tag{3.34b}$$

where m_ψ and m_ϕ are the masses of the fermion and boson fields, respectively.[13]

From now on we only consider explicitly the fermionic case as we only need the fermionic equation (3.32a) further in this work. More details on the bosonic case can be found in [129], for example.

Self-energy functions

The four real-time CTP self-energies (3.33a) are similar to the propagators (3.25). One important difference however is that the self-energies may contain a singular part [129]. We can extract it by defining

$$\Sigma_{ab}(x,y) \equiv c_{ab}\,\delta^{(4)}(x-y)\Sigma^{\mathrm{sg}}(x) + \widetilde{\Sigma}_{ab}(x,y), \tag{3.35}$$

where $\widetilde{\Sigma}_{ab}$ are non-singular. Note that the singular part has the same structure as the mass term in (3.34a). Hence, it can be absorbed to the inverse free propagator in equation (3.32a) as a spacetime dependent mass shift [113, 129]. We do this by *formally* replacing the mass m with the effective mass

$$\widetilde{m}(x) \equiv m + \Sigma^{\mathrm{sg}}(x). \tag{3.36}$$

[13] We also assumed here the standard form of the classical action in the Minkowski spacetime.

Now we may further define the non-singular self-energy functions

$$\Sigma^< \equiv -\Sigma^{+-}, \quad \Sigma^> \equiv \Sigma^{-+}, \quad \Sigma^{\mathrm{T}} \equiv \widetilde{\Sigma}^{++}, \quad \Sigma^{\overline{\mathrm{T}}} \equiv \widetilde{\Sigma}^{--}, \tag{3.37}$$

analogously to (3.25). Note that in these definitions the CTP branch indices are raised instead of lowered which would be the "natural" position according to equation (3.33a).

Relations between the self-energy functions (3.37) depend on the approximation scheme used to calculate the 2PIEA. In reasonable approximations the following relations, which are analogous to (3.27), are expected to hold: [129]

$$\Sigma^{\mathrm{T}}(u,v) = \quad \theta(u^0-v^0)\Sigma^>(u,v) - \theta(v^0-u^0)\Sigma^<(u,v), \tag{3.38a}$$

$$\Sigma^{\overline{\mathrm{T}}}(u,v) = -\theta(v^0-u^0)\Sigma^<(u,v) + \theta(v^0-u^0)\Sigma^>(u,v). \tag{3.38b}$$

Assuming this is the case we can then define the rest of the functions $\Sigma^{\mathrm{F},\mathcal{A}}$, $\Sigma^{r,a}$ and Σ^{H} like in section 3.3.1 so that *all* of the relations (3.28)–(3.30) hold analogously also for the self-energies. The self-energy functions should also satisfy the same Hermiticity conditions (3.31) as the corresponding propagators. However, we define the barred self-energies slightly differently compared to the propagators, with the matrix γ^0 on the other side: $\overline{\Sigma}^{<,>} \equiv \mathrm{i}\gamma^0\Sigma^{<,>}$, $\overline{\Sigma}^{r,a} \equiv \gamma^0\Sigma^{r,a}$ and $\overline{\Sigma}^{\mathrm{H},\mathcal{A}} \equiv \gamma^0\Sigma^{\mathrm{H},\mathcal{A}}$. This is convenient when manipulating the equations later on.

Kadanoff–Baym equations

In practice the Schwinger–Dyson equations in the form (3.32) must be inverted to solve them. The equivalent integro-differential form can be obtained by contracting the equations from the right by the full propagators. Equation (3.32a) then becomes

$$\big(\mathrm{i}\partial\!\!\!/_x - m\big)S^{ab}(x,y) = c^{ab}\delta^{(4)}(x-y) + \sum_{c=\pm} c\int_{t_{\mathrm{in}}}^{t_{\mathrm{f}}} \mathrm{d}^4z\, \Sigma^{ac}(x,z)S^{cb}(z,y). \tag{3.39}$$

This is a coupled set of non-linear partial integro-differential equations for the four real-time CTP propagators (3.25). The form (3.39) of the equations is still not very convenient for practical purposes because the statistical and spectral sectors are mixed together. This is where the various propagators defined in section 3.3.1 (and the corresponding self-energies) come in handy. Next we give three different equivalent formulations of equations (3.39) which are all useful in their own contexts. We also introduce the notation for the generalized convolution integral

$$(F * G)_{t_1}^{t_2}(x,y) \equiv \int_{t_1}^{t_2} \mathrm{d}^4z\, F(x,z)G(z,y) \tag{3.40}$$

and the effective inverse free propagator

$$\widetilde{S}_0^{-1}(x,y) \equiv \big[\mathrm{i}\partial\!\!\!/_x - \widetilde{m}(x)\big]\delta^{(4)}(x-y) \tag{3.41}$$

to make for a more streamlined notation in the subsequent equations.

First formulation. This is the most economic formulation with respect to the number of functions involved. It is possible to write a set of equations equivalent to (3.39) using only the statistical propagator S^{F} and the spectral function $S^{\mathcal{A}}$:

$$\big(\widetilde{S}_0^{-1} * S^{\mathcal{A}}\big)^{t_{\mathrm{f}}}_{t_{\mathrm{in}}}(x,y) = -2\mathrm{i}\big(\Sigma^{\mathcal{A}} * S^{\mathcal{A}}\big)^{x^0}_{y^0}(x,y), \tag{3.42a}$$

$$\big(\widetilde{S}_0^{-1} * S^{\mathrm{F}}\big)^{t_{\mathrm{f}}}_{t_{\mathrm{in}}}(x,y) = -2\mathrm{i}\big(\Sigma^{\mathcal{A}} * S^{\mathrm{F}}\big)^{x^0}_{t_{\mathrm{in}}}(x,y) + 2\mathrm{i}\big(\Sigma^{\mathrm{F}} * S^{\mathcal{A}}\big)^{y^0}_{t_{\mathrm{in}}}(x,y), \tag{3.42b}$$

$$S^{\mathcal{A}}(x,y)\,\delta(x^0-y^0) = \frac{1}{2}\gamma^0\,\delta^{(4)}(x-y). \tag{3.42c}$$

Second formulation. Here the statistical and spectral propagators are replaced by the Wightman functions S^s (with $s = <, >$) and the pole propagators S^p (with $p = r, a$), respectively:

$$\big[\big(\widetilde{S}_0^{-1} - \Sigma^p\big) * S^p\big]^{t_{\mathrm{f}}}_{t_{\mathrm{in}}}(x,y) = \delta^{(4)}(x-y), \tag{3.43a}$$

$$\big[\big(\widetilde{S}_0^{-1} - \Sigma^r\big) * S^s\big]^{t_{\mathrm{f}}}_{t_{\mathrm{in}}}(x,y) = \big(\Sigma^s * S^a\big)^{t_{\mathrm{f}}}_{t_{\mathrm{in}}}(x,y). \tag{3.43b}$$

Third formulation. The last formulation is a direct variant of equations (3.43) where the pole propagators have been traded for S^{H} and $S^{\mathcal{A}}$:

$$\big[\big(\widetilde{S}_0^{-1} - \Sigma^{\mathrm{H}}\big)*S^{\mathrm{H}}\big]^{t_{\mathrm{f}}}_{t_{\mathrm{in}}}(x,y) + \big(\Sigma^{\mathcal{A}} * S^{\mathcal{A}}\big)^{t_{\mathrm{f}}}_{t_{\mathrm{in}}}(x,y) = \delta^{(4)}(x-y), \tag{3.44a}$$

$$\big[\big(\widetilde{S}_0^{-1} - \Sigma^{\mathrm{H}}\big)*S^{\mathcal{A}}\big]^{t_{\mathrm{f}}}_{t_{\mathrm{in}}}(x,y) - \big(\Sigma^{\mathcal{A}} * S^{\mathrm{H}}\big)^{t_{\mathrm{f}}}_{t_{\mathrm{in}}}(x,y) = 0, \tag{3.44b}$$

$$\big[\big(\widetilde{S}_0^{-1} - \Sigma^{\mathrm{H}}\big)*S^{s}\big]^{t_{\mathrm{f}}}_{t_{\mathrm{in}}}(x,y) - \big(\Sigma^{s} * S^{\mathrm{H}}\big)^{t_{\mathrm{f}}}_{t_{\mathrm{in}}}(x,y) = \pm\mathcal{C}_{\mathrm{coll}}(x,y), \tag{3.44c}$$

where the $\pm$ corresponds to $s = \lessgtr$, and

$$\mathcal{C}_{\mathrm{coll}}(x,y) \equiv \frac{1}{2}\big(\Sigma^{>} * S^{<} - \Sigma^{<} * S^{>}\big)^{t_{\mathrm{f}}}_{t_{\mathrm{in}}}(x,y). \tag{3.45}$$

Equations (3.44c) are known as the Kadanoff–Baym (KB) equations where (3.45) is the collision term [129, 132].

All three sets of equations (3.42)–(3.44) are separately equivalent to (3.39) and hence also to each other. As we can see the original four equations (3.39) contained redundant information: the amount of equations was reduced to three in equations (3.42). Furthermore, equation (3.42c) is just the position-space representation of the *spectral sum rule* [101] which can also be derived directly from the canonical anticommutation relations.[14] In practice the sum rule fixes the equal-time values of the spectral function, including the value at the initial two-time point $(t_{\mathrm{in}}, t_{\mathrm{in}})$. This shows that the initial conditions of the system are not directly reflected in the spectral function.

The form (3.42) of the equations is useful because the structure of the convolution integrals shows that the equations are *causal*: only the past values of the propagators

[14] Nevertheless, the result (3.42) shows the consistency of the formalism: the canonical (anti)commutation relations are built-in even though they were not explicitly used in the derivation.

determine their future values [115]. Hence, the convolution integrals are also often called "memory integrals" as they integrate over the history of the time evolution. Being manifestly causal, equations (3.42) are also convenient for direct numerical calculations [115]. However, in realistic applications a full numerical implementation and solution can be very demanding because the complexity of the equations increases considerably with more degrees of freedom.

A commonly used approach to simplify the equations is to Fourier transform them into a mixed position-momentum representation. It is then possible to perform a gradient expansion to get more tractable equations [113, 129]. In equations (3.42) the time integration limits are finite and depend on the external arguments x^0, y^0 however, and this complicates the use of Fourier transforms. Equations (3.43) and (3.44) avoid this problem as all of the integration limits are extended to t_{in} and t_{f} (which can then be eventually taken to $-\infty$ and $+\infty$). In these two formulations there are again four equations but in practice not all of them are needed due to the relations (3.30).

Equations (3.44c) [or (3.43b)] are called the Kadanoff–Baym equations and equations (3.44a) and (3.44b) [or (3.43a)] are the pole equations. The KB equations are the main statistical evolution equations while the pole equations describe the dynamics of the spectral and dispersive properties of the system. The variant (3.43) of the equations is more compact to write down but equations (3.44) are physically more transparent because all of the interaction terms have clear interpretations. This makes the latter variant more convenient for spectral quasiparticle approximations, for example. The terms in (3.44) which explicitly contain Σ^{H} and $\Sigma^{\mathcal{A}}$ describe the dispersive corrections and the width of the propagators, respectively. Also the $\Sigma^s * S^{\mathrm{H}}$-term is related to the width [15, 133]. The collision term $\mathcal{C}_{\mathrm{coll}}$ on the right-hand side of the KB equation consists of generalized gain and loss terms which describe the equilibration process [129].

The KB equations can be used as a basis for deriving simpler kinetic equations which describe the evolution of particle distribution functions. For example, the equations can be reduced to semiclassical Boltzmann equations [77, 78, 132, 134]. In the context of kinetic transport theory the limit $t_{\mathrm{in}} \to -\infty$ is taken for the CTP contour which enables the use of the mixed representation and the gradient expansion.[15] This limit also discards the effects of the initial conditions set at t_{in}. The propagators are then prescribed at some finite time t_0 instead. This is a suitable approximation for systems with efficient equilibration processes (such as the electroweak plasma) [129] or when solving the equations for late times [77, 113].

Wigner representation

We now define the mixed momentum-position representation, called the Wigner representation. It is useful when considering kinetic equations but it is valid also

[15] The upper limit t_{f} of the CTP can always be taken to be arbitrarily large, see equation (3.4).

more generally. The equations can be transformed to this representation by using the *Wigner transform* (with $t_{\text{in}} \to -\infty$) [115, 129]

$$F(k,x) \equiv \int_{-\infty}^{\infty} \mathrm{d}^4 r \, \mathrm{e}^{\mathrm{i}k\cdot r} \, F\big(x + \tfrac{r}{2}, x - \tfrac{r}{2}\big), \tag{3.46}$$

where $F(u,v)$ is any two-point (or self-energy) function in the position representation.[16] The inverse transform is given by

$$F(u,v) \equiv \int \frac{\mathrm{d}^4 k}{(2\pi)^4} \, \mathrm{e}^{-\mathrm{i}k\cdot(u-v)} \, F\Big(k, \frac{u+v}{2}\Big). \tag{3.47}$$

Equation (3.46) is essentially a Fourier transform in the relative coordinate $r \equiv u - v$. In this transform the dependence on the pair of spacetime points (u,v) is exchanged to the four-momentum k and the average coordinate $x \equiv (u+v)/2$. In order to transform the equations of motion we also need the Wigner transform of the generalized convolution (3.40) (where $t_{1,2} \to \mp\infty$). The result is [8, 113]

$$(F * G)^{+\infty}_{-\infty}(k,x) = \mathrm{e}^{-\mathrm{i}\lozenge}\big\{F(k,x)\big\}\big\{G(k,x)\big\}, \tag{3.48}$$

where the right-hand side is called the Moyal product [135, 136] and we defined the derivative operator $\lozenge \equiv \frac{1}{2}(\partial_x^{(1)} \cdot \partial_k^{(2)} - \partial_k^{(1)} \cdot \partial_x^{(2)})$ [129]. Note that the only meaning of the curly brackets in (3.48) is to denote the first and second "slot" on which the derivatives $\partial^{(1)}$ and $\partial^{(2)}$ operate.

The pole and KB equations (3.43) can now be written straightforwardly in the Wigner representation by using equations (3.46)–(3.48):

$$\big(\not{k} + \tfrac{\mathrm{i}}{2}\not{\partial}_x\big) S^p - \mathrm{e}^{-\mathrm{i}\lozenge}\{\widetilde{\Sigma}^p\}\{S^p\} = \mathbf{1}, \tag{3.49a}$$

$$\big(\not{k} + \tfrac{\mathrm{i}}{2}\not{\partial}_x\big) S^s - \mathrm{e}^{-\mathrm{i}\lozenge}\{\widetilde{\Sigma}^r\}\{S^s\} = \mathrm{e}^{-\mathrm{i}\lozenge}\{\Sigma^s\}\{S^a\}. \tag{3.49b}$$

Here we denoted $\widetilde{\Sigma}^p(k,x) \equiv \widetilde{m}(x) + \Sigma^p(k,x)$ for both $p = r, a$ as it is now more convenient to group the mass term with the self-energy [$\widetilde{m}$ was defined in (3.36)]. We also suppressed the arguments (k,x) of all propagators and self-energies here for brevity. In the Wigner representation the sum rule (3.42c) also takes the more usual form

$$\int_{-\infty}^{\infty} \frac{\mathrm{d}k^0}{\pi} \, \overline{S}^{\mathcal{A}}(k,x) = \mathbf{1}. \tag{3.50}$$

Equations (3.49) are still exact and non-linear and they are equivalent to the original equations (under the simplification $t_{\text{in}} \to -\infty$). Instead of the non-local convolution integrals these equations contain infinite series of exponential gradient terms. The advantage of this form is that outside of periods of rapid oscillations it can often be assumed that the functions change slowly in the average coordinate x [113, 129]. Higher order terms in the gradient expansion can then be discarded and this reduces the complexity of the equations.

[16] We use the same notation for functions in both the position and the Wigner representation as these can be inferred from context.

Translational invariance. An important special case is when the propagators and self-energy functions are fully *translationally invariant* in their spacetime arguments and the mass m is constant (here we denote $\widetilde{m}$ by simply m). This implies that the Wigner representation functions have no dependence on the average coordinate x. The full equations (3.49) are in this case reduced to the algebraic matrix equations

$$\big(\not{k} - m - \Sigma^p_{\text{ti}}(k)\big) S^p_{\text{ti}}(k) = \mathbf{1}, \tag{3.51a}$$
$$\big(\not{k} - m - \Sigma^r_{\text{ti}}(k)\big) S^s_{\text{ti}}(k) = \Sigma^s_{\text{ti}}(k) S^a_{\text{ti}}(k), \tag{3.51b}$$

which have the (formal) solutions

$$S^p_{\text{ti}}(k) = \big(\not{k} - m - \Sigma^p_{\text{ti}}(k)\big)^{-1}, \tag{3.52a}$$
$$S^s_{\text{ti}}(k) = S^r_{\text{ti}}(k) \Sigma^s_{\text{ti}}(k) S^a_{\text{ti}}(k). \tag{3.52b}$$

Thermal equilibrium. If the system is also in *thermal equilibrium* the Wightman functions (3.52b) satisfy the Kubo–Martin–Schwinger (KMS) condition $S^>_{\text{eq}}(k) = \mathrm{e}^{\beta k^0} S^<_{\text{eq}}(k)$ [101], where $\beta \equiv 1/T$. The KMS condition follows from the (anti)periodicity of the field configurations in the standard way when the density operator ρ has the equilibrium form [101]. It may be described by adding the imaginary branch to the CTP [8, 113]. The thermal equilibrium solutions satisfy (3.52) and using the KMS condition the Wightman functions can be further simplified to

$$\mathrm{i} S^<_{\text{eq}}(k) = 2 S^{\mathcal{A}}_{\text{eq}}(k) f_{\text{FD}}(k^0), \tag{3.53a}$$
$$\mathrm{i} S^>_{\text{eq}}(k) = 2 S^{\mathcal{A}}_{\text{eq}}(k) \big(1 - f_{\text{FD}}(k^0)\big). \tag{3.53b}$$

Here $f_{\text{FD}}(k^0) \equiv 1/(\mathrm{e}^{\beta k^0} + 1)$ is the Fermi–Dirac distribution.[17] Equations (3.53) are equivalent to the fluctuation–dissipation relation $\mathrm{i} S^{\text{F}}_{\text{eq}}(k) = 2 S^{\mathcal{A}}_{\text{eq}}(k) \big(\frac{1}{2} - f_{\text{FD}}(k^0)\big)$ which is satisfied only in equilibrium [115]. The Kadanoff–Baym ansatz, which is often used to derive kinetic equations, is a generalization of (3.53) where the equilibrium distribution function f_{FD} is replaced by a more general non-equilibrium function [77, 115].

3.3.3 Spatially homogeneous and isotropic case

We now specialize to time-dependent systems which are spatially homogeneous and isotropic. This means that the propagators and self-energies have translational invariance in the spatial arguments and the singular contributions such as the mass m can only depend on the time variable. This special case is relevant for cosmology (e.g. leptogenesis) and other time-dependent phenomena which happen uniformly throughout space.

[17] Bosons have analogous solutions with the Bose–Einstein distribution $f_{\text{BE}}(k^0) \equiv 1/(\mathrm{e}^{\beta k^0} - 1)$ [II].

In this case it is useful to introduce another transformation of the two-point functions and self-energies: the *two-time representation*

$$F_{\boldsymbol{k}}(t_1, t_2) \equiv \int \mathrm{d}^3\boldsymbol{r}\, \mathrm{e}^{-\mathrm{i}\boldsymbol{k}\cdot\boldsymbol{r}}\, F\big((t_1, \boldsymbol{r}), (t_2, \boldsymbol{0})\big). \tag{3.54}$$

This is the spatial Fourier transform with the three-momentum $\boldsymbol{k}$. Its inverse is

$$F(u, v) \equiv \int \frac{\mathrm{d}^3\boldsymbol{k}}{(2\pi)^3}\, \mathrm{e}^{\mathrm{i}\boldsymbol{k}\cdot(\boldsymbol{u}-\boldsymbol{v})}\, F_{\boldsymbol{k}}\big(u^0, v^0\big). \tag{3.55}$$

In the representation (3.54) the pole and KB equations (3.43) become

$$\big[(\widetilde{S}^{-1}_{0,\boldsymbol{k}} - \Sigma^p_{\boldsymbol{k}}) * S^p_{\boldsymbol{k}}\big]^{t_\mathrm{f}}_{t_\mathrm{in}}(t_1, t_2) = \delta(t_1 - t_2), \tag{3.56a}$$

$$\big[(\widetilde{S}^{-1}_{0,\boldsymbol{k}} - \Sigma^r_{\boldsymbol{k}}) * S^s_{\boldsymbol{k}}\big]^{t_\mathrm{f}}_{t_\mathrm{in}}(t_1, t_2) = \big(\Sigma^s_{\boldsymbol{k}} * S^a_{\boldsymbol{k}}\big)^{t_\mathrm{f}}_{t_\mathrm{in}}(t_1, t_2), \tag{3.56b}$$

where

$$\widetilde{S}^{-1}_{0,\boldsymbol{k}}(t_1, t_2) = \big[\mathrm{i}\gamma^0\partial_{t_1} - \boldsymbol{\gamma}\cdot\boldsymbol{k} - \widetilde{m}(t_1)\big]\delta(t_1 - t_2), \tag{3.57}$$

and the convolutions are defined with only time integrals. The sum rule (3.42c) can be written in this case as

$$2\overline{S}^{\mathcal{A}}_{\boldsymbol{k}}(t, t) = \boldsymbol{1} \quad \text{for any } t. \tag{3.58}$$

Equations (3.56) are still very complicated, despite the reduction in the dimensions of the domain when compared to the more general equations (3.43).

The Wigner representation (3.46) can also be employed in the spatially homogeneous and isotropic case. The Wigner-transformed functions then have no dependence on the spatial average coordinate $\boldsymbol{x}$ and the corresponding spatial derivatives are dropped from equations (3.49). One can move between the Wigner and two-time representation (when $t_\mathrm{in} \to -\infty$) by doing the Wigner transform (3.46) and its inverse (3.47) with only the time and energy variables (see [II] for the explicit transformations). However, the two-time representation has the advantage of being more general as the initial time t_in can be kept finite.

Free time evolution

We first consider the free theory and introduce the associated free time evolution operator before analyzing the solutions in the full theory. This serves as an example of the solutions and, more importantly, it elucidates the special role of the spectral function and an important local property of the free solutions.

The free theory equations corresponding to (3.56) are

$$\big(S^{-1}_{0,\boldsymbol{k}} * S^p_{0,\boldsymbol{k}}\big)^{t_\mathrm{f}}_{t_\mathrm{in}}(t_1, t_2) = \delta(t_1 - t_2), \tag{3.59a}$$

$$\big(S^{-1}_{0,\boldsymbol{k}} * S^s_{0,\boldsymbol{k}}\big)^{t_\mathrm{f}}_{t_\mathrm{in}}(t_1, t_2) = 0, \tag{3.59b}$$

with the free pole propagators S_0^p and Wightman functions S_0^s. The equations are decoupled so it suffices to consider only the free KB equation (3.59b) which can be rewritten as

$$\partial_{t_1} \overline{S}^s_{0,\boldsymbol{k}}(t_1, t_2) = -\mathrm{i} H_{\boldsymbol{k}}(t_1) \overline{S}^s_{0,\boldsymbol{k}}(t_1, t_2). \tag{3.60}$$

Here $H_{\boldsymbol{k}}(t)$ is the Hermitian free Dirac Hamiltonian and we used the barred propagator notation defined below equations (3.31). The solutions to the free pole equations (3.59a) can be obtained from the spectral function $S^{\mathcal{A}}_{0,\boldsymbol{k}}$ after solving the Wightman functions from the free KB equation.

Equation (3.60) has a form similar to the general Schrödinger equation and thus its solutions can be found similarly by using a time-evolution operator [2]. We define the time-evolution operator $U_{0,\boldsymbol{k}}(t_1, t_2)$ of equation (3.60) as the unique solution with the initial condition $U_{0,\boldsymbol{k}}(t_{\mathrm{in}}, t_{\mathrm{in}}) = \mathbf{1}$. It is given explicitly by the time-ordered exponential (also called the Dyson series) [112, 137]

$$U_{0,\boldsymbol{k}}(t_1, t_2) \equiv \mathcal{T} \exp\left(-\mathrm{i} \int_{t_2}^{t_1} \mathrm{d}t' \, H_{\boldsymbol{k}}(t') \right). \tag{3.61}$$

It has the properties that $U_{0,\boldsymbol{k}}(t, t) = \mathbf{1}$, $U_{0,\boldsymbol{k}}(t_1, t_2)^\dagger = U_{0,\boldsymbol{k}}(t_2, t_1)$ and

$$\overline{S}_{\boldsymbol{k}}(t_1, t_2) = U_{0,\boldsymbol{k}}(t_1, t) \overline{S}_{\boldsymbol{k}}(t, t) U_{0,\boldsymbol{k}}(t, t_2), \tag{3.62}$$

for any $t, t_1, t_2 \geq t_{\mathrm{in}}$ and where $\overline{S}_{\boldsymbol{k}}$ stands for any solution of equation (3.60). These properties mean that $U_{0,\boldsymbol{k}}$ describes unitary time-evolution. Equation (3.62) implies that the complete solution $\overline{S}_{\boldsymbol{k}}$ can be calculated from its local value at *any* time t. In particular, the solution to equation (3.60) can be obtained from the initial value $\overline{S}_{\boldsymbol{k}}(t_{\mathrm{in}}, t_{\mathrm{in}})$ by setting $t = t_{\mathrm{in}}$ in equation (3.62). Furthermore, because the free spectral function $\overline{S}^{\mathcal{A}}_{0,\boldsymbol{k}}$ is also a solution to (3.60) and because it satisfies the sum rule (3.58) it actually coincides with the free time-evolution operator:

$$2\overline{S}^{\mathcal{A}}_{0,\boldsymbol{k}}(t_1, t_2) \equiv U_{0,\boldsymbol{k}}(t_1, t_2). \tag{3.63}$$

This result then yields the solutions to the free pole equations (3.59a) via the general definitions (3.29) and (3.54).

Formal full solutions

We now consider some exact properties of the full solutions to equations (3.56). To this end, we first rewrite the equations in the equivalent integral equation form:

$$S^p_{\boldsymbol{k}} = S^p_{0,\boldsymbol{k}} + S^p_{0,\boldsymbol{k}} * \Sigma^p_{\boldsymbol{k}} * S^p_{\boldsymbol{k}}, \tag{3.64a}$$

$$S^s_{\boldsymbol{k}} = S^s_{0,\boldsymbol{k}} + S^s_{0,\boldsymbol{k}} * \Sigma^a_{\boldsymbol{k}} * S^a_{\boldsymbol{k}} + S^r_{0,\boldsymbol{k}} * \Sigma^s_{\boldsymbol{k}} * S^a_{\boldsymbol{k}} + S^r_{0,\boldsymbol{k}} * \Sigma^r_{\boldsymbol{k}} * S^s_{\boldsymbol{k}}. \tag{3.64b}$$

Here we suppressed the external time arguments (t_1, t_2) of all terms and the time integration limits $t_{\mathrm{in}}, t_{\mathrm{f}}$ of the convolutions. Equations (3.64) can be derived straightforwardly by writing the Schwinger–Dyson equations (3.39) in the integral equation

form by contracting with the free propagator from the left. Equations (3.64) then result from using the definitions (3.25) and relations (3.30) for the different propagators (and the corresponding results for the self-energies).

We can obtain exact formal solutions to the integral equations (3.64) by suitably resumming them [II, 138]. The result is

$$S^p_{\boldsymbol{k}} = \left(S^{-1}_{0,\boldsymbol{k}} - \Sigma^p_{\boldsymbol{k}}\right)^{-1}, \tag{3.65a}$$

$$S^s_{\boldsymbol{k}} = S^s_{\mathrm{hom},\boldsymbol{k}} + S^s_{\mathrm{inh},\boldsymbol{k}}, \tag{3.65b}$$

with the *homogeneous* and *inhomogeneous* Wightman functions

$$S^s_{\mathrm{hom},\boldsymbol{k}} \equiv \left(S^r_{\boldsymbol{k}} * S^{-1}_{0,\boldsymbol{k}}\right) * S^s_{0,\boldsymbol{k}} * \left(S^{-1}_{0,\boldsymbol{k}} * S^a_{\boldsymbol{k}}\right), \tag{3.66a}$$

$$S^s_{\mathrm{inh},\boldsymbol{k}} \equiv S^r_{\boldsymbol{k}} * \Sigma^s_{\boldsymbol{k}} * S^a_{\boldsymbol{k}}. \tag{3.66b}$$

The homogeneous solution (3.66a) can be further simplified to

$$\overline{S}^s_{\mathrm{hom},\boldsymbol{k}}(t_1, t_2) = 2\overline{S}^{\mathcal{A}}_{\boldsymbol{k}}(t_1, t_{\mathrm{in}})\overline{S}^s_{\mathrm{hom},\boldsymbol{k}}(t_{\mathrm{in}}, t_{\mathrm{in}})2\overline{S}^{\mathcal{A}}_{\boldsymbol{k}}(t_{\mathrm{in}}, t_2), \tag{3.67}$$

when $t_1, t_2 \geq t_{\mathrm{in}}$ [II]. It is a solution to the KB equation (3.56b) with a vanishing right-hand side. The inhomogeneous solution (3.66b) is a particular solution to the full KB equation. It is notable that the homogeneous solution (3.67) has the same structure as the free solution given by equations (3.62) and (3.63). Even though in the full interacting case there is no such unitary time-evolution operator, the homogeneous solution is still "evolved" from the initial value by the full spectral function. However, a big difference to the free case is that in interacting dissipative systems the spectral function is exponentially damped in the absolute difference of its time arguments [II]. This means that the solution (3.67) is transient in nature and vanishes quickly when $t_1, t_2 \gg t_{\mathrm{in}}$.

Despite the formal solutions (3.65) appearing simpler than equations (3.64) they are generally still implicit non-linear integral equations because the self-energies generally depend on the Wightman functions S^s and the pole propagators S^p. However, the exact equations (3.65) are useful as a starting point for deriving approximative solutions. This is so especially if the self-energies Σ^s and Σ^p are some externally given functions or if they can be approximated so that they do not depend on the full solutions S^s and S^p. This is the case for example when the self-energy is dominated by a thermal equilibrium part. We will use this approach and put these results to use when we present the *local approximation method* in the next chapter.

4 COHERENT QUANTUM KINETIC EQUATIONS

The KB equations (3.43) describe the full non-equilibrium dynamics of fermions with all quantum effects, including quantum coherence. The price to pay for this generality is that the equations are very difficult to solve in realistic situations as they are coupled non-linear integro-differential equations for the two-point correlation functions S^α (with $\alpha = s, p$). The convolution integrals make the equations inherently non-local, as the evolution of the functions depends not only on their values at a local neighborhood of a given point but also on the values of the functions arbitrarily far away. In the equivalent formulation (3.42) of the equations this non-local time-evolution manifests explicitly as the causal memory integrals. In the Wigner representation (3.49), on the other hand, the non-locality is encoded in the exponential gradient operators, making the equations no easier to solve without approximations.

In this chapter we introduce two approximation methods to simplify the fermionic KB equations (3.56): the cQPA and the more general LA-method. The goal of these methods is to obtain quantum kinetic equations (QKEs) which are straightforward to solve while still containing all relevant quantum coherence effects. Both methods ultimately revolve around making the equations local. There is also the problem of several types of time-evolution mixed together in the propagator (e.g., there are several types of coherence). Next we describe the parametrization used to separate these different components of the propagator before getting into the approximation methods themselves.

4.1 Projection matrix parametrization

An essential part of the local quantum kinetic methods presented in this chapter is the projection matrix parametrization [I, II, 20, 21]. The fermion two-point function generally has both a Dirac and a flavor matrix structure. The components of the propagator have complicated time dependencies because the propagator describes different physical quantities and properties such as the abundance of the particle

species or the flavor and particle–antiparticle oscillations. The main purpose of the projection matrix parametrization is to efficiently separate the time-scales associated with the evolution of these different features.

The projection matrix parametrization can be motivated by the generic form of the *free* dynamical equation

$$\mathrm{i}\partial_t \mathcal{S}_{\boldsymbol{k}}(t) = \big[H_{\boldsymbol{k}}(t), \mathcal{S}_{\boldsymbol{k}}(t)\big]. \tag{4.1}$$

Here $H_{\boldsymbol{k}}$ is the free Dirac Hamiltonian and $\mathcal{S}_{\boldsymbol{k}}$ represents the local value of a generic fermion two-point function. As we will see later, the relevant equations of motion will take the form (4.1) in both the two-time representation (the equal-time or local equation) and the Wigner representation (the k^0-integrated equation). We assume that equation (4.1) is given in the mass eigenbasis, that is, $H_{\boldsymbol{k}}(t) = \boldsymbol{\alpha}\cdot\boldsymbol{k} + \gamma^0 m(t)$ with $\boldsymbol{\alpha} \equiv \gamma^0\boldsymbol{\gamma}$ and a diagonal and positive-semidefinite mass matrix $m(t)$.

The projection matrix parametrization for the flavored two-point function in a spatially homogeneous and isotropic system is then defined by [II]

$$\mathcal{S}_{\boldsymbol{k}ij}(t) = \sum_{h,s,s'=\pm} \mathcal{P}^{ss'}_{\boldsymbol{k}hij}(t)\, \mathcal{F}^{ss'}_{\boldsymbol{k}hij}(t), \tag{4.2a}$$

with

$$\mathcal{P}^{ss'}_{\boldsymbol{k}hij} \equiv N^{ss'}_{\boldsymbol{k}hij} \overbrace{P_{\boldsymbol{k}h} P^{s}_{\boldsymbol{k}i} \gamma^0 P^{s'}_{\boldsymbol{k}j}}^{\equiv P^{ss'}_{\boldsymbol{k}hij}}. \tag{4.2b}$$

Here $P_{\boldsymbol{k}h}$ and $P^s_{\boldsymbol{k}i}$ are the helicity and energy projection matrices, respectively. The basis matrices $P^{ss'}_{\boldsymbol{k}hij} \equiv P_{\boldsymbol{k}h} P^s_{\boldsymbol{k}i} \gamma^0 P^{s'}_{\boldsymbol{k}j}$ span the subalgebra of Dirac matrices consistent with homogeneity and isotropy and hence there is no loss of generality by using this parametrization [II, 20]. The quantities $\mathcal{F}^{ss'}_{\boldsymbol{k}hij}$ are generic complex-valued components of the local two-point function which can be viewed as generalized phase space distribution functions, and $N^{ss'}_{\boldsymbol{k}hij}$ are arbitrary normalization factors. The aforementioned projection matrices are given by

$$P_{\boldsymbol{k}h} = \frac{1}{2}\Big(\mathbf{1} + h\widehat{h}_{\boldsymbol{k}}\Big), \qquad P^s_{\boldsymbol{k}i} = \frac{1}{2}\left(\mathbf{1} + s\frac{H_{\boldsymbol{k}i}}{\omega_{\boldsymbol{k}i}}\right), \tag{4.3a}$$

where

$$\widehat{h}_{\boldsymbol{k}} \equiv \boldsymbol{\alpha}\cdot\hat{\boldsymbol{k}}\,\gamma^5, \qquad H_{\boldsymbol{k}i} \equiv \boldsymbol{\alpha}\cdot\boldsymbol{k} + \gamma^0 m_i, \tag{4.3b}$$

are the helicity operator and the diagonal element of the Hamiltonian, respectively. The helicity and energy indices take the values $h, s = \pm 1$, and $\omega_{\boldsymbol{k}i} \equiv \sqrt{|\boldsymbol{k}|^2 + {m_i}^2}$ is the free on-shell energy for the flavor state i. More details about the projection matrices and the parametrization can be found in [II]. However, unlike in [II], in this chapter we keep the normalization factors $N^{ss'}_{\boldsymbol{k}hij}$ unfixed in all equations.

The main idea of the parametrization (4.2) is that it separates different oscillation frequencies described by equation (4.1). Technically this happens because of the property

$$P^s_{\boldsymbol{k}i} H_{\boldsymbol{k}i} = H_{\boldsymbol{k}i} P^s_{\boldsymbol{k}i} = s\omega_{\boldsymbol{k}i} P^s_{\boldsymbol{k}i}, \tag{4.4}$$

that is, the Hamiltonian gets projected to the frequencies $\omega_{\boldsymbol{k}i}$ when it acts on the energy projection matrices. The parametrization thus separates the fast and slowly varying parts of the two-point function: each component $\mathcal{F}^{ss'}_{\boldsymbol{k}hij}$ has a distinct well-defined oscillation frequency. Finally, we define some notation for different combinations of the frequencies which are needed later:

$$\bar{\omega}_{\boldsymbol{k}ij} \equiv (\omega_{\boldsymbol{k}i} + \omega_{\boldsymbol{k}j})/2, \tag{4.5a}$$

$$\delta\omega_{\boldsymbol{k}ij} \equiv (\omega_{\boldsymbol{k}i} - \omega_{\boldsymbol{k}j})/2, \tag{4.5b}$$

$$\Delta\bar{\omega}^{ss'}_{\boldsymbol{k}ij} \equiv s\omega_{\boldsymbol{k}i} - s'\omega_{\boldsymbol{k}j}. \tag{4.5c}$$

4.2 Coherent quasiparticle approximation

The idea of cQPA, originally developed in [14–22], is to provide tractable QKEs where quantum coherence is included dynamically with interactions and decoherence. In practice, cQPA is a two-step method to solve the Wigner representation KB equations (3.49) in a spectral approximation. First the phase space structure is determined from the free equations with all gradients neglected. The resulting *spectral* (quasiparticle) shell structure contains the usual mass shells for all propagators and additional coherence shells for the Wightman functions. The second step is to use this spectral form, including coherence, as an ansatz for solving the full equations.

We consider here cQPA in the spatially homogeneous and isotropic case for fermions with a time dependent mass matrix. We present the improved way to derive both the cQPA ansatz and the resummed equations of motion given in [I], and review the main features of cQPA. We also generalize the treatment in [I] slightly by including multiple fermion flavors.

4.2.1 Spectral phase space structure

In the first step we derive the constraints for the phase space structure of the cQPA propagators. We start by dropping the collision terms and all gradients. The Hermitian part of equation (3.49b), which is also called the constraint equation, then becomes

$$2k^0 \overline{S}^<(k,t) = \big\{H_{\boldsymbol{k}}(t), \overline{S}^<(k,t)\big\}. \tag{4.6}$$

We assume a flavor-diagonal free Hamiltonian as described below equation (4.1), resulting in free theory dispersion relations. Generally in cQPA it is also possible to consider quasiparticle dispersion relations which originate from the interaction

terms with the dispersive self-energy Σ^{H}, but this is not necessary for the scope of this work.

Next we use the projection matrix basis (4.2b) to parametrize the Wightman function in terms of component functions $D^{ss'}_{hij}(k,t)$ [I]:

$$\overline{S}^{<}_{ij}(k,t) \equiv \sum_{h,s,s'} \mathcal{P}^{ss'}_{\boldsymbol{k}hij}\, D^{ss'}_{hij}(k,t). \tag{4.7}$$

After using the parametrization (4.7) in equation (4.6) and taking relevant projections and traces of the resulting equation we get the constraints [with notation (4.5)]

$$(k^0 - s\overline{\omega}_{\boldsymbol{k}ij}) D^{ss}_{hij}(k,t) = 0, \tag{4.8a}$$
$$(k^0 - s\delta\omega_{\boldsymbol{k}ij}) D^{s,-s}_{hij}(k,t) = 0. \tag{4.8b}$$

These equations admit the distributional solutions

$$D^{ss}_{hij}(k,t) = f^{m,s}_{\boldsymbol{k}hij}\, 2\pi\delta(k^0 - s\overline{\omega}_{\boldsymbol{k}ij}), \tag{4.9a}$$
$$D^{s,-s}_{hij}(k,t) = f^{c,s}_{\boldsymbol{k}hij}\, 2\pi\delta(k^0 - s\delta\omega_{\boldsymbol{k}ij}), \tag{4.9b}$$

where the unknown quantities

$$f^{m,\pm}_{\boldsymbol{k}hij} \equiv f^{\pm\pm}_{\boldsymbol{k}hij}, \qquad f^{c,\pm}_{\boldsymbol{k}hij} \equiv f^{\pm\mp}_{\boldsymbol{k}hij} \tag{4.10}$$

are called the mass shell functions and the coherence shell functions, respectively [20, 21]. Substituting the solutions (4.9) back to (4.7) we obtain the flavored spectral cQPA ansatz of [21] for the Wightman function:

$$\overline{S}^{<}_{ij}(k,t) = 2\pi \sum_{h,s} \Big(\mathcal{P}^{ss}_{\boldsymbol{k}hij} f^{m,s}_{\boldsymbol{k}hij}\, \delta(k^0 - s\overline{\omega}_{\boldsymbol{k}ij}) + \mathcal{P}^{s,-s}_{\boldsymbol{k}hij} f^{c,s}_{\boldsymbol{k}hij}\, \delta(k^0 - s\delta\omega_{\boldsymbol{k}ij}) \Big). \tag{4.11}$$

The ansatz (4.11) contains four different kinds of spectral shells and their corresponding phase space distribution functions f. These describe the usual mass shell excitations and different kinds of quantum coherence information as shown in table 1. Note that with this naming convention the mass shell functions $f^{m,\pm}_{\boldsymbol{k}hij}$ contain not only the flavor-diagonal particle and antiparticle excitations but also the off-diagonal flavor coherence which resides on the *average* energy shells $k^0 = \pm\overline{\omega}_{\boldsymbol{k}ij}$ (with $i \neq j$) in the phase space.

The same construction can naturally be done also for the other Wightman function $S^{>}(k,t)$ and the spectral function $S^{\mathcal{A}}(k,t)$, as they obey the same constraint equation (4.6). However, the spectral function is subject to an additional constraint, the sum rule (3.50). It fixes the spectral function in cQPA to a completely non-dynamical quantity with vanishing coherence shell functions [21]. In fact, when using free dispersion relations in cQPA the full spectral function has the same form as in free theory [21, 101].

f	i,j	Particle type	Information	Dispersion	Osc. freq.
$f^{m,\pm}_{\boldsymbol{k}hij}$	$i=j$	particle/antipart.	mass shell excit.	$k^0=\pm\omega_{\boldsymbol{k}i}$	$\nu=0$
$f^{m,\pm}_{\boldsymbol{k}hij}$	$i\neq j$	particle/antipart.	flavor coherence	$k^0=\pm\bar{\omega}_{\boldsymbol{k}ij}$	$\nu=\lvert 2\delta\omega_{\boldsymbol{k}ij}\rvert$
$f^{c,\pm}_{\boldsymbol{k}hij}$	$i=j$	particle–antipart.	coherence	$k^0=0$	$\nu=2\omega_{\boldsymbol{k}i}$
$f^{c,\pm}_{\boldsymbol{k}hij}$	$i\neq j$	particle–antipart.	flavor coherence	$k^0=\pm\delta\omega_{\boldsymbol{k}ij}$	$\nu=2\bar{\omega}_{\boldsymbol{k}ij}$

Table 1. Phase space distribution functions $f^{x,\pm}_{\boldsymbol{k}hij}$ $(x=m,c)$ of the projection matrix parametrization (4.2) and the type of information they describe (mass shell excitations or quantum coherence [21]). Given are also the dispersion relations of the corresponding (spectral) shells and the leading oscillation frequencies of the functions.

4.2.2 Dynamical equations

In the second step we derive the dynamical equations for the phase space distribution functions f^m and f^c. This is done by using the cQPA ansatz (4.11) in the antihermitian part of equation (3.49b), including all gradients and collision terms, and integrating over k^0. However, in practice there is a complication which we need to handle first. To see this, let us consider the free theory where the dynamical equation is

$$\mathrm{i}\partial_t\overline{S}^<(k,t)=\widehat{H}_{\boldsymbol{k}}(t)\overline{S}^<(k,t)-\mathrm{H.c.} \tag{4.12}$$

Here $\widehat{H}_{\boldsymbol{k}}(t)\equiv\boldsymbol{\alpha}\cdot\boldsymbol{k}+\gamma^0 m(t)\,\mathrm{e}^{-\frac{\mathrm{i}}{2}\overleftarrow{\partial}_t\partial_{k^0}}$ is the free Dirac Hamiltonian where we have included the exponential gradient operator originating from equation (3.49b) [21].

Now we insert the spectral ansatz (4.11) of the Wightman function into (4.12) and integrate over k^0 (and divide by 2π). Note that the resulting equation has the form (4.1). Taking again relevant projections and traces of the equation yields the integrated free dynamical equations

$$\partial_t f^{m,s}_{\boldsymbol{k}hij}=-2\mathrm{i}s\delta\omega_{\boldsymbol{k}ij}f^{m,s}_{\boldsymbol{k}hij}-\mathcal{L}^{m,s}_{\boldsymbol{k}hij}[f], \tag{4.13a}$$

$$\partial_t f^{c,s}_{\boldsymbol{k}hij}=\ -2\mathrm{i}s\bar{\omega}_{\boldsymbol{k}ij}f^{c,s}_{\boldsymbol{k}hij}-\mathcal{L}^{c,s}_{\boldsymbol{k}hij}[f]. \tag{4.13b}$$

Here $\mathcal{L}^{x,s}_{\boldsymbol{k}hij}[f]$ (with $x=m,c$) contain the terms proportional to the time-derivative of the projection matrices. Using analogous notation for $\mathcal{L}$ as for f in equation (4.10) (i.e. $\mathcal{L}^{m,\pm}=\mathcal{L}^{\pm\pm}$ and $\mathcal{L}^{c,\pm}=\mathcal{L}^{\pm\mp}$), we can write

$$\mathcal{L}^{ss'}_{\boldsymbol{k}hij}[f]=\sum_{r,r'}\frac{\mathrm{tr}\big[P^{s's}_{\boldsymbol{k}hji}\partial_t\mathcal{P}^{rr'}_{\boldsymbol{k}hij}\big]}{\mathrm{tr}\big[\mathcal{P}^{ss'}_{\boldsymbol{k}hij}\gamma^0\big]}f^{rr'}_{\boldsymbol{k}hij}. \tag{4.14}$$

In the end these terms are directly proportional to $\partial_t m$ and f. We can now see from equations (4.13) that the coherence functions f^c, and also f^m_{ij} for $i\neq j$, are very rapidly oscillating and the leading oscillation frequency is given by the first term on the right-hand side (see also table 1). These terms will give the leading behavior of

the distribution functions also in the full interacting equations, at least in the case of weak interactions. However, the main point that we wished to make here is that the oscillation frequencies are not suppressed by time-gradients.

4.2.3 Reorganized gradient expansion

Now that we understand the leading time-dependence of the cQPA propagator, we can see that there is a problem in the full interacting equations (3.49b). If we use the standard Moyal product (3.48) for the interaction terms the gradient expansion will include time-derivatives which operate on the rapidly oscillating coherence functions. This results in terms that grow at each order of the expansion. It is then not guaranteed to get valid approximations for the full equations by truncating the standard gradient expansion. This problem can be solved by *resumming* the leading behavior of the coherence function gradients to all orders, as was done in [20, 21]. The result is that the arguments of the self-energy functions are shifted so that they are always evaluated at the ordinary flavor-diagonal mass shells $k^0 = \pm\omega_{\boldsymbol{k}i}$.

A more direct way to derive the resummed equations is to rewrite the Moyal products in equations (3.49) so that the leading coherence gradient resummation is more transparent. The equations with the reorganized gradient expansion are [I]

$$\not{\Pi} S^p - \mathrm{e}^{-\frac{\mathrm{i}}{2}\partial_x^\Sigma\cdot\partial_k}\big[\widetilde{\Sigma}^p_{\mathrm{out}}(D,x)S^p\big] = \mathbf{1}, \tag{4.15a}$$

$$\not{\Pi} S^s - \mathrm{e}^{-\frac{\mathrm{i}}{2}\partial_x^\Sigma\cdot\partial_k}\big[\widetilde{\Sigma}^r_{\mathrm{out}}(D,x)S^s\big] = \mathrm{e}^{-\frac{\mathrm{i}}{2}\partial_x^\Sigma\cdot\partial_k}\big[\Sigma^s_{\mathrm{out}}(D,x)S^a\big], \tag{4.15b}$$

where $D \equiv k + \frac{\mathrm{i}}{2}\partial_x$ and we defined the "out-transform"

$$\Sigma_{\mathrm{out}}(k,x) \equiv \int \mathrm{d}^4 z\ \mathrm{e}^{\mathrm{i}k\cdot(x-z)}\,\Sigma(x,z) = \mathrm{e}^{\frac{\mathrm{i}}{2}\partial_x\cdot\partial_k}\Sigma(k,x). \tag{4.16}$$

In equations (4.15) the Moyal products have been reorganized into total k-derivatives and the exponential spacetime derivatives operate only on Σ. This form is useful already for the fact that the exponential gradient operator reduces to unity when integrating over k^0. However, the main point is that the self-energy functions have been generalized (via their Taylor expansions) to derivative operators which operate on the propagators. This can then be used to see directly how the coherence functions in S^s shift the arguments of the self-energy functions [I].

Next we illustrate how the gradient resummation shifts the argument of the self-energy in the multi-flavor case. Consider the k^0-integrated equation and a generic interaction term (in the spatially homogeneous and isotropic case)

$$\int\frac{\mathrm{d}k^0}{2\pi}\,\mathrm{e}^{-\frac{\mathrm{i}}{2}\partial_t^\Sigma\cdot\partial_{k^0}}\Big[\Sigma_{li}\big(k^0+\tfrac{\mathrm{i}}{2}\partial_t\big)S^<_{ij}(k,t)\Big] = \int\frac{\mathrm{d}k^0}{2\pi}\Sigma_{li}\big(k^0+\tfrac{\mathrm{i}}{2}\partial_t\big)S^<_{ij}(k,t), \tag{4.17}$$

where i,j,l are any flavor indices. When using the cQPA ansatz (4.11) here and performing the k^0-integral using the delta functions, the terms with f^m and f^c can

be approximated according to

$$\Sigma_{li}\big(k^0 + \tfrac{\mathrm{i}}{2}\partial_t\big) f^{m,s}_{\boldsymbol{k}hij}\, \delta(k^0 - s\bar{\omega}_{\boldsymbol{k}ij}) \quad \longrightarrow \quad \Sigma_{li}\big(\overbrace{s\bar{\omega}_{\boldsymbol{k}ij} + s\delta\omega_{\boldsymbol{k}ij}}^{= s\omega_{\boldsymbol{k}i}}\big) f^{m,s}_{\boldsymbol{k}hij}, \tag{4.18a}$$

$$\Sigma_{li}\big(k^0 + \tfrac{\mathrm{i}}{2}\partial_t\big) f^{c,s}_{\boldsymbol{k}hij}\, \delta(k^0 - s\delta\omega_{\boldsymbol{k}ij}) \quad \longrightarrow \quad \Sigma_{li}\big(s\delta\omega_{\boldsymbol{k}ij} + s\bar{\omega}_{\boldsymbol{k}ij}\big) f^{c,s}_{\boldsymbol{k}hij}. \tag{4.18b}$$

Here we used the leading behavior of $\partial_t f^m$ and $\partial_t f^c$ from equations (4.13). In both cases the k^0-argument of the self-energy reduces to $s\omega_{\boldsymbol{k}i}$. This prescription of course does not take into account the gradients that operate on the projection matrices and delta functions, but these are suppressed by the mass gradients and are thus controlled in most situations in a standard expansion. We can now see the main result of the resummation: in all cases the self-energy functions are effectively evaluated at the flavor-diagonal mass shell $k^0 = s\omega_{\boldsymbol{k}i}$ with the middle flavor index.

4.2.4 Resummed dynamical equations

We can now write the full integrated dynamical equations where the leading coherence-gradients have been resummed. This is done like described in section 4.2.2 but now starting from the antihermitian part of the KB equation (4.15b). The result is

$$\partial_t f^{m,s}_{\boldsymbol{k}hij} = -2\mathrm{i}s\delta\omega_{\boldsymbol{k}ij} f^{m,s}_{\boldsymbol{k}hij} - \mathcal{L}^{m,s}_{\boldsymbol{k}hij}[f] - \mathcal{C}^{m,s}_{\boldsymbol{k}hij}\big[\overline{\Sigma}^r_{\mathrm{out}}, f\big] - \mathcal{C}^{m,s}_{\boldsymbol{k}hij}\big[\mathrm{i}\overline{\Sigma}^<_{\mathrm{out}}, f^{(\mathcal{A})}\big], \tag{4.19a}$$

$$\partial_t f^{c,s}_{\boldsymbol{k}hij} = -2\mathrm{i}s\bar{\omega}_{\boldsymbol{k}ij} f^{c,s}_{\boldsymbol{k}hij} - \mathcal{L}^{c,s}_{\boldsymbol{k}hij}[f] - \mathcal{C}^{c,s}_{\boldsymbol{k}hij}\big[\overline{\Sigma}^r_{\mathrm{out}}, f\big] - \mathcal{C}^{c,s}_{\boldsymbol{k}hij}\big[\mathrm{i}\overline{\Sigma}^<_{\mathrm{out}}, f^{(\mathcal{A})}\big], \tag{4.19b}$$

where the projection matrix gradient terms $\mathcal{L}^{x,s}$ (with $x = m, c$) were defined in (4.14). Using similar notation ($\mathcal{C}^{m,\pm} = \mathcal{C}^{\pm\pm}$ and $\mathcal{C}^{c,\pm} = \mathcal{C}^{\pm\mp}$), the collision term projections in equations (4.19) are given by[18]

$$\mathcal{C}^{ss'}_{\boldsymbol{k}hij}[\Sigma, f] = \sum_{l,r}\Big(C^{srs'}_{\boldsymbol{k}hilj}[\Sigma]\, f^{rs'}_{\boldsymbol{k}hlj} + C^{\star,srs'}_{\boldsymbol{k}hilj}[\Sigma] f^{sr}_{\boldsymbol{k}hil}\Big), \tag{4.20a}$$

with

$$C^{srs'}_{\boldsymbol{k}hilj}[\Sigma] \equiv \frac{\mathrm{i}\,\mathrm{tr}\big[P^{s's}_{\boldsymbol{k}hji}\Sigma_{il}(r\omega_{\boldsymbol{k}l})\mathcal{P}^{rs'}_{\boldsymbol{k}hlj}\big]}{\mathrm{tr}\big[\mathcal{P}^{ss'}_{\boldsymbol{k}hij}\gamma^0\big]}, \tag{4.20b}$$

$$C^{\star,srs'}_{\boldsymbol{k}hilj}[\Sigma] \equiv \frac{-\mathrm{i}\,\mathrm{tr}\big[\mathcal{P}^{sr}_{\boldsymbol{k}hil}(\Sigma(r\omega_{\boldsymbol{k}l})^\dagger)_{lj}P^{s's}_{\boldsymbol{k}hji}\big]}{\mathrm{tr}\big[\mathcal{P}^{ss'}_{\boldsymbol{k}hij}\gamma^0\big]}. \tag{4.20c}$$

In order to be consistent with the used (quasi)particle approximation we also discarded the term $\propto \Sigma^< S^{\mathrm{H}}$ here [15]. This term is related to the spectral width as discussed below equation (3.44). Note that equations (4.19) also contain Σ^r which includes the dispersive self-energy Σ^{H}. It would be consistent to drop also Σ^{H} here because we have used the free dispersion relations in the cQPA ansatz. However, as we will see in the context of the more general LA-method it may still be included as a leading approximation to the dispersive corrections in these equations.

[18] Note that the collision term coefficients C and $C^\star$ used here are independent for arbitrary normalization N [which enters via equation (4.2b)].

An essential feature of cQPA is that the non-local degrees of freedom are treated non-dynamically in the collision terms [I]. This idea is further refined in the LA-method which we shall present in section 4.3. However, first we describe how to account for a more general mass matrix in these equations.

Mixing gradient terms

Above we assumed that the mass matrix $m(t)$ is diagonal with non-negative entries. In the more general case where it is non-diagonal and complex we first have to transform the equations to the mass eigenbasis before proceeding with the projection matrix parametrization. Here we only present the main points; details can be found in [21]. We use the singular value decomposition with unitary matrices U and V such that

$$m_{\mathrm{d}} \equiv UmV^{\dagger} \tag{4.21}$$

is diagonal with non-negative entries. The subscript d distinguishes the diagonal basis from the original where necessary. The free Hamiltonian generally has the form $H_{\boldsymbol{k}} = \boldsymbol{\alpha}\cdot\boldsymbol{k} + \gamma^0(P_{\mathrm{R}}m + P_{\mathrm{L}}m^{\dagger})$ in the original basis. Its transform is given by $H_{\mathrm{d},\boldsymbol{k}} \equiv Y H_{\boldsymbol{k}} Y^{\dagger} = \boldsymbol{\alpha}\cdot\boldsymbol{k} + \gamma^0 m_{\mathrm{d}}$ with the transformation matrix

$$Y \equiv P_{\mathrm{L}}U + P_{\mathrm{R}}V. \tag{4.22}$$

All equations can be transformed to the mass eigenbasis similarly by using the unitary matrix Y. Because of the time dependence of m and the matrices U and V this induces additional *mixing gradient* terms to the equations which are proportional to $\partial_t Y$. In the end the dynamical equations (4.19) are modified to

$$\partial_t f^{m,s}_{\boldsymbol{k}hij} = -2\mathrm{i}s\delta\omega_{\boldsymbol{k}ij} f^{m,s}_{\boldsymbol{k}hij} - \mathcal{L}^{m,s}_{\boldsymbol{k}hij}[f] - \mathcal{X}^{m,s}_{\boldsymbol{k}hij}[f] - (\cdots), \tag{4.23a}$$

$$\partial_t f^{c,s}_{\boldsymbol{k}hij} = -2\mathrm{i}s\bar{\omega}_{\boldsymbol{k}ij} f^{c,s}_{\boldsymbol{k}hij} - \mathcal{L}^{c,s}_{\boldsymbol{k}hij}[f] - \mathcal{X}^{c,s}_{\boldsymbol{k}hij}[f] - (\cdots), \tag{4.23b}$$

where the mixing gradient contribution is given by

$$\mathcal{X}^{ss'}_{\boldsymbol{k}hij}[f] = \sum_{l,r}\Big(X^{srs'}_{\boldsymbol{k}hilj}\, f^{rs'}_{\boldsymbol{k}hlj} + X^{\star,srs'}_{\boldsymbol{k}hilj}\, f^{sr}_{\boldsymbol{k}hil}\Big), \tag{4.24a}$$

with

$$X^{srs'}_{\boldsymbol{k}hilj} \equiv \frac{-\mathrm{i}\,\mathrm{tr}\big[P^{s's}_{\boldsymbol{k}hji}\,\dot{\Xi}_{il}\mathcal{P}^{rs'}_{\boldsymbol{k}hlj}\big]}{\mathrm{tr}\big[\mathcal{P}^{ss'}_{\boldsymbol{k}hij}\gamma^0\big]}, \qquad X^{\star,srs'}_{\boldsymbol{k}hilj} \equiv \frac{\mathrm{i}\,\mathrm{tr}\big[\mathcal{P}^{sr}_{\boldsymbol{k}hil}\,\dot{\Xi}_{lj}P^{s's}_{\boldsymbol{k}hji}\big]}{\mathrm{tr}\big[\mathcal{P}^{ss'}_{\boldsymbol{k}hij}\gamma^0\big]}. \tag{4.24b}$$

Here $\dot{\Xi}(t) \equiv \mathrm{i}Y(t)\partial_t Y^{\dagger}(t)$ is the mixing gradient matrix which is Hermitian. The ellipses in equations (4.23) stand for the collision terms which are the same as in (4.19) except that the self-energy functions have been transformed to the mass eigenbasis according to $\overline{\Sigma} \to Y\overline{\Sigma}Y^{\dagger}$.

4.3 The local approximation method

The local approximation (LA) method which was formulated in [II] is an improved method for obtaining straightforwardly solvable dynamical QKEs including quantum coherence. The LA-method provides a closed equation for the *local* Wightman function directly in the two-time representation. This is useful when calculating physical observables from the currents or the energy-momentum tensor because then knowledge of only the equal-time, or local, correlator $S^<_{\boldsymbol{k}}(t,t)$ is needed. The LA-method also sidesteps the need to specify the phase space shells of the full propagator as is required in a Wigner representation approach. This makes it more general than the cQPA, for example. Next we present the derivation and equations of the LA-method for fermions in a spatially homogeneous and isotropic system.

4.3.1 Dynamics of the local correlator

We start from the pole and KB equations (3.56) which we write explicitly as

$$\big[\mathrm{i}\partial_{t_1} - H_{\boldsymbol{k}}(t_1)\big]\overline{S}^p_{\boldsymbol{k}}(t_1,t_2) - (\overline{\Sigma}^p_{\boldsymbol{k}} * \overline{S}^p_{\boldsymbol{k}})(t_1,t_2) = \delta(t_1-t_2), \tag{4.25a}$$

$$\big[\mathrm{i}\partial_{t_1} - H_{\boldsymbol{k}}(t_1)\big]\overline{S}^s_{\boldsymbol{k}}(t_1,t_2) - (\overline{\Sigma}^r_{\boldsymbol{k}} * \overline{S}^s_{\boldsymbol{k}})(t_1,t_2) = (\overline{\Sigma}^s_{\boldsymbol{k}} * \overline{S}^a_{\boldsymbol{k}})(t_1,t_2). \tag{4.25b}$$

We again assume the mass eigenbasis with the free Hamiltonian $H_{\boldsymbol{k}}$ given below equation (4.1). To find the equation for the local Wightman function we first take the total derivative of $S^<_{\boldsymbol{k}}(t,t)$ and use the chain rule to get

$$\partial_t S^<_{\boldsymbol{k}}(t,t) \equiv \frac{\mathrm{d}}{\mathrm{d}t}\big[S^<_{\boldsymbol{k}}(t,t)\big] = \big(\partial_{t_1} S^<_{\boldsymbol{k}} + \partial_{t_2} S^<_{\boldsymbol{k}}\big)(t,t). \tag{4.26}$$

Equation (4.26) can then be used with the KB equation (4.25b) and its Hermitian conjugate to obtain the equation for the local function:[19]

$$\begin{aligned}\mathrm{i}\partial_t \overline{S}^<_{\boldsymbol{k}}(t,t) = \big[H_{\boldsymbol{k}}(t), \overline{S}^<_{\boldsymbol{k}}(t,t)\big] &+ (\overline{\Sigma}^r_{\boldsymbol{k}} * \overline{S}^<_{\boldsymbol{k}})(t,t) - (\overline{S}^<_{\boldsymbol{k}} * \overline{\Sigma}^a_{\boldsymbol{k}})(t,t) \\ &+ (\overline{\Sigma}^<_{\boldsymbol{k}} * \overline{S}^a_{\boldsymbol{k}})(t,t) - (\overline{S}^r_{\boldsymbol{k}} * \overline{\Sigma}^<_{\boldsymbol{k}})(t,t).\end{aligned} \tag{4.27}$$

The total derivative was required here to eventually produce an ordinary differential equation for the local correlator as a function of the single time variable t. Note that equation (4.27) is also consistent with the Hermiticity of $\overline{S}^<_{\boldsymbol{k}}(t,t)$.

Equation (4.27) is the starting point of the LA-method. The equation is still exact and hence of course not closed: it couples the local function $S^<_{\boldsymbol{k}}(t,t)$ to the non-local function $S^<_{\boldsymbol{k}}(t,t')$ (with $t \neq t'$) appearing in the interaction convolutions. The pole functions S^p also appear explicitly in the interaction terms. The LA-method consists of two steps to overcome these problems: (1) expansion around a suitable adiabatic background solution and (2) the local ansatz for the interaction terms.

[19] We assume that the local limit of $S^<_{\boldsymbol{k}}(t_1,t_2)$ exists and is well-enough-behaved (e.g. continuously differentiable). However, equation (4.27) may also be sensible with weaker assumptions. For example, if only one-sided limits $t_1 \to t_2$ exist, we can define $S^<_{\boldsymbol{k}}(t,t)$ as the symmetrized local limit.

4.3.2 Adiabatic background solution

The main purpose of the adiabatic background solution is to enable an approximation of equation (4.27) where the pole functions can be treated non-dynamically. The basis for this approximation is the assumption that the self-energy Σ is dominated by some known part Σ_{ad} which can be calculated non-dynamically. The adiabatic background solution S_{ad} for the two-point functions is then defined by a suitable approximation of the full equations where the full Σ is replaced by Σ_{ad}.

For given adiabatic two-point functions S_{ad} and self-energies Σ_{ad} we extract the dynamical parts (or deviations) δS and $\delta\Sigma$ from the full functions by defining

$$S^\alpha \equiv S^\alpha_{\text{ad}} + \delta S^\alpha, \tag{4.28a}$$
$$\Sigma^\alpha \equiv \Sigma^\alpha_{\text{ad}} + \delta\Sigma^\alpha. \tag{4.28b}$$

We then substitute (4.28a) into equation (4.27) to derive the equation for $\delta S^<_{\boldsymbol{k}}(t,t)$:

$$\mathrm{i}\partial_t \delta\overline{S}^<_{\boldsymbol{k}}(t,t) = \big[H_{\boldsymbol{k}}(t), \delta\overline{S}^<_{\boldsymbol{k}}(t,t)\big] + \big[(\overline{\Sigma}^r_{\boldsymbol{k}} * \delta\overline{S}^<_{\boldsymbol{k}})(t,t) + \overline{A}^<_{\boldsymbol{k}}(t) - \text{H.c.}\big], \tag{4.29}$$

with

$$\begin{aligned}\overline{A}^<_{\boldsymbol{k}}(t) \equiv{}& H_{\boldsymbol{k}}(t)\overline{S}^<_{\text{ad},\boldsymbol{k}}(t,t) + \big(\overline{\Sigma}^r_{\text{ad},\boldsymbol{k}} * \overline{S}^<_{\text{ad},\boldsymbol{k}} + \overline{\Sigma}^<_{\text{ad},\boldsymbol{k}} * \overline{S}^a_{\text{ad},\boldsymbol{k}}\big)(t,t)\\ &+ \big(\delta\overline{\Sigma}^r_{\boldsymbol{k}} * \overline{S}^<_{\text{ad},\boldsymbol{k}} + \delta\overline{\Sigma}^<_{\boldsymbol{k}} * \overline{S}^a_{\text{ad},\boldsymbol{k}} + \overline{\Sigma}^<_{\boldsymbol{k}} * \delta\overline{S}^a_{\boldsymbol{k}}\big)(t,t)\\ &- \tfrac{\mathrm{i}}{2}\partial_t \overline{S}^<_{\text{ad},\boldsymbol{k}}(t,t).\end{aligned} \tag{4.30}$$

Equation (4.29) is still just a reorganization of the exact equation (4.27) where $\overline{A}^<_{\boldsymbol{k}}(t)$ contains the terms which do not depend explicitly on $\delta S^<$. The idea is that the adiabatic solutions are defined so that the dynamical terms proportional to δS^p [the last term on the second line of (4.30) minus its Hermitian conjugate] will be small corrections compared to the leading terms with the non-dynamical S^α_{ad}.

There is a lot of freedom in the definition of the adiabatic functions [II], but a reasonable minimum requirement is that they satisfy the same generic properties and relations as the full functions. These include for example the Hermiticity properties (3.31) and the sum rule (3.58). An obvious choice with these properties is the translationally invariant solution (3.52). However, because we allow for a changing background, that is, the time-dependent mass $m(t)$, it is better to define the adiabatic functions as instantaneous generalizations of the solutions (3.52):

$$S^p_{\text{ad}}(k,t) \equiv \big[\not{k} - m(t) - \Sigma^p_{\text{ad}}(k,t)\big]^{-1}, \tag{4.31a}$$
$$S^s_{\text{ad}}(k,t) \equiv S^r_{\text{ad}}(k,t)\Sigma^s_{\text{ad}}(k,t)S^a_{\text{ad}}(k,t). \tag{4.31b}$$

Note that the definitions (4.31) are given in the Wigner representation so they must be transformed to the two-time representation when using them in equation (4.29), for example.

Expansion of the source term

Now with the adiabatic functions defined we can find the leading approximation for the "source term" $\overline{A}^<_{\boldsymbol{k}}(t)$ in (4.29). However, this still depends significantly on the physical situation at hand so we need to make some further assumptions. For example, the full self-energy quite generally depends on $\delta S^<$ itself so strictly speaking $\overline{A}^<_{\boldsymbol{k}}(t)$ is even not only a source term. Here we make the following assumptions which are sufficient in this work:

1. S^α_{ad} are given by equations (4.31).
2. Σ^s_{ad} contains a part satisfying the KMS condition.
3. Linearity: Σ does not depend on S itself at first order.

Assumption 1 implies that the adiabatic pole propagators satisfy the sum rule. A direct consequence is that the local part of the dynamical pole propagator vanishes, $\delta S^p_{\boldsymbol{k}}(t,t) = 0$. This together with dissipation has the effect that the convolution integral $\overline{\Sigma}^<_{\boldsymbol{k}} * \delta\overline{S}^a_{\boldsymbol{k}}$ in (4.30) is suppressed near both the upper and lower limits. Furthermore, examination of the full equation of motion in the Wigner representation shows that δS^p is also quite generally suppressed by either time gradients, coupling constants or $\delta\Sigma^p$.[20] When assuming weak interactions, it should then be a reasonable approximation to discard δS^p altogether. This makes the pole propagators entirely non-dynamical. Another consequence of assumption 1 is that the first line of equation (4.30) vanishes to zeroth order in gradients. The leading non-vanishing terms are also first order in both gradients and the interactions strength.

Assumptions 2 and 3 are related to the remaining terms in equation (4.30). Assumption 2 implies that $S^s_{\mathrm{ad}}(k,t)$ contains the (instantaneous) thermal equilibrium part, making it $\mathcal{O}(1)$ instead of first order in the interaction strength as might be naively expected from (4.31b) [II]. Assumption 3 is made so that equation (4.29) remains linear in $\delta S^<$ (in the leading approximation) and $\delta\Sigma$ can be more safely dropped from the equation. Together assumptions 1–3 imply that we can make the leading order approximation

$$\overline{A}^<_{\boldsymbol{k}}(t) \simeq -\tfrac{\mathrm{i}}{2}\partial_t \overline{S}^<_{\mathrm{ad},\boldsymbol{k}}(t,t) \tag{4.32}$$

in the interaction strength. In this approximation $\overline{A}^<_{\boldsymbol{k}}(t)$ then acts as a source term to $\delta\overline{S}^<_{\boldsymbol{k}}(t,t)$ in equation (4.29). The next-to-leading correction terms to equation (4.32) are proportional to (schematically) $\Sigma\,\partial_t S_{\mathrm{ad}}$, $\partial_t\Sigma\, S_{\mathrm{ad}}$ or $\delta\Sigma\, S_{\mathrm{ad}}$.

It should be borne in mind that the choice of the adiabatic background solutions (4.31) and the above assumptions 1–3 leading to the result (4.32) are specific to

[20] The Wightman functions $\delta S^s_{\boldsymbol{k}}(t,t)$ are not similarly suppressed because they are not restricted by the sum rule and they may also contain large initial transients.

the situation of a varying background (the mass) and a weak coupling to a thermal bath. For other situations this step may not be as simple and must be done more carefully. We also remark that the (non-local) pole propagator deviations δS^p cannot be solved perturbatively in the same way as the Wightman deviations δS^s [II]. Hence the only practical possibility is to set $\delta S^p \equiv 0$ in this approach. The background solution must then be calculated accurately enough for the considered application; its level of approximation essentially defines the approximation scheme [133].[21] However, in the situation considered in this work the results are not very sensitive to the approximation of the background solution and the error incurred to the dispersion and width of the propagators is small even with only a tree level approximation [II].

4.3.3 The local ansatz

The core of the LA-method is the technique used to localize the dynamical interaction convolutions. The problem is that the evolution of the local perturbation $\delta S^<_{\boldsymbol{k}}(t,t)$ in equation (4.29) generally depends on the values of $\delta S^<_{\boldsymbol{k}}(t_1,t_2)$ everywhere in the (t_1,t_2)-plane. However, when the system has dissipation this non-local dependence is suppressed [I] and the dominant contribution to the convolution integrals should come from the vicinity of the external local time t of equation (4.29). This is the basis for the local description of the non-equilibrium dynamics.

The idea is to use the structure of the homogeneous transient solution (3.67) to formulate the local approximation of the interaction convolutions. Suppose first that we had found the correct local value $\delta S^<_{\boldsymbol{k}}(t,t)$ for some time $t > t_{\rm in}$. Because most of the inhomogeneous solution (3.66b) is contained in the adiabatic solution (4.31b), it should then be reasonable to estimate the non-local values $\delta S^<_{\boldsymbol{k}}(t_1,t_2)$ by a transient solution similar to (3.67) where the initial time $t_{\rm in}$ is replaced by t (especially for t_1, t_2 close to t). Of course, we do not actually know the exact local values but we use this reasoning to *parametrize* the non-local values with the local ones [II]:

$$\delta\overline{S}^s_{\boldsymbol{k}}(t_1,t_2) = 2\overline{S}^{\mathcal{A}}_{\boldsymbol{k}}(t_1,t)\delta\overline{S}^s_{\boldsymbol{k}}(t,t)2\overline{S}^{\mathcal{A}}_{\boldsymbol{k}}(t,t_2), \quad \text{for any } t > t_{\rm in}. \tag{4.33}$$

We emphasize that this *local ansatz* is only to be used as a parametrization in the interaction convolutions. In particular, it must not be used to solve the entire time-evolution non-dynamically from the initial value. This would lead to contradictions with the local equation of motion, and it would for example exclude the use of thermal initial conditions (where $\delta S^s_{\boldsymbol{k}} = 0$ initially). In the interaction convolutions the ansatz (4.33) is effectively used with t_1, t_2 near the external time argument t.

[21] Also, the background self-energy $\Sigma_{\rm ad}$ may even include corrections from $\delta S^<$ itself. For example, it can include a part of $\delta\Sigma^<$ which can be arranged so that it *cancels* the term $\overline{\Sigma}^<_{\boldsymbol{k}} * \delta\overline{S}^a_{\boldsymbol{k}}$ in the equation (to lowest order in gradients) [133]. However, the adiabatic functions then become dynamical and have to be solved in an iterative way.

The dynamical interaction convolutions remaining in equation (4.29) can now be localized by using the ansatz (4.33). We replace the convolutions involving $\delta\overline{S}^<_{\boldsymbol{k}}$ according to

$$(\overline{\Sigma}^r_{\boldsymbol{k}} * \delta\overline{S}^<_{\boldsymbol{k}})(t,t) \longrightarrow \overline{\Sigma}^r_{\mathrm{eff},\boldsymbol{k}}(t,t)\delta\overline{S}^<_{\boldsymbol{k}}(t,t), \tag{4.34a}$$
$$(\delta\overline{S}^<_{\boldsymbol{k}} * \overline{\Sigma}^a_{\boldsymbol{k}})(t,t) \longrightarrow \delta\overline{S}^<_{\boldsymbol{k}}(t,t)\overline{\Sigma}^a_{\mathrm{eff},\boldsymbol{k}}(t,t), \tag{4.34b}$$

where we defined the *effective* self-energies

$$\overline{\Sigma}^r_{\mathrm{eff},\boldsymbol{k}}(t_1,t_2) \equiv (\overline{\Sigma}^r_{\boldsymbol{k}} * 2\overline{S}^{\mathcal{A}}_{\boldsymbol{k}})(t_1,t_2), \tag{4.35a}$$
$$\overline{\Sigma}^a_{\mathrm{eff},\boldsymbol{k}}(t_1,t_2) \equiv (2\overline{S}^{\mathcal{A}}_{\boldsymbol{k}} * \overline{\Sigma}^a_{\boldsymbol{k}})(t_1,t_2). \tag{4.35b}$$

Note that $\overline{\Sigma}^r_{\mathrm{eff},\boldsymbol{k}}(t_1,t_2)^\dagger = \overline{\Sigma}^a_{\mathrm{eff},\boldsymbol{k}}(t_2,t_1)$, so that the Hermiticity properties of equation (4.29) are preserved. The replacements (4.34) reduce the dynamical convolutions to simple matrix products of the local function $\delta S^<_{\boldsymbol{k}}(t,t)$ with the effective self-energy. The convolutions in the effective self-energy now involve the spectral function which is taken to be non-dynamical, $S^{\mathcal{A}} = S^{\mathcal{A}}_{\mathrm{ad}}$, as explained in section 4.3.2.

4.3.4 Closed local equation

We now use the local ansatz (4.33) as described in section 4.3.3 together with equations (4.29), (4.32) and (4.35) to write the first order local equation of motion for the local Wightman function $\delta\overline{S}^<_{\boldsymbol{k}}(t,t)$. We suppress the time arguments here for brevity as all quantities in the equation are now functions of the single time variable t. The equation, first presented in [II], takes a very simple form:

$$\partial_t\delta\overline{S}^<_{\boldsymbol{k}} = -\mathrm{i}\big[H_{\boldsymbol{k}}, \delta\overline{S}^<_{\boldsymbol{k}}\big] - \big(\mathrm{i}\overline{\Sigma}^r_{\mathrm{eff},\boldsymbol{k}}\,\delta\overline{S}^<_{\boldsymbol{k}} + \mathrm{H.c.}\big) - \partial_t\overline{S}^<_{\mathrm{ad},\boldsymbol{k}}. \tag{4.36}$$

Equation (4.36) is our main quantum transport equation for the fermion propagator. The equation is an ordinary matrix differential equation for $\delta\overline{S}^<_{\boldsymbol{k}}(t,t)$. It is a closed local equation due to the local ansatz which manifests as the effective self-energy functions Σ_{eff}. Despite its simple appearance and the used first order approximation the equation is still very general [II]. The form of the local function $\delta\overline{S}^<_{\boldsymbol{k}}(t,t)$ has not been restricted in any way so the equation can describe both flavor and particle–antiparticle coherence of mixing fermions. Equation (4.36) contains the effects of the thermal medium, including thermal width and dispersive corrections in the weak coupling expansion, via the adiabatic propagators in the effective self-energy and the source term. It also covers as special limits both the cQPA-method and the semiclassical Boltzmann equations [II]. We have summarized in table 2 the main points which were used to obtain the final closed local equation (4.36).

#	Step	Effect
1.	Expand the full solution around a non-dynamical background solution.	Decoupling of the pole equations from the local dynamical equation.
2.	Model the non-local part of the propagator as a homogeneous transient.	Closure of the interaction terms in the local dynamical equation.

Table 2. The steps used in the local approximation (LA) method to obtain a closed dynamical equation for the local propagator (in dissipative systems). The key point of the method is the local ansatz (4.33) used in step 2.

4.3.5 Generalized density matrix equations

In the LA-method the local equation (4.36) was formulated directly in the two-time presentation at the propagator level and the projection matrix parametrization was not needed (yet). This is in contrast to the cQPA where the projection matrix parametrization is used already in finding the ansatz (4.11) for the propagator. However, in the LA-method the projection matrix parametrization is equally essential when actually solving the equation as it separates the quickly and slowly varying components of the propagator. We adopt also here the terminology of mass and coherence shell functions used in cQPA, although in the more general LA-method these functions are not necessarily restricted to spectral phase space shells.

To derive the component equations we use the projection matrix parametrization (4.2) for the two-time representation propagator $\delta S^<_{\boldsymbol{k}}$ in the form

$$\delta\bar{S}^<_{\boldsymbol{k}ij}(t,t) = \sum_{h,s,s'=\pm} \mathcal{P}^{ss'}_{\boldsymbol{k}hij}(t)\, \delta f^{ss'}_{\boldsymbol{k}hij}(t). \tag{4.37}$$

Here $\delta f^{ss'}_{\boldsymbol{k}hij}$ are the phase space distribution functions of the non-equilibrium deviation $\delta S^<_{\boldsymbol{k}}(t,t)$. The mass and coherence shell functions are defined similarly to (4.10):

$$\delta f^{m,\pm}_{\boldsymbol{k}hij} \equiv \delta f^{\pm\pm}_{\boldsymbol{k}hij}, \qquad \delta f^{c,\pm}_{\boldsymbol{k}hij} \equiv \delta f^{\pm\mp}_{\boldsymbol{k}hij}. \tag{4.38}$$

The corresponding functions $f_{\rm ad}$ for the adiabatic function $S^<_{{\rm ad},\boldsymbol{k}}(t,t)$ are defined analogously [II]. Using the parametrization (4.37) in the local equation (4.36) yields the equation

$$\partial_t \delta f^{ss'}_{\boldsymbol{k}hij} = -{\rm i}\Delta\bar{\omega}^{ss'}_{\boldsymbol{k}ij}\delta f^{ss'}_{\boldsymbol{k}hij} - \mathcal{L}^{ss'}_{\boldsymbol{k}hij}[f] - \widetilde{\mathcal{C}}^{ss'}_{\boldsymbol{k}hij}\big[\bar{\Sigma}^r, \delta f\big] - \partial_t f^{ss'}_{{\rm ad},\boldsymbol{k}hij}, \tag{4.39}$$

where

$$\widetilde{\mathcal{C}}^{ss'}_{\boldsymbol{k}hij}[\Sigma, f] = \sum_{l,r}\Big(\widetilde{C}^{srs'}_{\boldsymbol{k}hilj}[\Sigma]\, f^{rs'}_{\boldsymbol{k}hlj} + \widetilde{C}^{\star,srs'}_{\boldsymbol{k}hilj}[\Sigma] f^{sr}_{\boldsymbol{k}hil}\Big), \tag{4.40a}$$

with

$$\widetilde{C}^{srs'}_{\boldsymbol{k}hilj}[\Sigma] \equiv \frac{\mathrm{i}\,\mathrm{tr}\big[P^{s's}_{\boldsymbol{k}hji}\Sigma_{\mathrm{eff},\boldsymbol{k}il}(t,t)\mathcal{P}^{rs'}_{\boldsymbol{k}hlj}\big]}{\mathrm{tr}\big[\mathcal{P}^{ss'}_{\boldsymbol{k}hij}\gamma^0\big]}, \tag{4.40b}$$

$$\widetilde{C}^{\star,srs'}_{\boldsymbol{k}hilj}[\Sigma] \equiv \frac{-\mathrm{i}\,\mathrm{tr}\big[\mathcal{P}^{sr}_{\boldsymbol{k}hil}(\Sigma_{\mathrm{eff},\boldsymbol{k}}(t,t)^\dagger)_{lj}P^{s's}_{\boldsymbol{k}hji}\big]}{\mathrm{tr}\big[\mathcal{P}^{ss'}_{\boldsymbol{k}hij}\gamma^0\big]}. \tag{4.40c}$$

Note that in equation (4.39) $f \equiv f_{\mathrm{ad}} + \delta f$, and the projection gradient terms $\mathcal{L}^{ss'}_{\boldsymbol{k}hij}[f]$ are the same as those already defined in (4.14). Also, the collision term functions (4.40) have the same structure as those defined in (4.20) but here they feature the effective self-energy. We also used here the notation (4.5c) for the leading term in (4.39) and wrote only a single equation which describes both δf^m and δf^c.

Equation (4.39) is our master equation for the non-equilibrium distribution functions $\delta f^{ss'}_{\boldsymbol{k}hij}$, and it has the form of a generalized density matrix equation. This equation was presented in [II] with the specific choice of the "symmetric" normalization

$$\big(N^{ss'}_{\boldsymbol{k}hij}\big)_{\mathrm{symm}} \equiv \mathrm{tr}\big(P^{ss'}_{\boldsymbol{k}hij}\gamma^0\big)^{-\frac{1}{2}} = \sqrt{\frac{2\omega_{\boldsymbol{k}i}\omega_{\boldsymbol{k}j}}{\omega_{\boldsymbol{k}i}\omega_{\boldsymbol{k}j} + ss'(m_im_j - |\boldsymbol{k}|^2)}} \tag{4.41}$$

which further simplifies the equation in several ways.[22] Here we have retained the more general form of equation (4.39) with an arbitrary normalization factor. In [II] we have also provided a simplified version of the equation where the rapidly oscillating coherence functions δf^c have been integrated out. This is possible when the mass shell flavor oscillations are slower than the particle–antiparticle oscillations and it greatly facilitates the practical numerical solution of these equations.

Comparison and reduction to cQPA

Equation (4.39) is very similar to the corresponding cQPA equations (4.19) but there are some major differences. The main ones are that equation (4.39) is formulated for the deviations δf instead of the total functions f and the collision term projections involve the effective self-energy Σ_{eff} instead of just Σ. In fact, in the LA-method the deviations δf are defined by the adiabatic functions f_{ad} which are provided externally to the equation. The evaluation of the effective self-energies (4.35) also depends on the supplied adiabatic spectral function. This means that the specification of the adiabatic functions controls the type of approximation used in the equation. This is in contrast to cQPA where the spectral limit is assumed from the outset.

Another advantage of the LA-method compared to the cQPA is that the leading coherence gradient resummation (considered in section 4.2.3) is built in to the effective self-energy. This is because the dispersion relation used for evaluating the self-energy is imposed by the adiabatic spectral function via the convolution integral (4.35).

[22] One is that when the normalization factors satisfy the condition $(N^{ss'}_{\boldsymbol{k}hij})^* = N^{s's}_{\boldsymbol{k}hji}$ then the collision term coefficients $\widetilde{C}$ and $\widetilde{C}^\star$ become related as $\widetilde{C}^{\star,srs'}_{\boldsymbol{k}hilj}[\Sigma] = (\widetilde{C}^{s'rs}_{\boldsymbol{k}hjli}[\Sigma])^*$.

Because the spectral function is non-dynamical and contains only "mass shells" the self-energy is then automatically evaluated with the correct dispersion.

It has been shown that the local ansatz (4.33) can be reduced to the cQPA ansatz (4.11) in a spectral approximation [II]. Equations (4.39) can be also directly reduced to the cQPA equations (4.19) by making the spectral approximation for the adiabatic propagators. This is done by dropping $\Sigma^{\mathcal{A}}$ in equation (4.31a) and using the free dispersion relations (or the quasiparticle relations if appropriate). For example, when using the free spectral function the collision term functions (4.40) are reduced to (4.20) at leading order in gradients [II]. In other words, the effective self-energy is then reduced to a regular self-energy projection [II]. There are some technical differences between the LA-equations and the cQPA-equations even after this but the difference of the equations should then be first order in both gradients and coupling expansion. Also, to get equations (4.39) explicitly into the form (4.19) one must still eliminate δf by using $f = f_{\mathrm{ad}} + \delta f$ and reinstate some terms proportional to the adiabatic functions which were estimated to be small [the terms corresponding to the first and second lines of (4.30)].

5 APPLICATIONS OF COHERENT QKES

In this chapter we apply the methods we have developed in chapter 4 to baryogenesis in the early universe setting. The cQPA is applied to a toy-model of electroweak baryogenesis as an example of features of coherent QKEs [I]. The LA-method is applied to resonant leptogenesis where we make a detailed analysis of the generation and evolution of the CP-asymmetry in the minimal leptogenesis model [II].

5.1 Electroweak baryogenesis

As an example on how to use cQPA we now consider a simple toy-model with one fermion flavor and a time-dependent complex mass. This setup, considered in [I], is a time-dependent analogue of the expanding bubble wall during a first order electroweak phase transition in EWBG. The main focus here is not on phenomenology but on the interplay between CP-violation and quantum coherence, and how coherence emerges and affects the results. We also confirm the shell structure predicted by cQPA in an analysis with exact solutions in a specific free case [I].

In EWBG the most prominent fermionic CP-violating source, contributing to the chiral asymmetry, is the axial vector current

$$j^{\mu 5}(x) \equiv \big\langle \overline{\psi}(x)\gamma^{\mu}\gamma^{5}\psi(x)\big\rangle. \tag{5.1}$$

It couples directly to the electroweak vacuum structure through the axial anomaly and can thus bias the sphaleron transitions which produce the baryon asymmetry [139]. Here we concentrate on the axial charge density j^{05} which is the zeroth component of the current (5.1). It is also more generally related to particle asymmetries. Using the definitions (3.25) we can write it in terms of the fermion CTP propagator as

$$j^{05}(x) = \mathrm{tr}\big[\gamma^{5}\overline{S}^{<}(x,x)\big], \tag{5.2}$$

where we used the barred propagator notation introduced below equations (3.31).

5.1.1 Single flavor cQPA with CP-violating mass

We consider a spatially homogeneous and isotropic system and a single Dirac fermion ψ with a complex time-dependent mass parameter $m_{\mathrm{c}}(t)$. The free part of the Lagrangian reads

$$\mathcal{L} = \mathrm{i}\overline{\psi}\partial\!\!\!/\psi - m_{\mathrm{c}}\overline{\psi}_{\mathrm{L}}\psi_{\mathrm{R}} - m_{\mathrm{c}}^{*}\overline{\psi}_{\mathrm{R}}\psi_{\mathrm{L}}. \tag{5.3}$$

The complex mass here is an effective description which can arise from complex scalar field vacuum expectation values, see for example [140]. This system will be CP-violating if the complex phase of the mass changes in time. Generally, time-dependence of the mass can be a result of the expansion of the universe, like considered in section 2.2, or it may arise from the changing Higgs vacuum expectation value in phase transitions in the early universe.

Equations in the mass eigenbasis

The cQPA equations for this system are the single flavor special case of the more general equations (4.19). The effect of the complex mass can be taken into account via the mixing gradient terms given in equations (4.23) and (4.24). We perform the transformations described in equations (4.21)–(4.24) using

$$m_{\mathrm{c}} = m\,\mathrm{e}^{\mathrm{i}\theta}, \tag{5.4a}$$

$$Y = \mathrm{e}^{-\mathrm{i}\frac{\theta}{2}}P_{\mathrm{L}} + \mathrm{e}^{\mathrm{i}\frac{\theta}{2}}P_{\mathrm{R}} = \mathrm{e}^{\mathrm{i}\frac{\theta}{2}\gamma^{5}}, \tag{5.4b}$$

$$\Xi = \tfrac{1}{2}\dot{\theta}\gamma^{5}, \tag{5.4c}$$

where $m \equiv |m_{\mathrm{c}}|$, $\theta \equiv \mathrm{Arg}(m_{\mathrm{c}})$ and $\dot{\theta} \equiv \partial_t\theta$. We also choose here the "symmetric" normalization (4.41) for the projection matrix parametrization (4.7):

$$N_{\boldsymbol{k}h}^{ss'} \equiv \mathrm{tr}\big(P_{\boldsymbol{k}h}^{ss'}\gamma^{0}\big)^{-\frac{1}{2}}, \qquad N_{\boldsymbol{k}h}^{ss} = \frac{\omega_{\boldsymbol{k}}}{m}, \qquad N_{\boldsymbol{k}h}^{s,-s} = \frac{\omega_{\boldsymbol{k}}}{|\boldsymbol{k}|}. \tag{5.5}$$

The resulting single-flavor cQPA equations can then be cast into the form

$$\partial_t f_{\boldsymbol{k}h}^{m,s} = \sum_r \Phi_{\boldsymbol{k}h}^{r} f_{\boldsymbol{k}h}^{c,r} - \mathrm{tr}\big[\mathcal{C}_{\mathrm{coll}}\mathcal{P}_{\boldsymbol{k}h}^{m,s}\big], \tag{5.6a}$$

$$\partial_t f_{\boldsymbol{k}hij}^{c,s} = -2\mathrm{i}s\Big[\omega_{\boldsymbol{k}} + \tfrac{|\boldsymbol{k}|}{m}\,\mathrm{Im}(\Phi_{\boldsymbol{k}h}^{-})\Big] f_{\boldsymbol{k}h}^{c,s} - \Phi_{\boldsymbol{k}h}^{-s}\sum_r f_{\boldsymbol{k}h}^{m,r} - \mathrm{tr}\big[\mathcal{C}_{\mathrm{coll}}\mathcal{P}_{\boldsymbol{k}h}^{c,-s}\big], \tag{5.6b}$$

$$\mathcal{C}_{\mathrm{coll}} = \sum_{h,s}\left(\Big[f_{\boldsymbol{k}h}^{m,s}\overline{\Sigma}^{\mathcal{A}}(s\omega_{\boldsymbol{k}}) - \frac{s}{2}\overline{\Sigma}^{<}(s\omega_{\boldsymbol{k}})\Big]\mathcal{P}_{\boldsymbol{k}h}^{m,s} + f_{\boldsymbol{k}h}^{c,s}\overline{\Sigma}^{\mathcal{A}}(s\omega_{\boldsymbol{k}})\mathcal{P}_{\boldsymbol{k}h}^{c,s}\right) + \mathrm{H.c.} \tag{5.6c}$$

We defined here

$$\Phi_{\boldsymbol{k}h}^{s} \equiv \frac{1}{2}\left(\frac{|\boldsymbol{k}|\dot{m}}{\omega_{\boldsymbol{k}}^{2}} + \mathrm{i}sh\frac{m\dot{\theta}}{\omega_{\boldsymbol{k}}}\right), \tag{5.7}$$

which contains the contributions from both projection gradient and mixing gradient terms: $\mathcal{L}_{\boldsymbol{k}h}^{ss'} \propto \dot{m}$ and $\mathcal{X}_{\boldsymbol{k}h}^{ss'} \propto \dot{\theta}$. Note that we have suppressed the flavor indices in

these equations because there is only one flavor. We also discarded the external gradient corrections of the self-energy by replacing Σ_{out} with Σ and we dropped the dispersive self-energy Σ^{H} from the equations for simplicity.

Equations (5.6) are equivalent to the single flavor cQPA equations given in [I], however here we used the mass eigenbasis in the projection matrix parametrization. The exact form of the equations is then different because in [I] the projection matrix parametrization was defined using the complex mass parameter directly. Equations (5.6) are also similar to the single flavor equations given in [21] but they too differ because of the different normalization (5.5). We chose here this different approach to be consistent with the multi-flavor case presented in section 4.2. In the multi-flavor case the diagonalization approach is mandatory if the original mass matrix is not real and diagonal. The symmetric normalization also makes the equations simpler. The resulting equations are also physically more transparent: one can see directly from the form of the equations (5.6) that a changing phase ($\dot{\theta} \neq 0$) is a source for helicity asymmetry of the distribution functions $f^{m,c}$. The helicity asymmetry in turn leads to CP-violation, as we will see below.

Connection to the complex mass basis. To bridge the gap to [I] we now give the relationship between the phase space distribution functions f^m and f^c used in (5.6) and the corresponding functions used in [I] which we denote here by $\widehat{f}^m$ and $\widehat{f}^c$. Since in both cases the Wightman function in the original complex mass basis (5.3) is the same, we have $\overline{\mathcal{S}}^< = Y\widehat{\mathcal{S}}^< Y^\dagger$ where $\overline{\mathcal{S}}^<$ and $\widehat{\mathcal{S}}^<$ denote the integrated Wightman functions in the different bases. Using the different projection matrix parametrizations on each side of the equation then yields

$$\frac{m}{\omega_{\boldsymbol{k}}} N^{ss}_{\boldsymbol{k}h}\, f^{m,s}_{\boldsymbol{k}h} = s\widehat{f}^{m,s}_{\boldsymbol{k}h}, \tag{5.8a}$$

$$\frac{|\boldsymbol{k}|}{\omega_{\boldsymbol{k}}} N^{s,-s}_{\boldsymbol{k}h} f^{c,s}_{\boldsymbol{k}h} = \frac{1}{m}\left(\frac{|\boldsymbol{k}|}{\omega_{\boldsymbol{k}}} m_{\text{R}} + \mathrm{i}shm_{\text{I}}\right)\widehat{f}^{c,s}_{\boldsymbol{k}h}. \tag{5.8b}$$

The normalization $N^{ss'}_{\boldsymbol{k}h}$ of the mass eigenbasis side is still general here. Choosing (5.5) reduces the coefficients of f^m and f^c on the left-hand side to unity. We also defined here

$$m_{\text{c}} \equiv m_{\text{R}} + \mathrm{i}m_{\text{I}}, \qquad (m_{\text{R}}, m_{\text{I}} \in \mathbb{R}) \tag{5.9}$$

and used $\mathrm{e}^{-\mathrm{i}\theta} = (m_{\text{R}} - \mathrm{i}m_{\text{I}})/m$ with the notation of equation (5.4a). We now also have the identities

$$\dot{m} = \frac{m_{\text{R}}\dot{m}_{\text{R}} + m_{\text{I}}\dot{m}_{\text{I}}}{m}, \qquad m\dot{\theta} = \frac{m_{\text{R}}\dot{m}_{\text{I}} - m_{\text{I}}\dot{m}_{\text{R}}}{m} = \frac{m_{\text{R}}^2}{m}\partial_t\Big(\frac{m_{\text{I}}}{m_{\text{R}}}\Big). \tag{5.10}$$

Using equations (5.4), (5.5) and (5.8)–(5.10) it can be verified after a lengthy but entirely straightforward calculation that equations (5.6) and (5.7) exactly reproduce the cQPA equations given in [I].

5.1.2 The mass profile

So far we have considered a general complex mass $m_c(t)$. We now choose the following tanh-profile which was used in [I]:

$$m_c(t) = m_1 + m_2 \tanh\left(-\frac{t}{\tau_w}\right). \tag{5.11}$$

This is a time-dependent analogue of the simplified tanh-profile [141, 142] for the bubble wall shape in a first order EWPT. For this reason we refer to the parameter τ_w, which describes the duration of the transition, simply as the wall width. The specific profile (5.11) was chosen because in the free theory exact analytic solutions for the fermion mode functions are then available [139]. It also serves as a toy-model for EWBG as it features CP-violation when m_1 and m_2 are complex.

The physical CP-violation arises from the relative complex phase of the parameters m_1 and m_2 in equation (5.11). To simplify the equations we assume that a global U(1) transformation of the chiral fermion fields has been performed which makes m_2 real [139]. Hence, we can assume with no loss of generality that $m_1 = m_{1R} + \mathrm{i}m_{1I}$ and $m_2 = m_{2R}$ with constant real parameters m_{1R}, m_{1I}, m_{2R}. Using the definition (5.9), this implies that

$$m_R(t) = m_{1R} + m_{2R} \tanh\left(-\frac{t}{\tau_w}\right), \tag{5.12a}$$

$$m_I(t) = m_{1I}. \tag{5.12b}$$

The identities (5.10) are now also simplified as the terms with $\dot{m}_I$ are dropped.

5.1.3 Axial charge density with interactions

Now we show an example calculation of the axial charge density evolution using cQPA with decohering interactions. The numerical results were calculated in [I]. The spatial Fourier transform of the axial charge density (5.2), calculated with the cQPA propagator, turns out to be[23]

$$j^{05}_{\boldsymbol{k}} = \sum_{h,s} \frac{h}{\omega_{\boldsymbol{k}}} \left(|\boldsymbol{k}| f^{m,s}_{\boldsymbol{k}h} - m f^{c,s}_{\boldsymbol{k}h} \right). \tag{5.13}$$

We can now see that this density is non-vanishing (and there is CP-violation) only if there is a helicity asymmetry in $f^{m(c)}_{\boldsymbol{k}h}$. Furthermore, from the form of equations (5.6) we saw that there will generically be helicity asymmetry, even in the free theory, as long as $\dot{\theta} \neq 0$. These features are not as transparent in the complex mass basis as presented in [I]. However, physical results for the current are of course the same in both conventions.

[23] The chiral transformation Y is not a symmetry of the Lagrangian so the current here is calculated in the original basis using $j^{05}_{\boldsymbol{k}} = \mathrm{tr}[\gamma^5 Y^\dagger \overline{S}^<_{\boldsymbol{k}}(t,t) Y]$. Equation (5.13) also has a corrected sign compared to [I], which affects the figures but has no effect on the main results.

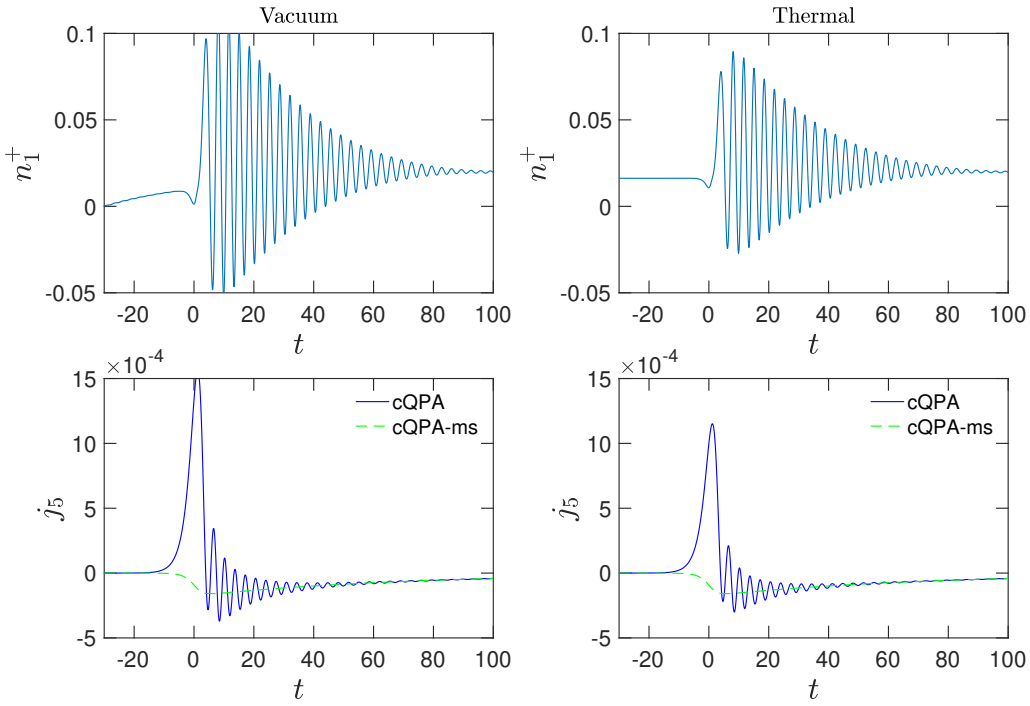

Figure 2. Time-evolution of the number density n_+^+ of positive helicity particles (top) and the axial charge density j^{05} (bottom) from interacting single-flavor cQPA with vacuum and thermal initial conditions. Mass profile (5.12) with parameters $m_{1\mathrm{R}} = 0.1$, $m_{2\mathrm{R}} = 1$, $m_{\mathrm{I}} = 0.1$ and $\tau_{\mathrm{w}} = 5$ was used. The green dashed line shows the result with only the mass-shell contribution throughout the evolution. Adapted from article [I] (CC BY 4.0), with corrected sign for j_5.

In figure 2 we show the results for the evolution of the total particle number density $n_+^+ \equiv \int \mathrm{d}^3\boldsymbol{k}/(2\pi)^3 n_{\boldsymbol{k}+}^+$ for particles ($s = +1$) of positive helicity and the total axial charge density $j^{05} = \int \mathrm{d}^3\boldsymbol{k}/(2\pi)^3 j_{\boldsymbol{k}}^{05}$ calculated from (5.13). Here we defined the phase space number densities as $n_{\boldsymbol{k}h}^+ \equiv f_{\boldsymbol{k}h}^{m,+}$ and $n_{\boldsymbol{k}h}^- \equiv 1 + f_{\boldsymbol{k}h}^{m,-}$ and the distribution functions $f_{\boldsymbol{k}h}^{m,s}$ obey the cQPA equations (5.6). As a simple example to demonstrate CP-violation and decoherence we used in the figure a chiral interaction with the following toy-model thermal equilibrium self-energy:

$$\begin{aligned} \overline{\Sigma}^{\mathcal{A}}_{\mathrm{eq}}(k) &= a(k^0, |\boldsymbol{k}|)\, \not{k} P_{\mathrm{L}} \gamma^0, \\ \overline{\Sigma}^{<}_{\mathrm{eq}}(k) &= 2\overline{\Sigma}^{\mathcal{A}}_{\mathrm{eq}}(k) f_{\mathrm{FD}}(k^0), \end{aligned} \qquad \left(\text{with} \quad \begin{aligned} a(\pm k^0, |\boldsymbol{k}|) &= \pm a(k^0, |\boldsymbol{k}|), \\ a(\omega_{\boldsymbol{k}}, |\boldsymbol{k}|) &= 0.03. \end{aligned} \right) \tag{5.14}$$

In the left panels of figure 2 we used the vacuum initial conditions $n_{\boldsymbol{k}h}^s = 0 = f_{\boldsymbol{k}h}^{c,s}$. The number density first begins to smoothly thermalize due to the interactions. In the transition region (centered around $t = 0$) it then starts oscillating rapidly due to the coherence that develops from the changing mass. The coherent oscillations also generate helicity asymmetry because of the CP-violating phase θ, and this leads to the generation of the axial charge. The chiral interaction is also responsible for

generating helicity asymmetry. This can be seen from the green dashed line where the f^c-functions have been artificially turned off. In this case the only source for helicity asymmetry is in the collision term. The decohering collisions also cause the rapid damping of the oscillations after the transition region. However, even without collisions the oscillations in these $\boldsymbol{k}$-integrated quantities would be damped (although not as strongly) because of the phase differences between different $\boldsymbol{k}$-modes [I]. In the right panels we show the same calculations with thermal initial conditions $n^s_{\boldsymbol{k}h} = f_{\rm FD}(\omega_{\boldsymbol{k}})$, $f^{c,s}_{\boldsymbol{k}h} = 0$. The results are similar but now the particle number stays initially at the thermal value. The final thermalized particle number is slightly higher than initially because the equilibrium distribution changes across the mass transition. We used units where $T = 1$ in all plots here.

5.1.4 Exact solution of the Dirac equation

We now turn to the analysis of the free theory. One of the main results of [I] is the independent demonstration of the shell structure, in particular the coherence shell at $k^0 = 0$, for the exact Wightman function without using cQPA. This is based on the exact mode function solutions of the free Dirac equation where the mass is a non-trivial function of time [139]. Specifically, we use the mass profile given by equation (5.11). We summarize here the most relevant steps and present the results. More details can be found in [I].

Mode function equations

We start with the canonical quantization of the fermion field operator $\hat{\psi}$. In a spatially homogeneous and isotropic system the field operator can be expanded using the mode functions and ladder operators as

$$\hat{\psi}(t,\boldsymbol{x}) = \sum_h \int \frac{\mathrm{d}^3\boldsymbol{k}}{(2\pi)^3 2\omega_-}\Big[\hat{a}_{\boldsymbol{k}h}U_{\boldsymbol{k}h}(t)\,\mathrm{e}^{\mathrm{i}\boldsymbol{k}\cdot\boldsymbol{x}} + \hat{b}^\dagger_{\boldsymbol{k}h}V_{\boldsymbol{k}h}(t)\,\mathrm{e}^{-\mathrm{i}\boldsymbol{k}\cdot\boldsymbol{x}}\Big]. \tag{5.15}$$

Here $2\omega_-$ is a normalization factor and we denote $\omega_\pm \equiv \omega_{\boldsymbol{k}}(t \to \pm\infty)$. We impose the standard canonical anticommutation relations for the field. We use the chiral representation of gamma matrices and decompose the particle and antiparticle spinors $U_{\boldsymbol{k}h}$ and $V_{\boldsymbol{k}h}$ as[24]

$$U_{\boldsymbol{k}h}(t) = \begin{bmatrix}\eta_{\boldsymbol{k}h}(t)\\ \zeta_{\boldsymbol{k}h}(t)\end{bmatrix}\otimes\xi_{\boldsymbol{k}h}, \qquad V_{\boldsymbol{k}h}(t) = \begin{bmatrix}\bar{\eta}_{\boldsymbol{k}h}(t)\\ \bar{\zeta}_{\boldsymbol{k}h}(t)\end{bmatrix}\otimes\xi_{\boldsymbol{k}h}. \tag{5.16}$$

Here $\otimes$ is the Kronecker product and $\xi_{\boldsymbol{k}h}$ are the helicity eigenfunctions ($h = \pm 1$) which satisfy $(\boldsymbol{\sigma}\cdot\hat{\boldsymbol{k}})\xi_{\boldsymbol{k}h} = h\xi_{\boldsymbol{k}h}$, where further $\boldsymbol{\sigma} \equiv (\sigma_1,\sigma_2,\sigma_3)$ and σ_i are the

[24] We use the chiral representation defined e.g. in [112] where $\gamma^5 = \mathrm{diag}(-\mathbf{1}_2, \mathbf{1}_2)$.

standard 2×2 Pauli matrices [112]. From the Dirac equation corresponding to the Lagrangian (5.3) it follows that the complex *mode functions* $\eta_{\boldsymbol{k}h}$ and $\zeta_{\boldsymbol{k}h}$ satisfy

$$\mathrm{i}\partial_t \eta_{\boldsymbol{k}h} + h|\boldsymbol{k}|\eta_{\boldsymbol{k}h} = m_\mathrm{c}(t)\zeta_{\boldsymbol{k}h}, \tag{5.17a}$$

$$\mathrm{i}\partial_t \zeta_{\boldsymbol{k}h} - h|\boldsymbol{k}|\zeta_{\boldsymbol{k}h} = m_\mathrm{c}^*(t)\eta_{\boldsymbol{k}h}. \tag{5.17b}$$

The complex mass $m_\mathrm{c}(t)$ is still general in these equations. The antiparticle mode functions $\bar{\eta}_{\boldsymbol{k}h}$ and $\bar{\zeta}_{\boldsymbol{k}h}$ satisfy equations analogous to (5.17) with the replacements $h \to -h$ and $m_\mathrm{c} \to -m_\mathrm{c}^*$.

It turns out that for the mass profile (5.12) the equations (5.17) can be transformed to the hypergeometric differential equation [139]. The solutions can then be written in terms of Gauss's hypergeometric functions ${}_2F_1$. There are two linearly independent solutions and for the numerical results we choose the one which corresponds to positive frequency particles (in vacuum) in the initial state [I]. The *initial* values for the particle mode functions are then fixed to

$$\eta_{\boldsymbol{k}h} = \sqrt{\omega_{\boldsymbol{k}} - h|\boldsymbol{k}|}\,\mathrm{e}^{-\mathrm{i}t\omega_{\boldsymbol{k}}}, \qquad \zeta_{\boldsymbol{k}h} = \sqrt{\omega_{\boldsymbol{k}} + h|\boldsymbol{k}|}\,\mathrm{e}^{-\mathrm{i}\theta}\,\mathrm{e}^{-\mathrm{i}t\omega_{\boldsymbol{k}}}, \tag{5.18}$$

where all time-dependent quantities are evaluated at $t \to -\infty$.

Wightman functions from mode functions

We can now construct the exact Wightman functions $S^{<,>}$, defined in equations (3.25), for this system from the vacuum expectation values of field operators by using (5.15). The different Wightman functions contain equivalent statistical information so either one suffices for the analysis here. We choose $S^>$ as it is constructed from the particle mode functions $\eta_{\boldsymbol{k}h}$ and $\zeta_{\boldsymbol{k}h}$. By using the properties of the ladder operators and the decomposition (5.16) of the spinors we can express the Wightman function $S^>$ in the two-time representation (3.54) as

$$\overline{S}^>_{\boldsymbol{k}}(t_1, t_2) = \sum_h M_{\boldsymbol{k}h}(t_1, t_2) \otimes P^{(2)}_{\boldsymbol{k}h}, \tag{5.19}$$

where

$$M_{\boldsymbol{k}h}(t_1, t_2) \equiv \frac{1}{2\omega_-} \begin{bmatrix} \eta_{\boldsymbol{k}h}(t_1)\eta^*_{\boldsymbol{k}h}(t_2) & \eta_{\boldsymbol{k}h}(t_1)\zeta^*_{\boldsymbol{k}h}(t_2) \\ \zeta_{\boldsymbol{k}h}(t_1)\eta^*_{\boldsymbol{k}h}(t_2) & \zeta_{\boldsymbol{k}h}(t_1)\zeta^*_{\boldsymbol{k}h}(t_2) \end{bmatrix}. \tag{5.20}$$

The two-dimensional helicity projection matrix is defined by $P^{(2)}_{\boldsymbol{k}h} \equiv \frac{1}{2}(\mathbf{1} + h\boldsymbol{\sigma}\cdot\hat{\boldsymbol{k}})$.

Now that we have equations (5.19) and (5.20) we can also easily calculate quantum currents from the mode functions. For example the axial charge density $j^{05}_{\boldsymbol{k}}$ which we considered before is given by

$$j^{05}_{\boldsymbol{k}}(t) = \frac{1}{2\omega_-} \sum_h \big(|\eta_{\boldsymbol{k}h}(t)|^2 - |\zeta_{\boldsymbol{k}h}(t)|^2\big). \tag{5.21}$$

To get this result we used the sum rule (3.58) in the form $(\overline{S}^>_{\boldsymbol{k}} + \overline{S}^<_{\boldsymbol{k}})(t,t) = \mathbf{1}$ to write the current in terms of $S^>$: $j^{05}_{\boldsymbol{k}} = \mathrm{tr}[\gamma^5 \overline{S}^<_{\boldsymbol{k}}(t,t)] = -\,\mathrm{tr}[\gamma^5 \overline{S}^>_{\boldsymbol{k}}(t,t)]$.

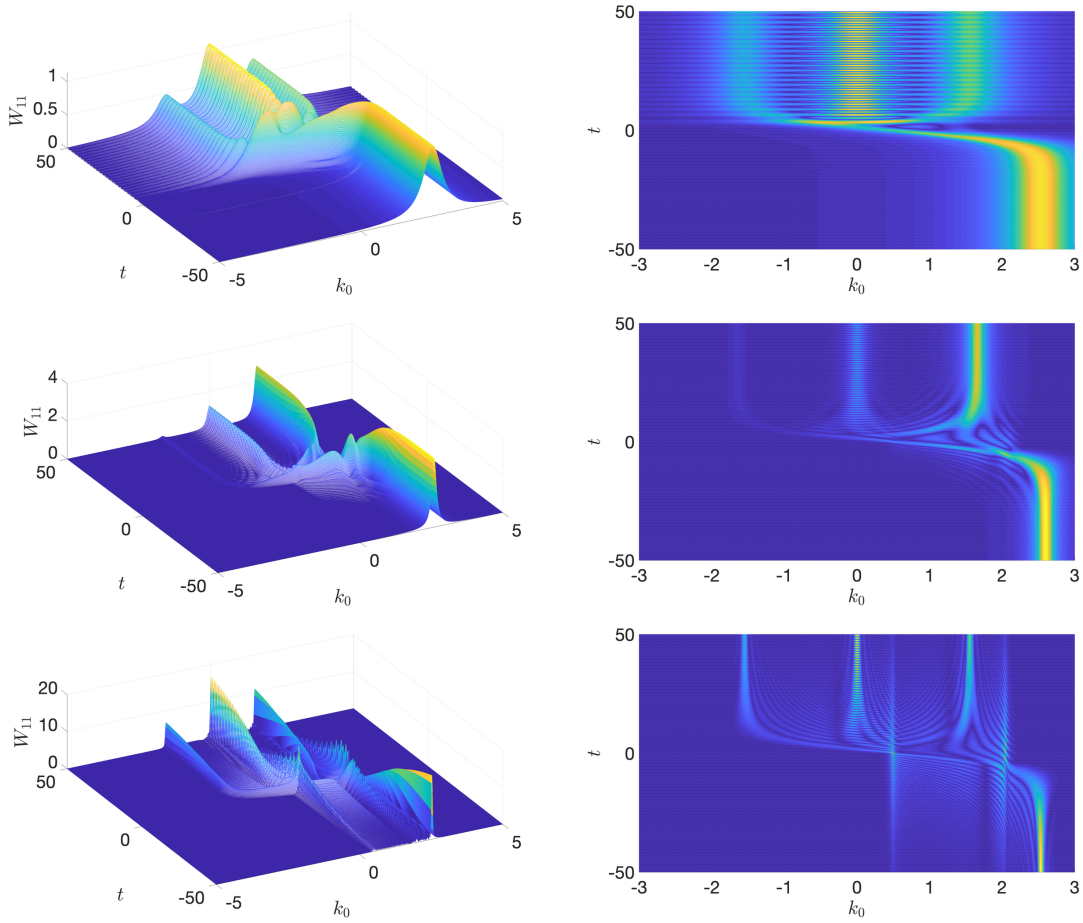

Figure 3. Phase space structure of the exact free Wightman function $S^>$. Shown is $\left|W^{(11)}_{\boldsymbol{k}h,\Gamma}\right|$ as a function of (k^0, t) for $h = +1$. The three pairs of plots have $|\boldsymbol{k}| = 0.4, 0.7, 0.4$ and $\Gamma_{\boldsymbol{k}} = 0.4, 0.1, 0.02$ from top to bottom, respectively. We used the mass profile (5.12) with $m_{1\mathrm{R}} = 0.5$, $m_{2\mathrm{R}} = 2$, $m_{\mathrm{I}} = -0.005$, $\tau_{\mathrm{w}} = 5$. From article [I] (CC BY 4.0).

Phase space structure

To study the phase space structure of the Wightman function we need to calculate the Wigner transform $\overline{S}^>(k, t)$ of (5.19) by using equations (3.46) and (3.55). However, with free particle mode functions the Wightman function (5.19) contains correlations over arbitrarily large time intervals. This is a physical result, but it also makes the Wigner transform divergent here. In a realistic system there would be interactions which would suppress the faraway correlations. We take this into account heuristically by adding a parametric *damping rate* $\Gamma_{\boldsymbol{k}h}$ and use the Wigner transform [I]

$$\overline{S}^>_\Gamma(k, t) \equiv \sum_h W_{\boldsymbol{k}h,\Gamma}(k^0, t) \otimes P^{(2)}_{\boldsymbol{k}h}, \tag{5.22a}$$

$$W_{\boldsymbol{k}h,\Gamma}(k^0, t) \equiv \int_{-\infty}^{\infty} \mathrm{d}r^0 \, \mathrm{e}^{\mathrm{i}k^0 r^0 - \Gamma_{\boldsymbol{k}h}|r^0|} \, M_{\boldsymbol{k}h}\big(t + \tfrac{r^0}{2}, t - \tfrac{r^0}{2}\big). \tag{5.22b}$$

The form of the damping factor $\mathrm{e}^{-\Gamma_{\boldsymbol{k}h}|r^0|}$ in equation (5.22b) is not arbitrary: it would result from a leading order calculation when taking the shifted poles of the interacting function into account [I]. Setting here $\Gamma_{\boldsymbol{k}h} = 0$ recovers the usual Wigner transform of (5.19).

In figure 3 we show the numerical results of the calculation of the absolute value of the $(1,1)$-component of $W_{\boldsymbol{k}h,\Gamma}$ [i.e. the component $\propto \eta\,\eta^*$ in (5.20)]. The other chiral components are qualitatively similar. The mode functions were calculated using the hypergeometric functions with the initial conditions (5.18) and these solutions were then used in equations (5.20) and (5.22b). The plots illustrate the phase space structure for varying momentum $|\boldsymbol{k}|$ and damping $\Gamma_{\boldsymbol{k}h}$. The results verify the shell structure predicted by cQPA, albeit the shells are smeared for larger Γ, as expected. The initial state particle is described by only the mass shell and the mass transition then develops coherence and creates particles and antiparticles at their respective shells (see table 1). The results also show the emergence of additional structures in the transition area and two new long-range shells in the limit of small Γ. These new structures are suppressed for larger Γ and the shell picture of cQPA remains valid even for moderately large values of Γ, however. A more thorough analysis of the additional shells and other features of these results is presented in [I].

Connection to cQPA

We now present a direct connection between the exact mode functions and cQPA in the free theory, which was not explicitly given in [I]. This can be done similarly to how we calculated the axial charge density (5.21) from the mode functions. The mode functions and the cQPA distribution functions can be related via the equal-time Wightman function. The connecting relation is

$$\sum_h M_{\boldsymbol{k}h}(t,t) \otimes P^{(2)}_{\boldsymbol{k}h} = \mathbf{1} - \sum_{h,s} Y^\dagger \big(f^{m,s}_{\boldsymbol{k}h} \mathcal{P}^{m,s}_{\boldsymbol{k}h} + f^{c,s}_{\boldsymbol{k}h} \mathcal{P}^{c,s}_{\boldsymbol{k}h} \big) Y, \tag{5.23}$$

where we also took into account the chiral transformation $Y = \mathrm{e}^{\mathrm{i}\frac{\theta}{2}\gamma^5}$. Writing here the four-dimensional projection matrices (4.2b) in the chiral representation and taking projections and traces of the equation eventually yields the explicit relations

$$f^{m,s}_{\boldsymbol{k}h} = s - \frac{1}{2}\Big[\big(s - \tfrac{h|\boldsymbol{k}|}{\omega_{\boldsymbol{k}}}\big) M^{(11)}_{\boldsymbol{k}h} + \big(s + \tfrac{h|\boldsymbol{k}|}{\omega_{\boldsymbol{k}}}\big) M^{(22)}_{\boldsymbol{k}h} + \tfrac{m_{\mathrm{c}}^*}{\omega_{\boldsymbol{k}}} M^{(12)}_{\boldsymbol{k}h} + \tfrac{m_{\mathrm{c}}}{\omega_{\boldsymbol{k}}} M^{(21)}_{\boldsymbol{k}h} \Big], \tag{5.24a}$$

$$f^{c,s}_{\boldsymbol{k}h} = -\frac{h}{2}\Big[\tfrac{m}{\omega_{\boldsymbol{k}}} \big(M^{(11)}_{\boldsymbol{k}h} - M^{(22)}_{\boldsymbol{k}h}\big) - \tfrac{m_{\mathrm{c}}^*}{m} \big(s - \tfrac{h|\boldsymbol{k}|}{\omega_{\boldsymbol{k}}}\big) M^{(12)}_{\boldsymbol{k}h} + \tfrac{m_{\mathrm{c}}}{m} \big(s + \tfrac{h|\boldsymbol{k}|}{\omega_{\boldsymbol{k}}}\big) M^{(21)}_{\boldsymbol{k}h} \Big]. \tag{5.24b}$$

Here $M^{(ij)}_{\boldsymbol{k}h}$ denotes the (i,j)-component of the mode function matrix $M_{\boldsymbol{k}h}(t,t)$. Equations (5.24) can also be inverted, for a given helicity h, to give the four different components $M^{(ij)}_{\boldsymbol{k}h}$ in terms of $f^{m,+}_{\boldsymbol{k}h}$, $f^{m,-}_{\boldsymbol{k}h}$ and $f^{c,+}_{\boldsymbol{k}h}$, $f^{c,-}_{\boldsymbol{k}h}$.

We have thus established that the cQPA phase space distribution functions $f^{m,s}_{\boldsymbol{k}h}$, $f^{c,s}_{\boldsymbol{k}h}$ are in a one-to-one correspondence to the components of the *equal-time* mode function matrix $M_{\boldsymbol{k}h}(t,t)$. We can go even further and actually derive the free cQPA equations of motion from the mode function equations. We just need to differentiate both sides of equations (5.24), use the mode function equations (5.17) with (5.20) and finally use the inverted form of equations (5.24) to eliminate the mode functions in the end. These steps reproduce exactly the single-flavor cQPA equations (5.6) without the collision term. Of course, this connection is ultimately not very surprising because the free cQPA and the mode functions are both based on the same Dirac equation. Nevertheless, it works as a consistency check and it is another verification for cQPA.

5.1.5 Comparison to the semiclassical approximation

Lastly, we compare the cQPA to the semiclassical method by calculating the axial charge density $j^{05}_{\boldsymbol{k}}$ numerically with both methods in the free theory. As we showed above, cQPA is exact in the free theory when calculating local quantities such as the currents. The results thus show how well the semiclassical method works outside its expected validity region $|\boldsymbol{k}|\tau_{\mathrm{w}} \gg 1$.

We consider here the method of semiclassical force (see [133] for a recent outline and more references) which is based on a gradient approximation of the KB equations. It was first formulated in the planar case in [47, 143–146] and later adapted to the time-dependent case in [139]. The general result for the axial charge density in this method is [I, 139]

$$j^{05}_{\boldsymbol{k}} = \sum_h \frac{\omega_- f^-_{3\boldsymbol{k}h}}{\omega_{3\boldsymbol{k}h}}, \qquad \omega_{3\boldsymbol{k}h} \equiv \omega_{\boldsymbol{k}} + h\frac{m^2\dot{\theta}}{2|\boldsymbol{k}|\omega_{\boldsymbol{k}}}, \tag{5.25}$$

where $\omega_{3\boldsymbol{k}h}$ is the shifted energy and $f^-_{3\boldsymbol{k}h} \equiv \lim_{t\to-\infty} \mathrm{tr}[\gamma^5 P_{\boldsymbol{k}h}\overline{S}^<_{\boldsymbol{k}}(t,t)]$ denotes the initial value of the helicity-projected axial charge density. The value which corresponds to the vacuum initial conditions used in figure 2, and equation (5.18), is

$$f^-_{3\boldsymbol{k}h} = -\frac{h|\boldsymbol{k}|}{\omega_-}. \tag{5.26}$$

The validity of the result (5.25) requires that $|m^2\dot{\theta}/(2|\boldsymbol{k}|\omega^2_{\boldsymbol{k}})| \ll 1$. Using this assumption and the initial condition (5.26) we can estimate

$$j^{05}_{\boldsymbol{k}} \simeq \frac{m^2\dot{\theta}}{\omega^3_{\boldsymbol{k}}}. \tag{5.27}$$

This is the expression that is used in the numerical comparison below. Note that the signs in equations (5.26) and (5.27) are corrected here when compared to [I] (similarly to equation (5.13); see footnote 23). This again has no effect on the conclusions.

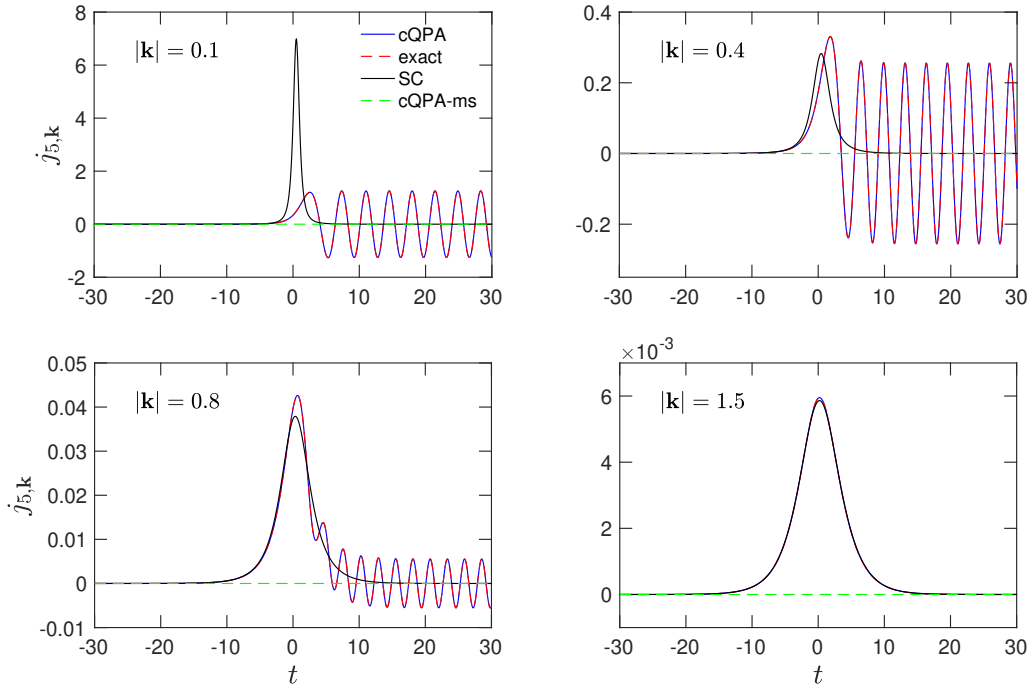

Figure 4. Time-evolution of different modes of the axial charge density $j^{05}_{\boldsymbol{k}}$ in free theory, calculated using single-flavor cQPA (blue line) and the semiclassical method (black line). We used vacuum initial conditions and the same mass profile parameters as in figure 2. Adapted from article [I] (CC BY 4.0), with corrected sign for j_5.

In figure 4 we show the results for the axial charge density $j^{05}_{\boldsymbol{k}}$ for varying modes $|\boldsymbol{k}|$ calculated from free cQPA using equation (5.13) and the semiclassical method using equation (5.27). We used again the mass profile given by equations (5.12). We also displayed the exact result (red dashed line) calculated from the mode functions which exactly matches the cQPA result as discussed earlier. In the free case the axial charge density is induced purely by coherence since the cQPA result vanishes when the coherence-functions are switched off (green dashed line). This is as expected from the forms of equations (5.6) and (5.13). The semiclassical result captures well the average of the oscillating current even for modes as small as $|\boldsymbol{k}|\tau_{\mathrm{w}} \approx 2$ but it misses the coherent oscillations outside the transition region. For larger modes there is virtually no difference between the semiclassical and the exact result. Also, the top-left panel in figure 4 (with $|\boldsymbol{k}|\tau_{\mathrm{w}} = 0.5$) is very far outside the validity region of the semiclassical approximation and the large spike in the result is entirely spurious and sensitive to the expression used for $j^{05}_{\boldsymbol{k}}$.

5.2 Resonant leptogenesis

In this section we apply the LA-method to resonant leptogenesis (RL), focusing on the details of the CP-asymmetry generation and evolution. We summarize the main results of the analysis done in [II] and also provide some supplementary results. The LA-method is well-suited for studying RL because the form of the propagator is not restricted in this approach. Hence the method captures the coherent flavor oscillations during the decays of the Majorana neutrinos which dominate the generation of the lepton asymmetry in the RL case. Because of this we only consider the one-loop self-energies as they are sufficient for capturing the decay and inverse decay processes of leptogenesis. In this case we can use our first order local transport equation (4.36), or the equivalent equations (4.39), to describe the Majorana neutrinos. There is also no RIS-problem because the LA-method is based on the KB equations derived from first principles in the CTP formalism.

In the SM sector we do a number of simplifications to reduce the complexity of the problem to a more manageable level. We assume that the SM lepton and Higgs fields are in kinetic equilibrium because of the electroweak gauge interactions, which are comparatively strong at the high temperature scale relevant for leptogenesis. We also neglect their decay widths and dispersive corrections and use tree level equilibrium forms for their propagators. Furthermore, we neglect the chemical potential of the Higgs field and assume a small lepton chemical potential so that its backreaction can be neglected in the Majorana neutrino equations. We also focus on the one-flavor approximation of leptogenesis where the Majorana neutrinos effectively couple to only one linear combination of the SM lepton flavors.

5.2.1 The minimal leptogenesis model

We consider the minimal leptogenesis model with two singlet Majorana neutrino fields N_i $(i = 1, 2)$ and one lepton doublet $\ell = (\ell_1, \ell_2)$ which represents the SM leptons (one-flavor approximation). These are coupled to the SM Higgs doublet $\phi = (\phi_1, \phi_2)$ via chiral Yukawa interactions. The Lagrangian is

$$\mathcal{L} = \frac{1}{2}\overline{N}_i(\mathrm{i}\partial\!\!\!/ - m_i)N_i + \bar{\ell}\,\mathrm{i}\partial\!\!\!/\,\ell + (\partial_\mu\phi^\dagger)(\partial^\mu\phi) - \Big(y_i^*(\bar{\ell}\widetilde{\phi})P_\mathrm{R}N_i + \mathrm{H.c.}\Big), \tag{5.28}$$

with an implicit summation over the neutrino flavor i. The complex Yukawa couplings are denoted by y_i and the SU(2)-conjugate Higgs doublet is $\widetilde{\phi} \equiv \mathrm{i}\sigma_2\phi^*$. We assume the mass eigenbasis of the neutrinos where m_i are the real Majorana masses. The neutrino fields satisfy the Majorana condition

$$N_i = N_i^c \equiv C\overline{N}_i^\mathsf{T}, \tag{5.29}$$

where C is the unitary charge conjugation matrix defined by $C(\gamma^\mu)^\mathsf{T}C^{-1} = -\gamma^\mu$.[25]

[25] It then follows that $C^\mathsf{T} = -C$, regardless of the used Dirac matrix representation [147].

Propagators and self-energies

We denote the CTP propagators of the neutrino, lepton and Higgs fields [in the contour notation defined in (3.24)] as

$$\mathrm{i}S_{ij}(x,y) \equiv \big\langle \mathcal{T}_\mathcal{C}\big[N_i(x)\overline{N}_j(y)\big]\big\rangle, \tag{5.30a}$$
$$\mathrm{i}S_{\ell,AB}(x,y) \equiv \big\langle \mathcal{T}_\mathcal{C}\big[\ell_A(x)\overline{\ell_B}(y)\big]\big\rangle, \tag{5.30b}$$
$$\mathrm{i}\Delta_{AB}(x,y) \equiv \big\langle \mathcal{T}_\mathcal{C}\big[\phi_A(x)\phi_B^\dagger(y)\big]\big\rangle, \tag{5.30c}$$

where $A, B = 1, 2$ are the SU(2)-doublet indices. We assume the SU(2)-symmetric phase where [75]

$$S_{\ell,AB}(x,y) \equiv S_\ell(x,y)\delta_{AB}, \tag{5.31a}$$
$$\Delta_{AB}(x,y) \equiv \Delta(x,y)\delta_{AB}. \tag{5.31b}$$

In the following we write the formulae and equations directly for the SU(2)-diagonal elements S_ℓ and Δ.

We calculate the CTP self-energies for this model using the 2PI effective action method introduced in section 3.2.1. We consider the two-loop truncation of Γ_2 which, for the Lagrangian (5.28), can be written in the contour notation as

$$\mathrm{i}\Gamma_2^{(2)} = c_\mathrm{w}\sum_{i,j} y_i^* y_j \iint_\mathcal{C} \mathrm{d}^4x\,\mathrm{d}^4y\,\mathrm{tr}\big[P_\mathrm{R}\mathrm{i}S_{ij}(x,y)P_\mathrm{L}\mathrm{i}S_\ell(y,x)\big]\mathrm{i}\Delta(y,x). \tag{5.32}$$

Equations (5.31) were used here to perform the sums over the SU(2)-indices resulting in the multiplicity factor $c_\mathrm{w} = 2$. The neutrino and lepton one-loop self-energies are calculated by using the functional derivative formula (3.33a). The results are [II]

$$\begin{aligned}\mathrm{i}\Sigma_{ij}(x,y) = c_\mathrm{w}\Big[&y_i y_j^* P_\mathrm{L}\mathrm{i}S_\ell(x,y)P_\mathrm{R}\mathrm{i}\Delta(x,y)\\ &+ y_i^* y_j P_\mathrm{R} C\mathrm{i}S_\ell(y,x)^\mathsf{T} C^{-1}P_\mathrm{L}\mathrm{i}\Delta(y,x)\Big],\end{aligned} \tag{5.33a}$$
$$\mathrm{i}\Sigma_\ell(x,y) = \sum_{i,j} y_i^* y_j P_\mathrm{R}\mathrm{i}S_{ij}(x,y)P_\mathrm{L}\mathrm{i}\Delta(y,x). \tag{5.33b}$$

The real-time self-energies can be obtained by inserting the CTP indices which simply follow the spacetime arguments x, y in equations (5.33). At this point we also introduce the tree-level kinetic equilibrium ansätze for the lepton and Higgs propagators so that the self-energies can be calculated explicitly. These are defined in the Wigner representation where the Wightman functions are [II]

$$\mathrm{i}S_\ell^\lessgtr(k,t) = 2\pi\,\mathrm{sgn}(k^0)P_\mathrm{L}\not{k}\,\delta(k^2)\,f_\mathrm{FD}\big(\pm(k^0-\mu_\ell)\big), \tag{5.34a}$$
$$\mathrm{i}\Delta^\lessgtr(k) = \pm 2\pi\,\mathrm{sgn}(k^0)\,\delta(k^2)\,f_\mathrm{BE}(\pm k^0) \equiv \mathrm{i}\Delta_\mathrm{eq}^\lessgtr(k). \tag{5.34b}$$

The equilibrium distributions $f_{\rm FD}$ and $f_{\rm BE}$ were defined below equations (3.53). The other real-time propagators can be recovered from (5.34) by using the general relations (3.30). In equations (5.34) μ_ℓ denotes the chemical potential of the leptons while the Higgs propagator has the thermal equilibrium form with zero chemical potential. The lepton propagator can be split into the thermal equilibrium part and the deviation,

$$S_\ell^{<,>}(k,t) \equiv S_{\ell,\rm eq}^{<,>}(k) + \delta S_\ell^{<,>}(k,t), \tag{5.35}$$

where the equilibrium part is defined by equation (5.34a) with $\mu_\ell = 0$. The one-loop self-energies can then be calculated explicitly as functions of k, T and μ_ℓ in the Wigner representation. In particular, the Majorana neutrino self-energy (5.33a) can be divided similarly to the thermal equilibrium part $\Sigma_{\rm eq}(k)$ and the deviation $\delta\Sigma(k,t)$. The needed self-energy components can be written as [II]

$$\Sigma^{\mathcal{A}}_{{\rm eq},ij}(k) = c_{\rm w}\big(y_i y_j^* P_{\rm L} + y_i^* y_j P_{\rm R}\big)\mathfrak{S}^{\mathcal{A}}_{\rm eq}(k), \tag{5.36a}$$

$$\Sigma^{{\rm H}(T)}_{{\rm eq},ij}(k) = c_{\rm w}\big(y_i y_j^* P_{\rm L} + y_i^* y_j P_{\rm R}\big)\mathfrak{S}^{{\rm H}(T)}_{\rm eq}(k), \tag{5.36b}$$

$$\mathrm{i}\delta\Sigma_{ij}^{<,>}(k,t) = c_{\rm w}\big(y_i y_j^* P_{\rm L} - y_i^* y_j P_{\rm R}\big)\delta\mathfrak{S}^{<,>}(k)\,\beta\mu_\ell. \tag{5.36c}$$

Explicit expressions for the different self-energy functions $\mathfrak{S}_{{\rm eq},\mu}$ and $\delta\mathfrak{S}_\mu$ are given in [II]. Note that we assume that the lepton asymmetry and hence the chemical potential μ_ℓ are small so we have expanded the deviations $\delta\Sigma$ to first order in $\beta\mu_\ell$.

5.2.2 Lepton asymmetry

The left chiral lepton asymmetry is related to the chiral current density of the SM lepton doublet, which can be defined generally as

$$j^\mu_{{\rm L},\ell}(x) \equiv \big\langle \bar{\ell}_A(x)\gamma^\mu P_{\rm L}\ell_A(x)\big\rangle. \tag{5.37}$$

Here an implicit summation over the SU(2)-index $A = 1, 2$ is understood. In this work we define the the *lepton asymmetry density* n_L as the non-equilibrium part of (the zeroth component of) the current (5.37): [II]

$$n_L \equiv \delta j^0_{{\rm L},\ell}(t) = c_{\rm w}\int \frac{\mathrm{d}^3\boldsymbol{k}}{(2\pi)^3}\,\mathrm{tr}\Big[P_{\rm L}\delta\overline{S}^{<}_{\ell,\boldsymbol{k}}(t,t)\Big]. \tag{5.38}$$

The relation to the chemical potential μ_ℓ is then given by the standard formula [6]

$$n_L = \frac{c_{\rm w}T^3}{6\pi^2}\left[\pi^2\Big(\frac{\mu_\ell}{T}\Big) + \Big(\frac{\mu_\ell}{T}\Big)^3\right] \simeq \frac{c_{\rm w}T^3}{6}\Big(\frac{\mu_\ell}{T}\Big), \tag{5.39}$$

once the free equilibrium form (5.34a) with (5.35) is used for the propagator.

The equation of motion for n_L can be derived from the equation of the lepton propagator S_ℓ via equations (5.35) and (5.38). For S_ℓ we use the KB equation (3.44c)

where we omit the terms with S^{H} and Σ^{H} on the left-hand side, because we neglect the width and dispersive corrections for the leptons. The evolution equation for the lepton asymmetry then is

$$\partial_t n_L = -\frac{c_{\mathrm{w}}}{2}\int \frac{\mathrm{d}^3\boldsymbol{k}}{(2\pi)^3}\,\mathrm{tr}\Big[\big(\overline{\Sigma}^{>}_{\ell,\boldsymbol{k}} * \overline{S}^{<}_{\ell,\boldsymbol{k}} - \overline{\Sigma}^{<}_{\ell,\boldsymbol{k}} * \overline{S}^{>}_{\ell,\boldsymbol{k}}\big)(t,t)\Big] + \mathrm{H.c.} \tag{5.40}$$

where Σ_ℓ is the lepton self-energy. Next we use the relations between the self-energies (5.33) to write the lepton collision term on the right-hand side of (5.40) in terms of the Majorana neutrino collision term [II]. This is possible because we are calculating a quantity that is local and diagonal in all indices. The result is

$$\partial_t n_L = \frac{1}{2}\int \frac{\mathrm{d}^3\boldsymbol{k}}{(2\pi)^3}\,\mathrm{Tr}\Big[P_{\mathrm{R}}\big(\overline{\Sigma}^{>}_{\boldsymbol{k}} * \overline{S}^{<}_{\boldsymbol{k}} - \overline{\Sigma}^{<}_{\boldsymbol{k}} * \overline{S}^{>}_{\boldsymbol{k}}\big)(t,t)\Big] + \mathrm{H.c.} \tag{5.41}$$

Here we can then use the LA-method to simplify the convolutions in the interaction terms [II]. Note that in principle we could have used the LA-method to derive also the lepton equation but the leading contribution to the source term (4.30) would then be different from (4.32). This is because the lepton is massless so $\partial_t S_{\ell,\mathrm{ad}} = 0$ (when choosing $S_{\ell,\mathrm{ad}} \equiv S_{\ell,\mathrm{eq}}$).

5.2.3 Quantum kinetic equations for leptogenesis

Next we present our leading-order QKEs for the Majorana neutrino distribution δf^m and the lepton asymmetry n_L. For the Majorana neutrinos we use the mass shell equations [II] which can be obtained from (4.39) by discarding the f^c-functions and choosing the symmetric normalization (4.41). We neglect the backreaction of the lepton asymmetry to the Majorana neutrinos by using the equilibrium self-energies (5.36) in the neutrino equation. The lepton equation is derived from (5.41) by using the division (4.28) (with $\Sigma_{\mathrm{ad}} = \Sigma_{\mathrm{eq}}$) and the local ansatz (4.33), and by expanding the equation to the leading order in gradients and interaction strength. The resulting equations are [II]

$$\begin{aligned}\partial_t \delta f^{m,+}_{\boldsymbol{k}hij} = {} & -\mathrm{i}\big(\omega_{\boldsymbol{k}i} - \omega_{\boldsymbol{k}j}\big)\delta f^{m,+}_{\boldsymbol{k}hij} - \partial_t f^{m,+}_{\mathrm{ad},\boldsymbol{k}hij} \\ & - \sum_l \Big[C^{+}_{\boldsymbol{k}hil}\delta f^{m,+}_{\boldsymbol{k}hlj} + \big(C^{+}_{\boldsymbol{k}hjl}\big)^{*}\delta f^{m,+}_{\boldsymbol{k}hil}\Big],\end{aligned} \tag{5.42a}$$

$$\partial_t n_L = S^m_{CP} + \big(\delta W^m + W_{\mathrm{ad}}\big)n_L, \tag{5.42b}$$

where in the neutrino equation (5.42a)

$$f^{m,+}_{\mathrm{ad},\boldsymbol{k}hij} = f_{\mathrm{FD}}(\omega_{\boldsymbol{k}i})\delta_{ij}, \tag{5.43}$$

$$\begin{aligned}C^{+}_{\boldsymbol{k}hil} = {} & \frac{c_{\mathrm{w}}N^m_{\boldsymbol{k}il}}{2\omega_{\boldsymbol{k}i}\omega_{\boldsymbol{k}l}}\Big[\mathrm{Re}(y_i^* y_l)\big(m_i k_{+l} + m_l k_{+i}\big)^{\mu} - \mathrm{i}h\,\mathrm{Im}(y_i^* y_l)\big(m_i k^{\perp}_{+l} + m_l k^{\perp}_{+i}\big)^{\mu}\Big] \\ & \times \Big(\mathfrak{S}^{\mathcal{A}}_{\mathrm{eq}}(k_{+l}) + \mathrm{i}\mathfrak{S}^{\mathrm{H}(T)}_{\mathrm{eq}}(k_{+l})\Big)_{\mu}.\end{aligned} \tag{5.44}$$

We used the free spectral approximation for the adiabatic functions and defined the four-vectors $(k_{si})^\mu \equiv (s\omega_{\boldsymbol{k}i}, \boldsymbol{k})$ and $(k^\perp)^\mu \equiv (|\boldsymbol{k}|, k^0\hat{\boldsymbol{k}})$, and denoted $N^m_{\boldsymbol{k}ij} \equiv N^{ss}_{\boldsymbol{k}hij}$ for the normalization. In the lepton equation (5.42b) the CP-violating source term S^m_{CP} and the washout term coefficients δW^m and W_{ad} are

$$\begin{aligned} S^m_{CP} = \sum_{i,j} \int \frac{\mathrm{d}^3\boldsymbol{k}}{(2\pi)^3} \frac{c_{\text{w}} N^m_{\boldsymbol{k}ij}}{2\omega_{\boldsymbol{k}i}\omega_{\boldsymbol{k}j}} \Big[& \operatorname{Re}(y_i^* y_j) \textstyle\sum_h h \operatorname{Re}(\delta f^{m,+}_{\boldsymbol{k}hij}) \big(m_i k^\perp_{+j} + m_j k^\perp_{+i}\big)^\mu \\ & - \operatorname{Im}(y_i^* y_j) \textstyle\sum_h \operatorname{Im}(\delta f^{m,+}_{\boldsymbol{k}hij}) \big(m_i k_{+j} + m_j k_{+i}\big)^\mu \Big] \\ & \times \Big(\mathfrak{S}^{\mathcal{A}}_{\text{eq}}(k_{+i}) + \mathfrak{S}^{\mathcal{A}}_{\text{eq}}(k_{+j}) \Big)_\mu , \end{aligned} \tag{5.45a}$$

$$\begin{aligned} \frac{c_{\text{w}} T^3}{6} \delta W^m = \sum_{i,j} \int \frac{\mathrm{d}^3\boldsymbol{k}}{(2\pi)^3} \frac{c_{\text{w}} N^m_{\boldsymbol{k}ij}}{2\omega_{\boldsymbol{k}i}\omega_{\boldsymbol{k}j}} \Big[& \operatorname{Re}(y_i^* y_j) \textstyle\sum_h \operatorname{Re}(\delta f^{m,+}_{\boldsymbol{k}hij}) \big(m_i k_{+j} + m_j k_{+i}\big)^\mu \\ & - \operatorname{Im}(y_i^* y_j) \textstyle\sum_h h \operatorname{Im}(\delta f^{m,+}_{\boldsymbol{k}hij}) \big(m_i k^\perp_{+j} + m_j k^\perp_{+i}\big)^\mu \Big] \\ & \times \Big(\delta\mathfrak{S}^{\mathcal{A}}(k_{+i}) + \delta\mathfrak{S}^{\mathcal{A}}(k_{+j}) \Big)_\mu , \end{aligned} \tag{5.45b}$$

$$\frac{c_{\text{w}} T^3}{6} W_{\text{ad}} = \sum_i \int \frac{\mathrm{d}^3\boldsymbol{k}}{(2\pi)^3} \frac{2c_{\text{w}}|y_i|^2}{\omega_{\boldsymbol{k}i}} k^\mu_{+i} \Big[2 f_{\text{FD}}(\omega_{\boldsymbol{k}i}) \delta\mathfrak{S}^{\mathcal{A}}_\mu(k_{+i}) - \delta\mathfrak{S}^<_\mu(k_{+i}) \Big]. \tag{5.45c}$$

To obtain these results we used the symmetry properties of the self-energy functions and the constraints between different components of the Majorana distribution functions δf^m [II]. It should also be noted that the explicit form of the collision term coefficient (5.44) is specific to the case of two Majorana neutrinos.

The Hubble expansion can be taken into account in these equations as described in sections 2.1 and 2.2. The equations then take the same form as given above when they are divided by appropriate powers of the scale factor, that is, when expressed in terms of physical (instead of comoving) quantities and the cosmic time t. The only changes to equations (5.42) are that the time-derivatives are replaced by total time-derivatives, the left-hand side of the lepton equation (5.42b) is changed to $[\frac{\mathrm{d}}{\mathrm{d}t}(n_L a^3)]/a^3$, and time-derivatives of the Majorana neutrino masses $\partial_t m_i$ are replaced by $\dot{a} m_i$ [II]. In practice, when solving the lepton asymmetry we also use the entropy-normalized yield parameter $Y_L \equiv n_L/s$. When assuming adiabatic expansion in the radiation dominated era we then have $[\frac{\mathrm{d}}{\mathrm{d}t}(n_L a^3)]/a^3 = s\frac{\mathrm{d}}{\mathrm{d}t} Y_L$. We also solve the equations by using the dimensionless variable $z \equiv m_1/T$, where m_1 is the mass of the lightest Majorana neutrino. It is related to the cosmic time t by $\mathrm{d}z = H(m_1)/z\,\mathrm{d}t$. Note also that in leptogenesis the standard (i.e. non-coherent) gradient corrections are suppressed because $H/T \ll 1$.

5.2.4 Helicity-symmetric approximation

We now simplify the leptogenesis QKEs (5.42a) and (5.42b) further by assuming helicity symmetry for the neutrino distribution functions $\delta f^{m,+}_{\boldsymbol{k}hij}$. This is a good approximation because the dominant contribution to the lepton asymmetry originates

from the helicity-even part of the source term S^m_{CP} (5.45a). This is true especially in the non-relativistic regime, that is, when the lepton asymmetry is generated mainly when $T \lesssim m_1$. With further approximations the helicity-symmetric equations can also be reduced to the form of semiclassical Boltzmann equations.

The helicity-symmetric equations are obtained by discarding the helicity-odd part of $\delta f^{m,+}_{\boldsymbol{k}hij}$ (i.e. setting $\delta f^{m,+}_{\boldsymbol{k},+1,ij} = \delta f^{m,+}_{\boldsymbol{k},-1,ij}$). For simplicity we also drop Σ^{H} here explicitly and work with vacuum dispersion relations. The resulting neutrino equations and the source term of the lepton asymmetry can be written as [II]

$$\partial_t \delta f_{\boldsymbol{k}11} = -\Gamma_{\boldsymbol{k}11}\, \delta f_{\boldsymbol{k}11} - \partial_t f_{\mathrm{ad},\boldsymbol{k}11} - \Gamma_{\boldsymbol{k}12}\, \mathrm{Re}(\delta f_{\boldsymbol{k}12}), \tag{5.46a}$$

$$\partial_t \delta f_{\boldsymbol{k}22} = -\Gamma_{\boldsymbol{k}22}\, \delta f_{\boldsymbol{k}22} - \partial_t f_{\mathrm{ad},\boldsymbol{k}22} - \Gamma_{\boldsymbol{k}21}\, \mathrm{Re}(\delta f_{\boldsymbol{k}12}), \tag{5.46b}$$

$$\partial_t \delta f_{\boldsymbol{k}12} = -\bar{\Gamma}_{\boldsymbol{k}12}\, \delta f_{\boldsymbol{k}12} - \mathrm{i}\Delta\omega_{\boldsymbol{k}12}\, \delta f_{\boldsymbol{k}12} - \frac{1}{2}\big(\Gamma_{\boldsymbol{k}21}\, \delta f_{\boldsymbol{k}11} + \Gamma_{\boldsymbol{k}12}\, \delta f_{\boldsymbol{k}22}\big), \tag{5.46c}$$

and

$$S^m_{CP} = -2\, \frac{\mathrm{Im}(y_1^* y_2)}{\mathrm{Re}(y_1^* y_2)} \int \frac{\mathrm{d}^3\boldsymbol{k}}{(2\pi)^3} \big(\Gamma_{21} + \Gamma_{12}\big)_{\boldsymbol{k}}\, \mathrm{Im}\big(\delta f_{\boldsymbol{k}12}\big). \tag{5.47}$$

Here the rates are defined as $\Gamma_{\boldsymbol{k}il} \equiv 2\,\mathrm{Re}(C^+_{\boldsymbol{k}hil})|_{\mathfrak{S}^H \to 0}$ with $C^+_{\boldsymbol{k}hil}$ given by equation (5.44). The coherence damping rate is given by the average $\bar{\Gamma}_{\boldsymbol{k}12} \equiv (\Gamma_{\boldsymbol{k}11} + \Gamma_{\boldsymbol{k}22})/2$. Its form agrees with the flavor coherence damping rate of mixing neutrinos found in the density matrix formalism [148–150]. We have suppressed the helicity indices in these equations as all quantities are now assumed to be the same for both helicities. Note that the equations could be written in a similar form in the helicity-dependent case also: there would just be additional helicity-mixing terms. It is also illustrative to integrate the off-diagonal equation (5.46c) into the form

$$\delta f_{\boldsymbol{k}12}(t) = -\frac{1}{2} \int_{t_0}^{t} \mathrm{d}u \, \big(\Gamma_{21} \delta f_{11} + \Gamma_{12} \delta f_{22}\big)_{\boldsymbol{k}}(u) \exp\bigg[- \int_u^t \mathrm{d}v \, \Big(\bar{\Gamma}_{12} + \mathrm{i}\Delta\omega_{12}\Big)_{\boldsymbol{k}}(v) \bigg], \tag{5.48}$$

where it was assumed that the flavor coherence vanishes initially, $\delta f_{\boldsymbol{k}12}(t_0) = 0$. In this form the oscillations and the role of the flavor coherence damping become even more clear.

Equations (5.46) and (5.47) can be reduced to the semiclassical Boltzmann equations in the decoupling limit where the off-diagonal function $\delta f_{\boldsymbol{k}12}$ is discarded from the diagonal equations (5.46a) and (5.46b) [II]. This is a valid approximation in the limit $\Delta m_{21} \gg \Gamma$. The equations of the diagonal functions $\delta f_{\boldsymbol{k}ii}$ then exactly match those derived in the semiclassical approach. The late-time limit of the lepton asymmetry then also matches the semiclassical result with the sum regulator (2.15c) for the CP-asymmetry. Analysis of the structure of the source term (5.47) also reveals that the *coherence damping rate* $\bar{\Gamma}_{\boldsymbol{k}12}$ is the origin of the regulator of the CP-asymmetry in the semiclassical approach [II].

Strong washout limit

A simplified solution to equations (5.46) and (5.47) can also be derived in the strong washout case $\Gamma_{ii} > H$. In this case one can derive a late-time approximation to the solution δf_{ij} by setting the left-hand sides of equations (5.46a)–(5.46c) to zero, resulting in an algebraic equation [76, 89, 91]. The idea is that the true solution relaxes towards this late-time limit and it is a good approximation if the relaxation happens before the lepton asymmetry freeze-out [76]. The solution to the algebraic equations leads to the approximation

$$S^m_{CP} \simeq \frac{\mathrm{Im}(y_1^* y_2)}{\mathrm{Re}(y_1^* y_2)} \int \frac{\mathrm{d}^3\boldsymbol{k}}{(2\pi)^3} \big(\Gamma_{21} + \Gamma_{12}\big)_{\boldsymbol{k}} \big(\Gamma_{21}\delta f_{11} + \Gamma_{12}\delta f_{22}\big)_{\boldsymbol{k}} \times \left[\frac{-\Delta\omega_{12}}{(\Delta\omega_{12})^2 + (\bar{\Gamma}_{12})^2\Big(1 - \frac{\Gamma_{12}\Gamma_{21}}{\Gamma_{11}\Gamma_{22}}\Big)}\right]_{\boldsymbol{k}} . \tag{5.49}$$

Here the diagonal distributions δf_{ii} are calculated without backreaction from the off-diagonal functions [II]. The factor $(1 - \Gamma_{12}\Gamma_{21}/[\Gamma_{11}\Gamma_{22}])$ takes effectively, but in a simplified way, into account the coupling between the diagonal and off-diagonal functions.

The result (5.49) illustrates the role of the coherence damping rate $\bar{\Gamma}_{\boldsymbol{k}12}$ as the regulator of the CP-asymmetry in the degeneracy limit $\Delta m_{21} \to 0$. In the quasidegenerate case $m_1 \simeq m_2$ the source (5.49) is also approximated by the standard Boltzmann form of the source term with the effective CP-asymmetry parameter

$$\varepsilon^{CP}_{i,\mathrm{eff}} = \frac{\mathrm{Im}\big[(y_1^* y_2)^2\big]}{|y_1|^2|y_2|^2} \frac{(m_2^2 - m_1^2) m_i \Gamma_j^{(0)}}{(m_2^2 - m_1^2)^2 + \big(m_1\Gamma_1^{(0)} + m_2\Gamma_2^{(0)}\big)^2 \sin^2\theta_{12}} . \quad (j \neq i) \tag{5.50}$$

This result corresponds to the effective regulator [76] given in equation (2.15d).

5.2.5 Results for the lepton asymmetry

Next we present our numerical results for the lepton asymmetry obtained from the main QKEs (5.42a) and (5.42b). We also compare the full results to the helicity-symmetric approximation given by equations (5.46) and (5.47) and to the semiclassical Boltzmann approach with the momentum-dependent version [II] of equations (2.11). We use $m_1 = 10^{13}\,\mathrm{GeV}$, $g_* = 110$, and $\theta_{12} = \pi/4$ with vacuum initial conditions here; more discussion about the parameter choices is given in [II]. We take the Hubble expansion into account as described in the end of section 5.2.3. We assume that there is no significant entropy production and that the universe expands adiabatically as described in section 2.1. This is a valid approximation if the Majorana neutrinos decay when $z < g_{*s}$ [64], which is typically the case in thermal leptogenesis and also here. We also discard the dispersive self-energy Σ^{H} in all results for simplicity. All of the results shown here have been calculated using the code package [IIb].

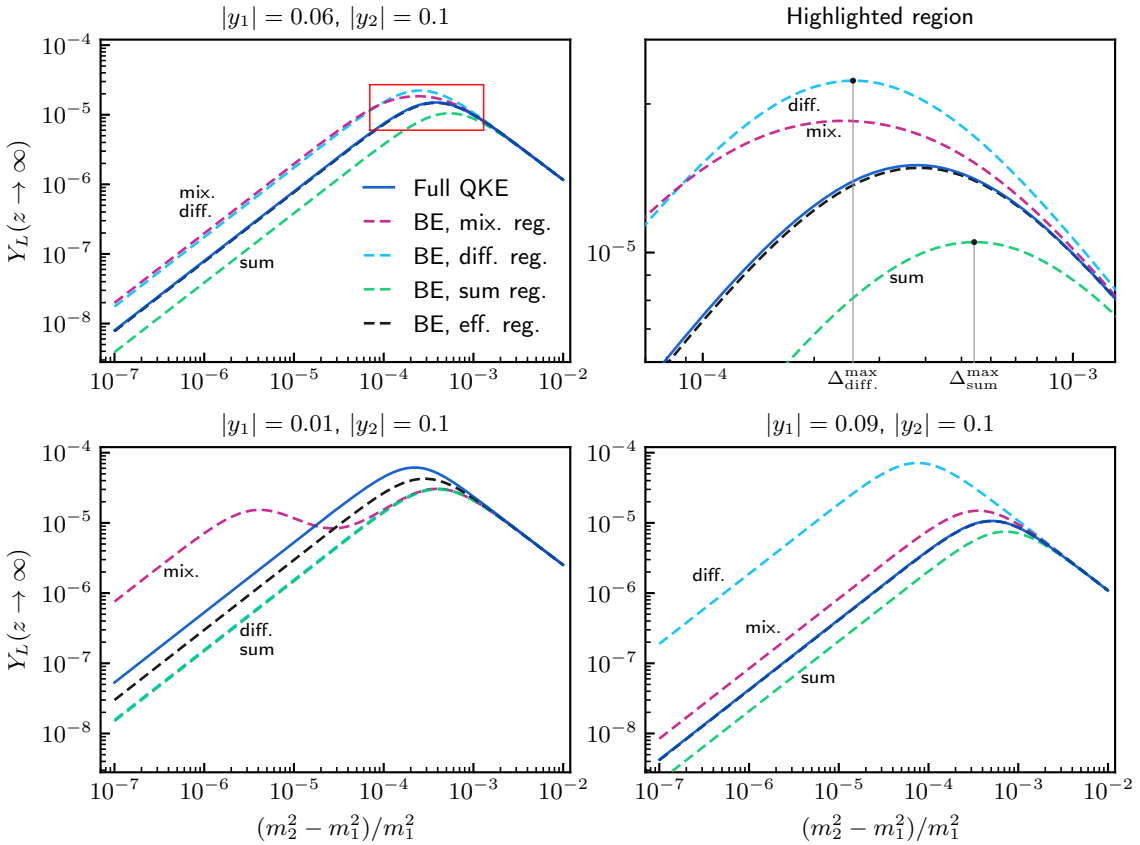

Figure 5. Final lepton asymmetry Y_L as a function of the relative mass-squared difference $\Delta m^2_{21}/m^2_1$, for different Yukawa couplings y_i. The full QKE results are compared to the Boltzmann equation (BE) results for four different regulators of the CP-asymmetry ε_i^{CP}. We used $m_1 = 10^{13}$ GeV, $\theta_{12} = \pi/4$ and vacuum initial conditions in all plots. The top-right panel shows the region highlighted in red on the left. From article [II] (CC BY 4.0).

In figure 5 we show the results for the asymptotic value of the lepton asymmetry yield parameter $Y_L \equiv n_L/s$ as a function of the relative mass-squared difference $\Delta m^2_{21}/m^2_1 \simeq 2\Delta m_{21}/m_1$. Our main QKE result is compared to the Boltzmann approach with the different CP-asymmetry regulators (2.15), and the results are shown for three different choices of the Yukawa couplings of the model. The lower left and right panel correspond to hierarchical and almost degenerate Yukawa couplings, respectively, whereas the upper panels show an intermediate case. The maximal resonant saturation of the CP-asymmetry, and consequently the maximum of the lepton asymmetry, occurs in all cases roughly when $\Delta m_{21} \sim \bar{\Gamma}_{12}$. There are however significant qualitative and quantitative differences between the full QKE and Boltzmann approaches in the resonant and quasidegenerate regions $\Delta m_{21} \lesssim \bar{\Gamma}_{12}$. Both approaches converge, as expected, in the region $\Delta m_{21} > \bar{\Gamma}_{12}$ where the flavor oscillations are fast and the diagonal Majorana neutrino distributions effectively decouple from the off-diagonal distributions [II].

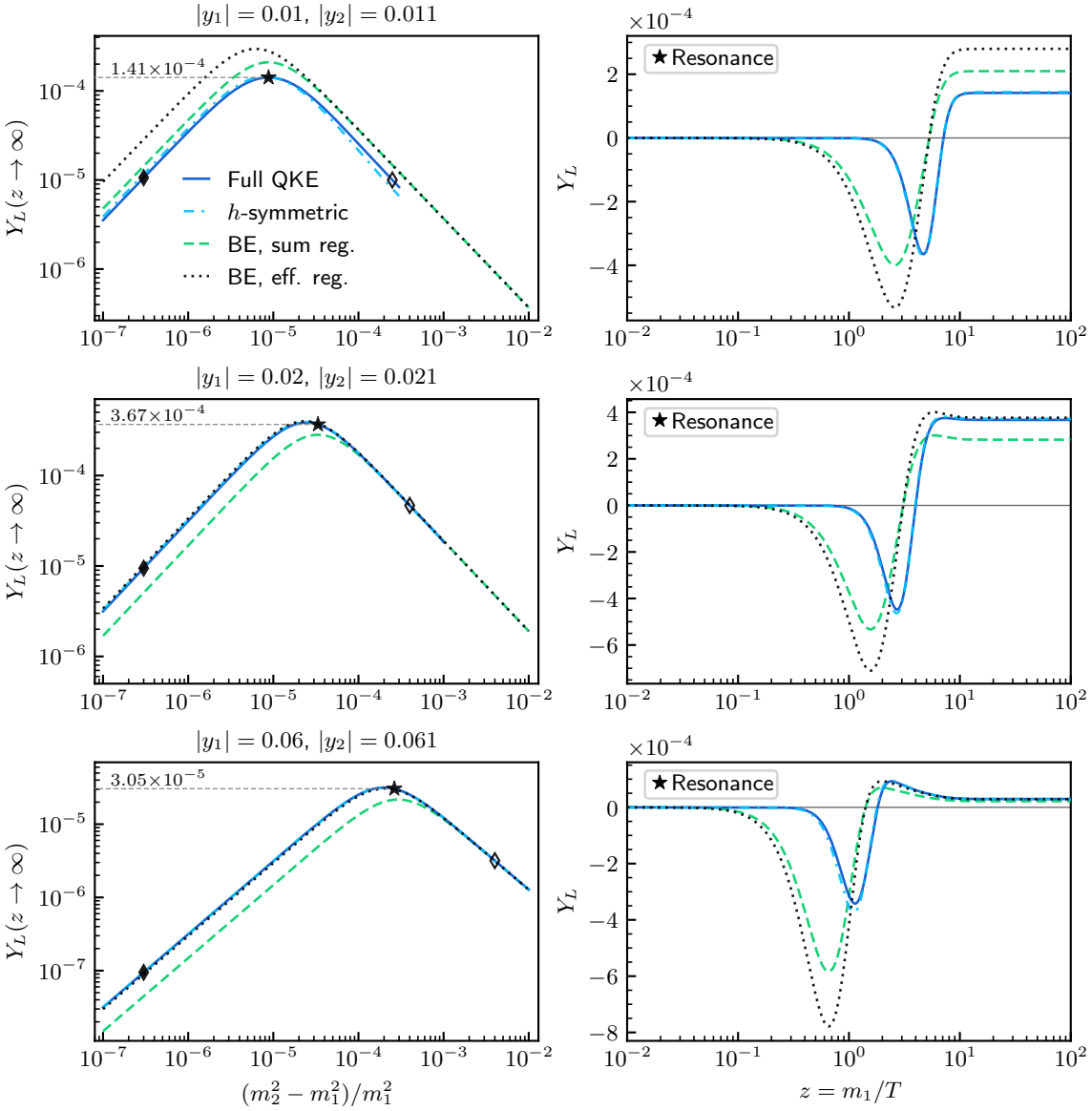

Figure 6. Final lepton asymmetry Y_L as a function of $\Delta m^2_{21}/m^2_1$ (left panels) and the full evolution of $Y_L(z)$ in the maximally resonant case (right panels) indicated with a star-marker (the diamond-markers are considered in figure 7). The results are shown in three different washout strength scenarios: weak (top panels), intermediate (middle panels) and strong (bottom panels).

In figure 6 we give a further comparison between three different washout strength scenarios: weak ($K_i \sim 0.1$), intermediate ($K_i \sim 1$) and strong ($K_i \sim 10$). The washout strength here is characterized by the parameter $K_i \equiv \Gamma_i^{(0)}/H(m_1)$ [II]. Note that in figure 5 (and in other results given in [II]) the total washout was still quite strong in all cases because at least one of the Yukawa couplings was large. In figure 6 we also compare the helicity-symmetric approximation given by equations (5.46)

and (5.47) to the full QKEs and the Boltzmann equations. Furthermore, we show the full evolution of the lepton asymmetry Y_L as a function of z for each scenario, in addition to the plots of the asymptotic asymmetry on the left. The mass difference parameters used in the right-hand side plots correspond to the maximal saturation points marked on the plots on the left-hand side. The left panels show that again the final lepton asymmetry is maximal at $\Delta m_{21} \sim \bar{\Gamma}_{12}$ and also that the largest value is obtained in the intermediate washout case (middle panels) when $\Delta m_{21} \sim \bar{\Gamma}_{12} \sim H$. This is as expected from general considerations [II].

In figure 7 we show the full evolution of the lepton asymmetry $Y_L(z)$ also in the overdamped ($\Delta m_{21} \ll \bar{\Gamma}_{12}$) and rapidly oscillating cases ($\Delta m_{21} \gg \bar{\Gamma}_{12}$), for the mass difference values indicated by the diamond-markers in figure 6. The full evolution plots in figures 6 and 7 show how increasing the interaction strength shifts the generation of the lepton asymmetry towards the relativistic region $z < 1$ in all cases. It can also be seen that the Boltzmann equations significantly overestimate the magnitude of the lepton asymmetry earlier during the evolution, when compared to our full QKEs. This can be explained by the static CP-asymmetry parameters $\varepsilon_i^{\mathrm{CP}}$ of the Boltzmann approach which do not take into account the finite build-up time [79] of the CP-asymmetry. For larger mass differences $\Delta m_{21} > \bar{\Gamma}_{12}$ the build-up time is shorter which is shown in the right-hand side panels of figure 7 [see also equations (5.47) and (5.48)]. There the initial lepton asymmetry spike (of the full QKE) is produced earlier when compared to the maximally resonant and overdamped cases.

The helicity-symmetric approximation tracks the full QKEs near-perfectly in most of the considered cases. It only fails somewhat in the fast oscillation regime ($\Delta m_{21} > \bar{\Gamma}_{12}$) as can be seen from the right-hand side panels in figure 7. However, the final lepton asymmetry still converges to the full QKE result in all cases, except the case of fast oscillations with weak washout. The effective sum regulator in the Boltzmann approach also gives a very good late-time match to our full QKEs in all considered cases except when the washout is weak. However, we do not expect the match to be this good more generally because the validity of the effective regulator is sensitive to the size of the CP-violating phase θ_{12} of the Yukawa couplings [76]. The results do not take this into account as we used only a single value for θ_{12}.

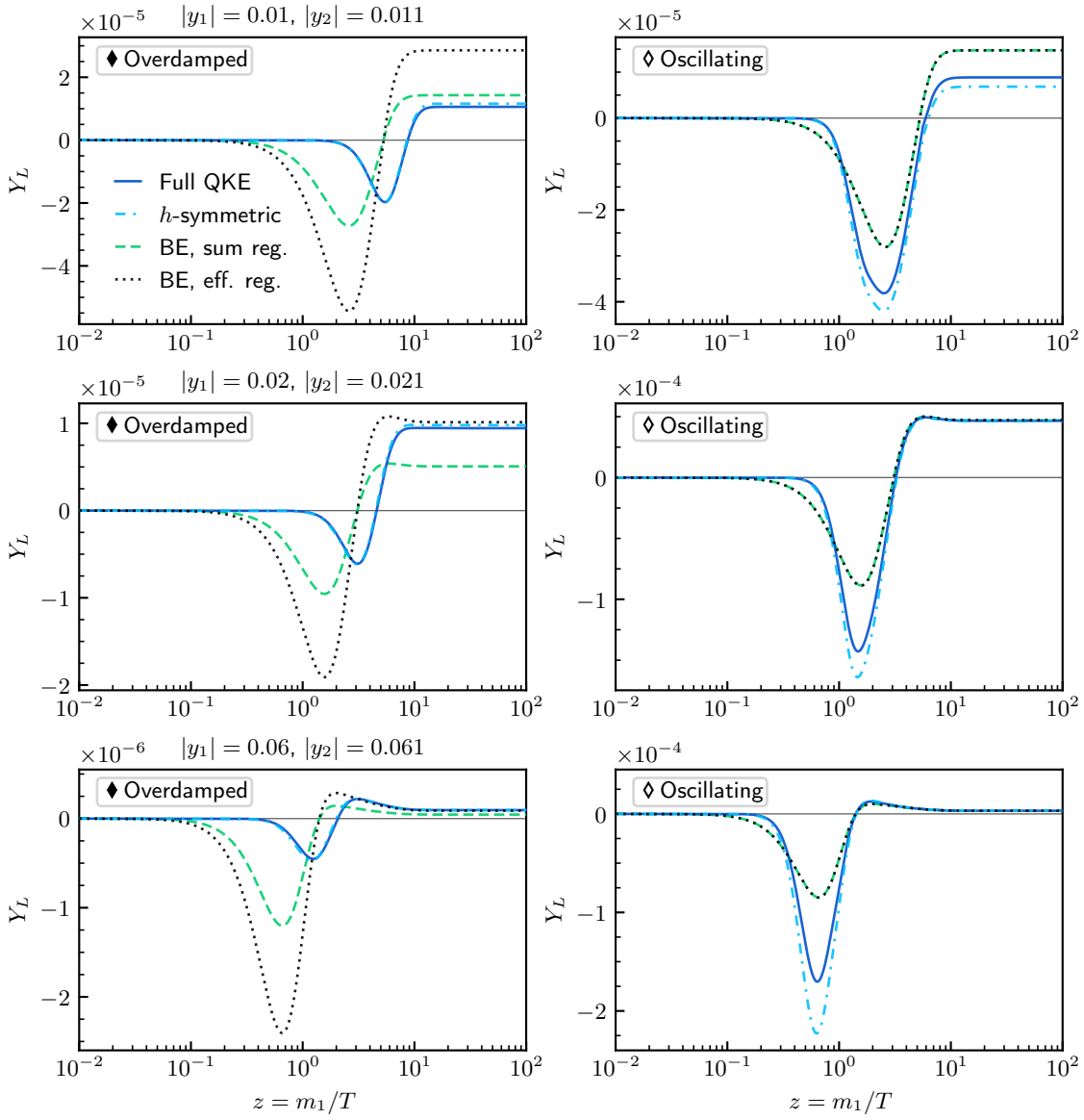

Figure 7. Continuation of figure 6, showing the full evolution of $Y_L(z)$ in the overdamped and rapidly oscillating cases for each washout scenario. The used mass difference values in each panel are indicated with the filled or empty diamond-markers (in figure 6).

6 DISCUSSION AND CONCLUSIONS

We have developed approximation methods in non-equilibrium QFT for deriving local quantum kinetic equations including interactions and *quantum coherence*. Our main results are the formulation of the new local approximation (LA) method [II] and also the improvement [I] of the coherent quasiparticle approximation (cQPA) developed earlier in [14–22]. We focused on fermions in spatially homogeneous and isotropic systems with a time-dependent mass and a weak coupling to a thermal bath. The motivation for this setting was the early universe and especially baryogenesis. The presented flavored QKEs in these systems can describe both flavor coherence and particle–antiparticle coherence and the related oscillations (summarized in table 1).

6.1 Coherent quantum kinetic equations

In section 4.2 we presented a new derivation of the cQPA equations of motion. We gave a straightforward way to derive the cQPA ansatz by using the projection matrix parametrization. We introduced a new way of organizing the gradient expansion, leading to a transparent method for performing the coherence gradient resummation [21] of the collision term. It follows that the coherence-resummed self-energy functions (4.18) are always evaluated at the conventional flavor-diagonal mass shells instead of the coherence shells. While this result is already known [20], the more easy-to-use method presented here has been long needed (see e.g. [91]).

In section 5.1 we formulated the transport equations (5.6) using cQPA for a generic interacting fermion with a CP-violating complex mass. These equations are a generalization of semiclassical Boltzmann equations which take into account local coherence between particles and antiparticles. The structure of the equations shows that a changing mass ($\dot{m} \neq 0$) induces coherent particle production while a changing complex phase of the mass ($\dot{\theta} \neq 0$) generates helicity asymmetry (leading to CP-asymmetry) via the coherence functions f^c. We used the equations to study the evolution of axial charge density with the mass profile (5.11) which is a time-

dependent analogue of a first order phase transition in EWBG. The results (figures 2 and 4) indicate that in the middle of the transition (i.e. inside the transition wall), where the mass changes rapidly, almost all of the axial charge is due to coherence. Full quantum treatment of coherence can thus be important in the thin wall case [151–153] of EWBG. In other regions the mass shell functions f^m are able to track the average of the oscillating axial charge. This result also supports the exclusion of the f^c-functions in the leptogenesis application where the background is slowly-changing. We showed explicitly that semiclassical effects are included in cQPA.

We also verified the shell structure of cQPA by using exact solutions of the Dirac equation in a non-interacting system with the mass profile (5.11). The results (figure 3) additionally revealed the important twofold role of damping in the emergence of the local kinetic picture. A spectral quasiparticle description with well-distinguished shells requires that there is not too much damping as it smears the shells. On the other hand, if there is too little damping the two-point function becomes overwhelmed by non-local temporal correlations [I]. This implies the breakdown of the simple shell picture and the description of time-evolution by local quantities. This observation is important for the development of more general local approximation methods.

Our results also establish that cQPA is exact when calculating local quantities in non-interacting systems. We derived the one-to-one correspondence between the local mode function matrix and the cQPA phase space distribution functions, which was not done explicitly in [I]. This is another important consistency check for the basic structure of the coherent phase space functions, even though the true utility of cQPA is of course in the interacting case. However, these developments lead to an important insight about cQPA, ultimately transcending it: the key feature is that the non-local correlations are treated non-dynamically while the local correlations related to the average time coordinate are fully included [I]. This insight was used as the main idea for developing the more general LA-method.

6.2 Improved local description of non-equilibrium dynamics

In section 4.3 we formulated the new LA-method and used it to derive improved coherent QKEs (4.39) where the effects of spectral width can be included. The main idea of the method is to form a closed dynamical equation directly for the local two-point function $S^<_{\boldsymbol{k}}(t,t)$. This can be achieved in dissipative systems by two steps (summarized in table 2): (1) identification of a suitable background solution $S_{\rm ad}$ and expansion of the full solution S around it, and (2) parametrization of the non-local parts of the deviation δS by its local values. The second step with the local ansatz (4.33) is the core part of the method which enables the local description of the non-equilibrium dynamics.

An essential part in the derivation of the improved QKEs was also the projection matrix parametrization which separates different components of the local

propagator which vary in different time-scales. This is crucial for separating the rapid particle–antiparticle oscillations from the flavor oscillations. Furthermore, there is no loss of generality with this parametrization in homogeneous and isotropic systems; equations (4.39) and (4.36) are equivalent.

The LA-method can be viewed as an improved and generalized version of the cQPA. The improved QKEs (4.39) can be reduced to the cQPA equations in a spectral approximation. However, the local transport equation (4.36) in the LA-method is formulated directly in the two-time representation at the propagator level without needing to solve the phase space structure. The method can thus be used in a spectral approximation but also more generally when accounting for the spectral width. A major practical advantage is also that the gradient resummation of the collision term is automatically imposed by the local ansatz in the LA-method.

6.2.1 Resonant leptogenesis with coherent QKEs

In section 5.2 we derived local coherent QKEs for leptogenesis by using the LA-method. The most general form of the equations contains all local quantum coherence effects of the Majorana neutrinos and also thermal medium effects in a weak coupling expansion [II]. The simpler QKEs (5.42) for the minimal leptogenesis model are still valid for arbitrary mass differences and fully include the coherent flavor oscillations of the Majorana neutrinos. Our main goal with these equations was to study the details of the CP-asymmetry generation in resonant leptogenesis. We gave even simpler helicity-symmetric equations (5.46) and (5.47) which provide a good approximation to the full QKEs (5.42) and from which the CP-asymmetry generation mechanism can be more easily analyzed. We also reduced the equations to the conventional Boltzmann equation form in the decoupling limit (and with further approximations) [II].

Our results imply that the flavor-coherence damping rate $\bar{\Gamma}_{\boldsymbol{k}12}$ of the Majorana neutrinos is the origin of the CP-asymmetry regulator in the Boltzmann approach. The result corresponds to the sum-regulator derived earlier in the CTP approach [75, 88, 89]. The damping of flavor-coherence, rather than the oscillations averaging out (cf. [79]), also explains why the Boltzmann equations and the full QKEs converge to the same late-time lepton asymmetry in the decoupling limit (i.e. when $\Delta m_{21} \gg \bar{\Gamma}_{12}$) [II]. Our numerical results agree with these findings.

We performed a thorough numerical analysis of our QKEs in the resonant case and compared them to the conventional Boltzmann equations [II]. The exact form of the CP-asymmetry regulator in the Boltzmann approach has been debated in the literature [69, 70, 75, 76, 91, 95]. Therefore we included several different regulators for the Boltzmann equations in the comparison of the final lepton asymmetry calculated from the different approaches. Our results in figures 5–7 show that the maximal resonant saturation occurs roughly when $\Delta m_{21} \simeq \bar{\Gamma}_{12}$ in all approaches. However, in the quasidegenerate regime $\Delta m_{21} \lesssim \bar{\Gamma}_{12}$ there are significant qualitative differences

between different Boltzmann regulators. We found that the sum regulator (and its effective variant) gives the best qualitative match to our full QKEs in the late-time limit, but there can still be differences by at least a factor of 2. The late-time results of all approaches also converge in the weakly resonant regime $\bar{\Gamma}_{12} \ll \Delta m_{21} \ll m_1$ (except for very weak washout, $\bar{\Gamma}_{12} \ll H$). This provides a consistency check for our full QKEs in the validity region of the semiclassical approach.

Finally, our QKEs are in line with several other studies based on the CTP method. In particular, our RL results are similar to the results of [75, 88, 89] and our equations agree with those derived in [87]. However, our approach is also more general in several ways: we do not need to restrict the values of the Yukawa couplings, the size of the deviation from equilibrium, or the mass difference of the Majorana neutrinos. Further comparison to other studies is given in [II].

6.3 Outlook

So far we have compared our methods mainly to simple semiclassical equations. More precise comparisons should be made to other methods and results found in the literature. For example, in leptogenesis with quasidegenerate Majorana neutrinos the question if the CP-asymmetry has separate contributions from mixing and oscillations remains unsettled [95, 98]. While our results point to the interpretation that the conventional mixing source arises from the coherent oscillations in a particular limit ($\Delta m_{21} \gg \bar{\Gamma}_{12}$) [II], a more careful investigation is needed. A thorough analysis of corrections to the adiabatic propagators and the effective self-energies is challenging but may also be required for more conclusive answers to this question.

Our leptogenesis equations could also be improved and extended in other ways. An obvious improvement would be the inclusion of scattering processes and multiple SM lepton flavors. It would then be very interesting to apply our equations to low-scale RL and ARS scenarios in a unified framework similarly to [62]. The numerical results could also be extended straightforwardly to include leading dispersive corrections for the Majorana neutrinos. Covering the hierarchical regime of leptogenesis and investigating the size of the CP-asymmetry from particle–antiparticle coherence [II] would also be very interesting. At a more general level, a numerical analysis to test the local ansatz (4.33) against the full memory integrals would also be desirable.

A long standing goal, which has remained elusive so far, has also been to extend the coherent quantum transport methods to the planar symmetric case [14]. This is required for a proper description of coherence in realistic EWBG models. The transport equations developed here could also be combined with the results of [154] to study particle production during reheating in a realistic setup. Another interesting application of the coherent equations is the field-theoretic description of SM neutrino oscillations.

REFERENCES

[1] L. de Broglie, *"Waves and Quanta"*, Nature **112**, 540 (1923), DOI: 10.1038/112540a0.

[2] M. Le Bellac, *"Quantum Physics"* (Cambridge University Press, 2006), ISBN: 978-0-521-85277-7, DOI: 10.1017/CBO9780511616471.

[3] C. Giunti and C. W. Kim, *"Fundamentals of Neutrino Physics and Astrophysics"* (Oxford University Press, 2007), ISBN: 978-0-19-850871-7, DOI: 10.1093/acprof:oso/9780198508717.001.0001.

[4] N. Aghanim et al. (Planck Collaboration), *"Planck 2018 results. VI. Cosmological parameters"*, Astron. Astrophys. **641**, A6 (2020), DOI: 10.1051/0004-6361/201833910, [arXiv: 1807.06209 (astro-ph.CO)].

[5] A. G. Cohen, A. De Rujula, and S. L. Glashow, *"A Matter - antimatter universe?"*, Astrophys. J. **495**, 539 (1998), DOI: 10.1086/305328, [arXiv: astro-ph/9707087].

[6] E. W. Kolb and M. S. Turner, *"The Early Universe"* (Addison-Wesley, 1990), ISBN: 978-0-201-62674-2, DOI: 10.1201/9780429492860.

[7] S. M. Bilenky and S. T. Petcov, *"Massive Neutrinos and Neutrino Oscillations"*, Rev. Mod. Phys. **59**, 671 (1987), DOI: 10.1103/RevModPhys.59.671.

[8] E. A. Calzetta and B.-L. B. Hu, *"Nonequilibrium Quantum Field Theory"* (Cambridge University Press, 2008), ISBN: 978-0-521-64168-5, DOI: 10.1017/CBO9780511535123.

[9] V. A. Kuzmin, V. A. Rubakov, and M. E. Shaposhnikov, *"On the Anomalous Electroweak Baryon Number Nonconservation in the Early Universe"*, Phys. Lett. B **155**, 36 (1985), DOI: 10.1016/0370-2693(85)91028-7.

[10] A. G. Cohen, D. B. Kaplan, and A. E. Nelson, *"Progress in electroweak baryogenesis"*, Ann. Rev. Nucl. Part. Sci. **43**, 27 (1993), DOI: 10.1146/annurev.ns.43.120193.000331, [arXiv: hep-ph/9302210].

[11] V. A. Rubakov and M. E. Shaposhnikov, *"Electroweak baryon number non-conservation in the early universe and in high-energy collisions"*, Usp. Fiz. Nauk **166**, 493 (1996), DOI: 10.1070/PU1996v039n05ABEH000145, [arXiv: hep-ph/9603208].

[12] M. Fukugita and T. Yanagida, *"Baryogenesis Without Grand Unification"*, Phys. Lett. B **174**, 45 (1986), DOI: 10.1016/0370-2693(86)91126-3.

[13] E. K. Akhmedov, V. A. Rubakov, and A. Y. Smirnov, *"Baryogenesis via neutrino oscillations"*, Phys. Rev. Lett. **81**, 1359 (1998), DOI: 10.1103/PhysRevLett.81.1359, [arXiv: hep-ph/9803255].

[14] M. Herranen, K. Kainulainen, and P. M. Rahkila, *"Towards a kinetic theory for fermions with quantum coherence"*, Nucl. Phys. B **810**, 389 (2009), DOI: 10.1016/j.nuclphysb.2008.09.032, [arXiv: 0807.1415 (hep-ph)].

[15] M. Herranen, K. Kainulainen, and P. M. Rahkila, *"Quantum kinetic theory for fermions in temporally varying backgrounds"*, J. High Energy Phys. **09**, 032 (2008), DOI: 10.1088/1126-6708/2008/09/032, [arXiv: 0807.1435 (hep-ph)].

[16] M. Herranen, K. Kainulainen, and P. M. Rahkila, *"Kinetic transport theory with quantum coherence"*, Nucl. Phys. A **820**, edited by J. Smit, 203C (2009), DOI: 10.1016/j.nuclphysa.2009.01.050, [arXiv: 0811.0936 (hep-ph)].

[17] M. Herranen, K. Kainulainen, and P. M. Rahkila, *"Kinetic theory for scalar fields with nonlocal quantum coherence"*, J. High Energy Phys. **05**, 119 (2009), DOI: 10.1088/1126-6708/2009/05/119, [arXiv: 0812.4029 (hep-ph)].

[18] M. Herranen, *"Quantum kinetic theory with nonlocal coherence"*, PhD thesis (Jyvaskyla U., 2009), [arXiv: 0906.3136 (hep-ph)].

[19] M. Herranen, K. Kainulainen, and P. M. Rahkila, *"Coherent quasiparticle approximation (cQPA) and nonlocal coherence"*, J. Phys. Conf. Ser. **220**, edited by M. Bonitz and K. Balzer, 012007 (2010), DOI: 10.1088/1742-6596/220/1/012007, [arXiv: 0912.2490 (hep-ph)].

[20] M. Herranen, K. Kainulainen, and P. M. Rahkila, *"Coherent quantum Boltzmann equations from cQPA"*, J. High Energy Phys. **12**, 072 (2010), DOI: 10.1007/JHEP12(2010)072, [arXiv: 1006.1929 (hep-ph)].

[21] C. Fidler, M. Herranen, K. Kainulainen, and P. M. Rahkila, *"Flavoured quantum Boltzmann equations from cQPA"*, J. High Energy Phys. **02**, 065 (2012), DOI: 10.1007/JHEP02(2012)065, [arXiv: 1108.2309 (hep-ph)].

[22] M. Herranen, K. Kainulainen, and P. M. Rahkila, *"Flavour-coherent propagators and Feynman rules: Covariant cQPA formulation"*, J. High Energy Phys. **02**, 080 (2012), DOI: 10.1007/JHEP02(2012)080, [arXiv: 1108.2371 (hep-ph)].

[23] S. Weinberg, *"Gravitation and Cosmology: Principles and Applications of the General Theory of Relativity"* (John Wiley and Sons, 1972), ISBN: 978-0-471-92567-5.

[24] S. Weinberg, *"Cosmology"* (Oxford University Press, Oxford, 2008), ISBN: 978-0-19-852682-7, DOI: 10.1007/s10714-008-0728-z.

[25] A. H. Guth, *"The Inflationary Universe: A Possible Solution to the Horizon and Flatness Problems"*, Phys. Rev. D **23**, edited by L.-Z. Fang and R. Ruffini, 347 (1981), DOI: 10.1103/PhysRevD.23.347.

[26] P. A. Zyla et al. (Particle Data Group), *"Review of Particle Physics"*, Prog. Theor. Exp. Phys. **2020**, 083C01 (2020), DOI: 10.1093/ptep/ptaa104.

[27] N. D. Birrell and P. C. W. Davies, *"Quantum Fields in Curved Space"* (Cambridge University Press, 1982), ISBN: 978-0-521-27858-4, DOI: 10.1017/CBO9780511622632.

[28] M. Dine and A. Kusenko, *"The Origin of the matter - antimatter asymmetry"*, Rev. Mod. Phys. **76**, 1 (2003), DOI: 10.1103/RevModPhys.76.1, [arXiv: hep-ph/0303065].

[29] B. D. Fields, K. A. Olive, T.-H. Yeh, and C. Young, *"Big-Bang Nucleosynthesis after Planck"*, J. Cosmol. Astropart. Phys. **03**, [Erratum: JCAP 11, E02 (2020)], 010 (2020), DOI: 10.1088/1475-7516/2020/03/010, [arXiv: 1912.01132 (astro-ph.CO)].

[30] J. M. Cline, *"Baryogenesis"*, in Les Houches Summer School - Session 86: Particle Physics and Cosmology: The Fabric of Spacetime (Sept. 2006), [arXiv: hep-ph/0609145].

[31] J. M. Cline, *"TASI Lectures on Early Universe Cosmology: Inflation, Baryogenesis and Dark Matter"*, PoS **TASI2018**, 001 (2019), [arXiv: 1807.08749 (hep-ph)].

[32] D. Bodeker and W. Buchmuller, *"Baryogenesis from the weak scale to the grand unification scale"*, Rev. Mod. Phys. **93**, 035004 (2021), DOI: 10.1103/RevModPhys.93.035004, [arXiv: 2009.07294 (hep-ph)].

[33] A. D. Sakharov, *"Violation of CP Invariance, C asymmetry, and baryon asymmetry of the universe"*, Pisma Zh. Eksp. Teor. Fiz. **5**, 32 (1967), DOI: 10.1070/PU1991v034n05ABEH002497.

[34] D. E. Morrissey and M. J. Ramsey-Musolf, *"Electroweak baryogenesis"*, New J. Phys. **14**, 125003 (2012), DOI: 10.1088/1367-2630/14/12/125003, [arXiv: 1206.2942 (hep-ph)].

[35] K. Kajantie, M. Laine, K. Rummukainen, and M. E. Shaposhnikov, *"Is there a hot electroweak phase transition at $m_H \gtrsim m_W$?"*, Phys. Rev. Lett. **77**, 2887 (1996), DOI: 10.1103/PhysRevLett.77.2887, [arXiv: hep-ph/9605288].

[36] G. 't Hooft, *"Symmetry Breaking Through Bell-Jackiw Anomalies"*, Phys. Rev. Lett. **37**, edited by M. A. Shifman, 8 (1976), DOI: 10.1103/PhysRevLett.37.8.

[37] G. 't Hooft, *"Computation of the Quantum Effects Due to a Four-Dimensional Pseudoparticle"*, Phys. Rev. D **14**, edited by M. A. Shifman, [Erratum: Phys.Rev.D 18, 2199 (1978)], 3432 (1976), DOI: 10.1103/PhysRevD.14.3432.

[38] S. L. Adler, *"Axial vector vertex in spinor electrodynamics"*, Phys. Rev. **177**, 2426 (1969), DOI: 10.1103/PhysRev.177.2426.

[39] J. S. Bell and R. Jackiw, *"A PCAC puzzle: $\pi^0 \to \gamma\gamma$ in the σ model"*, Nuovo Cim. A **60**, 47 (1969), DOI: 10.1007/BF02823296.

[40] F. R. Klinkhamer and N. S. Manton, *"A Saddle Point Solution in the Weinberg-Salam Theory"*, Phys. Rev. D **30**, 2212 (1984), DOI: 10.1103/PhysRevD.30.2212.

[41] N. S. Manton, *"Topology in the Weinberg-Salam Theory"*, Phys. Rev. D **28**, 2019 (1983), DOI: 10.1103/PhysRevD.28.2019.

[42] P. B. Arnold and L. D. McLerran, *"Sphalerons, Small Fluctuations and Baryon Number Violation in Electroweak Theory"*, Phys. Rev. D **36**, 581 (1987), DOI: 10.1103/PhysRevD.36.581.

[43] P. B. Arnold and L. D. McLerran, *"The Sphaleron Strikes Back"*, Phys. Rev. D **37**, 1020 (1988), DOI: 10.1103/PhysRevD.37.1020.

[44] T. Konstandin, *"Quantum Transport and Electroweak Baryogenesis"*, Phys. Usp. **56**, 747 (2013), DOI: 10.3367/UFNe.0183.201308a.0785, [arXiv: 1302.6713 (hep-ph)].

[45] J. A. Harvey and M. S. Turner, *"Cosmological baryon and lepton number in the presence of electroweak fermion number violation"*, Phys. Rev. D **42**, 3344 (1990), DOI: 10.1103/PhysRevD.42.3344.

[46] V. Andreev et al. (ACME), *"Improved limit on the electric dipole moment of the electron"*, Nature **562**, 355 (2018), DOI: 10.1038/s41586-018-0599-8.

[47] J. M. Cline, M. Joyce, and K. Kainulainen, *"Supersymmetric electroweak baryogenesis"*, J. High Energy Phys. **07**, 018 (2000), DOI: 10.1088/1126-6708/2000/07/018, [arXiv: hep-ph/0006119].

[48] J. M. Cline and K. Kainulainen, *"A New source for electroweak baryogenesis in the MSSM"*, Phys. Rev. Lett. **85**, 5519 (2000), DOI: 10.1103/PhysRevLett.85.5519, [arXiv: hep-ph/0002272].

[49] J. M. Cline, K. Kainulainen, P. Scott, and C. Weniger, *"Update on scalar singlet dark matter"*, Phys. Rev. D **88**, [Erratum: Phys.Rev.D 92, 039906 (2015)], 055025 (2013), DOI: 10.1103/PhysRevD.88.055025, [arXiv: 1306.4710 (hep-ph)].

[50] T. Alanne, K. Kainulainen, K. Tuominen, and V. Vaskonen, *"Baryogenesis in the two doublet and inert singlet extension of the Standard Model"*, J. Cosmol. Astropart. Phys. **08**, 057 (2016), DOI: 10.1088/1475-7516/2016/08/057, [arXiv: 1607.03303 (hep-ph)].

[51] J. M. Cline, K. Kainulainen, and D. Tucker-Smith, *"Electroweak baryogenesis from a dark sector"*, Phys. Rev. D **95**, 115006 (2017), DOI: 10.1103/PhysRevD.95.115006, [arXiv: 1702.08909 (hep-ph)].

[52] J. M. Cline and K. Kainulainen, *"Improved Electroweak Phase Transition with Subdominant Inert Doublet Dark Matter"*, Phys. Rev. D **87**, 071701 (2013), DOI: 10.1103/PhysRevD.87.071701, [arXiv: 1302.2614 (hep-ph)].

[53] J. M. Cline and K. Kainulainen, *"Electroweak baryogenesis and dark matter from a singlet Higgs"*, J. Cosmol. Astropart. Phys. **01**, 012 (2013), DOI: 10.1088/1475-7516/2013/01/012, [arXiv: 1210.4196 (hep-ph)].

[54] J. M. Cline, K. Kainulainen, and M. Trott, *"Electroweak Baryogenesis in Two Higgs Doublet Models and B meson anomalies"*, J. High Energy Phys. **11**, 089 (2011), DOI: 10.1007/JHEP11(2011)089, [arXiv: 1107.3559 (hep-ph)].

[55] S. Davidson, E. Nardi, and Y. Nir, *"Leptogenesis"*, Phys. Rept. **466**, 105 (2008), DOI: 10.1016/j.physrep.2008.06.002, [arXiv: 0802.2962 (hep-ph)].

[56] A. Pilaftsis, *"The Little Review on Leptogenesis"*, J. Phys. Conf. Ser. **171**, edited by J. Bernabeu, F. J. Botella, N. E. Mavromatos, and V. A. Mitsou, 012017 (2009), DOI: 10.1088/1742-6596/171/1/012017, [arXiv: 0904.1182 (hep-ph)].

[57] S. Blanchet and P. Di Bari, *"The minimal scenario of leptogenesis"*, New J. Phys. **14**, 125012 (2012), DOI: 10.1088/1367-2630/14/12/125012, [arXiv: 1211.0512 (hep-ph)].

[58] A. Pilaftsis and T. E. Underwood, *"Resonant leptogenesis"*, Nucl. Phys. B **692**, 303 (2004), DOI: 10.1016/j.nuclphysb.2004.05.029, [arXiv: hep-ph/0309342].

[59] S. Davidson and A. Ibarra, *"A Lower bound on the right-handed neutrino mass from leptogenesis"*, Phys. Lett. B **535**, 25 (2002), DOI: 10.1016/S0370-2693(02)01735-5, [arXiv: hep-ph/0202239].

[60] A. Granelli, K. Moffat, and S. T. Petcov, *"Flavoured resonant leptogenesis at sub-TeV scales"*, Nucl. Phys. B **973**, 115597 (2021), DOI: 10.1016/j.nuclphysb.2021.115597, [arXiv: 2009.03166 (hep-ph)].

[61] M. Drewes, B. Garbrecht, P. Hernandez, M. Kekic, J. Lopez-Pavon, J. Racker, N. Rius, J. Salvado, and D. Teresi, *"ARS Leptogenesis"*, Int. J. Mod. Phys. A **33**, 1842002 (2018), DOI: 10.1142/S0217751X18420022, [arXiv: 1711.02862 (hep-ph)].

[62] J. Klarić, M. Shaposhnikov, and I. Timiryasov, *"Uniting Low-Scale Leptogenesis Mechanisms"*, Phys. Rev. Lett. **127**, 111802 (2021), DOI: 10.1103/PhysRevLett.127.111802, [arXiv: 2008.13771 (hep-ph)].

[63] E. W. Kolb and S. Wolfram, *"Baryon Number Generation in the Early Universe"*, Nucl. Phys. B **172**, [Erratum: Nucl.Phys.B 195, 542 (1982)], 224 (1980), DOI: 10.1016/0550-3213(82)90012-8.

[64] M. Luty, *"Baryogenesis via leptogenesis"*, Phys. Rev. D **45**, 455 (1992), DOI: 10.1103/PhysRevD.45.455.

[65] A. Basboll and S. Hannestad, *"Decay of heavy Majorana neutrinos using the full Boltzmann equation including its implications for leptogenesis"*, J. Cosmol. Astropart. Phys. **01**, 003 (2007), DOI: 10.1088/1475-7516/2007/01/003, [arXiv: hep-ph/0609025].

[66] W. Buchmuller, P. Di Bari, and M. Plumacher, *"Leptogenesis for pedestrians"*, Annals Phys. **315**, 305 (2005), DOI: 10.1016/j.aop.2004.02.003, [arXiv: hep-ph/0401240].

[67] A. Pilaftsis, *"CP violation and baryogenesis due to heavy Majorana neutrinos"*, Phys. Rev. D **56**, 5431 (1997), DOI: 10.1103/PhysRevD.56.5431, [arXiv: hep-ph/9707235].

[68] W. Buchmuller and M. Plumacher, *"CP asymmetry in Majorana neutrino decays"*, Phys. Lett. B **431**, 354 (1998), DOI: 10.1016/S0370-2693(97)01548-7, [arXiv: hep-ph/9710460].

[69] A. Anisimov, A. Broncano, and M. Plumacher, *"The CP-asymmetry in resonant leptogenesis"*, Nucl. Phys. B **737**, 176 (2006), DOI: 10.1016/j.nuclphysb.2006.01.003, [arXiv: hep-ph/0511248].

[70] P. Bhupal Dev, P. Millington, A. Pilaftsis, and D. Teresi, *"Flavour Covariant Transport Equations: an Application to Resonant Leptogenesis"*, Nucl. Phys. B **886**, 569 (2014), DOI: 10.1016/j.nuclphysb.2014.06.020, [arXiv: 1404.1003 (hep-ph)].

[71] W. Buchmuller and M. Plumacher, *"Spectator processes and baryogenesis"*, Phys. Lett. B **511**, 74 (2001), DOI: 10.1016/S0370-2693(01)00614-1, [arXiv: hep-ph/0104189].

[72] E. Nardi, Y. Nir, J. Racker, and E. Roulet, *"On Higgs and sphaleron effects during the leptogenesis era"*, J. High Energy Phys. **01**, 068 (2006), DOI: 10.1088/1126-6708/2006/01/068, [arXiv: hep-ph/0512052].

[73] A. Pilaftsis and T. E. J. Underwood, *"Electroweak-scale resonant leptogenesis"*, Phys. Rev. D **72**, 113001 (2005), DOI: 10.1103/PhysRevD.72.113001, [arXiv: hep-ph/0506107].

[74] G. Giudice, A. Notari, M. Raidal, A. Riotto, and A. Strumia, *"Towards a complete theory of thermal leptogenesis in the SM and MSSM"*, Nucl. Phys. B **685**, 89 (2004), DOI: 10.1016/j.nuclphysb.2004.02.019, [arXiv: hep-ph/0310123].

[75] M. Garny, A. Kartavtsev, and A. Hohenegger, *"Leptogenesis from first principles in the resonant regime"*, Annals Phys. **328**, 26 (2013), DOI: 10.1016/j.aop.2012.10.007, [arXiv: 1112.6428 (hep-ph)].

[76] P. S. B. Dev, M. Garny, J. Klarić, P. Millington, and D. Teresi, *"Resonant enhancement in leptogenesis"*, Int. J. Mod. Phys. **A33**, 1842003 (2018), DOI: 10.1142/S0217751X18420034, [arXiv: 1711.02863 (hep-ph)].

[77] M. Lindner and M. M. Muller, *"Comparison of Boltzmann equations with quantum dynamics for scalar fields"*, Phys. Rev. D **73**, 125002 (2006), DOI: 10.1103/PhysRevD.73.125002, [arXiv: hep-ph/0512147].

[78] W. Buchmüller and S. Fredenhagen, *"Quantum mechanics of baryogenesis"*, Phys. Lett. **B483**, 217 (2000), DOI: 10.1016/S0370-2693(00)00573-6, [arXiv: hep-ph/0004145 (hep-ph)].

[79] A. De Simone and A. Riotto, *"Quantum Boltzmann Equations and Leptogenesis"*, J. Cosmol. Astropart. Phys. **0708**, 002 (2007), DOI: 10.1088/1475-7516/2007/08/002, [arXiv: hep-ph/0703175 (hep-ph)].

[80] A. De Simone and A. Riotto, *"On Resonant Leptogenesis"*, J. Cosmol. Astropart. Phys. **0708**, 013 (2007), DOI: 10.1088/1475-7516/2007/08/013, [arXiv: 0705.2183 (hep-ph)].

[81] V. Cirigliano, A. De Simone, G. Isidori, I. Masina, and A. Riotto, *"Quantum Resonant Leptogenesis and Minimal Lepton Flavour Violation"*, J. Cosmol. Astropart. Phys. **0801**, 004 (2008), DOI: 10.1088/1475-7516/2008/01/004, [arXiv: 0711.0778 (hep-ph)].

[82] M. Garny, A. Hohenegger, A. Kartavtsev, and M. Lindner, *"Systematic approach to leptogenesis in nonequilibrium QFT: Self-energy contribution to the CP-violating parameter"*, Phys. Rev. **D81**, 085027 (2010), DOI: 10.1103/PhysRevD.81.085027, [arXiv: 0911.4122 (hep-ph)].

[83] M. Garny, A. Hohenegger, A. Kartavtsev, and M. Lindner, *"Systematic approach to leptogenesis in nonequilibrium QFT: Vertex contribution to the CP-violating parameter"*, Phys. Rev. **D80**, 125027 (2009), DOI: 10.1103/PhysRevD.80.125027, [arXiv: 0909.1559 (hep-ph)].

[84] M. Beneke, B. Garbrecht, M. Herranen, and P. Schwaller, *"Finite Number Density Corrections to Leptogenesis"*, Nucl. Phys. **B838**, 1 (2010), DOI: 10.1016/j.nuclphysb.2010.05.003, [arXiv: 1002.1326 (hep-ph)].

[85] M. Beneke, B. Garbrecht, C. Fidler, M. Herranen, and P. Schwaller, *"Flavoured Leptogenesis in the CTP Formalism"*, Nucl. Phys. **B843**, 177 (2011), DOI: 10.1016/j.nuclphysb.2010.10.001, [arXiv: 1007.4783 (hep-ph)].

[86] A. Anisimov, W. Buchmüller, M. Drewes, and S. Mendizabal, *"Quantum Leptogenesis I"*, Annals Phys. **326**, [Erratum: Annals Phys.338,376(2011)], 1998 (2011), DOI: 10.1016/j.aop.2011.02.002,10.1016/j.aop.2013.05.00, [arXiv: 1012.5821 (hep-ph)].

[87] B. Garbrecht and M. Herranen, *"Effective Theory of Resonant Leptogenesis in the Closed-Time-Path Approach"*, Nucl. Phys. **B861**, 17 (2012), DOI: 10.1016/j.nuclphysb.2012.03.009, [arXiv: 1112.5954 (hep-ph)].

[88] S. Iso, K. Shimada, and M. Yamanaka, *"Kadanoff-Baym approach to the thermal resonant leptogenesis"*, J. High Energy Phys. **04**, 062 (2014), DOI: 10.1007/JHEP04(2014)062, [arXiv: 1312.7680 (hep-ph)].

[89] S. Iso and K. Shimada, *"Coherent Flavour Oscillation and CP Violating Parameter in Thermal Resonant Leptogenesis"*, J. High Energy Phys. **08**, 043 (2014), DOI: 10.1007/JHEP08(2014)043, [arXiv: 1404.4816 (hep-ph)].

[90] A. Hohenegger and A. Kartavtsev, *"Leptogenesis in crossing and runaway regimes"*, J. High Energy Phys. **07**, 130 (2014), DOI: 10.1007/JHEP07(2014)130, [arXiv: 1404.5309 (hep-ph)].

[91] B. Garbrecht, F. Gautier, and J. Klarić, *"Strong Washout Approximation to Resonant Leptogenesis"*, J. Cosmol. Astropart. Phys. **1409**, 033 (2014), DOI: 10.1088/1475-7516/2014/09/033, [arXiv: 1406.4190 (hep-ph)].

[92] P. S. B. Dev, P. Millington, A. Pilaftsis, and D. Teresi, *"Kadanoff–Baym approach to flavour mixing and oscillations in resonant leptogenesis"*, Nucl. Phys. **B891**, 128 (2015), DOI: 10.1016/j.nuclphysb.2014.12.003, [arXiv: 1410.6434 (hep-ph)].

[93] A. Kartavtsev, P. Millington, and H. Vogel, *"Lepton asymmetry from mixing and oscillations"*, J. High Energy Phys. **06**, 066 (2016), DOI: 10.1007/JHEP06(2016)066, [arXiv: 1601.03086 (hep-ph)].

[94] M. Drewes, B. Garbrecht, D. Gueter, and J. Klarić, *"Leptogenesis from Oscillations of Heavy Neutrinos with Large Mixing Angles"*, J. High Energy Phys. **12**, 150 (2016), DOI: 10.1007/JHEP12(2016)150, [arXiv: 1606.06690 (hep-ph)].

[95] P. S. B. Dev, P. Di Bari, B. Garbrecht, S. Lavignac, P. Millington, and D. Teresi, *"Flavor effects in leptogenesis"*, Int. J. Mod. Phys. **A33**, 1842001 (2018), DOI: 10.1142/S0217751X18420010, [arXiv: 1711.02861 (hep-ph)].

[96] B. Garbrecht, *"Why is there more matter than antimatter? Calculational methods for leptogenesis and electroweak baryogenesis"*, Prog. Part. Nucl. Phys. **110**, 103727 (2020), DOI: 10.1016/j.ppnp.2019.103727, [arXiv: 1812.02651 (hep-ph)].

[97] P. F. Depta, A. Halsch, J. Hütig, S. Mendizabal, and O. Philipsen, *"Complete leading-order standard model corrections to quantum leptogenesis"*, J. High Energy Phys. **09**, 036 (2020), DOI: 10.1007/JHEP09(2020)036, [arXiv: 2005.01728 (hep-ph)].

[98] J. Racker, *"CP violation in mixing and oscillations for leptogenesis. Part II. The highly degenerate case"*, J. High Energy Phys. **11**, 027 (2021), DOI: 10.1007/JHEP11(2021)027, [arXiv: 2109.00040 (hep-ph)].

[99] J. Berges and J. Serreau, *"Progress in nonequilibrium quantum field theory II"*, in 6th International Conference on Strong and Electroweak Matter (2005), pp. 102–116, DOI: 10.1142/9789812702159_0011, [arXiv: hep-ph/0410330].

[100] J. Berges, *"Controlled nonperturbative dynamics of quantum fields out-of-equilibrium"*, Nucl. Phys. A **699**, 847 (2002), DOI: 10.1016/S0375-9474(01)01295-7, [arXiv: hep-ph/0105311].

[101] M. Le Bellac, *"Thermal Field Theory"* (Cambridge University Press, 1996), ISBN: 978-0-521-65477-7, DOI: 10.1017/CBO9780511721700.

[102] J. I. Kapusta and C. Gale, *"Finite-Temperature Field Theory: Principles and Applications"* (Cambridge University Press, 2006), ISBN: 978-0-521-82082-0, DOI: 10.1017/CBO9780511535130.

[103] J. S. Schwinger, *"Brownian motion of a quantum oscillator"*, J. Math. Phys. **2**, 407 (1961), DOI: 10.1063/1.1703727.

[104] L. V. Keldysh, *"Diagram technique for nonequilibrium processes"*, Zh. Eksp. Teor. Fiz. **47**, [Sov. Phys. JETP20,1018(1965)], 1515 (1964).

[105] P. M. Bakshi and K. T. Mahanthappa, *"Expectation value formalism in quantum field theory. 1."* J. Math. Phys. **4**, 1 (1963), DOI: 10.1063/1.1703883.

[106] R. P. Feynman and F. L. Vernon Jr., *"The Theory of a general quantum system interacting with a linear dissipative system"*, Annals Phys. **24**, edited by L. M. Brown, 118 (1963), DOI: 10.1016/0003-4916(63)90068-X.

[107] K.-c. Chou, Z.-b. Su, B.-l. Hao, and L. Yu, *"Closed time path Green's functions and critical dynamics"*, Phys. Rev. B **22**, 3385 (1980), DOI: 10.1103/PhysRevB.22.3385.

[108] B. S. DeWitt, *"Effective action for expectation values"*, in Quantum Concepts In Space and Time (1986), pp. 325–336, ISBN: 0-19-851972-9.

[109] R. D. Jordan, *"Effective Field Equations for Expectation Values"*, Phys. Rev. D **33**, 444 (1986), DOI: 10.1103/PhysRevD.33.444.

[110] Z.-b. Su, L.-Y. Chen, X.-t. Yu, and K.-c. Chou, *"Influence functional and closed-time-path Green's function"*, Phys. Rev. B **37**, 9810 (1988), DOI: 10.1103/PhysRevB.37.9810.

[111] K.-c. Chou, Z.-b. Su, B.-l. Hao, and L. Yu, *"Equilibrium and Nonequilibrium Formalisms Made Unified"*, Phys. Rept. **118**, 1 (1985), DOI: 10.1016/0370-1573(85)90136-X.

[112] M. E. Peskin and D. V. Schroeder, *"An Introduction to quantum field theory"* (Westview Press, 1995), ISBN: 978-0-201-50397-5, DOI: 10.1201/9780429503559.

[113] J. Berges, *"Nonequilibrium Quantum Fields: From Cold Atoms to Cosmology"*, (2015), [arXiv: 1503.02907 (hep-ph)].

[114] E. Calzetta and B. L. Hu, *"Nonequilibrium Quantum Fields: Closed Time Path Effective Action, Wigner Function and Boltzmann Equation"*, Phys. Rev. D **37**, 2878 (1988), DOI: 10.1103/PhysRevD.37.2878.

[115] J. Berges, *"Introduction to nonequilibrium quantum field theory"*, AIP Conf. Proc. **739**, edited by M. Bracco, M. Chiapparini, E. Ferreira, and T. Kodama, 3 (2004), DOI: 10.1063/1.1843591, [arXiv: hep-ph/0409233].

[116] J. Berges and J. Cox, *"Thermalization of quantum fields from time reversal invariant evolution equations"*, Phys. Lett. B **517**, 369 (2001), DOI: 10.1016/S0370-2693(01)01004-8, [arXiv: hep-ph/0006160].

[117] J. Berges and J. Serreau, *"Progress in nonequilibrium quantum field theory"*, in 5th Internationa Conference on Strong and Electroweak Matter (2003), pp. 111–126, DOI: 10.1142/9789812704498_0011, [arXiv: hep-ph/0302210].

[118] J. Berges, *"N-particle irreducible effective action techniques for gauge theories"*, Phys. Rev. D **70**, 105010 (2004), DOI: 10.1103/PhysRevD.70.105010, [arXiv: hep-ph/0401172].

[119] M. Brown and I. Whittingham, *"Two-particle irreducible effective actions versus resummation: analytic properties and self-consistency"*, Nucl. Phys. B **900**, 477 (2015), DOI: 10.1016/j.nuclphysb.2015.09.021, [arXiv: 1503.08664 (hep-th)].

[120] T. D. Lee and C. N. Yang, *"Many-Body Problem in Quantum Statistical Mechanics. 4. Formulation in Terms of Average Occupation Number in Momentum Space"*, Phys. Rev. **117**, 22 (1960), DOI: 10.1103/PhysRev.117.22.

[121] J. M. Luttinger and J. C. Ward, *"Ground state energy of a many fermion system. 2."* Phys. Rev. **118**, 1417 (1960), DOI: 10.1103/PhysRev.118.1417.

[122] G. Baym, *"Selfconsistent approximation in many body systems"*, Phys. Rev. **127**, 1391 (1962), DOI: 10.1103/PhysRev.127.1391.

[123] J. M. Cornwall, R. Jackiw, and E. Tomboulis, *"Effective Action for Composite Operators"*, Phys. Rev. **D10**, 2428 (1974), DOI: 10.1103/PhysRevD.10.2428.

[124] M. Garny and U. Reinosa, *"Renormalization out of equilibrium in a super-renormalizable theory"*, Phys. Rev. D **94**, 045012 (2016), DOI: 10.1103/PhysRevD.94.045012, [arXiv: 1504.06643 (hep-ph)].

[125] R. Jackiw, *"Functional evaluation of the effective potential"*, Phys. Rev. D **9**, 1686 (1974), DOI: 10.1103/PhysRevD.9.1686.

[126] U. Reinosa and J. Serreau, *"Ward Identities for the 2PI effective action in QED"*, J. High Energy Phys. **11**, 097 (2007), DOI: 10.1088/1126-6708/2007/11/097, [arXiv: 0708.0971 (hep-th)].

[127] E. A. Calzetta, *"The Two particle irreducible effective action in gauge theories"*, Int. J. Theor. Phys. **43**, edited by E. Gunzig, V. F. Mukhanov, and E. Verdaguer, 767 (2004), DOI: 10.1023/B:IJTP.0000048174.83795.3f, [arXiv: hep-ph/0402196].

[128] J. Berges, S. Borsanyi, and J. Serreau, *"Thermalization of fermionic quantum fields"*, Nucl. Phys. B **660**, 51 (2003), DOI: 10.1016/S0550-3213(03)00261-X, [arXiv: hep-ph/0212404].

[129] T. Prokopec, M. G. Schmidt, and S. Weinstock, *"Transport equations for chiral fermions to order h bar and electroweak baryogenesis. Part 1"*, Annals Phys. **314**, 208 (2004), DOI: 10.1016/j.aop.2004.06.002, [arXiv: hep-ph/0312110].

[130] G. Baym and L. P. Kadanoff, *"Conservation Laws and Correlation Functions"*, Phys. Rev. **124**, 287 (1961), DOI: 10.1103/PhysRev.124.287.

[131] L. P. Kadanoff and G. Baym, *"Quantum Statistical Mechanics"* (W. A. Benjamin, 1962), ISBN: 978-0-201-41046-4, DOI: 10.1201/9780429493218.

[132] P. Danielewicz, *"Quantum Theory of Nonequilibrium Processes. 1."* Annals Phys. **152**, 239 (1984), DOI: 10.1016/0003-4916(84)90092-7.

[133] K. Kainulainen, *"CP-violating transport theory for electroweak baryogenesis with thermal corrections"*, J. Cosmol. Astropart. Phys. **11**, 042 (2021), DOI: 10.1088/1475-7516/2021/11/042, [arXiv: 2108.08336 (hep-ph)].

[134] M. Drewes, S. Mendizabal, and C. Weniger, *"The Boltzmann Equation from Quantum Field Theory"*, Phys. Lett. B **718**, 1119 (2013), DOI: 10.1016/j.physletb.2012.11.046, [arXiv: 1202.1301 (hep-ph)].

[135] J. E. Moyal, *"Quantum mechanics as a statistical theory"*, Proc. Cambridge Phil. Soc. **45**, 99 (1949), DOI: 10.1017/S0305004100000487.

[136] H. J. Groenewold, *"On the Principles of elementary quantum mechanics"*, Physica **12**, 405 (1946), DOI: 10.1016/S0031-8914(46)80059-4.

[137] S. Weinberg, *"The Quantum theory of fields. Vol. 1: Foundations"* (Cambridge University Press, 1995), ISBN: 978-0-521-55001-7, DOI: 10.1017/CBO9781139644167.

[138] C. Greiner and S. Leupold, *"Stochastic interpretation of Kadanoff-Baym equations and their relation to Langevin processes"*, Annals Phys. **270**, 328 (1998), DOI: 10.1006/aphy.1998.5849, [arXiv: hep-ph/9802312].

[139] T. Prokopec, M. G. Schmidt, and J. Weenink, *"Exact solution of the Dirac equation with CP violation"*, Phys. Rev. D **87**, 083508 (2013), DOI: 10.1103/PhysRevD.87.083508, [arXiv: 1301.4132 (hep-th)].

[140] J. M. Cline and K. Kainulainen, *"Electroweak baryogenesis at high bubble wall velocities"*, Phys. Rev. D **101**, 063525 (2020), DOI: 10.1103/PhysRevD.101.063525, [arXiv: 2001.00568 (hep-ph)].

[141] J. M. Cline, *"Is electroweak baryogenesis dead?"*, edited by E. Auge, J. Dumarchez, and J. Tran Thanh Van, 339 (2017), DOI: 10.1098/rsta.2017.0116, [arXiv: 1704.08911 (hep-ph)].

[142] D. Bodeker, L. Fromme, S. J. Huber, and M. Seniuch, *"The Baryon asymmetry in the standard model with a low cut-off"*, J. High Energy Phys. **02**, 026 (2005), DOI: 10.1088/1126-6708/2005/02/026, [arXiv: hep-ph/0412366].

[143] J. M. Cline, M. Joyce, and K. Kainulainen, *"Supersymmetric electroweak baryogenesis in the WKB approximation"*, Phys. Lett. B **417**, [Erratum: Phys.Lett.B 448, 321–321 (1999)], 79 (1998), DOI: 10.1016/S0370-2693(97)01361-0, [arXiv: hep-ph/9708393].

[144] J. M. Cline, M. Joyce, and K. Kainulainen, *"Erratum for 'Supersymmetric electroweak baryogenesis'"*, (2001), [arXiv: hep-ph/0110031].

[145] K. Kainulainen, T. Prokopec, M. G. Schmidt, and S. Weinstock, *"First principle derivation of semiclassical force for electroweak baryogenesis"*, J. High Energy Phys. **06**, 031 (2001), DOI: 10.1088/1126-6708/2001/06/031, [arXiv: hep-ph/0105295].

[146] K. Kainulainen, T. Prokopec, M. G. Schmidt, and S. Weinstock, *"Semiclassical force for electroweak baryogenesis: Three-dimensional derivation"*, Phys. Rev. D **66**, 043502 (2002), DOI: 10.1103/PhysRevD.66.043502, [arXiv: hep-ph/0202177].

[147] P. B. Pal, *"Dirac, Majorana and Weyl fermions"*, Am. J. Phys. **79**, 485 (2011), DOI: 10.1119/1.3549729, [arXiv: 1006.1718 (hep-ph)].

[148] K. Enqvist, K. Kainulainen, and J. Maalampi, *"Refraction and Oscillations of Neutrinos in the Early Universe"*, Nucl. Phys. B **349**, 754 (1991), DOI: 10.1016/0550-3213(91)90397-G.

[149] K. Enqvist, K. Kainulainen, and M. J. Thomson, *"Stringent cosmological bounds on inert neutrino mixing"*, Nucl. Phys. B **373**, 498 (1992), DOI: 10.1016/0550-3213(92)90442-E.

[150] K. Kainulainen, *"Light Singlet Neutrinos and the Primordial Nucleosynthesis"*, Phys. Lett. B **244**, 191 (1990), DOI: 10.1016/0370-2693(90)90054-A.

[151] G. R. Farrar and M. E. Shaposhnikov, *"Baryon asymmetry of the universe in the standard electroweak theory"*, Phys. Rev. D **50**, 774 (1994), DOI: 10.1103/PhysRevD.50.774, [arXiv: hep-ph/9305275].

[152] M. Joyce, T. Prokopec, and N. Turok, *"Nonlocal electroweak baryogenesis. Part 1: Thin wall regime"*, Phys. Rev. D **53**, 2930 (1996), DOI: 10.1103/PhysRevD.53.2930, [arXiv: hep-ph/9410281].

[153] J. M. Cline, K. Kainulainen, and A. P. Vischer, *"Dynamics of two Higgs doublet CP violation and baryogenesis at the electroweak phase transition"*, Phys. Rev. D **54**, 2451 (1996), DOI: 10.1103/PhysRevD.54.2451, [arXiv: hep-ph/9506284].

[154] K. Kainulainen and O. Koskivaara, *"Non-equilibrium dynamics of a scalar field with quantum backreaction"*, J. High Energy Phys. **12**, 190 (2021), DOI: 10.1007/JHEP12(2021)190, [arXiv: 2105.09598 (hep-ph)].

ORIGINAL PAPERS

I

QUANTUM TRANSPORT AND THE PHASE SPACE STRUCTURE OF THE WIGHTMAN FUNCTIONS

by

Jukkala, Henri & Kainulainen, Kimmo & Koskivaara, Olli 2020

Journal of High Energy Physics, 2020, 12

DOI:10.1007/JHEP01(2020)012

Published for SISSA by Springer

Received: October 30, 2019
Accepted: December 16, 2019
Published: January 3, 2020

Quantum transport and the phase space structure of the Wightman functions

Henri Jukkala,[a,b] **Kimmo Kainulainen**[a,b,c] **and Olli Koskivaara**[a,b]

[a] *Department of Physics, University of Jyväskylä, P.O. Box 35 (YFL), FI-40014 Jyväskylä, Finland*
[b] *Helsinki Institute of Physics, University of Helsinki, P.O. Box 64, FI-00014 Helsinki, Finland*
[c] *Theoretical Physics Department, CERN, 1211 Geneva 23, Switzerland*

E-mail: henri.a.jukkala@student.jyu.fi, kimmo.kainulainen@jyu.fi, olli.a.koskivaara@student.jyu.fi

Abstract: We study the phase space structure of exact quantum Wightman functions in spatially homogeneous, temporally varying systems. In addition to the usual mass shells, the Wightman functions display additional coherence shells around zero frequency $k_0 = 0$, which carry the information of the local quantum coherence of particle-antiparticle pairs. We find also other structures, which encode non-local correlations in time, and discuss their role and decoherence. We give a simple derivation of the cQPA formalism, a set of quantum transport equations, that can be used to study interacting systems including the local quantum coherence. We compute quantum currents created by a temporal change in a particle's mass, comparing the exact Wightman function approach, the cQPA and the semiclassical methods. We find that the semiclassical approximation, which is fully encompassed by the cQPA, works surprisingly well even for very sharp temporal features. This is encouraging for the application of semiclassical methods in electroweak baryogenesis with strong phase transitions.

Keywords: Thermal Field Theory, CP violation, Quantum Dissipative Systems

ArXiv ePrint: 1910.10979

https://doi.org/10.1007/JHEP01(2020)012

Contents

1 Introduction

Quantum coherence plays an important role in many physical problems in cosmology. Examples include CP-violating particle-wall interactions during the electroweak phase transition, out-of-equilibrium decay of nearly degenerate heavy neutrinos during leptogenesis, particle production during phase transitions and reheating at the end of inflation. The key quantity in the analysis of such intrinsically quantum systems is the two-point correlation function, whose evolution is described by the Schwinger-Dyson equations [1, 2], or in the phase space picture by the Kadanoff-Baym equations [3–5]. The phase space picture in particular has provided a useful basis for deriving approximate transport formalisms, the prime example being the standard Boltzmann theory.

In this paper we study an exact, damped, spatially homogeneous and isotropic two-point correlation function of a fermion with a possibly complex, time-varying mass term. We show that the mixed representation correlation function contains novel shell structures which carry information about different types of quantum coherences. For example we find

a shell at $k_0 = 0$, which encodes the information of a coherently mixing particle-antiparticle system. This shell was previously seen in the context of the coherent quasiparticle approximation (cQPA) [6–12] in the spectral limit, but our derivation is more general, being exact in the non-interacting case. In addition we find also other shell-structures, corresponding to non-local (in the relative time coordinate), long range correlations.

All phase space structures depend sensitively on the existence and the magnitude of damping. In the non-interacting case non-local coherences dominate the system, preventing a free particle interpretation of the phase space structure in non-trivial backgrounds. Damping suppresses the non-local coherences and leads to the emergence of a local limit for time intervals $\Delta t > 1/\Gamma$, where Γ is the damping width. For small enough Γ the local correlation function can be well approximated by a spectral ansatz, leading to the cQPA-picture mentioned above.

We will introduce a new, elegant way to reorganise the gradient expansion in the mixed representation Kadanoff-Baym equations. We then use it to give a simple derivation of the cQPA equations complete with explicit collision integrals for arbitrary types of interactions. These equations are one of the main results of this paper: they generalise the usual Boltzmann transport theory to systems including coherent particle-antiparticle states. In particular we argue that the cQPA completely encompasses the well known semiclassical effects. Possible applications of these equations include baryogenesis during phase transitions and particle production during and after inflation.

We compute the axial current densities using the exact mixed representation correlation functions as well as their cQPA counterparts and compare these to the ones obtained in the semiclassical approximation. We find that the semiclassical methods work reasonably well even in systems where the relevant modes have a wavelength as small as half of the wall width.[1] This is encouraging for the application of semiclassical methods in the related problem of electroweak phase baryogenesis with very strong electroweak phase transitions. These typically create sharp transition walls and are often encountered in the context of models producing large, observable gravitational wave signals [13–18].

This paper is organised as follows: in section 2 we first review the derivation of the cQPA formalism including the spectral Wightman functions. In section 3 we construct the exact free Wightman function from mode functions, generalised to account for the damping. Some numerical examples for the phase space solutions are shown in section 4. In section 5, we compute and compare currents in different approximations in the non-interacting case. In section 6 we present cQPA transport equations in the interacting case with explicit expressions for collision terms and compute cQPA currents with interactions. Finally, in section 7, we give our conclusions.

[1] Throughout this paper we use the word 'wall' to refer to the temporal transition in the mass, see e.g. figure 2a.

2 Wightman functions and cQPA

We are using the Schwinger-Keldysh formalism [1, 2] of finite temperature field theory. The key quantities are the two-point Wightman functions

$$\begin{aligned} \mathrm{i}S^{<}(u,v) &= \big\langle \overline{\psi}(v)\psi(u)\big\rangle, \\ \mathrm{i}S^{>}(u,v) &= \big\langle \psi(u)\overline{\psi}(v)\big\rangle, \end{aligned} \tag{2.1}$$

which describe the quantum statistical properties of the non-equilibrium system.[2] We also need the retarded and advanced correlation functions $\mathrm{i}S^{\mathrm{r}}(u,v) = 2\theta(u_0-v_0)\mathcal{A}(u,v)$ and $\mathrm{i}S^{\mathrm{a}}(u,v) = -2\theta(v_0-u_0)\mathcal{A}(u,v)$, where the *spectral function* is $\mathcal{A} \equiv \frac{1}{2}\langle\{\psi(u),\overline{\psi}(v)\}\rangle = \frac{\mathrm{i}}{2}(S^{>}+S^{<}) = \frac{\mathrm{i}}{2}(S^{\mathrm{r}}-S^{\mathrm{a}})$.

To get a phase space description of the system we perform the Wigner transformation

$$S(k,x) \equiv \int \mathrm{d}^4 r\, \mathrm{e}^{\mathrm{i}k\cdot r} S\left(x+\frac{r}{2}, x-\frac{r}{2}\right), \tag{2.2}$$

where $r \equiv u-v$ and $x \equiv \frac{1}{2}(u+v)$ are the relative and average coordinates, corresponding to microscopic and macroscopic scales, respectively. In this mixed Wigner representation correlation functions obey the Kadanoff-Baym equations [3]

$$\left(\not{k} + \frac{\mathrm{i}}{2}\not{\partial}\right) S^{p} - \mathrm{e}^{-\mathrm{i}\diamondsuit}\{\Sigma^{p}\}\{S^{p}\} = 1, \tag{2.3}$$

$$\left(\not{k} + \frac{\mathrm{i}}{2}\not{\partial}\right) S^{s} - \mathrm{e}^{-\mathrm{i}\diamondsuit}\{\Sigma^{\mathrm{r}}\}\{S^{s}\} = \mathrm{e}^{-\mathrm{i}\diamondsuit}\{\Sigma^{s}\}\{S^{\mathrm{a}}\}, \tag{2.4}$$

where $s = <, >$ and $p = \mathrm{r}, \mathrm{a}$ refer to the retarded and advanced functions, respectively, Σ is the fermion self-energy and $\diamondsuit\{f\}\{g\} \equiv \frac{1}{2}[\partial_x f\cdot\partial_k g - \partial_k f\cdot\partial_x g]$ is the Moyal product. Note that we absorb the mass terms into the singular parts of $\Sigma^{\mathrm{r,a}}$, unless explicitly stated otherwise.

Moyal products are not the optimal way for organising the gradient expansions, and we find it useful to introduce another self-energy function:

$$\Sigma_{\mathrm{out}}(k,x) \equiv \int \mathrm{d}^4 z\, \mathrm{e}^{\mathrm{i}k\cdot(x-z)}\Sigma(x,z) = \mathrm{e}^{\frac{\mathrm{i}}{2}\overleftarrow{\partial_x^{\Sigma}}\cdot\overrightarrow{\partial_k^{\Sigma}}}\Sigma(k,x). \tag{2.5}$$

Using equation (2.5) we can rewrite Moyal products in a form that reorganises the gradients into total k-derivatives controlled by the scale of variation of Σ, while all dependence on (dynamical) gradients acting on S is fully accounted for by iterative resummation:

$$\not{\hat{K}} S^{p} - \mathrm{e}^{-\frac{\mathrm{i}}{2}\overleftarrow{\partial_x^{\Sigma}}\cdot\partial_k}[\Sigma^{p}_{\mathrm{out}}(\hat{K},x)S^{p}] = 1, \tag{2.6}$$

$$\not{\hat{K}} S^{s} - \mathrm{e}^{-\frac{\mathrm{i}}{2}\overleftarrow{\partial_x^{\Sigma}}\cdot\partial_k}[\Sigma^{\mathrm{r}}_{\mathrm{out}}(\hat{K},x)S^{s}] = \mathrm{e}^{-\frac{\mathrm{i}}{2}\overleftarrow{\partial_x^{\Sigma}}\cdot\partial_k}[\Sigma^{s}_{\mathrm{out}}(\hat{K},x)S^{\mathrm{a}}], \tag{2.7}$$

where $\hat{K} \equiv k + \frac{\mathrm{i}}{2}\partial_x$. This form of the Kadanoff-Baym equations is particularly well suited for obtaining finite order expansions and iterative solutions. The mass operator is included in the singular part Σ_{sg} of the retarded/advanced self-energy functions:

$$\Sigma^{\mathrm{r,a}}(k,x) = \Sigma_{\mathrm{sg}}(x) + \Sigma^{\mathrm{H}}_{\mathrm{nsg}}(k,x) \mp \mathrm{i}\Sigma^{\mathcal{A}}(k,x), \tag{2.8}$$

[2] Note that we define the Wightman function $S^{<}$ with a positive sign. We also suppress Dirac indices when there is no danger of confusion.

where $\Sigma^{\rm H}_{\rm nsg}$ is the non-singular Hermitian part and $\Sigma^{\mathcal{A}}$ is the anti-Hermitian part of the self-energy. To be specific, we consider a fermion field with a complex, spacetime-dependent mass $m(x)$:

$$\mathcal{L} = \mathrm{i}\overline{\psi}\partial\!\!\!/\psi - m^*(x)\overline{\psi}_{\rm R}\psi_{\rm L} - m(x)\overline{\psi}_{\rm L}\psi_{\rm R}, \tag{2.9}$$

where $\psi_{\rm L,R} \equiv \frac{1}{2}(1 \mp \gamma^5)\psi$. In the Wigner representation the spacetime-dependent mass gives rise to an operator:

$$(\hat{m}_{\rm R} + \mathrm{i}\gamma^5\hat{m}_{\rm I})S(k,x) \equiv \mathrm{e}^{-\frac{\mathrm{i}}{2}\partial_x^m\cdot\partial_k}\left\{[m_{\rm R}(x) + \mathrm{i}\gamma^5 m_{\rm I}(x)]S(k,x)\right\}, \tag{2.10}$$

where $m_{\rm R}(x)$ and $m_{\rm I}(x)$ are the real and imaginary parts of $m(x)$, respectively.

Equations (2.6) and (2.7) are practically impossible to solve exactly and one needs to find approximation schemes that maintain the essential physics at hand. The cQPA developed in refs. [6–12] is one such scheme, which allows to study particular non-equilibrium systems with quantum coherence. The crux of the cQPA is to solve equations (2.6) and (2.7) in two steps. First one solves for the phase space structure of the system at the lowest order in gradients and ignoring collision terms. This leads to spectral solutions for both pole and Wightman functions, where the latter contain new coherence shells in addition to the usual mass shell solutions. In the second step, one inserts these solutions back to the full equations, which are then reduced to a set of Boltzmann-like equations for generalised particle distribution functions [10, 11].

2.1 cQPA-solution in a spatially homogeneous system

Let us consider a spatially homogeneous and isotropic system, where $m(x) \to m(t)$ in equations (2.9) and (2.10). The Wigner transform (2.2) with respect to spatial coordinates then reduces to a Fourier transform, and we will denote the Wigner transform $S(k,x)$ as $S_{\boldsymbol{k}}(k_0,t)$. We also consider explicitly only the equation for $S^<$, as the derivation for $S^>$ is completely analogous. At first we will ignore interactions and work to the lowest order in gradients. The Hermitian part of equation (2.7) for $\overline{S}^< \equiv \mathrm{i}S^<\gamma^0$ then reduces to

$$2k_0\overline{S}^<_{\boldsymbol{k}}(k_0,t) = \{H_{\boldsymbol{k}}(t), \overline{S}^<_{\boldsymbol{k}}(k_0,t)\}, \tag{2.11}$$

where $H_{\boldsymbol{k}}(t) \equiv \boldsymbol{\alpha}\cdot\boldsymbol{k} + \gamma^0[m_{\rm R}(t) + \mathrm{i}\gamma^5 m_{\rm I}(t)]$ is the free Dirac Hamiltonian.

In spatially homogeneous and isotropic systems the Wightman functions have 8 independent components and can be parametrised without any loss of generality as follows:

$$\overline{S}^<_{\boldsymbol{k}}(k_0,t) \equiv \sum_{h,\pm,\pm'} P^{(4)}_{h\boldsymbol{k}} P^{\pm}_{\boldsymbol{k}}\gamma^0 P^{\pm'}_{\boldsymbol{k}}\, D^{\pm\pm'}_{h\boldsymbol{k}}(k_0,t), \tag{2.12}$$

where the helicity and energy projection operators are defined, respectively, as

$$P^{(4)}_{h\boldsymbol{k}} \equiv \frac{1}{2}\big(\mathbb{1} + h\boldsymbol{\alpha}\cdot\hat{\boldsymbol{k}}\gamma^5\big), \qquad P^{\pm}_{\boldsymbol{k}} \equiv \frac{1}{2}\left(\mathbb{1} \pm \frac{H_{\boldsymbol{k}}}{\omega_{\boldsymbol{k}}}\right), \tag{2.13}$$

with $\hat{\boldsymbol{k}} \equiv \boldsymbol{k}/|\boldsymbol{k}|$ and $\omega_{\boldsymbol{k}} \equiv \sqrt{\boldsymbol{k}^2 + |m(t)|^2}$. Inserting the parametrisation (2.12) to equation (2.11) gives algebraic constraints to the time- and energy-dependent coefficient functions $D^{\pm\pm'}_{h\boldsymbol{k}}(k_0,t)$:

$$\begin{aligned}(k_0 \mp \omega_{\boldsymbol{k}})D^{\pm\pm}_{h\boldsymbol{k}}(k_0,t) &= 0,\\ k_0 D^{\pm\mp}_{h\boldsymbol{k}}(k_0,t) &= 0.\end{aligned} \tag{2.14}$$

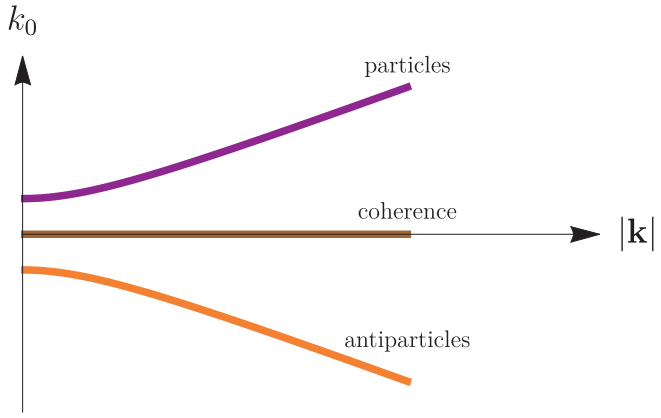

Figure 1. The shell structure of the cQPA Wightman function $S^<_{\boldsymbol{k}}(k_0, t)$, showing the particle shell where $k_0 = \omega_{\boldsymbol{k}}$ (purple), the antiparticle shell where $k_0 = -\omega_{\boldsymbol{k}}$ (orange) and the particle-antiparticle coherence shell where $k_0 = 0$ (brown).

Functions $D^{\pm\pm}_{h\boldsymbol{k}}(k_0, t) \propto \delta(k_0 \mp \omega_{\boldsymbol{k}})$ correspond to the usual mass shell excitations, while $D^{\pm\mp}_{h\boldsymbol{k}}(k_0, t) \propto \delta(k_0)$ are the new coherence functions found in refs. [7–11]. The spectral cQPA-solution can then be written as:

$$\overline{S}^<_{\boldsymbol{k}}(k_0, t) = 2\pi \sum_{h,\pm} \left[P^{m\pm}_{h\boldsymbol{k}} f^{m\pm}_{h\boldsymbol{k}} \delta(k_0 \mp \omega_{\boldsymbol{k}}) + P^{c\pm}_{h\boldsymbol{k}} f^{c\pm}_{h\boldsymbol{k}} \delta(k_0) \right]. \tag{2.15}$$

where we defined the projection operators

$$\begin{aligned} P^{m\pm}_{h\boldsymbol{k}} &\equiv \pm \frac{\omega_{\boldsymbol{k}}}{m_{\mathrm{R}}} P^{(4)}_{h\boldsymbol{k}} P^{\pm}_{\boldsymbol{k}} \gamma^0 P^{\pm}_{\boldsymbol{k}} = P^{(4)}_{h\boldsymbol{k}} P^{\pm}_{\boldsymbol{k}}, \\ P^{c\pm}_{h\boldsymbol{k}} &\equiv P^{(4)}_{h\boldsymbol{k}} P^{\pm}_{\boldsymbol{k}} \gamma^0 P^{\mp}_{\boldsymbol{k}} = P^{(4)}_{h\boldsymbol{k}} \left(\gamma^0 \pm \frac{m_{\mathrm{R}}}{\omega_{\boldsymbol{k}}} \right) P^{\mp}_{\boldsymbol{k}}. \end{aligned} \tag{2.16}$$

With this normalisation the mass shell functions $f^{m\pm}_{h\boldsymbol{k}}(t)$ coincide with the usual Fermi-Dirac distributions in the thermal limit: $f^{m\pm}_{h\boldsymbol{k}} \to f_{\mathrm{eq}}(\pm\omega_{\boldsymbol{k}})$, where $f_{\mathrm{eq}}(k_0) \equiv (\mathrm{e}^{k_0/T} + 1)^{-1}$. Note that due to the Hermiticity of $\overline{S}^<_{h\boldsymbol{k}}(k_0, t)$ the shell functions obey $(f^{m\pm}_{h\boldsymbol{k}})^* = f^{m\pm}_{h\boldsymbol{k}}$ and $(f^{c\pm}_{h\boldsymbol{k}})^* = f^{c\mp}_{h\boldsymbol{k}}$. The phase space structure of the cQPA Wightman functions is shown in figure 1.

The cQPA evolution equations are then obtained by inserting the spectral ansatz (2.15) to the anti-Hermitian part of equation (2.7), now including all gradients and interaction terms, and integrating over the energy. However, let us again first consider this equation in the non-interacting limit and to lowest order in gradients:

$$\mathrm{i}\partial_t \overline{S}^<_{\boldsymbol{k}}(k_0, t) = \left[H_{\boldsymbol{k}}, \overline{S}^<_{\boldsymbol{k}}(k_0, t) \right]. \tag{2.17}$$

Substituting the spectral solution (2.15) for $\overline{S}^<_{\boldsymbol{k}}(k_0, t)$ to equation (2.17) and integrating over k_0 it is easy to derive the leading behaviour of the shell-functions:

$$\begin{aligned} \partial_t f^{m\pm}_{h\boldsymbol{k}} &= \dots, \\ \partial_t f^{c\pm}_{h\boldsymbol{k}} &= \mp 2\mathrm{i}\omega_{\boldsymbol{k}} f^{c\pm}_{h\boldsymbol{k}} + \dots, \end{aligned} \tag{2.18}$$

where the ellipses denote terms proportional to gradient terms (and eventually self-energy terms when interactions are included).

The point we wish to make here is that the coherence shell solutions $f^{c\pm}_{h\boldsymbol{k}}$ are oscillating rapidly with frequencies that are not suppressed by gradients. Anticipating this oscillation was the reason for our careful organisation of gradient terms in equations (2.6) and (2.7): whenever the operator $\hat{K}_0 = k_0 + \frac{\mathrm{i}}{2}\partial_t$ is acting on a coherence shell function $f^{c\pm}_{h\boldsymbol{k}}$, one must replace $\hat{K}_0 \to k_0 \pm \omega_{\boldsymbol{k}}$ as the effective momentum argument of the operator, at the *lowest* order in gradients. Indeed, in cQPA:

$$
\begin{aligned}
&\int \frac{\mathrm{d}k_0}{2\pi}\, \mathrm{e}^{-\frac{\mathrm{i}}{2}\partial^{\Sigma}_x\cdot\partial_k}\left[\Sigma_{\mathrm{out},\boldsymbol{k}}\left(k_0+\frac{\mathrm{i}}{2}\partial_t\right)\overline{S}^{<}_{h\boldsymbol{k}}(k_0,t)\right]\\
&=\sum_{\pm}\int \mathrm{d}k_0\,\Sigma_{\mathrm{out},\boldsymbol{k}}\left(k_0+\frac{\mathrm{i}}{2}\partial_t\right)\left[P^{m\pm}_{h\boldsymbol{k}}(t)f^{m\pm}_{h\boldsymbol{k}}(t)\delta(k_0\mp\omega_{\boldsymbol{k}})+P^{c\pm}_{h\boldsymbol{k}}(t)f^{c\pm}_{h\boldsymbol{k}}(t)\delta(k_0)\right]\\
&\simeq\sum_{\pm}\int \mathrm{d}k_0\left[\Sigma_{\mathrm{out},\boldsymbol{k}}(k_0)P^{m\pm}_{h\boldsymbol{k}}(t)f^{m\pm}_{h\boldsymbol{k}}(t)\delta(k_0\mp\omega_{\boldsymbol{k}})+\Sigma_{\mathrm{out},\boldsymbol{k}}(k_0\pm\omega_{\boldsymbol{k}})P^{c\pm}_{h\boldsymbol{k}}(t)f^{c\pm}_{h\boldsymbol{k}}(t)\delta(k_0)\right]\\
&=\sum_{\pm}\Sigma_{\mathrm{out},\boldsymbol{k}}(\pm\omega_{\boldsymbol{k}})\left[P^{m\pm}_{h\boldsymbol{k}}(t)f^{m\pm}_{h\boldsymbol{k}}(t)+P^{c\pm}_{h\boldsymbol{k}}(t)f^{c\pm}_{h\boldsymbol{k}}(t)\right]
\end{aligned}
\tag{2.19}
$$

for a generic self-energy function Σ. That is, coherence shell projections are not evaluated at the shell $k_0 = 0$, but on the mass shells instead. It would be straightforward to include higher order gradient corrections to shell positions generated by the $\hat{K}_0$-operator, but doing so consistently, we should also solve the cQPA-ansatz to higher order in gradients. The gradient corrections to collision terms arising from such an expansion (collisional source terms) were studied in ref. [19] for the electroweak baryogenesis problem using semiclassical methods. They were in general found to be very small and we shall not pursue them here further. For the same reason we shall, in what follows, set $\Sigma_{\mathrm{out},\boldsymbol{k}} \to \Sigma_{\boldsymbol{k}}$, dropping the corrections coming from the expansion of the Σ_{out}-function in equation (2.5).[3]

We will also work with the vacuum dispersion relations, setting $\Sigma^{\mathrm{H}}_{\mathrm{nsg}} \to 0$ and $\Sigma_{\mathrm{sg}} \to m_{\mathrm{R}} + \mathrm{i}\gamma^5 m_{\mathrm{I}}$. Furthermore, we shall drop the term $\propto S_{\mathrm{H}}\Sigma^{<}$, as this is required by the consistency of the spectral limit with respect to the pole equations [7]. With these simplifications it is now straightforward to show that the full cQPA equations can be written as

$$
\partial_t f^{m\pm}_{h\boldsymbol{k}} = \pm\frac{1}{2}\sum_s \dot{\Phi}^s_{h\boldsymbol{k}} f^{cs}_{h\boldsymbol{k}} + \mathrm{Tr}\left[\mathcal{C}_{\mathrm{coll}}P^{m\pm}_{h\boldsymbol{k}}\right], \tag{2.20a}
$$

$$
\partial_t f^{c\pm}_{h\boldsymbol{k}} = \mp 2\mathrm{i}\omega_{\boldsymbol{k}} f^{c\pm}_{h\boldsymbol{k}} + \xi_{\boldsymbol{k}}\dot{\Phi}^{\mp}_{h\boldsymbol{k}}\left[\frac{m_{\mathrm{R}}}{\omega_{\boldsymbol{k}}}f^{c\pm}_{h\boldsymbol{k}} - \frac{1}{2}\left(f^{m+}_{h\boldsymbol{k}} - f^{m-}_{h\boldsymbol{k}}\right)\right] + \xi_{\boldsymbol{k}}\,\mathrm{Tr}\left[\mathcal{C}_{\mathrm{coll}}P^{c\mp}_{h\boldsymbol{k}}\right], \tag{2.20b}
$$

where

$$
\mathcal{C}_{\mathrm{coll}} = \sum_{h,s}\left[\left(\frac{1}{2}\overline{\Sigma}^{<}_{\boldsymbol{k}}(s\omega_{\boldsymbol{k}}) - f^{ms}_{h\boldsymbol{k}}\,\overline{\Sigma}^{\mathcal{A}}_{\boldsymbol{k}}(s\omega_{\boldsymbol{k}})\right)P^{ms}_{h\boldsymbol{k}} - f^{cs}_{h\boldsymbol{k}}\,\overline{\Sigma}^{\mathcal{A}}_{\boldsymbol{k}}(s\omega_{\boldsymbol{k}})P^{cs}_{h\boldsymbol{k}}\right] + \mathrm{h.c.} \tag{2.21}
$$

[3] Note however that the expansion of $\Sigma_{\mathrm{out},\boldsymbol{k}}$ may contain lowest order gradients that need to be resummed in the same way as we did above in equation (2.19). This is the case whenever the self-energy function contains an internal propagator containing the coherence function connected to the external leg in the diagram. For more details see refs. [11, 12].

and we defined

$$\dot{\Phi}^{\pm}_{h\boldsymbol{k}} \equiv \partial_t\left(\frac{m_{\mathrm{R}}}{\omega_{\boldsymbol{k}}}\right) \pm \mathrm{i}\frac{h|\boldsymbol{k}|}{\omega_{\boldsymbol{k}}^2}\,\partial_t m_{\mathrm{I}}, \qquad \xi_{\boldsymbol{k}} \equiv \frac{\omega_{\boldsymbol{k}}^2}{\omega_{\boldsymbol{k}}^2 - m_{\mathrm{R}}^2}. \tag{2.22}$$

We shall return to study interacting theories in section 6. For now, we shall take a closer look into the phase space structure of the exact non-interacting Wightman functions.

3 Constructing the exact Wightman function

In the previous section we showed that Wightman functions may acquire novel phase space structures in the spectral limit. The new coherence functions $f^{c\pm}_{h\boldsymbol{k}}$ on the $k_0 = 0$ shell describe quantum coherence in correlated particle-antiparticle states. These correlations can be interpreted in terms of squeezed states and the functions $f^{c\pm}_{h\boldsymbol{k}}$ can be related to Bogolyubov coefficients [12]. Condensation of the coherence information onto a sharp phase space shell is still surprising. It is therefore of interest to see how such structures arise in an exactly solvable system.

3.1 Non-interacting Wightman function

The Lagrangian density (2.9) provides a suitable system for our study. In the spatially homogeneous case it implies the equation of motion

$$\mathrm{i}\partial\!\!\!/\psi - m^*(t)\psi_{\mathrm{L}} - m(t)\psi_{\mathrm{R}} = 0. \tag{3.1}$$

We quantise this model with the usual canonical procedure. Because three-momentum $\boldsymbol{k}$ and helicity h are conserved, the field operator $\hat{\psi}(x)$ may be expanded in terms of mode functions as

$$\hat{\psi}_{\mathrm{free}}(t,\boldsymbol{x}) = \sum_h \int \frac{\mathrm{d}^3\boldsymbol{k}}{(2\pi)^3 2\omega_-}\Big[\hat{a}_{h\boldsymbol{k}}U_{h\boldsymbol{k}}(t)\mathrm{e}^{\mathrm{i}\boldsymbol{k}\cdot\boldsymbol{x}} + \hat{b}^\dagger_{h\boldsymbol{k}}V_{h\boldsymbol{k}}(t)\mathrm{e}^{-\mathrm{i}\boldsymbol{k}\cdot\boldsymbol{x}}\Big], \tag{3.2}$$

where $\omega_- = \sqrt{\boldsymbol{k}^2 + |m(-\infty)|^2}$. The vacuum state is annihilated as $\hat{a}_{h\boldsymbol{k}}|\Omega\rangle = \hat{b}_{h\boldsymbol{k}}|\Omega\rangle = 0$ and our normalisation is such that

$$\begin{aligned}\{\hat{a}_{h\boldsymbol{k}}, \hat{a}^\dagger_{h'\boldsymbol{k}'}\} &= (2\pi)^3 2\omega_- \delta^{(3)}(\boldsymbol{k}-\boldsymbol{k}')\delta_{hh'},\\ \{\hat{b}_{h\boldsymbol{k}}, \hat{b}^\dagger_{h'\boldsymbol{k}'}\} &= (2\pi)^3 2\omega_- \delta^{(3)}(\boldsymbol{k}-\boldsymbol{k}')\delta_{hh'},\end{aligned} \tag{3.3}$$

while all other anticommutators vanish. The normalisation of the spinor $\hat{\psi}_{\mathrm{free}}$ is chosen to be such that

$$\{\hat{\psi}_{\mathrm{free},\alpha}(t,\boldsymbol{x}), \hat{\psi}^\dagger_{\mathrm{free},\beta}(t,\boldsymbol{y})\} = \delta_{\alpha\beta}\delta^{(3)}(\boldsymbol{x}-\boldsymbol{y}), \tag{3.4}$$

with the mode functions $U_{h\boldsymbol{k}}$ and $V_{h\boldsymbol{k}}$ normalised accordingly. The particle and antiparticle spinors can be decomposed in terms of helicity as follows:

$$U_{h\boldsymbol{k}}(t) = \begin{bmatrix}\eta_{h\boldsymbol{k}}(t)\\ \zeta_{h\boldsymbol{k}}(t)\end{bmatrix} \otimes \xi_{h\boldsymbol{k}}, \qquad V_{h\boldsymbol{k}}(t) = \begin{bmatrix}\bar{\eta}_{h\boldsymbol{k}}(t)\\ \bar{\zeta}_{h\boldsymbol{k}}(t)\end{bmatrix} \otimes \xi_{h\boldsymbol{k}}, \tag{3.5}$$

where $\xi_{h\boldsymbol{k}}$ are the eigenfunctions of helicity satisfying

$$(\boldsymbol{\sigma}\cdot\hat{\boldsymbol{k}})\xi_{h\boldsymbol{k}} = h\,\xi_{h\boldsymbol{k}}, \qquad h=\pm 1, \tag{3.6}$$

and $\eta_{h\boldsymbol{k}}$, $\zeta_{h\boldsymbol{k}}$, $\bar{\eta}_{h\boldsymbol{k}}$ and $\bar{\zeta}_{h\boldsymbol{k}}$ are yet unknown mode functions that depend on $m(t)$.[4] The particle mode functions $\eta_{h\boldsymbol{k}}$ and $\zeta_{h\boldsymbol{k}}$ satisfy the equations

$$\mathrm{i}\partial_t\eta_{h\boldsymbol{k}} + h|\boldsymbol{k}|\eta_{h\boldsymbol{k}} = m(t)\zeta_{h\boldsymbol{k}}, \tag{3.7a}$$

$$\mathrm{i}\partial_t\zeta_{h\boldsymbol{k}} - h|\boldsymbol{k}|\zeta_{h\boldsymbol{k}} = m^*(t)\eta_{h\boldsymbol{k}}, \tag{3.7b}$$

while the equations for the antiparticle mode functions $\bar{\eta}_{h\boldsymbol{k}}$ and $\bar{\zeta}_{h\boldsymbol{k}}$ contained in $V_{h\boldsymbol{k}}(t)$ can be obtained from equations (3.7) by the replacements $h\to -h$ and $m\to -m^*$.

The exact Wightman functions for the non-interacting system can now be constructed as expectation values of field operators in the vacuum defined by our annihilation operators. While both Wightman functions $S^>$ and $S^<$ contain the same degrees of freedom, the positive energy solutions, which we shall be using as an example below, are most straightforward to identify from $S^>$. Continuing to work in the helicity basis we find

$$\mathrm{i}S^>_{hh'\boldsymbol{k}}(k_0,t) = \int \mathrm{d}^4 r\, \mathrm{e}^{\mathrm{i}k_0 r_0 - \mathrm{i}\boldsymbol{k}\cdot\boldsymbol{r}} \big\langle\Omega\big|\hat{\psi}_{h,\mathrm{free}}\Big(x+\frac{r}{2}\Big)\hat{\bar{\psi}}_{h',\mathrm{free}}\Big(x-\frac{r}{2}\Big)\big|\Omega\big\rangle. \tag{3.8}$$

Using the definition (3.2) (with $\hat{\psi}_{\mathrm{free}} \equiv \sum_h \hat{\psi}_{h,\mathrm{free}}$), decompositions (3.5) and spatial translation invariance, this can be written as

$$\bar{S}^>_{hh'\boldsymbol{k}}(k_0,t) = \delta_{hh'}\int_{-\infty}^{\infty}\mathrm{d}r_0\,\mathrm{e}^{\mathrm{i}k_0 r_0} M^>_{h\boldsymbol{k}}\Big(t+\frac{r_0}{2}, t-\frac{r_0}{2}\Big)\otimes P^{(2)}_{h\boldsymbol{k}}, \tag{3.9}$$

where $P^{(2)}_{h\boldsymbol{k}} = \xi_{h\boldsymbol{k}}\xi^\dagger_{h\boldsymbol{k}} = \frac{1}{2}(\mathbb{1} + h\boldsymbol{\sigma}\cdot\hat{\boldsymbol{k}})$ and only the chiral component matrix $M^>_{h\boldsymbol{k}}$ depends on the mode functions:

$$M^>_{h\boldsymbol{k}}\Big(t+\frac{r_0}{2}, t-\frac{r_0}{2}\Big) \equiv \frac{1}{2\omega_-}\begin{bmatrix} \eta_{h\boldsymbol{k}}\big(t+\frac{r_0}{2}\big)\eta^*_{h\boldsymbol{k}}\big(t-\frac{r_0}{2}\big) & \eta_{h\boldsymbol{k}}\big(t+\frac{r_0}{2}\big)\zeta^*_{h\boldsymbol{k}}\big(t-\frac{r_0}{2}\big) \\ \zeta_{h\boldsymbol{k}}\big(t+\frac{r_0}{2}\big)\eta^*_{h\boldsymbol{k}}\big(t-\frac{r_0}{2}\big) & \zeta_{h\boldsymbol{k}}\big(t+\frac{r_0}{2}\big)\zeta^*_{h\boldsymbol{k}}\big(t-\frac{r_0}{2}\big)\end{bmatrix}. \tag{3.10}$$

When the component mode functions are solved, it is straightforward to construct the Wightman function using fast Fourier transform methods.

3.2 Including damping

In the absence of dissipative processes, the free particle solutions (3.9) are correlated over arbitrarily large time intervals, because the Wigner transform correlates mode functions over all relative times $\pm\frac{r_0}{2}$ at each value of t. This is of course a physical result. However, our typical applications concern interacting systems, where such correlations are naturally suppressed by decohering interactions.

Taking interactions completely into account would require solving the full Kadanoff-Baym equations, which is beyond the scope of this paper. However, one can account for

[4] We are using the chiral basis, where the Dirac matrices are given by $\gamma^0 = \rho^1\otimes\mathbb{1}$, $\gamma^i = \mathrm{i}\rho^2\otimes\sigma^i$ and $\gamma^5 = -\rho^3\otimes\mathbb{1}$. Here both ρ^i and σ^i are just the usual 2×2 Pauli matrices. The former encode the chiral and the latter the helicity degrees of freedom of a given spinor.

their most important effect for the phase space structure in a rather simple manner. We observe that the information encoded in the relative coordinate must be damped by the rate of interactions that measure the state of the system (in this case whether the system is a particle or an antiparticle). If we denote this rate by $\Gamma_{h\boldsymbol{k}}$ for each mode with momentum $\boldsymbol{k}$ and helicity h, then the appropriately damped correlation function should be

$$\begin{aligned}\overline{S}^{>}_{h\boldsymbol{k},\Gamma}(k_0,t) &\equiv \int \mathrm{d}^4 r\, \mathrm{e}^{\mathrm{i}k_0 r_0 - \mathrm{i}\boldsymbol{k}\cdot\boldsymbol{r} - \Gamma_{h\boldsymbol{k}}|r_0|} \big\langle\Omega\big|\hat{\psi}_{h,\mathrm{free}}\Big(x+\frac{r}{2}\Big)\hat{\bar{\psi}}_{h,\mathrm{free}}\Big(x-\frac{r}{2}\Big)\big|\Omega\big\rangle\gamma^0 \\ &= \int_{-\infty}^{\infty} \mathrm{d}r_0\, \mathrm{e}^{\mathrm{i}k_0 r_0 - \Gamma_{h\boldsymbol{k}}|r_0|} M^{>}_{h\boldsymbol{k}}\Big(t+\frac{r_0}{2}, t-\frac{r_0}{2}\Big)\otimes P^{(2)}_{h\boldsymbol{k}} \\ &\equiv W^{>}_{h\boldsymbol{k},\Gamma}(k_0,t)\otimes P^{(2)}_{h\boldsymbol{k}}. \end{aligned} \tag{3.11}$$

The only difference to the exact free case (3.9) is the introduction of the exponential damping factor $\mathrm{e}^{-\Gamma_{h\boldsymbol{k}}|r_0|}$, where the damping rate $\Gamma_{h\boldsymbol{k}}$ is the imaginary part of the pole of the full propagator. The exponential accounts for the most relevant effect of interactions here. Taking the self-energy fully into account would also modify the matrix $M^{>}_{h\boldsymbol{k}}$, which we here approximate with the free result. Equation (3.11) is thus reasonable in the usual weak coupling limit, where particles are assumed to propagate freely between relatively infrequent collisions.[5] When collisions occur they affect "measurements" of the quantum state, which over time leads to a loss of coherence.

The appearance of the exponential damping factor in equation (3.11) can also be motivated by studying the case of thermal equilibrium, where the full correlation function in Wigner representation is given by $\overline{S}^{>}_{h\boldsymbol{k}}(k_0,t) = 2\overline{\mathcal{A}}_{h\boldsymbol{k}}(k_0,t)(1-f_{\mathrm{eq}}(k_0))$. (Remember that $\overline{S}^{>}_{h\boldsymbol{k}} + \overline{S}^{<}_{h\boldsymbol{k}} = 2\overline{\mathcal{A}}_{h\boldsymbol{k}}$). The damping factor in this case arises from the absorptive self-energy corrections to the single particle poles of the pole propagators $S^{\mathrm{r,a}}_{h\boldsymbol{k}}$. When neglecting gradient corrections one can show that in the small coupling limit

$$\overline{S}^{>}_{h\boldsymbol{k}}(k_0,t) \simeq \int \mathrm{d}r_0\, \mathrm{e}^{\mathrm{i}k_0 r_0 - \Gamma_{h\boldsymbol{k}}(t)|r_0|}\overline{S}^{>}_{0,h\boldsymbol{k}}\Big(t+\frac{r_0}{2}, t-\frac{r_0}{2}\Big), \tag{3.12}$$

where

$$\overline{S}^{>}_{0,h\boldsymbol{k}}\Big(t+\frac{r_0}{2}, t-\frac{r_0}{2}\Big) = \sum_{\pm} \mathrm{e}^{\mp\mathrm{i}\omega_{\boldsymbol{k}}(t)r_0}\Big[1-f_{\mathrm{eq}}\big(\pm\omega_{\boldsymbol{k}}(t)\big)\Big]P^{(4)}_{h\boldsymbol{k}}P^{\pm}_{\boldsymbol{k}}(t) \tag{3.13}$$

is the two-time representation of the free thermal correlation function (derived using the usual plane wave mode functions). We have only kept the absorptive corrections to the single particle poles of $S^{\mathrm{r,a}}_{h\boldsymbol{k}}(k_0,t)$, which are then located at $k_0 = \omega_{\boldsymbol{k}}(t) \mp \mathrm{i}\Gamma_{h\boldsymbol{k}}(t)$. The damping factor in equation (3.11) relates the free correlation function to the full one in exactly the same way as in equation (3.12), generalising the latter into the case of a non-thermal system with coherence structures.

3.3 Explicit solutions for mode functions

We shall now study the correlation function (3.11) explicitly in a simple toy model. For quantitative results we must define the mass function $m(t)$. We assume that it approaches

[5] In fact we are accounting also for the soft interactions with the background fields that lead to the time-varying mass term. It would be straightforward to extend this to other dispersive processes by the use of quasiparticle eigenstates.

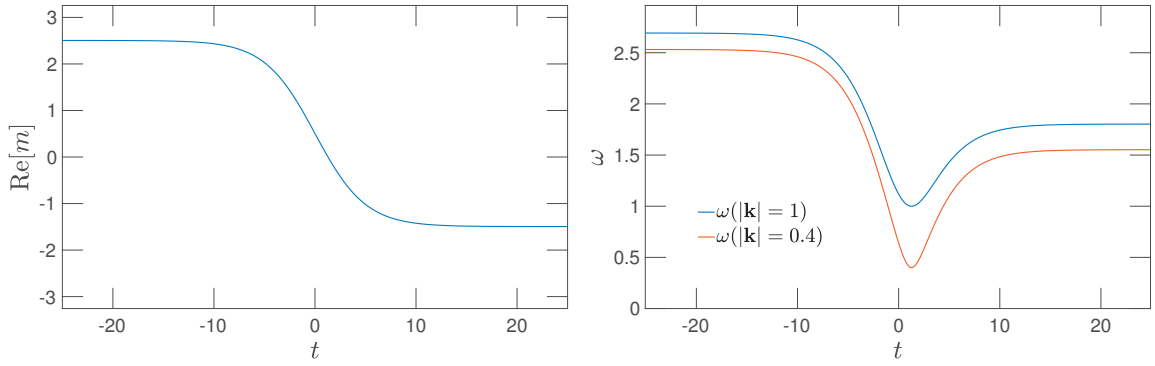

(a) (b)

Figure 2. Left panel (a): the real part of the mass profile $m(t)$ of equation (3.15), with parameters $m_1 = 0.5 + 0.005\mathrm{i}$, $m_2 = 2$ and $\tau_\mathrm{w} = 5$, in arbitrary units. Right panel (b): the positive energy eigenvalue $\omega_{\boldsymbol{k}}(t) = \sqrt{\boldsymbol{k}^2 + |m(t)|^2}$ with the same mass function as in the left panel and with both $|\boldsymbol{k}| = 1$ and 0.4.

asymptotically constant values $m_\mp$ at early and late times, respectively, and that it changes between the asymptotic values over a characteristic time interval τ_w around time $t = 0$. This is the situation e.g. in a phase transition interpolating between the broken and unbroken phases. At early and late times such solutions approach asymptotically plane waves (with spinor normalisation $U^\dagger_{h\boldsymbol{k}} U_{h\boldsymbol{k}} = V^\dagger_{h\boldsymbol{k}} V_{h\boldsymbol{k}} = 2\omega_-$):

$$U^\infty_{h\boldsymbol{k}} = \begin{bmatrix} \sqrt{\omega_- - h|\boldsymbol{k}|} \\ \sqrt{\omega_- + h|\boldsymbol{k}|}\mathrm{e}^{-\mathrm{i}\theta} \end{bmatrix} \otimes \xi_{h\boldsymbol{k}} \mathrm{e}^{-\mathrm{i}\omega_- t}, \tag{3.14a}$$

$$V^\infty_{h\boldsymbol{k}} = \begin{bmatrix} \sqrt{\omega_- + h|\boldsymbol{k}|} \\ -\sqrt{\omega_- - h|\boldsymbol{k}|}\mathrm{e}^{\mathrm{i}\theta} \end{bmatrix} \otimes \xi_{h\boldsymbol{k}} \mathrm{e}^{\mathrm{i}\omega_- t}, \tag{3.14b}$$

where θ is the phase of the constant mass in the asymptotic limit: $m \to |m_\pm|\mathrm{e}^{\mathrm{i}\theta_\pm}$. To be specific, we use the following mass profile for which the mode functions can be solved analytically [20]:

$$m(t) = m_1 + m_2 \tanh\left(-\frac{t}{\tau_\mathrm{w}}\right), \tag{3.15}$$

where $m_1 = m_{1\mathrm{R}} + \mathrm{i}m_{1\mathrm{I}}$ and $m_2 = m_{2\mathrm{R}} + \mathrm{i}m_{2\mathrm{I}}$ are constant complex coefficients and τ_w is a parameter describing the width of the transition in time. At early times ($t \to -\infty$) we then have $m \to m_- = m_1 + m_2$ and at late times ($t \to \infty$) $m \to m_+ = m_1 - m_2$. For solving the mode functions, the imaginary part of m_2 is removed by a global rotation of the spinors (see ref. [20] for details), which of course does not change the dynamics of the system. The remaining imaginary part is simply denoted by m_I. Figure 2 illustrates the shape of the mass function and the corresponding energy for representative parameters.

Equations (3.7) with the mass profile (3.15) were solved in ref. [20] and here we just quote the results relevant for our purposes. Defining a new basis for the mode functions,

$$\phi^{\pm}_{h\boldsymbol{k}}(t) \equiv \frac{1}{\sqrt{2}}\big[\eta_{h\boldsymbol{k}}(t) \pm \zeta_{h\boldsymbol{k}}(t)\big], \tag{3.16a}$$

$$\bar{\phi}^{\pm}_{h\boldsymbol{k}}(t) \equiv \frac{1}{\sqrt{2}}\big[\bar{\eta}_{h\boldsymbol{k}}(t) \pm \bar{\zeta}_{h\boldsymbol{k}}(t)\big], \tag{3.16b}$$

one can show that the solutions can be written in terms of Gauss' hypergeometric functions:

$$\phi^{\pm(1)}_{h\boldsymbol{k}} = C^{\pm(1)}_{h\boldsymbol{k}}\, z^{\alpha}(1-z)^{\beta}\ {}_2F_1(a_{\pm}, b_{\pm}, c; z), \tag{3.17a}$$

$$\phi^{\pm(2)}_{h\boldsymbol{k}} = C^{\pm(2)}_{h\boldsymbol{k}}\, z^{-\alpha}(1-z)^{\beta}\ {}_2F_1(1+a_{\pm}-c, 1+b_{\pm}-c, 2-c; z), \tag{3.17b}$$

where $C^{\pm(1,2)}_{h\boldsymbol{k}}$ are constants and

$$\begin{aligned} z &= \frac{1}{2}\left[1 - \tanh\left(-\frac{t}{\tau_{\rm w}}\right)\right], \qquad \alpha = -\frac{\mathrm{i}}{2}\tau_{\rm w}\omega_-, \qquad \beta = -\frac{\mathrm{i}}{2}\tau_{\rm w}\omega_+, \\ \omega_{\mp} &= \sqrt{\boldsymbol{k}^2 + m_{\rm I}^2 + (m_{1\rm R} \pm m_{2\rm R})^2}, \\ a_{\pm} &\equiv 1 + \alpha + \beta \mp \mathrm{i}\tau_{\rm w} m_{2\rm R}, \qquad b_{\pm} \equiv \alpha + \beta \pm \mathrm{i}\tau_{\rm w} m_{2\rm R}, \quad c \equiv 1 + 2\alpha. \end{aligned} \tag{3.18}$$

Superscripts (1) and (2) label the two linearly independent solutions. The solutions for $\bar{\phi}^{\pm}_{h\boldsymbol{k}}$ can be obtained by changing the sign of helicity in equations (3.17), $h \to -h$. (Helicity enters the solution through the boundary conditions as will be seen below.)

Using the properties of the hypergeometric functions it is easy to check that at early times

$$\phi^{\pm(1)}_{h\boldsymbol{k}} \xrightarrow{t\to-\infty} C^{\pm(1)}_{h\boldsymbol{k}} \mathrm{e}^{-\mathrm{i}t\omega_-}, \qquad \phi^{\pm(2)}_{h\boldsymbol{k}} \xrightarrow{t\to-\infty} C^{\pm(2)}_{h\boldsymbol{k}} \mathrm{e}^{\mathrm{i}t\omega_-}. \tag{3.19}$$

At late times these solutions split into mixtures of positive and negative frequency states:

$$\phi^{\pm(1)}_{h\boldsymbol{k}} \xrightarrow{t\to\infty} C^{\pm(1)}_{h\boldsymbol{k}} \frac{\Gamma(c)\Gamma(c-a_{\pm}-b_{\pm})}{\Gamma(c-a_{\pm})\Gamma(c-b_{\pm})} \mathrm{e}^{\mathrm{i}t\omega_+} + C^{\pm(1)}_{h\boldsymbol{k}} \frac{\Gamma(c)\Gamma(a_{\pm}+b_{\pm}-c)}{\Gamma(a_{\pm})\Gamma(b_{\pm})} \mathrm{e}^{-\mathrm{i}t\omega_+}, \tag{3.20}$$

which manifests the fact that a varying mass mixes particle and antiparticle states. Indeed, in systems without time-translation invariance the division to particles and antiparticles is not unique. Locally a clear identification can be made however, and with the asymptotic limits given above we can construct different initial and final states we wish to study.

Let us now specify our initial state as a positive frequency particle, i.e. the solution (3.17a), corresponding to the constant mass one-particle state (3.14a) at $t \to -\infty$. This determines the constants

$$C^{\pm(1)}_{h\boldsymbol{k}} = \frac{1}{\sqrt{2}}\left(\sqrt{\omega_- - h|\boldsymbol{k}|} \pm \sqrt{\omega_- + h|\boldsymbol{k}|}\mathrm{e}^{-\mathrm{i}\theta_-}\right), \tag{3.21}$$

where $\theta_- = \mathrm{Arg}(m_{1\rm R} + m_{2\rm R} + \mathrm{i}m_{\rm I})$. Figure 3 shows these solutions for a representative set of parameters. It is evident that the solutions asymptote to plane waves very quickly on each side of the transition region.

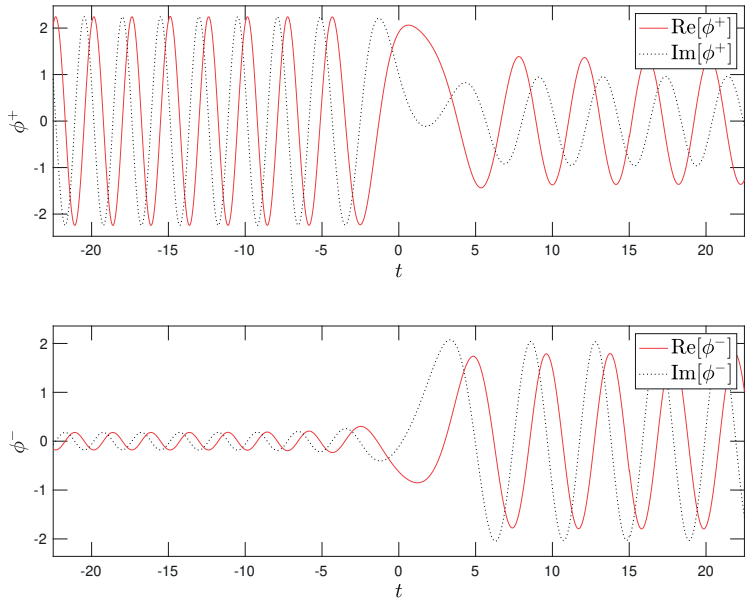

Figure 3. Shown are the real and imaginary parts of the exact free mode functions $\phi^{\pm(1)}_{h\boldsymbol{k}}$, defined in equation (3.17a), across the transition defined by the mass profile (3.15). We used the initial conditions (3.21) and the same parameters as in figure 2a with $|\boldsymbol{k}| = 0.4$ and $h = 1$.

4 Phase space of the exact Wightman function

Having solved the mode functions, we can now calculate the Wightman functions $S^s_{h\boldsymbol{k}}$ and $S^s_{h\boldsymbol{k},\Gamma}$. It suffices to concentrate on one type of them, say $S^>$, since both functions exhibit the same phase space structures. We evaluate the Wightman functions by inserting the mode functions solved from equations (3.16) and (3.17) with the boundary conditions (3.21) into the matrix $M^>_{h\boldsymbol{k}}$ (3.10) and performing the integral over the relative coordinate in equation (3.11) numerically for each $\boldsymbol{k}$-mode. Results of these computations for varying parameter sets are shown in figures 4–6.

Figure 4 shows the absolute value of the $(1,1)$-component of the function $W^>_{h\boldsymbol{k},\Gamma}(k_0,t)$, defined in equation (3.11), for a system initially prepared to a pure positive frequency state. (Other three chiral components are qualitatively similar.) The surface plot in the left panel displays a clearly peaked structure, where the initial particle peak branches at the transition region to three separate peaks corresponding to particle and antiparticle solutions at $k_0 = \pm\omega_{\boldsymbol{k}}(t)$ and a coherence peak at $k_0 = 0$. This reproduces the cQPA-shell structure predicted in the previous section. Note that the coherence shell solution is rapidly oscillating in time as predicted by the cQPA equation (2.18). The feature is slightly obscured by the absolute value, but it shows up in the "digitised" structure of the coherence solution in the projected plot on the right panel. Due to a rather large interaction rate Γ the shell structures are wide enough in frequency to overlap a little, which can after the transition be seen as a leakage of the coherence shell oscillations into the mass shells. At early times the sole positive frequency shell contains no oscillations. Physically, what we are seeing, is particle production by a temporally changing mass parameter and the

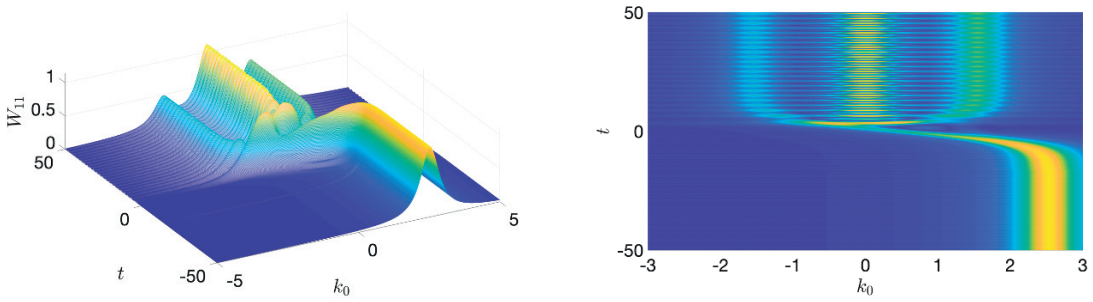

Figure 4. Shown is the absolute value of the $(1,1)$-component of the exact free Wightman function $W^{>}_{h\boldsymbol{k},\Gamma}$ defined in equation (3.11), for parameters $h = 1$, $|\boldsymbol{k}| = 0.4$, $m_{1\mathrm{R}} = 0.5$, $m_{2\mathrm{R}} = 2$, $m_{\mathrm{I}} = -0.005$, $\tau_{\mathrm{w}} = 5$ and $\Gamma = 0.4$. Note that time flows from bottom to top in the right panel.

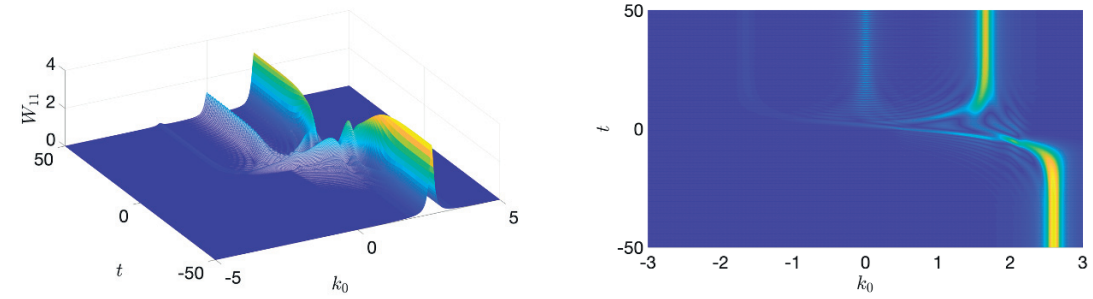

Figure 5. The same as in figure 4, but for parameters $h = 1$, $|\boldsymbol{k}| = 0.7$, $m_{1\mathrm{R}} = 0.5$, $m_{2\mathrm{R}} = 2$, $m_{\mathrm{I}} = -0.005$, $\tau_{\mathrm{w}} = 5$ and $\Gamma = 0.1$.

fundamental relation of the phenomenon to the quantum coherence between positive and negative frequency states.

In figure 4 we assumed a quite large damping factor and correspondingly the shell structures were rather broad in frequency. In figure 5 we show for comparison a solution with a smaller wavelength and a much smaller damping coefficient. As expected, the shell structure gets more sharply peaked because of the smaller width.[6] At the same time the antiparticle shell after the transition becomes much less pronounced, reflecting the fact that a larger initial energy is less affected by the mass change. (The same qualitative behaviour would of course be obtained by increasing the width of the wall, leading to less efficient particle production.) Indeed, for a very large $|\boldsymbol{k}|$ the whole novel shell structure vanishes, making way for a single shell following a classical energy path such as the ones shown in figure 2b.

Right at the transition region one can distinguish additional fine-structures, which are not related to the cQPA solution of equation (2.15). This is partly because our derivation of cQPA assumed lowest order expansion in gradients. It would be interesting (and possible) to generalise cQPA to a singular higher order expansion in gradients and check if the emerging discrete sequence of shells could reproduce the structures seen here. However,

[6] In fact it is easy to show in an even simpler toy model, where the mass-function is replaced by a step-function, that the peaks become Breit-Wigner-functions in frequency [21]. The spectral cQPA-solution can then be seen explicitly as the Breit-Wigner forms approach delta functions in the limit $\Gamma \to 0$.

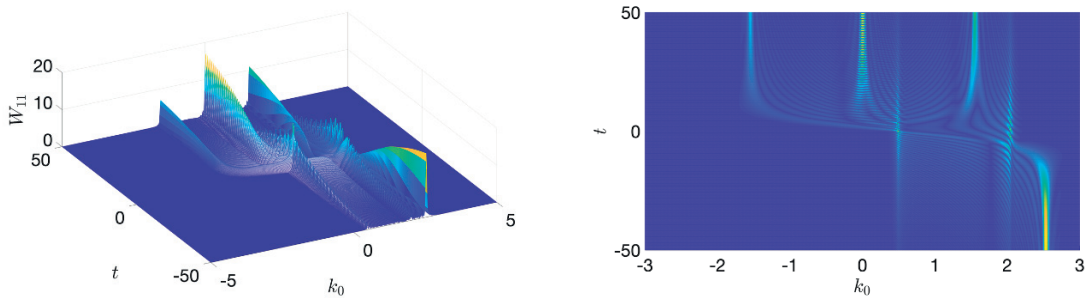

Figure 6. The same as in figure 4, but for parameters $h = 1$, $|\boldsymbol{k}| = 0.4$, $m_{1\mathrm{R}} = 0.5$, $m_{2\mathrm{R}} = 2$, $m_{\mathrm{I}} = -0.005$, $\tau_{\mathrm{w}} = 5$ and $\Gamma = 0.02$.

these structures may also reflect the onset of the new non-local correlations that we shall turn to next.[7]

4.1 Non-local coherence in time

In figure 6 we again plot $|W^{>}_{h\boldsymbol{k},\Gamma,11}|$ with the same parameters as in figure 4, but with a much smaller decay term. The shells become even more peaked as expected, but in addition a much richer phase space structure emerges, extending well outside the transition region. From the projection plot one recognises that two new spectral shells have entered the play, together with a rich network of secondary fine-structures around the transition region. From the surface plot it is evident, compared to the earlier cases, that the cQPA-shells are suppressed near the transition region, while the new shells grow in amplitude there. Far away from the transition region the situation is reversed and the new shells (which are also oscillating) fade away, making room for the usual cQPA-shells that allow for a clear particle and antiparticle identification.

The new shells correspond to non-local correlations between the early- and late-time solutions across the wall; in the particle interpretation the system appears to become aware of the change in its energy levels already before the transition occurs. This is completely expected behaviour for a quantum system and, again, these shells can also be seen analytically in the simple step-function model [21]. One can show, and also observe in the projection plot, that the new shells coincide with the average frequencies

$$k_0 = \frac{1}{2}\left(\sqrt{\boldsymbol{k}^2 + |m_-|^2} \pm \sqrt{\boldsymbol{k}^2 + |m_+|^2}\right), \tag{4.1}$$

which reveals that they correspond to particle-particle and particle-antiparticle correlations across the wall. The reason why these solutions are suppressed at large time differences is the damping; the information about the transition can be propagated only up to a distance

[7] Let us clarify our use of the notion of (non-)locality in this paper: first, by non-local coherence we mean coherence over the relative coordinate in the two-point correlation function. Then, by local limit, we mean the limit where the two time-arguments in the correlation function are the same. The local correlation function still supports the particle-antiparticle coherence, which is non-local in the sense that creating it requires coherent evolution over a finite interval in the average time uninterrupted by collisions, which differentiate particles from antiparticles.

$\Delta t \sim 1/\Gamma$ in the relative coordinate. Beyond this time interval only local correlations can survive. Decreasing Γ further makes the non-local coherence structures ever more prominent and if one removes damping entirely, the system becomes completely overwhelmed by them. In this limit the system is intrinsically quantum; local particle-like solutions are irrelevant and the system is globally sensitive to the initial conditions and the size of the time-domain.

4.2 Physical and practical significance of the phase space structures

We have seen that a quantum system with negligible damping is strongly correlated over large time intervals. However, in interacting systems damping suppresses non-local correlations, eventually reducing correlation functions to the local limit. This decoherence enables the quasiparticle picture and eventually the Boltzmann limit in slowly varying backgrounds. In the language of a direct space Kadanoff-Baym approach, damping removes contributions from memory integrals over long relative time differences. Note however, that damping does *not* destroy the coherence shell at $k_0 = 0$; spectral cQPA shells get finite widths, but the coherence between particles and antiparticles survives. Of course, equations (2.6) and (2.7) contain also other (hard) collisions terms, which we have omitted so far. If these collisions depend on the particle-antiparticle nature of the state, they constitute measurements which destroy this coherence. A complete treatment of particle production in phase transitions, for example, should account for this effect as well, as was indeed done for example in refs. [7, 8] in the cQPA context.

From a practical point of view our solutions show that in the weakly interacting limit $\tau_{\rm w}\Gamma \ll 1$, a complete phase space solution of the interacting problem would require very fine resolution in frequency space in order to account for all the fine-structures in the transition region. In this region, because of the large number of transient shell structures, the quasiparticle picture appears impractical.[8] On the other hand, even for a moderately strongly interacting system $\tau_{\rm w}\Gamma \gtrsim 0.5$, the phase space structure is smoothed out and the *coherent* quasiparticle picture of refs. [6–12] should provide a good description of the system.

5 Currents and connection to the semiclassical limit

In the previous sections we showed that the phase space of a system with a varying mass profile has non-trivial phase space structures, whose intricacy depends on the size of the mode momentum $\boldsymbol{k}$ and the damping strength Γ. We also argued that the quasiparticle picture may provide a reasonable description of the system (even for very small $\tau_{\rm w}\Gamma$). We now change slightly our perspective, and ask how our results compare with the semiclassical treatment, which should be applicable when $\tau_{\rm w}|\boldsymbol{k}| \gg 1$. Semiclassical methods have been

[8] The situation is not as bad as one might think even in the limit $\tau_{\rm w}\Gamma \ll 1$. Let us consider the problem from the point of view of the cQPA method, which includes local coherence shells but ignores the non-local structures. Because the quasiparticle picture is appropriate far from the transition region and one expects only few interactions within the transition area, the evolution of the quasiparticle distributions may be only weakly sensitive to the new transient structures (the evolution of the quasiparticle functions is affected by the new shells only through the collision integrals). If the physics one is interested in is sensitive only to the late time correlations, it should be rather well described by the cQPA.

widely used to describe CP-violating dynamics in electroweak baryogenesis models [5, 19, 22–30]. While we are dealing with a purely time-dependent system here, the results should be qualitatively representative.

To be specific, we shall compare different methods for computing the expectation values of fermionic currents. A generic current corresponding to a Dirac operator $\mathcal{O}$ can be computed as

$$j^{\mathcal{O}}_{h\boldsymbol{k}}(t) \equiv \int \frac{\mathrm{d}^3\boldsymbol{r}}{(2\pi)^3}\, \mathrm{e}^{\mathrm{i}\boldsymbol{k}\cdot\boldsymbol{r}} \big\langle \hat{\bar{\psi}}_h\big(t,\boldsymbol{x}+\boldsymbol{r}\big)\mathcal{O}\hat{\psi}_h\big(t,\boldsymbol{x}\big)\big\rangle = \int \frac{\mathrm{d}k_0}{2\pi}\, \mathrm{Tr}\big[\mathcal{O}\,\mathrm{i}S^<_{h\boldsymbol{k}}(k_0,t)\big]. \tag{5.1}$$

In particular, we will be interested in the axial charge density

$$j_{5,h\boldsymbol{k}}(t) \equiv \int \frac{\mathrm{d}^3\boldsymbol{r}}{(2\pi)^3}\, \mathrm{e}^{\mathrm{i}\boldsymbol{k}\cdot\boldsymbol{r}} \big\langle \hat{\bar{\psi}}_h\big(t,\boldsymbol{x}+\boldsymbol{r}\big)\gamma^0\gamma^5\hat{\psi}_h\big(t,\boldsymbol{x}\big)\big\rangle, \tag{5.2}$$

which is related to particle asymmetries.

With the exact solutions (3.17) at hand it is a simple numerical task to compute $j_{5,h\boldsymbol{k}}$ for the kink profile using equation (5.1). Furthermore, in cQPA it can be calculated in terms of the shell functions $f^{(m,c)\pm}_{h\boldsymbol{k}}$ as follows:

$$j^{\mathrm{cQPA}}_{5,h\boldsymbol{k}} = \sum_{s=\pm}\left[-\frac{sh|\boldsymbol{k}|}{\omega_{\boldsymbol{k}}}\, f^{ms}_{h\boldsymbol{k}} + \left(\frac{h|\boldsymbol{k}|m_{\mathrm{R}}}{\omega^2_{\boldsymbol{k}}} + \frac{\mathrm{i}sm_{\mathrm{I}}}{\omega_{\boldsymbol{k}}}\right) f^{cs}_{h\boldsymbol{k}}\right]. \tag{5.3}$$

5.1 Collisionless case

We first point out that currents computed with the exact Wightman function fully agree with the cQPA currents in the collisionless limit. This may look surprising, because cQPA relies on a spectral ansatz derived to lowest order in gradients. Yet, at the integrated level the collisionless cQPA is in fact *exact* and cQPA shell functions are in one-to-one correspondence with the *local limit* of the correlation functions [12], and the correspondence is not affected by the introduction of a damping term. This can be illustrated explicitly e.g. with equations (3.12) and (2.15): integrating equation (3.12) over k_0 gives

$$\begin{aligned}\int \frac{\mathrm{d}k_0}{2\pi}\, \overline{S}^<_{h\boldsymbol{k},\Gamma}(k_0,t) &= \int \frac{\mathrm{d}k_0}{2\pi} \int \mathrm{d}r_0\, \mathrm{e}^{\mathrm{i}k_0 r_0 - \Gamma_{h\boldsymbol{k}}|r_0|}\overline{S}^<_{h\boldsymbol{k}}\left(t+\frac{r_0}{2}, t-\frac{r_0}{2}\right)\\ &= \overline{S}^<_{h\boldsymbol{k}}(t,t) \overset{\mathrm{cQPA}}{\longrightarrow} \sum_{\pm}\left[P^{m\pm}_{h\boldsymbol{k}} f^{m\pm}_{h\boldsymbol{k}} + P^{c\pm}_{h\boldsymbol{k}} f^{c\pm}_{h\boldsymbol{k}}\right],\end{aligned} \tag{5.4}$$

where in the last line we used the cQPA-ansatz (2.15). Thus, *the essential feature of the cQPA is* not the expansion in gradients or the ensuing spectral approximation, but *the assumption that non-local degrees of freedom are not dynamical.* In particular this result shows that cQPA retains the full quantum information relative to the average time coordinate t.

Finally, let us stress the delicate role the decay width Γ plays in the emergence of the cQPA-scheme. On one hand, we have seen that if Γ was vanishing, non-local temporal correlations would dominate the correlation function; the quality of the local approximation then crucially depends on a non-zero damping. Yet, the spectral limit formally corresponds

to taking $\Gamma \to 0$. That is, Γ must be large enough to ensure that non-local correlations can be neglected, and yet small enough so that a spectral quasiparticle picture is valid. Fortunately this is typically the case. We shall elaborate more on these issues in a forthcoming publication [31].

5.2 Semiclassical approximation

While the cQPA is designed to capture the local quantum effects in a generic evolving background, a different method exists for systems in slowly varying backgrounds. The *semiclassical approximation* was introduced in refs. [22–25] for systems with spatial inhomogeneities, and the details for temporally varying systems can be found in ref. [5]. The semiclassical approximation is also local, but in contrast to cQPA, one applies the gradient expansion directly to the *unintegrated* equations of motion, eliminating off-diagonal chiral degrees of freedom. This leads to a loss of information in comparison to cQPA.

We do not get into the details of the derivation, but merely quote the results relevant for our purposes. The Wightman function is decomposed into a helicity block-diagonal form

$$2\mathrm{i}\gamma^0 S^<_{h\boldsymbol{k}}(k_0,t) = \sigma^a g_{ah\boldsymbol{k}}(k_0,t) \otimes P^{(2)}_{h\boldsymbol{k}}, \tag{5.5}$$

where $a \in \{0,1,2,3\}$, $\sigma^0 \equiv \mathbb{1}$, σ^i are the Pauli matrices, and g_{ah} are the unknown coefficient functions to be solved. The main outcome of the semiclassical formalism is that, when considered to the first order in the gradients of a time-dependent mass $m = |m|\mathrm{e}^{\mathrm{i}\theta}$, the axial part of the helicity correlation function $g_{3h\boldsymbol{k}}$ is found to be living on a shifted energy shell: $g_{3h\boldsymbol{k}} \sim \delta\left(k_0^2 - \omega^2_{3h\boldsymbol{k}}\right)$, with

$$\omega_{3h\boldsymbol{k}} \equiv \omega_{\boldsymbol{k}}(t) + h\frac{|m|^2\partial_t\theta(t)}{2|\boldsymbol{k}|\omega_{\boldsymbol{k}}(t)}. \tag{5.6}$$

The shift has an opposite sign for particles with opposite helicities, and it obviously vanishes for translationally invariant systems.[9]

Defining the integrated phase space densities

$$f_{ah\boldsymbol{k}}(t) \equiv \int \frac{\mathrm{d}k_0}{2\pi}\, g_{ah\boldsymbol{k}}(k_0,t) \tag{5.7}$$

one finds the following collisionless equation of motion for the axial density $f_{3h\boldsymbol{k}}$ [5]:

$$\left[\omega_{3h\boldsymbol{k}}\partial_t + F_{h\boldsymbol{k}}\partial_{k_0}\right] f_{3h\boldsymbol{k}} = 0, \tag{5.8}$$

where $F_{h\boldsymbol{k}}$ is the *semiclassical force*

$$F_{h\boldsymbol{k}} = \frac{\partial_t|m|^2}{2\omega_{3h\boldsymbol{k}}} + h\frac{\partial_t(|m|^2\partial_t\theta)}{2|\boldsymbol{k}|\omega_{\boldsymbol{k}}}. \tag{5.9}$$

This process of going from quantum equations (cQPA) to the semiclassical force is analogous to going from the Schrödinger equation to a spin-dependent force when calculating

[9] For problems with a spatially varying mass a similar shift occurs for the zeroth component g_0, and is proportional to the spin of the particle [24, 25].

an electron's movement in a magnetic field (the Stern-Gerlach experiment). Noticing that $F_{h\boldsymbol{k}} = \partial_t \omega_{3h\boldsymbol{k}}$, one can see that the collisionless equation (5.8) is solved by

$$f^{\mathrm{sc}}_{3h\boldsymbol{k}}(t) = \frac{\omega_- f^-_{3h\boldsymbol{k}}}{\omega_{3h\boldsymbol{k}}(t)}, \tag{5.10}$$

where $f^-_{3h\boldsymbol{k}} \equiv f_{3h\boldsymbol{k}}(t \to -\infty)$ is determined by the desired initial conditions. These formulae are valid for an arbitrary form of the mass function. Note that the definition of the phase space function $f_{3h\boldsymbol{k}}$ exactly coincides with our definition of the current $j_{5,h\boldsymbol{k}}$ in equations (5.1) and (5.2).

5.3 Range of validity of the different formalism

Let us now compare the axial quantum currents to their semiclassical approximation in different kinematical regions. We use the initial conditions described in section 3.3, which correspond to choosing $f^-_{3h\boldsymbol{k}} = h|\boldsymbol{k}|/\omega_-$ in equation (5.10). In cQPA the equivalent initial configuration for $S^<$ is $f^{m-}_{h\boldsymbol{k}}(-\infty) = 1$ with other shell functions vanishing. In this case the semiclassical approximation gives the following form for the helicity-summed axial density of our kink-mass system:

$$j^{\mathrm{sc}}_{5,\boldsymbol{k}}(t) = \sum_h f^{\mathrm{sc}}_{3h\boldsymbol{k}}(t) = -\frac{m_{\mathrm{I}} m_{2\mathrm{R}}}{\tau_{\mathrm{w}}\, \omega^3_{\boldsymbol{k}}(t) \cosh^2(t/\tau_{\mathrm{w}})}. \tag{5.11}$$

In figure 7 we show the helicity summed axial density $j_{5,\boldsymbol{k}} \equiv \sum_h j_{5,h\boldsymbol{k}}$ as a function of time for a few representative values for $|\boldsymbol{k}|$, computed from the semiclassical equation (5.11), using our exact solutions with equation (5.1) and using the cQPA methods via equation (5.3). As explained above, the full cQPA-currents coincide with the exact currents in the collisionless limit. In this case the cQPA-current is *pure coherence*, since the cQPA-solution restricted to mass shells (green dashed lines) gives a vanishing axial current.

The general comparison to the semiclassical approximation is as expected: prominent oscillations appearing in the exact solutions for small $|\boldsymbol{k}|$ are absent in the semiclassical solution. This is as it should be, since quantum coherence effects are included in the semiclassical formalism only in an average sense. However, the oscillations turn off quickly for large $|\boldsymbol{k}|$, such that already for $|\boldsymbol{k}| = 1.5$ the semiclassical and quantum currents are practically identical. Moreover, the semiclassical current captures the *average* of the exact solution very well for $|\boldsymbol{k}| = 0.8$ and reasonably well even for $|\boldsymbol{k}| = 0.4$. The broad range of validity of the semiclassical approximation is slightly surprising. On general grounds one would assume it to work when at least one wavelength fits to the wall width, corresponding to $\frac{2\pi}{|\boldsymbol{k}|} < \tau_{\mathrm{w}}$. However, our results suggest that it works quite well even when the wall width is but a fraction of the wave length of the mode.

The validity of the semiclassical approximation is even more pronounced when one considers the integrated current

$$j_5(t) \equiv \frac{1}{2\pi^2} \int \mathrm{d}|\boldsymbol{k}|\, \boldsymbol{k}^2 \sum_h j_{5,h\boldsymbol{k}}(t). \tag{5.12}$$

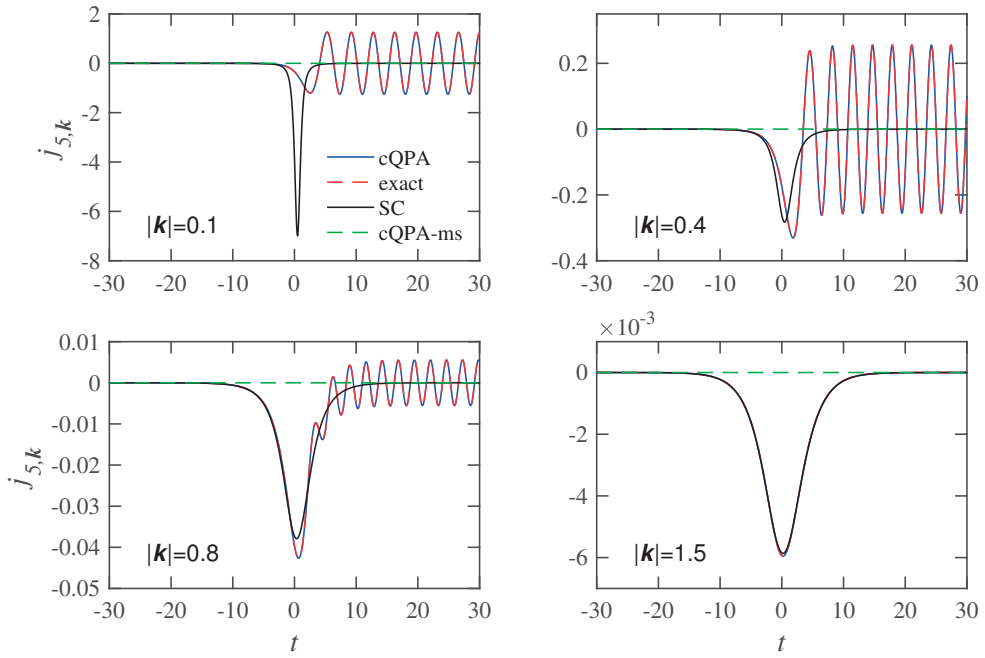

Figure 7. The helicity summed axial charge density $j_{5,\boldsymbol{k}}$ from the exact solutions (red dashed line), and from the semiclassical approximation (black line). Blue solid line (exactly matching the red dashed line) is the full cQPA solution and the green line is cQPA solution restricted to the mass shells. In each figure we have $m_{1\mathrm{R}} = 0.1$, $m_{2\mathrm{R}} = 1$, $m_{\mathrm{I}} = 0.1$, $\tau_{\mathrm{w}} = 5$ and $\Gamma = 0.2$, while $|\boldsymbol{k}| = 0.1$, 0.4, 0.8 and 1.5 in different panels as indicated.

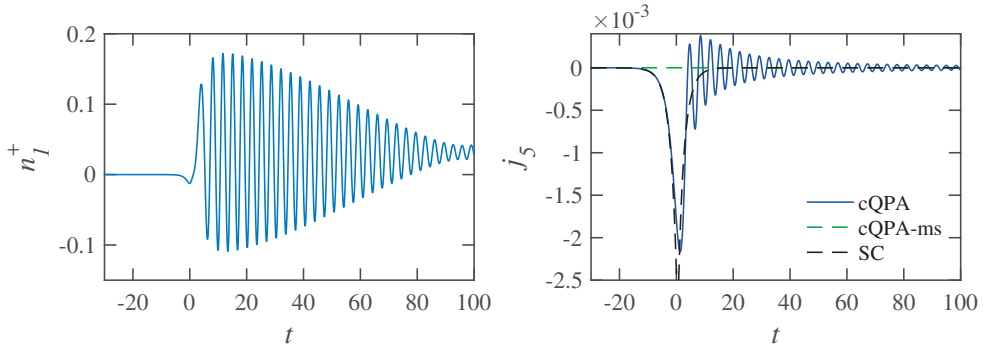

Figure 8. Shown is the integrated number density n_1^+ of positive helicity particles (left graph) and the integrated axial charge density j_5 (right graph) for a vacuum initial condition in the non-interacting case. We used the same set of mass parameters as in figure 7.

In the right panel of figure 8 we show the result of the calculation of $j_5(t)$ for the same set of parameters as considered in figure 7. Apart from the oscillations right after the mass change, the semiclassical solution follows the full solution quite well. In the left panel we show the behaviour of the integrated number density n_1^+ of positive helicity particles. (The individual number densities are defined below in section 6.) Indeed, oscillations tend to be much larger in the individual components, but they mostly cancel out at the level of currents.

Our results in the non-interacting case are qualitatively similar to those of ref. [20]; the semiclassical approximation captures the mean trend of the currents quite well. However, while ref. [20] emphasized the fact that the semiclassical approximation misses the late time oscillations, we do not think that this is necessarily a significant problem. First, we see that the oscillations damp quite quickly. Second, a typical application of a calculation presented here would be to compute the particle-antiparticle asymmetry arising from the transition. The axial current would then be closely related to the source of the asymmetry. In such a case the effect of oscillations around the mean would tend to cancel out, leaving a mean effect that could be well captured by the semiclassical result.

Let us emphasize that the cQPA result for the current indeed contains and generalises the semiclassical result. This is so despite the fact that the cQPA-dispersion relation was derived formally to lower order in gradients than the semiclassical one. The reason for this apparently contradicting result was already emphasized in the beginning of this section: at the integrated level the non-interacting cQPA is in fact exact. Similarly then, the interacting cQPA-equations (2.20) constitute a generalisation of the interacting semiclassical Boltzmann theory to the fully quantum case. We now turn to study such interacting systems in the context of cQPA. This requires that we define explicitly the collision terms in equations (2.20).

6 cQPA with collisions

Let us now assume that the self-energy satisfies the KMS-relation $\Sigma^{>} = \mathrm{e}^{\beta k_0}\Sigma^{<}$. This is perhaps the most often recurring application, so we write down the full single flavour interacting cQPA-equations (2.20) explicitly for this case. After some algebra we find:

$$\partial_t n^{\pm}_{h\boldsymbol{k}} = \frac{1}{2}\sum_s \dot{\Phi}^s_{h\boldsymbol{k}}\, f^{cs}_{h\boldsymbol{k}} - \sum_s \Big[\big(n^s_{h\boldsymbol{k}} - n^s_{\mathrm{eq}}\big)T^{hs\pm}_{mm} + f^{cs}_{h\boldsymbol{k}}\, T^{hs\pm}_{cm}\Big]\,, \tag{6.1a}$$

$$\begin{aligned}\partial_t f^{c\pm}_{h\boldsymbol{k}} = {}& \mp 2\mathrm{i}\omega_{\boldsymbol{k}} f^{c\pm}_{h\boldsymbol{k}} + \xi_{\boldsymbol{k}}\dot{\Phi}^{\mp}_{h\boldsymbol{k}}\left[\frac{m_{\mathrm{R}}}{\omega_{\boldsymbol{k}}} f^{c\pm}_{h\boldsymbol{k}} + \frac{1}{2}\big(1 - n^{+}_{h\boldsymbol{k}} - n^{-}_{h\boldsymbol{k}}\big)\right] \\ & - \xi_{\boldsymbol{k}}\sum_s \Big[\big(n^s_{h\boldsymbol{k}} - n^s_{\mathrm{eq}}\big)T^{hs\pm}_{mc} + f^{cs}_{h\boldsymbol{k}}\, T^{hs\pm}_{cc}\Big]\,,\end{aligned} \tag{6.1b}$$

where $\dot{\Phi}^{\pm}_{h\boldsymbol{k}}$ and $\xi_{\boldsymbol{k}}$ were defined in equation (2.22) and we replaced the mass shell functions by the number densities $n^{+}_{h\boldsymbol{k}} \equiv f^{m+}_{h\boldsymbol{k}}$ and $n^{-}_{h\boldsymbol{k}} \equiv 1 - f^{m-}_{h\boldsymbol{k}}$ (these are the usual 1-particle Boltzmann distribution functions) and $n^s_{\mathrm{eq}} \equiv f_{\mathrm{eq}}(+\omega_{\boldsymbol{k}})$. Finally, the $T^{hs\pm}_{ab}$-functions encode the collision terms for generic thermal interactions. In the spatially homogeneous and isotropic system the most general form of the self-energy function can be expanded as

$$\Sigma^{\mathcal{A}}_{\boldsymbol{k}}(k_0, t) \equiv \sum_i c^{\mathcal{A}}_i(k, t)\sigma_i(k). \tag{6.2}$$

Here $\sigma_i(k)$ are the Dirac structures given in the leftmost column of table 1 and $c^{\mathcal{A}}_i(k,t)$ are some four-momentum- and possibly time-dependent functions.[10] Interaction terms

[10] Note that the last four rows in table 1 contain redundant information. For example, using the fact that $\not{k}P_{h\boldsymbol{k}} = (k_0\gamma^0 - h|\boldsymbol{k}|\gamma^0\gamma^5)P_{h\boldsymbol{k}}$, one finds that $(\mathcal{T}_{\not{k}})^{hss'}_{ab} = \omega_{\boldsymbol{k}}(\mathcal{T}_{\mathrm{sgn}(k_0)\gamma^0})^{hss'}_{ab} - h|\boldsymbol{k}|(\mathcal{T}_{\gamma^0\gamma^5})^{hss'}_{ab}$. It is easy to

σ_i	$(\mathcal{T}_i)^{hss'}_{mm}$	$(\mathcal{T}_i)^{hss'}_{cm}$	$(\mathcal{T}_i)^{hss'}_{mc}$	$(\mathcal{T}_i)^{hss'}_{cc}$
$\mathbb{1}$	$2s\delta_{ss'}\frac{m_\mathrm{R}}{\omega_{\boldsymbol{k}}}$	$s'/\xi_{\boldsymbol{k}}$	$s/\xi_{\boldsymbol{k}}$	$2s\delta_{ss'}\frac{m_\mathrm{R}}{\omega_{\boldsymbol{k}}}/\xi_{\boldsymbol{k}}$
γ^5	$-2\mathrm{i}s\delta_{ss'}\frac{m_\mathrm{I}}{\omega_{\boldsymbol{k}}}$	$s'B^{s}_{h\boldsymbol{k}}$	$sB^{-s'}_{h\boldsymbol{k}}$	$-2\mathrm{i}s\delta_{ss'}\frac{m_\mathrm{I}}{\omega_{\boldsymbol{k}}}/\xi_{\boldsymbol{k}}$
$\mathrm{sgn}(k_0)\gamma^0$	$2s\delta_{ss'}$	0	0	$2s\delta_{ss'}/\xi_{\boldsymbol{k}}$
$\gamma^0\gamma^5$	$2s\delta_{ss'}h\frac{\lvert\boldsymbol{k}\rvert}{\omega_{\boldsymbol{k}}}$	$-s'A^{s}_{h\boldsymbol{k}}$	$-sA^{-s'}_{h\boldsymbol{k}}$	$2s\delta_{ss'}h\frac{\lvert\boldsymbol{k}\rvert}{\omega_{\boldsymbol{k}}}/\xi_{\boldsymbol{k}}$
$\not{k}$	$2s\delta_{ss'}\frac{\lvert m\rvert^2}{\omega_{\boldsymbol{k}}}$	$s'h\lvert\boldsymbol{k}\rvert A^{s}_{h\boldsymbol{k}}$	$sh\lvert\boldsymbol{k}\rvert A^{-s'}_{h\boldsymbol{k}}$	$2s\delta_{ss'}\frac{\lvert m\rvert^2}{\omega_{\boldsymbol{k}}}/\xi_{\boldsymbol{k}}$
$\not{k}\gamma^5$	0	$\omega_{\boldsymbol{k}}A^{s}_{h\boldsymbol{k}}$	$-\omega_{\boldsymbol{k}}A^{-s'}_{h\boldsymbol{k}}$	0
$\frac{1}{2}[\gamma^0,\not{k}]$	$2\mathrm{i}s\delta_{ss'}h\lvert\boldsymbol{k}\rvert\frac{m_\mathrm{I}}{\omega_{\boldsymbol{k}}}$	$-s'h\lvert\boldsymbol{k}\rvert B^{s}_{h\boldsymbol{k}}$	$-sh\lvert\boldsymbol{k}\rvert B^{-s'}_{h\boldsymbol{k}}$	$2\mathrm{i}s\delta_{ss'}h\lvert\boldsymbol{k}\rvert\frac{m_\mathrm{I}}{\omega_{\boldsymbol{k}}}/\xi_{\boldsymbol{k}}$
$\frac{1}{2}[\gamma^0,\not{k}]\gamma^5$	$-2s\delta_{ss'}h\lvert\boldsymbol{k}\rvert\frac{m_\mathrm{R}}{\omega_{\boldsymbol{k}}}$	$-s'h\lvert\boldsymbol{k}\rvert/\xi_{\boldsymbol{k}}$	$-sh\lvert\boldsymbol{k}\rvert/\xi_{\boldsymbol{k}}$	$-2s\delta_{ss'}h\lvert\boldsymbol{k}\rvert\frac{m_\mathrm{R}}{\omega_{\boldsymbol{k}}}/\xi_{\boldsymbol{k}}$

Table 1. Collision term coefficients for different self-energy components $\sigma_i(k)$ of $\Sigma_{\boldsymbol{k}}$.

corresponding to equation (6.2) are given by

$$\begin{aligned}
T^{hss'}_{mm}(|\boldsymbol{k}|,t) &= \sum_i c_i^{\mathcal{A}}(s)(\mathcal{T}_i)^{hss'}_{mm}(|\boldsymbol{k}|),\\
T^{hss'}_{cm}(|\boldsymbol{k}|,t) &= \sum_i \left[\frac{c_i^{\mathcal{A}}(s)+c_i^{\mathcal{A}}(-s)}{2} - ss'\frac{c_i^{\mathcal{A}}(s)-c_i^{\mathcal{A}}(-s)}{2}\right](\mathcal{T}_i)^{hss'}_{cm}(|\boldsymbol{k}|),\\
T^{hss'}_{mc}(|\boldsymbol{k}|,t) &= \sum_i c_i^{\mathcal{A}}(s)(\mathcal{T}_i)^{hss'}_{mc}(|\boldsymbol{k}|),\\
T^{hss'}_{cc}(|\boldsymbol{k}|,t) &= \sum_i \frac{c_i^{\mathcal{A}}(s)-c_i^{\mathcal{A}}(-s)}{2}(\mathcal{T}_i)^{hss'}_{cc}(|\boldsymbol{k}|),
\end{aligned} \tag{6.3}$$

where $c_i^{\mathcal{A}}(s) \equiv c_i^{\mathcal{A}}(s\omega_{\boldsymbol{k}},|\boldsymbol{k}|,t)$ and the functions $(\mathcal{T}_i)^{hss'}_{ab}$ can be read from table 1, where we further defined

$$A^{s}_{h\boldsymbol{k}} \equiv h\frac{|\boldsymbol{k}|m_\mathrm{R}}{\omega_{\boldsymbol{k}}^2} + \mathrm{i}s\frac{m_\mathrm{I}}{\omega_{\boldsymbol{k}}}, \tag{6.4}$$

$$B^{s}_{h\boldsymbol{k}} \equiv sh\frac{|\boldsymbol{k}|}{\omega_{\boldsymbol{k}}} + \mathrm{i}\frac{m_\mathrm{R}m_\mathrm{I}}{\omega_{\boldsymbol{k}}^2}. \tag{6.5}$$

The collision terms of equations (6.3) together with table 1 allow for completely general coefficient functions $c_i(k,t)$ of the self-energy (6.2). However, in thermal equilibrium the functions $c_i(k,t)$ are typically either even or odd functions of k_0. As an example, we consider a thermal self-energy with a chiral interaction given by

$$\Sigma^{\mathcal{A}}_{\boldsymbol{k}}(k_0) = (a\not{k} + b\not{u})P_\mathrm{L}, \tag{6.6}$$

check that this relation is satisfied by the entries of table 1. Similarly $\frac{1}{2}[\gamma^0,\not{k}]P_{h\boldsymbol{k}} = -h|\boldsymbol{k}|\gamma^5 P_{h\boldsymbol{k}}$, which implies that the last two rows are just $-h|\boldsymbol{k}|$ times the first two lines in reverse order. However, rather than being minimalistic, we give a complete list of the possible structures.

where u_μ is the fluid four-velocity. We further assume that, in the rest frame of the thermal plasma where $\not{u} \to \gamma^0$, the coefficient $a = a(k_0, |\boldsymbol{k}|)$ is an odd and $b = b(k_0, |\boldsymbol{k}|)$ an even function of k_0. Using table 1, we then get the following collision terms for equations (6.1):

$$\begin{aligned}
T^{hss'}_{mm}(|\boldsymbol{k}|, t) &= \left[\frac{|m|^2}{\omega_{\boldsymbol{k}}} a_{\boldsymbol{k}} + \left(1 - sh\frac{|\boldsymbol{k}|}{\omega_{\boldsymbol{k}}}\right) b_{\boldsymbol{k}}\right] \delta_{ss'}, \\
T^{hss'}_{cm}(|\boldsymbol{k}|, t) &= \frac{s'}{2}\Big[(\omega_{\boldsymbol{k}} - s'h|\boldsymbol{k}|)a_{\boldsymbol{k}} + b_{\boldsymbol{k}}\Big] A^{s}_{h\boldsymbol{k}}, \\
T^{hss'}_{mc}(|\boldsymbol{k}|, t) &= \frac{s}{2}\Big[(\omega_{\boldsymbol{k}} + sh|\boldsymbol{k}|)a_{\boldsymbol{k}} + b_{\boldsymbol{k}}\Big] A^{-s'}_{h\boldsymbol{k}}, \\
T^{hss'}_{cc}(|\boldsymbol{k}|, t) &= \frac{1}{\xi_{\boldsymbol{k}}}\left[\frac{|m|^2}{\omega_{\boldsymbol{k}}} a_{\boldsymbol{k}} + b_{\boldsymbol{k}}\right] \delta_{ss'}.
\end{aligned} \tag{6.7}$$

Here $a_{\boldsymbol{k}} \equiv a(\omega_{\boldsymbol{k}}, |\boldsymbol{k}|)$, $b_{\boldsymbol{k}} \equiv b(\omega_{\boldsymbol{k}}, |\boldsymbol{k}|)$ and we used the parity properties $a(s\omega_{\boldsymbol{k}}, |\boldsymbol{k}|) = s a_{\boldsymbol{k}}$ and $b(s\omega_{\boldsymbol{k}}, |\boldsymbol{k}|) = b_{\boldsymbol{k}}$. Also, given that $a_{\boldsymbol{k}}, b_{\boldsymbol{k}} > 0$, note how $T^{hss'}_{mm}$ and $T^{hss'}_{cc}$ are always positive.

Let us finally point out that it is easy to generalise equations (6.1) to the case with a non-thermal self-energy that does *not* obey the KMS-relation. One just needs to replace the two terms involving the equilibrium distribution function $n^s_{\rm eq}$ as follows:

$$(n^s_{h\boldsymbol{k}} - n^s_{\rm eq}) T^{hss'}_{ma}(|\boldsymbol{k}|, t) \to \sum_i s\left(f^{ms}_{h\boldsymbol{k}} c^{\mathcal{A}}_i(s) - \frac{1}{2} c^{<}_i(s)\right) (\mathcal{T}_i)^{hss'}_{ma}(|\boldsymbol{k}|, t) \tag{6.8}$$

for $a = m, c$, where we defined $\mathrm{i}\Sigma^{<}_{\boldsymbol{k}}(k_0, t) \equiv \sum_i c^{<}_i(k, t)\sigma_i(k)$. We remind, however, that evaluating the self-energy diagrams involving coherent propagators as internal lines requires special techniques developed in refs. [11, 12].

6.1 A numerical example

In figure 9 we show a result of a model calculation with a non-vanishing interaction rate using a self-energy of the form (6.6) with $a_{\boldsymbol{k}} = 0.03$ and $b_{\boldsymbol{k}} = 0$. The left panels, where we imposed the vacuum initial conditions $n^{\pm}_{h\boldsymbol{k}} = f^{c\pm}_{h\boldsymbol{k}} = 0$, correspond to the interacting version of the case studied in figure 8. Initially, the particle number approaches smoothly the thermal value. At the onset of the transition it again starts oscillating, but the amplitude is strongly damped in comparison to the non-interacting case. In the right panels we show the analogous calculation with equilibrium initial conditions $n^{\pm}_{h\boldsymbol{k}} = n^{\pm}_{\rm eq}$ with $T = 1$ in the units we are working with and $f^{c\pm}_{h\boldsymbol{k}} = 0$. Now the particle number stays unchanged until the onset of the transition, after which it oscillates approaching asymptotically the same post-transition equilibrium value as in the case with vacuum initial conditions. Pushing the starting point further away from the transition region would make the later evolution indistinguishable in the two cases.

The main difference to the non-interacting case is that the left-chiral interaction, in connection with the coherent CP-violating oscillations, creates a temporary non-zero average chiral current after transition. This is due to the fact that the chiral interaction term (6.6) breaks the helicity symmetry. The average current is well captured at late times by the pure mass shell contribution, shown in green dashed line in figure 9. However at

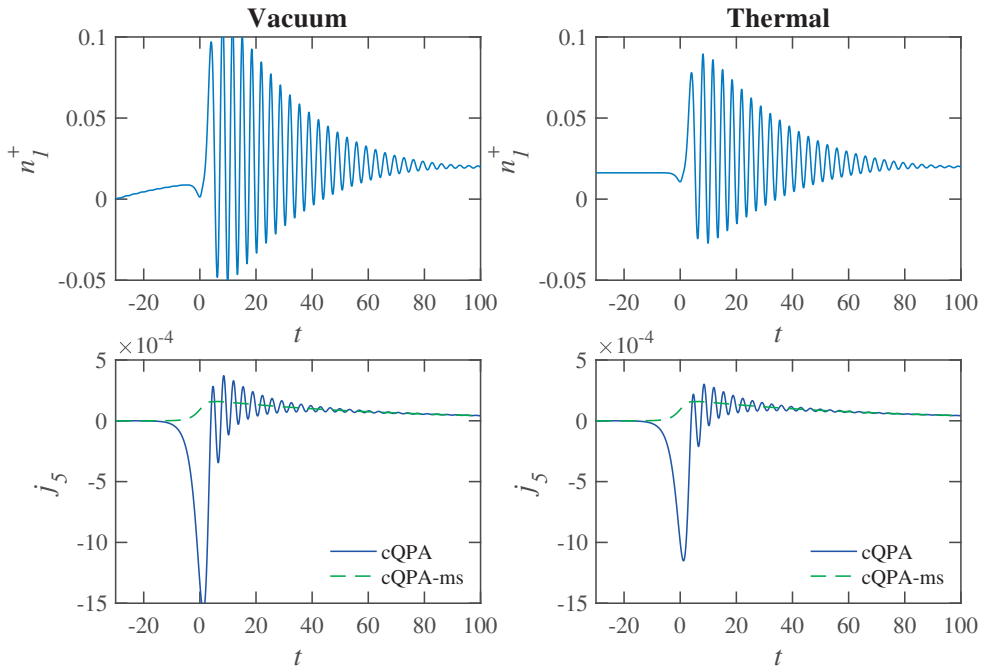

Figure 9. Shown is the integrated number density n_1^+ of positive helicity particles (the upper panels) and the integrated axial charge density j_5 (the lower panels) in interacting cQPA. The left panels correspond to the vacuum initial condition and the right panels to the thermal initial condition with $T = 1$. We used the same set of mass parameters as in figure 7.

the transition point the main peak is still pure coherence. While the current eventually equilibrates to zero, the region where it is non-vanishing could act as a seed for example for a particle-antiparticle asymmetry creation in such a transition.

The calculation we presented here was just a toy model whose sole purpose was to show how to implement the method and display some of the effects of interactions. There are several interesting applications for the formalism that we shall pursue in the future. One avenue is the study of baryogenesis in abrupt spatially homogeneous phase transitions in the early universe, such as the models considered in the context of the cold baryogenesis [32–34]. Another application is to study the reheating phase after inflation. It is straightforward to couple equations (6.1) with an equation of motion for the inflaton and model the reheating phase including all quantum effects and interactions. Our formalism, extended to the flavour mixing case [12], can also be applied to the study of leptogenesis. It is of particular interest to compare our approach with several other transport theory formulations that also employ the closed time path (CTP) methods, such as those presented in refs. [35–42].

7 Conclusions and outlook

We have studied the phase space structure of a fermionic two-point function with a varying complex mass. We computed the Wightman function of a non-interacting system for a specific mass profile, and demonstrated that its phase space contains, in addition to the usual mass shell solutions, a shell-like structure located at $k_0 = 0$. This zero-momentum

shell describes local-in-time quantum coherence between particles and antiparticles and it was discovered earlier in the context of the cQPA-formalism [6–12]. However, our present derivation did not rely on any approximations, but derived the free Wightman function from the exact mode functions of the system.

In addition to the cQPA-solutions we found other, non-local coherence structures in the exact Wightman function. These structures look peculiar, appearing to let the system become aware of the transition before it actually takes place in the local time coordinate, but of course they are just a reflection of the usual quantum non-locality in the phase space picture. We argued that the non-local correlations would dominate the phase space structure in large non-dissipative systems. However, when dissipation is included (modelled here by a damping term coupled to the relative time coordinate), the non-locality gets confined to the neighbourhood of the transition region. These results underline the delicate role of dissipation in the emergence of the local (cQPA) limit, and eventually (in the nearly translationally invariant systems) of the familiar Boltzmann transport theory.

In section 2 we introduced a new and particularly useful way to reorganise the gradient expansion in the mixed representation Kadanoff-Baym equations. Then, based on this form, we gave a simple and transparent derivation of the cQPA equations. In section 6 we completed the analysis by providing explicit collision integrals for generic interaction self-energies. The resulting equations (6.1) are one of the main results of this paper: they generalise the Boltzmann transport theory to systems with local coherence between particles and antiparticles. In particular they fully encompass the well known semiclassical effects. Such coherences may be relevant for example for baryogenesis during phase transitions and for particle production at the end of inflation.

We further computed axial phase space densities out of the Wightman functions and compared these to the same quantities obtained from the semiclassical approximation. We found out that the semiclassical methods work reasonably well even in systems where the relevant modes have wavelengths down to a half of the wall width. This is encouraging for baryogenesis studies in very strong electroweak phase transitions, often encountered in the context of models producing large, observable gravitational wave signals [17, 18].

In this work we only considered a time-dependent mass. A natural follow-up, relevant for the baryogenesis problem, would be to generalise the analysis to a mass depending on one spatial coordinate. Part of this program is straightforward, but some new features emerge as well, such as the tunneling solutions, whose proper description at the phase space level is non-trivial. But there are practical applications of the time-dependent formalism as well, which we shall be pursuing. One is the baryogenesis at a phase transition as discussed in section 6 and already studied in the context of a simple toy model in ref. [11]. Another immediate goal is to use equations (6.1), coupled to the one-point function of the inflaton, to model accurately the reheating phase at the end of the inflation. Also, we are pursuing a generalisation of the present formalism to the case with mixing fermion fields, in the context of resonant leptogenesis [43].

Acknowledgments

This work was supported by the Academy of Finland grant 318319. HJ was in addition supported by grants from the Väisälä Fund of the Finnish Academy of Science and Letters and OK by a grant from the Magnus Ehrnrooth Foundation. We wish to thank Pyry Rahkila and Werner Porod for many enlightening discussions.

References

[1] J.S. Schwinger, *Brownian motion of a quantum oscillator*, *J. Math. Phys.* **2** (1961) 407 [INSPIRE].

[2] L.V. Keldysh, *Diagram technique for nonequilibrium processes*, *Zh. Eksp. Teor. Fiz.* **47** (1964) 1515 [*Sov. Phys. JETP* **20** (1965) 1018] [INSPIRE].

[3] G. Baym and L.P. Kadanoff, *Conservation laws and correlation functions*, *Phys. Rev.* **124** (1961) 287 [INSPIRE].

[4] G. Mahan, *Quantum transport equation for electric and magnetic fields*, *Phys. Rept.* **145** (1987) 251.

[5] T. Prokopec, M.G. Schmidt and S. Weinstock, *Transport equations for chiral fermions to order ħ and electroweak baryogenesis. Part* 1, *Annals Phys.* **314** (2004) 208 [hep-ph/0312110] [INSPIRE].

[6] M. Herranen, K. Kainulainen and P.M. Rahkila, *Towards a kinetic theory for fermions with quantum coherence*, *Nucl. Phys.* **B 810** (2009) 389 [arXiv:0807.1415] [INSPIRE].

[7] M. Herranen, K. Kainulainen and P.M. Rahkila, *Quantum kinetic theory for fermions in temporally varying backgrounds*, *JHEP* **09** (2008) 032 [arXiv:0807.1435] [INSPIRE].

[8] M. Herranen, K. Kainulainen and P.M. Rahkila, *Kinetic theory for scalar fields with nonlocal quantum coherence*, *JHEP* **05** (2009) 119 [arXiv:0812.4029] [INSPIRE].

[9] M. Herranen, *Quantum kinetic theory with nonlocal coherence*, Ph.D. thesis, Jyväskylä U., Jyväskylä, Finland (2009) [arXiv:0906.3136] [INSPIRE].

[10] M. Herranen, K. Kainulainen and P.M. Rahkila, *Coherent quasiparticle approximation (cQPA) and nonlocal coherence*, *J. Phys. Conf. Ser.* **220** (2010) 012007 [arXiv:0912.2490] [INSPIRE].

[11] M. Herranen, K. Kainulainen and P.M. Rahkila, *Coherent quantum Boltzmann equations from cQPA*, *JHEP* **12** (2010) 072 [arXiv:1006.1929] [INSPIRE].

[12] C. Fidler, M. Herranen, K. Kainulainen and P.M. Rahkila, *Flavoured quantum Boltzmann equations from cQPA*, *JHEP* **02** (2012) 065 [arXiv:1108.2309] [INSPIRE].

[13] M. Hindmarsh, S.J. Huber, K. Rummukainen and D.J. Weir, *Gravitational waves from the sound of a first order phase transition*, *Phys. Rev. Lett.* **112** (2014) 041301 [arXiv:1304.2433] [INSPIRE].

[14] M. Hindmarsh, S.J. Huber, K. Rummukainen and D.J. Weir, *Numerical simulations of acoustically generated gravitational waves at a first order phase transition*, *Phys. Rev.* **D 92** (2015) 123009 [arXiv:1504.03291] [INSPIRE].

[15] M. Hindmarsh, S.J. Huber, K. Rummukainen and D.J. Weir, *Shape of the acoustic gravitational wave power spectrum from a first order phase transition*, *Phys. Rev.* **D 96** (2017) 103520 [arXiv:1704.05871] [INSPIRE].

[16] D. Cutting, M. Hindmarsh and D.J. Weir, *Gravitational waves from vacuum first-order phase transitions: from the envelope to the lattice*, *Phys. Rev.* **D 97** (2018) 123513 [arXiv:1802.05712] [INSPIRE].

[17] G.C. Dorsch, S.J. Huber, T. Konstandin and J.M. No, *A second Higgs doublet in the early universe: baryogenesis and gravitational waves*, *JCAP* **05** (2017) 052 [arXiv:1611.05874] [INSPIRE].

[18] V. Vaskonen, *Electroweak baryogenesis and gravitational waves from a real scalar singlet*, *Phys. Rev.* **D 95** (2017) 123515 [arXiv:1611.02073] [INSPIRE].

[19] T. Prokopec, M.G. Schmidt and S. Weinstock, *Transport equations for chiral fermions to order ħ and electroweak baryogenesis. Part* 2, *Annals Phys.* **314** (2004) 267 [hep-ph/0406140] [INSPIRE].

[20] T. Prokopec, M.G. Schmidt and J. Weenink, *Exact solution of the Dirac equation with CP-violation*, *Phys. Rev.* **D 87** (2013) 083508 [arXiv:1301.4132] [INSPIRE].

[21] O. Koskivaara, *Exact solutions of a Dirac equation with a varying CP-violating mass profile and coherent quasiparticle approximation*, Master's thesis, Jyväskylä U., Jyväskylä, Finland (2015).

[22] J.M. Cline, M. Joyce and K. Kainulainen, *Supersymmetric electroweak baryogenesis*, *JHEP* **07** (2000) 018 [hep-ph/0006119] [INSPIRE].

[23] J.M. Cline, M. Joyce and K. Kainulainen, *Erratum for 'Supersymmetric electroweak baryogenesis'*, hep-ph/0110031 [INSPIRE].

[24] K. Kainulainen, T. Prokopec, M.G. Schmidt and S. Weinstock, *First principle derivation of semiclassical force for electroweak baryogenesis*, *JHEP* **06** (2001) 031 [hep-ph/0105295] [INSPIRE].

[25] K. Kainulainen, T. Prokopec, M.G. Schmidt and S. Weinstock, *Semiclassical force for electroweak baryogenesis: three-dimensional derivation*, *Phys. Rev.* **D 66** (2002) 043502 [hep-ph/0202177] [INSPIRE].

[26] L. Fromme, S.J. Huber and M. Seniuch, *Baryogenesis in the two-Higgs doublet model*, *JHEP* **11** (2006) 038 [hep-ph/0605242] [INSPIRE].

[27] L. Fromme and S.J. Huber, *Top transport in electroweak baryogenesis*, *JHEP* **03** (2007) 049 [hep-ph/0604159] [INSPIRE].

[28] J.M. Cline and K. Kainulainen, *Electroweak baryogenesis and dark matter from a singlet Higgs*, *JCAP* **01** (2013) 012 [arXiv:1210.4196] [INSPIRE].

[29] J.M. Cline, K. Kainulainen, P. Scott and C. Weniger, *Update on scalar singlet dark matter*, *Phys. Rev.* **D 88** (2013) 055025 [*Erratum ibid.* **D 92** (2015) 039906] [arXiv:1306.4710] [INSPIRE].

[30] J.M. Cline, K. Kainulainen and D. Tucker-Smith, *Electroweak baryogenesis from a dark sector*, *Phys. Rev.* **D 95** (2017) 115006 [arXiv:1702.08909] [INSPIRE].

[31] H. Jukkala, K. Kainulainen and O. Koskivaara, in preparation.

[32] A. Tranberg, A. Hernandez, T. Konstandin and M.G. Schmidt, *Cold electroweak baryogenesis with Standard Model CP-violation*, *Phys. Lett.* **B 690** (2010) 207 [arXiv:0909.4199] [INSPIRE].

[33] A. Tranberg and B. Wu, *On using cold baryogenesis to constrain the two-Higgs doublet model*, *JHEP* **01** (2013) 046 [arXiv:1210.1779] [INSPIRE].

[34] A. Tranberg and B. Wu, *Cold electroweak baryogenesis in the two Higgs-doublet model*, *JHEP* **07** (2012) 087 [arXiv:1203.5012] [INSPIRE].

[35] M. Beneke, B. Garbrecht, M. Herranen and P. Schwaller, *Finite number density corrections to leptogenesis*, *Nucl. Phys.* **B 838** (2010) 1 [arXiv:1002.1326] [INSPIRE].

[36] M. Beneke, B. Garbrecht, C. Fidler, M. Herranen and P. Schwaller, *Flavoured leptogenesis in the CTP formalism*, *Nucl. Phys.* **B 843** (2011) 177 [arXiv:1007.4783] [INSPIRE].

[37] B. Garbrecht and M. Herranen, *Effective theory of resonant leptogenesis in the closed-time-path approach*, *Nucl. Phys.* **B 861** (2012) 17 [arXiv:1112.5954] [INSPIRE].

[38] B. Garbrecht, *Why is there more matter than antimatter? Calculational methods for leptogenesis and electroweak baryogenesis*, arXiv:1812.02651 [INSPIRE].

[39] B. Dev, M. Garny, J. Klaric, P. Millington and D. Teresi, *Resonant enhancement in leptogenesis*, *Int. J. Mod. Phys.* **A 33** (2018) 1842003 [arXiv:1711.02863] [INSPIRE].

[40] M. Garny, A. Kartavtsev and A. Hohenegger, *Leptogenesis from first principles in the resonant regime*, *Annals Phys.* **328** (2013) 26 [arXiv:1112.6428] [INSPIRE].

[41] A. Kartavtsev, P. Millington and H. Vogel, *Lepton asymmetry from mixing and oscillations*, *JHEP* **06** (2016) 066 [arXiv:1601.03086] [INSPIRE].

[42] P.S. Bhupal Dev, P. Millington, A. Pilaftsis and D. Teresi, *Kadanoff-Baym approach to flavour mixing and oscillations in resonant leptogenesis*, *Nucl. Phys.* **B 891** (2015) 128 [arXiv:1410.6434] [INSPIRE].

[43] H. Jukkala, K. Kainulainen and P. Rahkila, in preparation.

II

FLAVOUR MIXING TRANSPORT THEORY AND RESONANT LEPTOGENESIS

by

Jukkala, Henri & Kainulainen, Kimmo & Rahkila, Pyry M. 2021

Journal of High Energy Physics, 2021, 119

DOI: 10.1007/JHEP09(2021)119

Published for SISSA by Springer

Received: *April 20, 2021*
Revised: *August 16, 2021*
Accepted: *August 26, 2021*
Published: *September 20, 2021*

Flavour mixing transport theory and resonant leptogenesis

Henri Jukkala, Kimmo Kainulainen and Pyry M. Rahkila

Department of Physics, University of Jyväskylä,
P.O. Box 35 (YFL), FI-40014 Jyväskylä, Finland
Helsinki Institute of Physics, University of Helsinki,
P.O. Box 64, FI-00014 Helsinki, Finland

E-mail: henri.a.jukkala@jyu.fi, kimmo.kainulainen@jyu.fi, pyry.m.rahkila@jyu.fi

Abstract: We derive non-equilibrium quantum transport equations for flavour-mixing fermions. We develop the formalism mostly in the context of resonant leptogenesis with two mixing Majorana fermions and one lepton flavour, but our master equations are valid more generally in homogeneous and isotropic systems. We give a hierarchy of quantum kinetic equations, valid at different approximations, that can accommodate helicity and arbitrary mass differences. In the mass-degenerate limit the equations take the familiar form of density matrix equations. We also derive the semiclassical Boltzmann limit of our equations, including the CP-violating source, whose regulator corresponds to the flavour coherence damping rate. Boltzmann equations are accurate and insensitive to the particular form of the regulator in the weakly resonant case $\Delta m \gg \Gamma$, but for $\Delta m \lesssim \Gamma$ they are qualitatively correct at best, and their accuracy crucially depends on the form of the CP-violating source.

Keywords: Cosmology of Theories beyond the SM, CP violation, Thermal Field Theory

ArXiv ePrint: 2104.03998

https://doi.org/10.1007/JHEP09(2021)119

Contents

1 Introduction

Quantum coherence, and the related mixing and oscillation of quantum states, plays an important role in many interesting phenomena in particle physics and in the early universe. Examples include neutrino mixing and oscillations [1–9], particle scattering from phase transition walls in baryogenesis [10–18], mixing of Majorana neutrinos in leptogenesis [19–21], and particle production after inflation or in phase transitions [22–24]. In these applications a quantum field theoretical treatment of coherence is essential. Several different types of coherence may be relevant depending on the problem: particle production is driven by the particle-antiparticle coherence, and coherent mixing of left- and right-moving particles can be the engine for creating the particle-antiparticle asymmetry during the electroweak phase transition. Finally, coherence between different flavour states powers the familiar phenomenon of neutrino oscillations as well as the particle-antiparticle asymmetry generation in leptogenesis, which is the main topic of this paper.

The primary goal of this work is to develop a general and transparent formalism for treating problems involving quantum flavour coherence. While our results are more general, a large part of the development will be done in the context of (resonant) leptogenesis. We will develop a series of implementations of quantum transport equations with different levels of sophistication. At the most general level our formalism includes also the particle-antiparticle coherences. From there we move by a well defined reduction process to equations fully describing the flavour coherence separately in the particle and antiparticle sectors. These equations are valid for arbitrary helicities and neutrino masses. We also show how these equations can be further reduced to a helicity-symmetric density matrix equation and eventually to the Boltzmann limit with a soundly motivated form for

the CP-violating source in the leptogenesis application. This hierarchy of implementations serves both to compare our results against the existing literature, and provides a "library of methods" from where one can choose the one that is best suitable for the given application at hand.

In the leptogenesis scenario [19] an initial lepton asymmetry n_L gets converted to the baryon asymmetry via the $B + L$-violating sphaleron processes [25] present in the standard model (SM) [26–29]. Several versions of the leptogenesis mechanism exist [20, 21]. In standard thermal leptogenesis n_L is generated by CP-violating out-of-equilibrium decays of heavy Majorana neutrinos and the same basic mechanism carries over to resonant leptogenesis. In the latter the neutrino masses are nearly degenerate however, which leads to an enhanced efficiency. The enhancement is maximal when the timescale $\sim 1/\Delta m$ of the flavour oscillations is comparable to the timescale $\sim 1/\Gamma$ of the change of the neutrino abundances. In this case the flavour mixing has been found to be the dominant source of the lepton asymmetry [20, 21]. Thermal leptogenesis can be well treated using standard kinetic equations, but the resonant case needs a more refined treatment to correctly account for the flavour mixing.

We will use the Schwinger-Keldysh closed time path (CTP) formalism [30, 31] to derive Kadanoff-Baym evolution equations [32, 33] for the two-point correlation function of the mixing fermions from first principles, using the two-particle irreducible effective action (2PIEA) method [34, 35]. We specialize to spatially homogeneous and isotropic systems and include the expansion of the universe, relevant for the leptogenesis application. The central object for our study is the *local* Wightman function $S^<_{\boldsymbol{k}}(t,t)$, which encodes the statistical properties of the system including flavour diagonal and off-diagonal correlations. The key element of our approach is finding a closed equation for $S^<_{\boldsymbol{k}}(t,t)$. Our method does not rely on restricted forms of the correlation function, such as the Kadanoff-Baym or quasiparticle ansätze [33, 36]. Rather, it is based on the identification of a proper background solution and a judicious approximation to compute the collision terms. This makes it well suited for a study of dynamical mixing as all components of the correlation function are treated on an equal footing. We point out that leptogenesis has already been studied extensively using first principles methods [37–56] and resonant leptogenesis in particular [57–71]. Technically our approach is closest to that of ref. [61].

Our formalism is a generalisation of the coherent quasiparticle approximation (cQPA) first developed in [72–78] and further studied in [79]. The cQPA is a two-step approximation where the structure of the Wightman function is solved first in a collisionless approximation in the Wigner representation. This results in a spectral shell structure, including particle and coherence shells, which is then used to solve the full dynamical equation. The present method is not restricted to spectral structures as the equations are solved directly in the two-time representation, which allows taking into account a finite width of the pole propagators. If the width is neglected however, our equations are equivalent to cQPA equations.

Our main results include the quantum transport equations (5.7) and (5.15), the helicity symmetric equations (8.1)–(8.3) and the Boltzmann equation source term (8.10) with the CP-violating parameter (8.11). We provide an explicit implementation for a benchmark model with two Majorana neutrinos and one lepton flavour including decay and inverse

decay interactions, but generalising to more complicated fermion sectors and scattering processes would be straightforward. Numerically all approaches are in good agreement in the weakly resonant case, $m \gg \Delta m \gg \Gamma$, and the helicity-symmetric equation is in good agreement with the full master equation for all parameter values. However, when $\Delta m \lesssim \Gamma$ the Boltzmann equation results depend strongly on the choice of the CP-violating source, the precise form of which has been debated in the literature [55, 62, 66, 70]. Our result agrees with ref. [62]. We show that the effective width that defines this source corresponds to the off-diagonal damping of flavour coherence in the density matrix equations. We also find that the Boltzmann equations equipped with this source are in best numerical agreement with the full master equation results.

This paper is organised as follows: in section 2 we review the underlying CTP formalism and examine the general structure of solutions. In section 3 we derive the transport equation for the local correlation function $S^<_{\boldsymbol{k}}(t,t)$ and the key approximation leading to a closure is introduced in section 3.2. In section 4 we introduce the leptogenesis model, compute the self-energy functions for the decay processes, find the adiabatic background solutions and adapt the transport equations of section 3 to the leptogenesis case. We conclude the section with renormalised master equations for leptogenesis, including an equation for the lepton asymmetry and explicit forms for the source and washout terms. In section 5 we project the neutrino master equation onto different frequency, helicity and flavour quantum states, recasting it as a generalised density matrix equation, which we then further simplify by averaging over the particle-antiparticle oscillations. In section 6 we generalise to the case of an expanding universe and in section 7 we give detailed numerical results for the lepton asymmetry in some benchmark cases. In section 8 we introduce further approximations, first by dropping the helicity dependence and then reducing the master equation to a density matrix equation in the quasidegenerate case and finally into a Boltzmann equation in the decoupling limit, including a semiclassical source term. In section 9 we present detailed comparisons to earlier work in the literature. Further details of the derivation are presented in several appendices. Finally, section 10 contains our conclusions and outlook.

2 Kadanoff-Baym equations

For completeness and to introduce the notations, we start with a brief review of the CTP formalism. The basic quantity of interest in the CTP quantum transport theory is the contour-time ordered two-point correlation function. For flavoured fermions it is defined by

$$\mathrm{i}S_{ij,\alpha\beta}(u,v) \equiv \big\langle \mathcal{T}_{\mathcal{C}}\big[\psi_{i,\alpha}(u)\overline{\psi}_{j,\beta}(v)\big]\big\rangle, \tag{2.1}$$

where $\mathcal{C}$ is a complex time contour and the expectation value is defined as a trace weighted by the non-equilibrium density operator of the system. We will usually suppress the Dirac (α, β) and flavour (i, j) indices when possible, as they follow the spacetime coordinates u and v of the fermion field ψ. All products involving the two-point and self-energy functions are thus implicitly matrix products in Dirac as well as flavour indices. In this paper we consider the Schwinger-Keldysh path shown in figure 1 and parametrise the

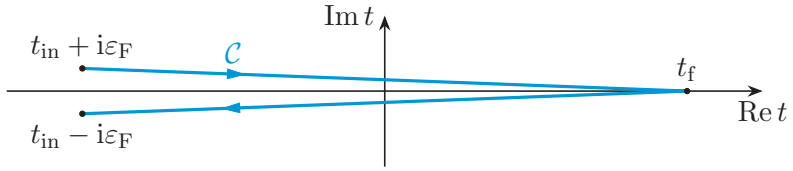

Figure 1. Shown is the Schwinger-Keldysh closed time path $\mathcal{C}$. Arrows show the direction of increasing contour-time.

contour function (2.1) in terms of four real-time valued correlation functions: the Wightman functions

$$ {\rm i}S^{<}(u,v) \equiv \langle \overline{\psi}(v)\psi(u)\rangle, \tag{2.2a} $$

$$ {\rm i}S^{>}(u,v) \equiv \langle \psi(u)\overline{\psi}(v)\rangle, \tag{2.2b} $$

and the retarded and advanced pole propagators[1]

$$ {\rm i}S^{r}(u,v) \equiv \quad 2\theta(u^0-v^0)\mathcal{A}(u,v), \tag{2.3a} $$

$$ {\rm i}S^{a}(u,v) \equiv -2\theta(v^0-u^0)\mathcal{A}(u,v). \tag{2.3b} $$

Here $\mathcal{A}(u,v) \equiv \frac{1}{2}\langle\{\psi(u),\overline{\psi}(v)\}\rangle$ is the spectral function, which satisfies $\mathcal{A} = \frac{\rm i}{2}(S^{>}+S^{<}) = \frac{\rm i}{2}(S^{r}-S^{a})$. We also denote $\mathcal{A} = S^{\mathcal{A}}$ below. We also need the Hermitian part of the pole propagators $S^{\rm H} \equiv \frac{1}{2}(S^{r}+S^{a})$. The fermion self-energy Σ can be divided into real-time components similarly and the various self-energy functions $\Sigma^{<,>}$, $\Sigma^{r,a}$, $\Sigma^{\mathcal{A},{\rm H}}$ satisfy analogous relations.

With the leptogenesis application in mind, we now specialize to spatially homogeneous and isotropic systems where the correlation and self-energy functions $F \in \{S,\Sigma\}$ have spatial translational invariance: $F(u,v) = F(u^0,v^0;\boldsymbol{u}-\boldsymbol{v})$. In this case it is convenient to use the two-time representation

$$ F_{\boldsymbol{k}}(t_1,t_2) \equiv \int {\rm d}^3\boldsymbol{r}\, {\rm e}^{-{\rm i}\boldsymbol{k}\cdot\boldsymbol{r}} F(t_1,t_2;\boldsymbol{r}), \tag{2.4} $$

which is just the spatial Fourier transform and $\boldsymbol{k}$ is the Euclidean three-momentum vector.

The Schwinger-Dyson equation obeyed by the two-point function (2.1) can be cast into four real-time Kadanoff-Baym (KB) equations for the real-time correlation and self-energy functions. In the homogeneous and isotropic case and in the two-time representation (2.4) they are given by

$$ \big[(S^{-1}_{0,\boldsymbol{k}} - \Sigma^{p}_{\boldsymbol{k}}) * S^{p}_{\boldsymbol{k}}\big](t_1,t_2) = \delta(t_1-t_2), \tag{2.5a} $$

$$ \big[(S^{-1}_{0,\boldsymbol{k}} - \Sigma^{r}_{\boldsymbol{k}}) * S^{s}_{\boldsymbol{k}}\big](t_1,t_2) = (\Sigma^{s}_{\boldsymbol{k}} * S^{a}_{\boldsymbol{k}})(t_1,t_2), \tag{2.5b} $$

[1] A related parametrisation is S^{ab}, where $a,b = \pm$ denote the CTP branches of the time arguments u^0 and v^0: $+$ referring to the upper and $-$ to the lower branch in figure 1. Then $S^{<} = -S^{+-}$ and $S^{>} = S^{-+}$, while $S^{++} = S^{\rm T}$ and $S^{--} = S^{\overline{\rm T}}$ are the time-ordered and reverse time-ordered propagators. Note that our definition of $S^{<}$ has an additional minus sign for fermions compared to what is often used elsewhere in the literature.

where $p = r, a$ and $s = <, >$. The convolution appearing here is defined by

$$(F_{\boldsymbol{k}} * G_{\boldsymbol{k}})(t_1, t_2) \equiv \int_{t_{\rm in}}^{\infty} \mathrm{d}t\, F_{\boldsymbol{k}}(t_1, t) G_{\boldsymbol{k}}(t, t_2), \tag{2.6}$$

where $t_{\rm in}$ is the initial time of the CTP, and we have taken the limit $t_{\rm f} \to \infty$ for the final time. We will eventually also take the limit $t_{\rm in} \to -\infty$ when deriving the kinetic transport equations. Finally, the inverse free propagator in equations (2.5) is given by

$$S^{-1}_{0,\boldsymbol{k}}(t_1, t_2) \equiv [\mathrm{i}\gamma^0 \partial_{t_1} - \boldsymbol{\gamma} \cdot \boldsymbol{k} - m(t_1)]\delta(t_1 - t_2). \tag{2.7}$$

The time dependent, real mass matrix $m(t)$, can be viewed as a singular contribution to the Hermitian part of the self-energy, but with our immediate application to leptogenesis in mind, it is useful to write it explicitly.

Later on we make frequent use of the Hermiticity relations of the propagators and the self-energies. In the two-time representation we can write them as

$$\overline{S}^{<,>}_{\boldsymbol{k}}(t_1, t_2)^\dagger = \overline{S}^{<,>}_{\boldsymbol{k}}(t_2, t_1), \tag{2.8a}$$
$$\overline{S}^{\mathcal{A},\mathrm{H}}_{\boldsymbol{k}}(t_1, t_2)^\dagger = \overline{S}^{\mathcal{A},\mathrm{H}}_{\boldsymbol{k}}(t_2, t_1), \tag{2.8b}$$
$$\overline{S}^{r,a}_{\boldsymbol{k}}(t_1, t_2)^\dagger = \overline{S}^{a,r}_{\boldsymbol{k}}(t_2, t_1), \tag{2.8c}$$

where we defined $\overline{S}^{<,>} \equiv \mathrm{i}S^{<,>}\gamma^0$, $\overline{S}^{r,a} \equiv S^{r,a}\gamma^0$ and $\overline{S}^{\mathcal{A},\mathrm{H}} \equiv S^{\mathcal{A},\mathrm{H}}\gamma^0$. The relations (2.8) follow straightforwardly from the definitions (2.2)–(2.4). Note that Hermitian conjugation exchanges the pole propagators in addition to their time arguments. Similar Hermiticity properties hold among the self-energy functions (with S replaced by Σ in equations (2.8)) with the definitions $\overline{\Sigma}^{<,>} \equiv \gamma^0 \mathrm{i}\Sigma^{<,>}$, $\overline{\Sigma}^{r,a} \equiv \gamma^0 \Sigma^{r,a}$ and $\overline{\Sigma}^{\mathcal{A},\mathrm{H}} \equiv \gamma^0 \Sigma^{\mathcal{A},\mathrm{H}}$. We will also need the spectral sum rule, which in the two-time representation reads

$$2\overline{\mathcal{A}}_{\boldsymbol{k}}(t, t) = \mathbf{1} \quad \text{for any } t. \tag{2.9}$$

Equation (2.9) is a direct consequence of the canonical equal-time anti-commutation relations, and it can be also derived from the definitions (2.3), the analogous relations for the self-energy functions and equations (2.5a) and (2.7).

The coupled integro-differential equations (2.5) would be difficult to solve even if the self-energies were some externally given functions. The fact that self-energies are in general functionals of the correlation functions $S^{r,a,<,>}$, makes (2.5) also non-linear and consequently much more complicated. Our main goal is to find a tractable and efficient approximation scheme for these equations, which still captures the relevant physics.

2.1 Formal solutions

Before introducing our approximations, it is useful to study some general properties of the solutions. We start by rewriting (2.5) in an alternative, but equivalent form of Schwinger-Dyson integral equations:

$$S^p_{\boldsymbol{k}} = S^p_{0,\boldsymbol{k}} + S^p_{0,\boldsymbol{k}} * \Sigma^p_{\boldsymbol{k}} * S^p_{\boldsymbol{k}}, \tag{2.10a}$$
$$S^s_{\boldsymbol{k}} = S^s_{0,\boldsymbol{k}} + S^s_{0,\boldsymbol{k}} * \Sigma^a_{\boldsymbol{k}} * S^a_{\boldsymbol{k}} + S^r_{0,\boldsymbol{k}} * \Sigma^s_{\boldsymbol{k}} * S^a_{\boldsymbol{k}} + S^r_{0,\boldsymbol{k}} * \Sigma^r_{\boldsymbol{k}} * S^s_{\boldsymbol{k}}, \tag{2.10b}$$

where the free propagators S_0^p and S_0^s satisfy

$$S_{0,\boldsymbol{k}}^{-1} * S_{0,\boldsymbol{k}}^{p} = \mathbf{1}, \tag{2.11a}$$

$$S_{0,\boldsymbol{k}}^{-1} * S_{0,\boldsymbol{k}}^{s} = 0, \tag{2.11b}$$

and again $p = r, a$ and $s = <, >$.[2] We suppressed the now obvious coordinate dependencies and used $\mathbf{1}$ to denote the functional identity matrix (i.e. the delta function in time variables).

We can turn (2.10) into formal solutions by iterating and rearranging the infinite series solutions suitably (intermediate steps of the procedure are given in appendix A). The formal pole propagator solutions are given by

$$S_{\boldsymbol{k}}^{p} = \left(S_{0,\boldsymbol{k}}^{-1} - \Sigma_{\boldsymbol{k}}^{p}\right)^{-1}. \tag{2.12}$$

The Wightman functions $S_{\boldsymbol{k}}^{s}$ can be broken into *homogeneous* and *inhomogeneous* parts: $S_{\boldsymbol{k}}^{s} = S_{\mathrm{hom},\boldsymbol{k}}^{s} + S_{\mathrm{inh},\boldsymbol{k}}^{s}$, where

$$S_{\mathrm{hom},\boldsymbol{k}}^{s} \equiv (\mathbf{1} + S_{\boldsymbol{k}}^{r} * \Sigma_{\boldsymbol{k}}^{r}) * S_{0,\boldsymbol{k}}^{s} * (\mathbf{1} + \Sigma_{\boldsymbol{k}}^{a} * S_{\boldsymbol{k}}^{a}), \tag{2.13}$$

$$S_{\mathrm{inh},\boldsymbol{k}}^{s} \equiv S_{\boldsymbol{k}}^{r} * \Sigma_{\boldsymbol{k}}^{s} * S_{\boldsymbol{k}}^{a}. \tag{2.14}$$

The inhomogeneous part $S_{\mathrm{inh},\boldsymbol{k}}^{s}$ is a particular solution to the full KB equation (2.5b), while the homogeneous part $S_{\mathrm{hom},\boldsymbol{k}}^{s}$ satisfies the same equation with the right-hand side put to zero. Solutions (2.12)–(2.14) are still completely general, but indeed purely formal because the self-energies in general depend on $S_{\boldsymbol{k}}$.[3] However, they provide important insight as to how to define and set up approximative solutions and equations. For example, if the self-energy functions are dominated by some known part, such as the equilibrium contribution, they suggest how to split the pole-functions and the inhomogeneous part of the Wightman function to a leading part and a perturbation, following schematically the division $\Sigma_{\boldsymbol{k}} = \Sigma_{\mathrm{eq},\boldsymbol{k}} + \delta\Sigma_{\boldsymbol{k}}$. We shall put this observation into good use in section 3 below.

2.2 Homogeneous solutions

We can gain further insight to the homogeneous solution (2.13), simplifying it further (still in full generality) by using the KB equations. To this end we first substitute the inverse free propagator (2.7) to equations (2.5) and write them explicitly as

$$\left[\mathrm{i}\partial_{t_1} - H_{\boldsymbol{k}}(t_1)\right]\overline{S}_{\boldsymbol{k}}^{p}(t_1,t_2) - (\overline{\Sigma}_{\boldsymbol{k}}^{p} * \overline{S}_{\boldsymbol{k}}^{p})(t_1,t_2) = \delta(t_1 - t_2), \tag{2.15a}$$

$$\left[\mathrm{i}\partial_{t_1} - H_{\boldsymbol{k}}(t_1)\right]\overline{S}_{\boldsymbol{k}}^{s}(t_1,t_2) - (\overline{\Sigma}_{\boldsymbol{k}}^{r} * \overline{S}_{\boldsymbol{k}}^{s})(t_1,t_2) = (\overline{\Sigma}_{\boldsymbol{k}}^{s} * \overline{S}_{\boldsymbol{k}}^{a})(t_1,t_2). \tag{2.15b}$$

Here $H_{\boldsymbol{k}}(t) \equiv \boldsymbol{\alpha}\cdot\boldsymbol{k} + \gamma^0 m(t)$ is the free Dirac Hamiltonian with $\boldsymbol{\alpha} \equiv \gamma^0\boldsymbol{\gamma}$, and we used the barred propagators $\overline{S}$ and self-energies $\overline{\Sigma}$ defined below equations (2.8). Using the pole

[2] It is easy to show, using (2.11a) and (2.11b) that any solution S^s to (2.10b) is also a solution to (2.5b).

[3] Of course, when one makes approximations, such as the 2PI expansion for the self-energy, the generality of these equations is restricted. In particular, when using the 2PIEA-method, one also makes an implicit assumption of Gaussianity of the initial state [62, 80]. This is not always warranted, but the nontrivial correlations induced tend to be short lived, lasting only over $t \lesssim \mathcal{O}(1-10)/m$ [81].

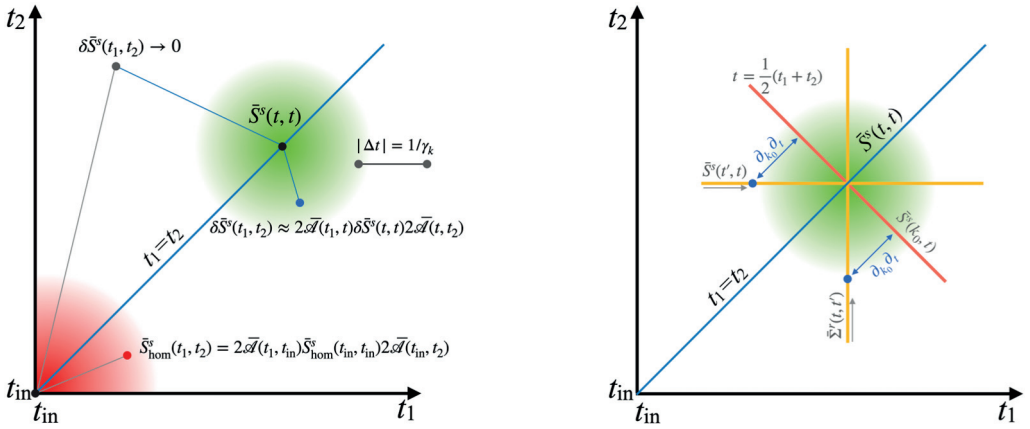

Figure 2. Left panel: schematics of the propagation of the homogeneous correlation from the initial condition set at $(t_1,t_2)=(t_{\rm in},t_{\rm in})$ (red) and the extent of the non-local correlation around a local solution defined at $(t_1,t_2)=(t,t)$ (green, see section 3.2). The strength of the colour illustrates the strength of the correlation. Outside the spheres, with $|\Delta t|\gg 1/\gamma_{\boldsymbol{k}}$, points are no longer correlated (with $(t_{\rm in},t_{\rm in})$ and (t,t) respectively) because of the dissipation. Right panel: shown are the particular time-contours of relevance for the local equation as discussed in section 3.3.

equation (2.15a) and its Hermitian conjugate in equation (2.13) then leads to

$$\begin{aligned}
&\overline{S}^s_{{\rm hom},\boldsymbol{k}}(t_1,t_2)\\
&=\int_{t_{\rm in}}^{\infty}\int_{t_{\rm in}}^{\infty}{\rm d}t\,{\rm d}t'\,\overline{S}^r_{\boldsymbol{k}}(t_1,t)\big[-{\rm i}\overleftarrow{\partial}_t-H_{\boldsymbol{k}}(t)\big]\overline{S}^s_{0,\boldsymbol{k}}(t,t')\big[{\rm i}\partial_{t'}-H_{\boldsymbol{k}}(t')\big]\overline{S}^a_{\boldsymbol{k}}(t',t_2)\\
&=2\overline{\mathcal{A}}_{\boldsymbol{k}}(t_1,t_{\rm in})\overline{S}^s_{0,\boldsymbol{k}}(t_{\rm in},t_{\rm in})2\overline{\mathcal{A}}_{\boldsymbol{k}}(t_{\rm in},t_2)\\
&=2\overline{\mathcal{A}}_{\boldsymbol{k}}(t_1,t_{\rm in})\overline{S}^s_{{\rm hom},\boldsymbol{k}}(t_{\rm in},t_{\rm in})2\overline{\mathcal{A}}_{\boldsymbol{k}}(t_{\rm in},t_2).
\end{aligned}\tag{2.16}$$

To get the second equality we integrated the derivative terms by parts, used equation (2.11b) and its Hermitian conjugate and the definitions (2.3). The only remaining term in the expression is then the boundary term involving the initial time $t_{\rm in}$. Note that it is essential in this derivation that $t_{\rm in}$ is smaller than both t_1 and t_2. Finally, we used the sum rule (2.9) at $t=t_{\rm in}$ to identify $\overline{S}^s_{0,\boldsymbol{k}}(t_{\rm in},t_{\rm in})=\overline{S}^s_{{\rm hom},\boldsymbol{k}}(t_{\rm in},t_{\rm in})$.

The result (2.16) is exact and it shows that homogeneous solutions describe transients evolving from initial conditions set at a finite initial time $t_{\rm in}$. Indeed, it is easy to show that the spectral function is the unitary time-evolution operator for two-point functions in the free theory limit: $2\overline{\mathcal{A}}_0(t_1,t_2)=U(t_1,t_2)$, for which the spectral sum rule (2.9) imposes the correct normalisation $U(t,t)=1$. However, in dissipative systems this time-evolution is no longer unitary. Dissipation shows up as a finite width of the pole functions in the Wigner representation. Going to the Wigner representation, finding quasiparticle poles and computing the corresponding quasiparticle widths $\gamma_{\boldsymbol{k}}$, and transforming back to the two-time representation, one could then obtain a more general $\mathcal{A}_{\boldsymbol{k}}$ effecting an explicit non-unitary decay of correlations in the relative time [79]: $2\overline{\mathcal{A}}_{\boldsymbol{k}}(t_1,t_2)\sim{\rm e}^{-\gamma_{\boldsymbol{k}}|t_1-t_2|}$.[4] As

[4] In this qualitative explanation we do not explicitly account for flavour dependence. It is clear however, that flavour dependent $\gamma_{\boldsymbol{k}}$'s correspond to the widths of quasi-states in the locally diagonalised matter basis.

a result, if the initial time is pushed to the past infinity, $t_{\rm in} \to -\infty$, all memory of the initial conditions will vanish, leaving only the inhomogeneous solution. We illustrate this phenomenon schematically in figure 2.

We find the homogeneous solutions of the form (2.16) to be very useful still in another way, which is crucial to our scheme. We will return to this issue in section 3.2 below.

3 Local quantum kinetic equation

The main source of complexity in equations (2.15) comes from their non-locality and the associated need for a complete accounting of the memory effects. Yet, all physical observables are expressible in terms of the local correlation function $S_{\boldsymbol{k}}(t,t)$, and moreover, we have seen that dissipative processes in general wash out memory effects over time intervals $|\Delta t| \geq 1/\gamma_{\boldsymbol{k}}$. This suggests to try to find an approximative equation that involves *only* the local correlation function. Such an equation is easy to set up formally: we first use the chain rule to write[5]

$$\partial_t S^<_{\boldsymbol{k}}(t,t) = \Big[(\partial_t + \partial_{t'}) S^<_{\boldsymbol{k}}(t,t')\Big]_{t'=t}. \tag{3.1}$$

Using this with the KB equation (2.15b) and its Hermitian conjugate together with the Hermiticity relations (2.8) yields the equal-time equation

$$\begin{aligned} \mathrm{i}\partial_t \overline{S}^<_{\boldsymbol{k}}(t,t) = \big[H_{\boldsymbol{k}}(t), \overline{S}^<_{\boldsymbol{k}}(t,t)\big] &+ (\overline{\Sigma}^r_{\boldsymbol{k}} * \overline{S}^<_{\boldsymbol{k}})(t,t) - (\overline{S}^<_{\boldsymbol{k}} * \overline{\Sigma}^a_{\boldsymbol{k}})(t,t) \\ &+ (\overline{\Sigma}^<_{\boldsymbol{k}} * \overline{S}^a_{\boldsymbol{k}})(t,t) - (\overline{S}^r_{\boldsymbol{k}} * \overline{\Sigma}^<_{\boldsymbol{k}})(t,t). \end{aligned} \tag{3.2}$$

This equation is still exact, but of course not closed because it still involves the non-local function $S^<_{\boldsymbol{k}}(t,t')$ with $t \neq t'$ explicitly in the interaction convolution terms $\overline{\Sigma}^r_{\boldsymbol{k}} * \overline{S}^<_{\boldsymbol{k}}$ and $\overline{S}^<_{\boldsymbol{k}} * \overline{\Sigma}^a_{\boldsymbol{k}}$ and implicitly within the self-energies. It also depends explicitly on the pole functions $S^{r,a}_{\boldsymbol{k}}(t_1,t_2)$. To make (3.2) self-contained, we need to supply it with enough information of these particular correlations, without going back to the full KB equations.

3.1 Perturbation around the adiabatic solution

Let us first address the coupling between the Wightman functions and the pole functions. This issue is intimately connected to finding a good approximation for the inhomogeneous solution for the Wightman functions as is suggested by equations (2.12) and (2.14). We start by formally dividing the correlation functions into some known adiabatic background solution and a perturbation:

$$S^\alpha_{\boldsymbol{k}} = S^\alpha_{\mathrm{ad},\boldsymbol{k}} + \delta S^\alpha_{\boldsymbol{k}}. \tag{3.3}$$

where $\alpha = r, a, <, >$. There is some freedom as to how to choose the adiabatic solutions. For example, in a system near thermal equilibrium, the instantaneous thermal equilibrium solutions would be an obvious choice. More formally, the adiabatic Wightman function can be defined as a solution that reduces to the stationary solution of (3.2), when ignoring

[5] In order to get an equation for the local correlation function, it is essential that the derivative acts on both time-variables. Otherwise the limiting procedure introduces other independent functions (first moment of the propagator in the mixed representation) to the left hand side of the equation (3.2).

all local time dependence.[6] When $S^{\alpha}_{\mathrm{ad},\boldsymbol{k}}$ fulfil this requirement, inserting the division (3.3) into equation (3.2) leads to

$$\begin{aligned}\mathrm{i}\partial_t \delta\overline{S}^{<}_{\boldsymbol{k}}(t,t) \simeq [H_{\boldsymbol{k}}(t), \delta\overline{S}^{<}_{\boldsymbol{k}}(t,t)] &+ (\overline{\Sigma}^{r}_{\boldsymbol{k}} * \delta\overline{S}^{<}_{\boldsymbol{k}})(t,t) - (\delta\overline{S}^{<}_{\boldsymbol{k}} * \overline{\Sigma}^{a}_{\boldsymbol{k}})(t,t) \\ &+ (\overline{\Sigma}^{<}_{\boldsymbol{k}} * \delta\overline{S}^{a}_{\boldsymbol{k}})(t,t) - (\delta\overline{S}^{r}_{\boldsymbol{k}} * \overline{\Sigma}^{<}_{\boldsymbol{k}})(t,t) \\ &- \mathrm{i}\partial_t \overline{S}^{<}_{\mathrm{ad},\boldsymbol{k}}(t,t). \end{aligned} \tag{3.4}$$

The source $-\mathrm{i}\partial_t \overline{S}^{<}_{\mathrm{ad},\boldsymbol{k}}(t,t)$ is the leading correction left from the terms involving the adiabatic solution in the full dynamical equation. Note that as the Wightman function can contain also a homogeneous transient, $\delta S^{<}_{\boldsymbol{k}}$ is not necessarily small even when the adiabatic solution is an equilibrium solution.

The equal-time pole functions, on the other hand, can be taken to be purely adiabatic with no dynamical perturbations: $\delta S^{p}_{\boldsymbol{k}} = 0$. In the equal-time limit this condition is actually strictly imposed by the spectral sum rule (2.9) and the relations (2.3) between the pole functions and the spectral function. One can also show that $\partial_t S^{p}_{\mathrm{ad},\boldsymbol{k}}(t,t) = 0$ exactly at least in a non-interacting theory. This suggests that no perturbations in the pole functions can be included in a truncation to the local limit. It is then remarkable, that in the truncation scheme for the collision terms developed in the next section, the non-local pole function perturbations vanish consistently with their vanishing equal-time counterparts. This means that pole functions become entirely non-dynamical quantities that account for the structure of the phase space only. With this information, equation (3.4) further reduces to

$$\mathrm{i}\partial_t \delta\overline{S}^{<}_{\boldsymbol{k}}(t,t) \simeq \big[H_{\boldsymbol{k}}(t), \delta\overline{S}^{<}_{\boldsymbol{k}}(t,t)\big] - \mathrm{i}\partial_t \overline{S}^{<}_{\mathrm{ad},\boldsymbol{k}}(t,t) + \big[(\overline{\Sigma}^{r}_{\boldsymbol{k}} * \delta\overline{S}^{<}_{\boldsymbol{k}})(t,t) - \mathrm{H.c.}\big]. \tag{3.5}$$

This equation no longer depends explicitly on the pole functions. They only have limited influence on (3.5) through the source function and the self-energy functions, as we shall discuss below.

On the choice of the adiabatic solution. Explicit forms for the adiabatic solutions are most conveniently given in the Wigner representation, which is defined as the Fourier transform of the two-time representation (2.4) with respect to the relative time-coordinate:

$$F(k,t) \equiv \int_{-\infty}^{\infty} \mathrm{d}r^0 \, \mathrm{e}^{\mathrm{i}k^0 r^0} F_{\boldsymbol{k}}(t + \tfrac{r^0}{2}, t - \tfrac{r^0}{2}). \tag{3.6}$$

Here $t = (t_1 + t_2)/2$ is the average time coordinate and k^0 is the internal energy conjugate to the relative time coordinate $r^0 = t_1 - t_2$. Note that we always take the limit $t_{\mathrm{in}} \to -\infty$ before calculating any Wigner transforms. We now define the adiabatic solutions with

[6] This corresponds to working to lowest order in gradients in the Wigner representation.

instantaneous mass $m(t)$ and self-energies as follows:[7]

$$S^p_{\rm ad}(k,t) = \big[\not{k} - m(t) - \Sigma^p_{\rm ad}(k,t)\big]^{-1}, \tag{3.7a}$$

$$S^s_{\rm ad}(k,t) = S^r_{\rm ad}(k,t)\Sigma^s_{\rm ad}(k,t)S^a_{\rm ad}(k,t). \tag{3.7b}$$

There still is significant freedom left in these solutions related to the choice of the self-energy functions $\Sigma^\alpha_{\rm ad}$. For example, one might choose to ignore or include the Hermitian part $\Sigma^{\rm H}_{\rm ad}$ of the pole self-energy functions, leading to solutions either with vacuum or quasiparticle dispersion relations. Moreover, if one neglects the finite width, setting $\Sigma^{\mathcal{A}}_{\rm ad} = 0$, the corresponding solutions become spectral (either vacuum or quasiparticle). This is the choice made in the derivation of cQPA-formalism [72–79], as well as in the usual Boltzmann theory [82]. If one includes a finite width however, the adiabatic part of the solution spreads out in phase space, with a consequent change in the source term in the equation (3.5) for the perturbation $\delta S^<_{\boldsymbol{k}}$. One can even include corrections from the perturbations $\delta S^<_{\boldsymbol{k}}$ in the self-energies, without changing the basic structure of the equation for the perturbation $\delta S^<_{\boldsymbol{k}}$ itself. The point is that the validity of all these approximations is controlled by the coupling constant expansion.

3.2 Local approximation

The division into an adiabatic background and the perturbation simplified the original equal-time equation considerably. However, the problem of closure still remains: our equation describes the evolution of the perturbation only along the diagonal $t_1 = t_2$ in figure 2, but the collision integrals depend on $\delta S^<_{\boldsymbol{k}}(t_1,t_2)$ everywhere in the two-time plane. In a system with dissipation, these *memory effects* are suppressed however, and there is hope that a strictly local description can be found. We use the evolution of the homogeneous perturbation (2.16) as our guiding principle to reach this goal.

Indeed, imagine first that we somehow have found the correct solution $\delta S^s_{\boldsymbol{k}}(t,t)$ along the diagonal. For $t_{1,2}$ not too far from the time t, the true non-local solution $\delta S^s_{\boldsymbol{k}}(t_1,t_2)$ should be correlated with $\delta S^s_{\boldsymbol{k}}(t,t)$, and even reasonably well approximated by a homogeneous solution similar to equation (2.16), with the initial time $t_{\rm in}$ replaced by the local time t. Even when we do not know the local solution beforehand, we can *parametrise* the non-local solution with the local one. Specifically, we make the *local ansatz*

$$\delta\overline{S}^s_{\boldsymbol{k}}(t_1,t_2) = 2\overline{\mathcal{A}}_{\boldsymbol{k}}(t_1,t)\delta\overline{S}^s_{\boldsymbol{k}}(t,t)2\overline{\mathcal{A}}_{\boldsymbol{k}}(t,t_2) \quad \text{for any } t. \tag{3.8}$$

Note in particular that the spectral function is not a dynamical quantity in (3.8); following the discussion of the previous section, the generalised time evolution operator $2\overline{\mathcal{A}}_{\boldsymbol{k}}(t_1,t_2)$ is a non-dynamical adiabatic solution that can be computed to the desired accuracy independently from the local correlation function $\delta S^s_{\boldsymbol{k}}(t,t)$. We stress that the ansatz (3.8) will

[7] More precisely, we should replace the self-energies $\Sigma(k,t)$ in equations (3.7) by their "out-versions" defined below equation (3.9). This is important when the self-energy depends on the perturbation δS itself and may thus contain rapidly oscillating coherence functions [76, 77, 79]. However, this phenomenon is not relevant for us in this paper where we eventually will average over such fast fluctuations and both definitions correspond to the same local correlator in the two-time representation.

only be used in the convolution terms describing the interactions. Indeed, if taken to hold universally for all t, it would generally be too restrictive and in contradiction with the local equation of motion (3.5).

cQPA and Boltzmann theory limit. It should be stressed that the ansatz (3.8) is an exact relation in free theory and for spectral quasiparticles, where the full solution is homogeneous and the free spectral function is the unitary time evolution operator. Indeed, we can derive the cQPA-correlation function [77, 79], and eventually the Boltzmann theory limit directly from (3.8). First choosing $t = (t_1+t_2)/2$ and then Wigner-transforming (3.8), one finds (here we write the results explicitly for $S^<$ but analogous results hold for $S^>$)

$$\delta\overline{S}^<(k,t) = \int \frac{\mathrm{d}p^0}{\pi} 2\overline{\mathcal{A}}_{\mathrm{in},\boldsymbol{k}}(p^0,t)\delta\overline{S}^<_{\boldsymbol{k}}(t,t)2\overline{\mathcal{A}}_{\mathrm{out},\boldsymbol{k}}(2k^0-p^0,t), \tag{3.9}$$

where $\mathcal{A}_{\mathrm{out}}(k,t) \equiv \mathrm{e}^{\frac{\mathrm{i}}{2}\partial_t\partial_{k^0}}\mathcal{A}(k,t)$ and $\mathcal{A}_{\mathrm{in}}(k,t) \equiv \mathrm{e}^{-\frac{\mathrm{i}}{2}\partial_t\partial_{k^0}}\mathcal{A}(k,t)$. This form is still valid for any adiabatic solution for the spectral function. Working to lowest order in gradients and using the free adiabatic spectral function,

$$\overline{\mathcal{A}}^{(0)}_{\boldsymbol{k}ij}(k^0,t) = \pi\,\mathrm{sgn}(k^0)(\not{k}+m_i(t))\gamma^0\,\delta(k^2-m_i^2)\delta_{ij}, \tag{3.10}$$

equation (3.9) reduces to the spectral form

$$\delta\overline{S}^<_{ij}(k,t) = 2\pi\sum_{h,\pm,\pm'} P_{\boldsymbol{k}h}P^{\pm}_{\boldsymbol{k}i}\,\delta\overline{S}^<_{\boldsymbol{k}hij}(t,t)\,P^{\pm'}_{\boldsymbol{k}j}\delta(k^0 \mp \tfrac{1}{2}\omega_{\boldsymbol{k}i} \mp' \tfrac{1}{2}\omega_{\boldsymbol{k}j}), \tag{3.11}$$

where the helicity and energy projection matrices are defined by

$$P_{\boldsymbol{k}h} = \frac{1}{2}\Big(\mathbf{1} + h\hat{h}_{\boldsymbol{k}}\Big), \qquad P^s_{\boldsymbol{k}i} = \frac{1}{2}\Big(\mathbf{1} + s\frac{H_{\boldsymbol{k}i}}{\omega_{\boldsymbol{k}i}}\Big), \tag{3.12}$$

with $\hat{h}_{\boldsymbol{k}} \equiv \boldsymbol{\alpha}\cdot\hat{\boldsymbol{k}}\,\gamma^5$, $H_{\boldsymbol{k}i} = \boldsymbol{\alpha}\cdot\boldsymbol{k} + \gamma^0 m_i$ and $\omega_{\boldsymbol{k}i} = \sqrt{|\boldsymbol{k}|^2 + {m_i}^2}$. The helicity and energy indices both take values $h, s = \pm$. It is easy to show that the projectors $P_{\boldsymbol{k}h}P^{\pm}_{\boldsymbol{k}i}\gamma^0 P^{\pm'}_{\boldsymbol{k}j}$ form a complete basis of matrices consistent with homogeneity and isotropy (this will be elaborated further in section 5.1). In the spectral limit the adiabatic solutions and the perturbations can be combined on the common shell functions. Expanding the corresponding full $\overline{S}^<_{\boldsymbol{k}}(t,t)$ in this basis (for the precise definition of $\mathcal{P}^{ss'}_{\boldsymbol{k}hij}$ see equation (5.2) below), we can rewrite equation (3.11) as

$$\overline{S}^<_{ij}(k,t) = 2\pi\sum_{h,\pm}\Big(\mathcal{P}^{\pm\pm}_{\boldsymbol{k}hij}f^{m,\pm}_{\boldsymbol{k}hij}\delta(k^0 \mp \bar{\omega}_{\boldsymbol{k}ij}) + \mathcal{P}^{\pm\mp}_{\boldsymbol{k}hij}f^{c,\pm}_{\boldsymbol{k}hij}\delta(k^0 \mp \tfrac{1}{2}\Delta\omega_{\boldsymbol{k}ij})\Big), \tag{3.13}$$

where $\bar{\omega}_{\boldsymbol{k}ij} \equiv (\omega_{\boldsymbol{k}i}+\omega_{\boldsymbol{k}j})/2$ and $\Delta\omega_{\boldsymbol{k}ij} \equiv \omega_{\boldsymbol{k}i}-\omega_{\boldsymbol{k}j}$. This is the flavoured cQPA-propagator, up to normalisation, derived in [77] and it carries information of all coherence structures consistent with homogeneity and isotropy in the spectral limit.

If one ignores all coherence information, equation (3.13) reduces to a generalised KB-ansatz

$$\overline{S}^<_{ij}(k,t) = \sum_h P_{\boldsymbol{k}h}f^{m,\mathrm{sgn}(k^0)}_{\boldsymbol{k}hii}\,2\overline{\mathcal{A}}^{(0)}_{\boldsymbol{k}ij}(k^0,t)\,\mathrm{sgn}(k^0), \tag{3.14}$$

which corresponds to the Boltzmann theory limit with distribution functions that are diagonal in flavour and helicity. The extra $\mathrm{sgn}(k^0)$ factor could be absorbed to normalisation, but the present normalisation will be more convenient later. Moreover, if one imposes the thermal equilibrium Kubo-Martin-Schwinger (KMS) condition for the cQPA Wightman functions, $S^>(k,t) = \mathrm{e}^{\beta k^0} S^<(k,t)$, which now is equivalent to $\overline{S}^<_{ij}(k,t) = 2\overline{\mathcal{A}}^{(0)}_{\boldsymbol{k}ij}(k^0,t) f_{\mathrm{FD}}(k^0)$, the distribution function further reduces to the thermal Fermi-Dirac distribution: $f^{m,\pm}_{\boldsymbol{k}hii} = \pm f_{\mathrm{FD}}(\pm\omega_{\boldsymbol{k}i})$ (cf. [79]).

3.3 Local transport equation

For us, the most important utility of the local approximation (3.8) is that it allows closure in equation (3.5), reducing all interaction convolutions containing the non-local function $\delta\overline{S}^<_{\boldsymbol{k}}(t,t')$ to simple matrix products involving only the local function $\delta\overline{S}^<_{\boldsymbol{k}}(t,t)$. For example,

$$\begin{aligned}(\overline{\Sigma}^r_{\boldsymbol{k}} * \delta\overline{S}^<_{\boldsymbol{k}})(t,t) &= \int_{t_{\mathrm{in}}}^{\infty} \mathrm{d}t'\, \overline{\Sigma}^r_{\boldsymbol{k}}(t,t')\delta\overline{S}^<_{\boldsymbol{k}}(t',t) \\ &\simeq \left[\int_{t_{\mathrm{in}}}^{\infty} \mathrm{d}t'\, \overline{\Sigma}^r_{\boldsymbol{k}}(t,t') 2\overline{\mathcal{A}}_{\boldsymbol{k}}(t',t)\right] \delta\overline{S}^<_{\boldsymbol{k}}(t,t) \\ &\equiv \overline{\Sigma}^r_{\mathrm{eff},\boldsymbol{k}}(t,t)\delta\overline{S}^<_{\boldsymbol{k}}(t,t), \end{aligned} \tag{3.15}$$

where we introduced the effective self-energy $\overline{\Sigma}^r_{\mathrm{eff},\boldsymbol{k}}$. We remind that the spectral function is adiabatic $\mathcal{A} \equiv \mathcal{A}_{\mathrm{ad}}$ in these expressions, consistent with our approximation scheme. While the effective self-energy

$$\overline{\Sigma}^r_{\mathrm{eff},\boldsymbol{k}}(t,t) = (\overline{\Sigma}^r_{\boldsymbol{k}} * 2\overline{\mathcal{A}}_{\boldsymbol{k}})(t,t) \tag{3.16}$$

is still a convolution, it can be computed at any time during the solution based only on the local solution itself, or independently of it, depending on the approximation one uses for the adiabatic functions, as discussed in section 3.1.

We now use the local approximation (3.8) to obtain closure in equation (3.5). This amounts to using (3.15) and its Hermitian conjugate with (3.16) in equation (3.5), resulting in the local equation of motion

$$\partial_t \delta\overline{S}^<_{\boldsymbol{k}}(t,t) + \mathrm{i}\big[H_{\boldsymbol{k}}(t), \delta\overline{S}^<_{\boldsymbol{k}}(t,t)\big] = -\partial_t \overline{S}^<_{\mathrm{ad},\boldsymbol{k}}(t,t) - \big(\mathrm{i}\overline{\Sigma}^r_{\mathrm{eff},\boldsymbol{k}}(t,t)\delta\overline{S}^<_{\boldsymbol{k}}(t,t) + \mathrm{H.c.}\big). \tag{3.17}$$

Equation (3.17) is our final quantum kinetic equation (QKE) for non-equilibrium evolution of mixing fermions. The non-local memory integrals have been truncated by the local approximation, so it is an ordinary (matrix) differential equation for the local non-equilibrium correlation function $\delta\overline{S}^<_{\boldsymbol{k}}(t,t)$. Equation (3.17) still describes both flavour and particle-antiparticle coherence effects of the mixing fermions. It also takes into account quantum statistical effects of the thermal medium (within the weak coupling expansion), and it can accommodate thermal corrections to the dispersion relations via the effective self-energy and the adiabatic source term. We have shown that (3.17) encompasses the coherent cQPA-formalism and consequently the usual Boltzmann theory including also semiclassical corrections [79], but it is a more general formulation in that it is not restricted to the spectral limit. We will apply this equation in the leptogenesis setting to describe the evolution of the right-handed Majorana neutrinos in the next section.

On the accuracy of the local ansatz. Despite its wide range of applicability, the ansatz (3.8) should eventually break down if the system develops significant temporal correlations (a memory) over large time intervals. When would this happen and how large would the corrections be? Ultimately one would like to compare the results obtained using the local equation (3.17) with a numerical solution of the full non-local two-time equations (2.15), but we can get a good idea of the size of the memory effects by studying their origin in the Wigner representation.

We first note that the Wigner transform (3.6) encodes all dependence on the relative time $r^0 = t_1 - t_2$ at constant average time slices $t = \frac{1}{2}(t_1 + t_2)$ in the frequency components $S_{\boldsymbol{k}}(k^0, t)$ (see the right panel of figure 2 for illustration). In the weak coupling limit this information gets concentrated on narrow shells in frequency space and eventually to spectral solutions when widths are neglected. The non-local information relevant for equations (3.5) and (3.17) is contained in the convolution integrals that can be expressed as follows:

$$(\overline{\Sigma}^r_{\boldsymbol{k}} * \overline{G}_{\boldsymbol{k}})(t,t) = \int \mathrm{d}t'\, \overline{\Sigma}^r_{\boldsymbol{k}}(t,t')\overline{G}_{\boldsymbol{k}}(t',t) = \int \frac{\mathrm{d}k^0}{2\pi}\, \overline{\Sigma}^r_{\mathrm{out}}(k + \tfrac{\mathrm{i}}{2}\partial_t, t)\overline{G}(k,t), \tag{3.18}$$

where $\overline{G} = \delta\overline{S}^<$ in (3.5) and $\overline{G} = \overline{\mathcal{A}}$ in (3.17).[8] Clearly, for a fixed t the non-local information of $G_{\boldsymbol{k}}(t', t)$ contained in the two-time convolution (along the contour $t_2 = t$) is fully encoded in the gradients in the Wigner representation, since $G(k, t)$ only contains information along the contour $\frac{1}{2}(t_1 + t_2) = t$. This correspondence is schematically illustrated by the blue arrows in figure 2.

Finally then, the validity of the local approximation (3.8) boils down to the smallness of the gradient corrections and assuming that $\delta S(k, t)$ has a similar phase space structure as the adiabatic solution. In the leptogenesis application gradient corrections are controlled by the Hubble expansion and hence they are small since $H/T \ll 1$. The phase space structures of the adiabatic solution and the perturbation $\delta S(k, t)$ should be similar because the latter is created by the former. Also, both solutions become spectral when the width is zero, so this approximation becomes good also in the weak coupling limit.

4 Leptogenesis

We now apply our methods to study lepton asymmetry production in the early universe. Leptogenesis has different variants, including the original thermal leptogenesis [19], resonant leptogenesis [83, 84] and the freeze-in, or Akhmedov-Rubakov-Smirnov (ARS) leptogenesis [85]. For more discussion see e.g. [20, 21]. Our methods apply, with minor modifications, to all these variants, but we will focus to the resonant scenario in the minimal model with two heavy Majorana neutrinos coupled to a single light SM lepton doublet and a Higgs doublet. Generalisation to more neutrino flavours, or more SM lepton flavours necessary

[8] There is one subtlety if we take $\overline{G} = \delta\overline{S}^<$ as in equation (3.5). In this case one has to account for the gradient operator in the argument of $\overline{\Sigma}^r_{\mathrm{out}}$, when it acts on the rapidly oscillating coherence solutions in $\delta\overline{S}^<$. This ensures that the coherence shell contributions get computed on correct frequency shells in the cQPA-formulation (see e.g. [79]). One of the nice features of the ansatz (3.8) is that it fully automatises this resummation, also when evaluating higher loop self-energy functions [77]. Indeed, the issue clearly does not arise when $\overline{G} = \overline{\mathcal{A}}$, because $\mathcal{A}$ is an adiabatic function.

e.g. for low scale leptogenesis [86, 87] and the ARS-mechanism, would be straightforward. We will also only include the decay and inverse decay interactions, neglecting the $2 \to 2$ scattering processes. This limits the range of validity of our predictions, but our goal is not the maximal phenomenological reach, but the accuracy of the quantum transport formulation and detailed comparisons between different approximations. Again, generalisation to more complex interactions would be straightforward.

In principle all particle species involved in the problem could be treated on the same footing in the CTP-context, resulting in a network of local transport equations. However, a number of simplifying approximations can be made for the SM fields. For example we can neglect the decay widths of the lepton and Higgs fields and assume that they are in kinetic equilibrium due to the SM gauge interactions. To first order, we can also neglect the chemical potential of the Higgs field, which then decouples from the dynamics. The lepton chemical potential μ_ℓ is essential of course, but we can assume μ_ℓ/T to be small, which allows us to neglect the backreaction of μ_ℓ to the dynamics of the Majorana neutrinos. We can then solve the coupled neutrino and lepton equations consecutively instead of simultaneously. For neutrinos we will use the local transport equation (3.17) with full phase space structure and flavour coherence information. Since we are only accounting for one-loop self-energies, we include only the indirect or ε-type self-energy contribution to the CP-violation. Including the direct ε'-type contribution would require a two-loop self-energy calculation, but we refrain from doing this, because the indirect contribution is dominant in the resonant regime.

In summary, the objective of this section is to derive an explicit local quantum transport equation for the mixing Majorana neutrinos, coupled with an equation for the particle-antiparticle asymmetry of the SM lepton doublet. We will compute explicitly all self-energy functions and the adiabatic background solutions for the neutrinos, as well as the source and washout terms for the lepton asymmetry equation. We will work consistently to the leading order in the coupling constant expansion and discuss the renormalisation procedure necessary for the loop calculations.

4.1 The minimal model

Our model contains two singlet Majorana neutrino fields N_i, coupled to an active lepton SU(2)-doublet ℓ and the complex scalar Higgs doublet ϕ via chiral Yukawa interactions:

$$\mathcal{L} = \sum_i \Big[\frac{1}{2}\overline{N}_i(\mathrm{i}\partial\!\!\!/ - m_i)N_i - y_i^*(\bar{\ell}\widetilde{\phi})P_{\mathrm{R}}N_i - y_i\overline{N}_i P_{\mathrm{L}}(\widetilde{\phi}^\dagger\ell)\Big] + \bar{\ell}\,\mathrm{i}\partial\!\!\!/\,\ell + (\partial_\mu\phi^\dagger)(\partial^\mu\phi). \tag{4.1}$$

We work in the mass basis for the Majorana neutrinos, where m_i are the lepton number violating real Majorana masses. The lepton and Higgs fields are assumed to be massless as leptogenesis must take place in a high temperature in the electroweak symmetric phase. Finally, the SU(2)-conjugate Higgs doublet is defined by $\widetilde{\phi} \equiv \varepsilon\phi^*$ where ε is the anti-symmetric 2×2 matrix with $\varepsilon_{12} = 1$. The CP-violating phases necessary for leptogenesis are contained in the complex coupling constants y_i.

The CTP propagators of the neutrino, lepton and Higgs fields are given by

$$\mathrm{i}S_{ij}(x,y) \equiv \langle \mathcal{T}_\mathcal{C}[N_i(x)\overline{N}_j(y)]\rangle, \tag{4.2a}$$

$$\mathrm{i}S_{\ell,AB}(x,y) \equiv \langle \mathcal{T}_\mathcal{C}[\ell_A(x)\overline{\ell_B}(y)]\rangle, \tag{4.2b}$$

$$\mathrm{i}\Delta_{AB}(x,y) \equiv \langle \mathcal{T}_\mathcal{C}[\phi_A(x)\phi_B^\dagger(y)]\rangle, \tag{4.2c}$$

respectively, with the various real-time propagators defined as in section 2.[9] Here we have explicitly marked the SU(2)-doublet indices ($A, B = 1, 2$) of the lepton and Higgs propagators and the Majorana flavour indices (i, j) of the neutrino propagator. Because of the SU(2) symmetry the lepton and Higgs propagators are diagonal in the SU(2)-indices: $S_{\ell,AB} \equiv S_\ell\,\delta_{AB}$ and $\Delta_{AB} \equiv \Delta\,\delta_{AB}$. In the following we work directly with the diagonal elements S_ℓ and Δ. On the other hand, the Majorana fields N_i satisfy the Majorana condition

$$N_i = N_i^c \equiv C\overline{N}_i^\mathrm{T}, \tag{4.3}$$

where C is the unitary and antisymmetric charge conjugation matrix. An important consequence of the condition (4.3) is that the neutrino propagator is constrained by

$$S(x,y) = CS(y,x)^\mathrm{T}C^{-1}. \tag{4.4}$$

Note that here the transpose acts on all of the flavour, Dirac and CTP indices of the propagator.

4.2 Self-energy functions

We calculate the self-energies in the 2PIEA formalism, where the self-energies are defined as functional derivatives of the non-trivial part Γ_2 of the effective action with respect to the propagators. The non-trivial part Γ_2 contains contributions of vacuum diagrams with two or more loops. The two-loop contribution (see figure 3a) arising from the Yukawa interaction in the Lagrangian (4.1) is given by

$$\mathrm{i}\Gamma_2^{(2)} = c_\mathrm{w}\sum_{i,j} y_i^* y_j \iint_\mathcal{C} \mathrm{d}^4x\,\mathrm{d}^4y\,\mathrm{tr}[P_\mathrm{R}\mathrm{i}S_{ij}(x,y)P_\mathrm{L}\mathrm{i}S_\ell(y,x)]\mathrm{i}\Delta(y,x). \tag{4.5}$$

Here $c_\mathrm{w} = 2$ is a multiplicity factor from the trace over the SU(2)-doublet indices, and $\mathcal{C}$ denotes integration over the CTP.

To calculate the Majorana neutrino self-energy we need to take the functional derivative of Γ_2 with respect to the neutrino propagator S. As the propagator is constrained by the Majorana condition (4.4), its functional derivative is defined by

$$\begin{aligned}\frac{\delta S_{ij,\alpha\beta}(x,y)}{\delta S_{kl,\gamma\delta}(w,z)} &= \delta_{ik}\delta_{jl}\delta_{\alpha\gamma}\,\delta_{\beta\delta}\;\delta^{(4)}(x-w)\delta^{(4)}(y-z)\\ &\quad + \delta_{il}\delta_{jk}C_{\alpha\delta}C^*_{\beta\gamma}\delta^{(4)}(x-z)\delta^{(4)}(y-w),\end{aligned} \tag{4.6}$$

where the flavour and Dirac indices have been indicated explicitly. For an unconstrained Dirac particle the second term on the right-hand side of equation (4.6) would not be present.

[9] The real-time components of the complex scalar propagator are defined similarly to equations (2.2) and (2.3): for example the Wightman functions are $\Delta^<(u,v) \equiv \langle\phi^\dagger(v)\phi(u)\rangle$ and $\Delta^>(u,v) \equiv \langle\phi(u)\phi^\dagger(v)\rangle$. The only difference to the fermionic case is that the bosonic spectral function is a commutator of the fields, rather than an anti-commutator, and we use the standard sign convention $\Delta^< = \Delta^{+-}$ for bosons.

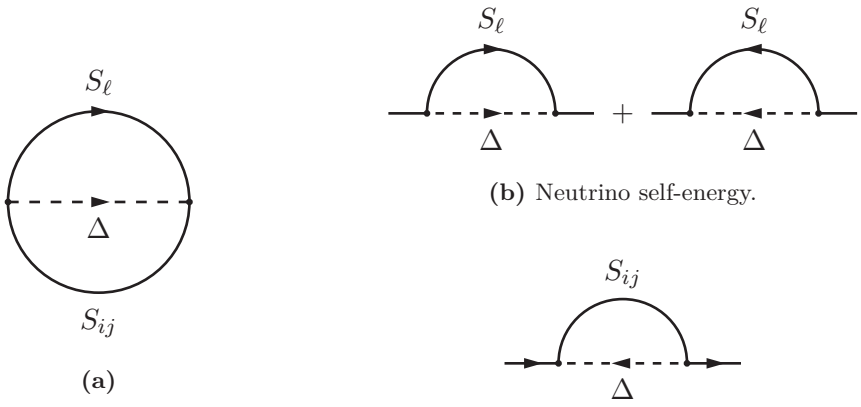

(a)

(b) Neutrino self-energy.

(c) Lepton self-energy.

Figure 3. Shown on the left (a) is the 2PI two-loop vacuum diagram in theory (4.1). The corresponding 1PI diagrams contributing to the Majorana neutrino (b) and lepton (c) self-energies are shown on the right.

The one-loop Majorana neutrino self-energy Σ_{ij} (figure 3b), calculated using equations (4.5) and (4.6), is then given in direct space by

$$\begin{aligned} \mathrm{i}\Sigma_{ij}(x,y) \equiv \frac{\delta\Gamma_2}{\delta S_{ji}(y,x)} = c_\mathrm{w}\Big[&y_i y_j^* P_\mathrm{L}\mathrm{i}S_\ell(x,y)P_\mathrm{R}\mathrm{i}\Delta(x,y) \\ &+ y_i^* y_j P_\mathrm{R} C\mathrm{i}S_\ell(y,x)^\mathrm{T} C^{-1} P_\mathrm{L}\mathrm{i}\Delta(y,x)\Big]. \end{aligned} \tag{4.7}$$

The lepton self-energy (figure 3c) is calculated similarly, and the result for the SU(2)-diagonal element is

$$\mathrm{i}\Sigma_\ell(x,y) = \sum_{i,j} y_i^* y_j P_\mathrm{R}\mathrm{i}S_{ij}(x,y)P_\mathrm{L}\mathrm{i}\Delta(y,x). \tag{4.8}$$

From these it is straightforward to calculate the real-time self-energies by inserting the CTP indices (which follow the spacetime arguments) and using the relations of the different propagators. Later we need the following neutrino self-energy functions (given now in the Wigner representation):

$$\begin{aligned} \mathrm{i}\Sigma_{ij}^{<,>}(k,t) = c_\mathrm{w}\int\frac{\mathrm{d}^4p}{(2\pi)^4}\Big[&y_i y_j^* P_\mathrm{L}\mathrm{i}S_\ell^{<,>}(p,t)P_\mathrm{R}\mathrm{i}\Delta^{<,>}(k-p,t) \\ &- y_i^* y_j P_\mathrm{R} C\mathrm{i}S_\ell^{>,<}(-p,t)^\mathrm{T} C^{-1} P_\mathrm{L}\mathrm{i}\Delta^{>,<}(p-k,t)\Big], \end{aligned} \tag{4.9}$$

$$\begin{aligned} \Sigma_{ij}^\mathrm{H}(k,t) = c_\mathrm{w}\int\frac{\mathrm{d}^4p}{(2\pi)^4}\Big[&y_i y_j^* P_\mathrm{L} S_\ell^\mathrm{H}(p,t)P_\mathrm{R}\mathrm{i}\Delta^\mathrm{F}(k-p,t) \\ &+ y_i y_j^* P_\mathrm{L}\mathrm{i}S_\ell^\mathrm{F}(p,t)P_\mathrm{R}\Delta^\mathrm{H}(k-p,t) \\ &+ y_i^* y_j P_\mathrm{R} C S_\ell^\mathrm{H}(-p,t)^\mathrm{T} C^{-1} P_\mathrm{L}\mathrm{i}\Delta^\mathrm{F}(p-k,t) \\ &+ y_i^* y_j P_\mathrm{R} C\mathrm{i}S_\ell^\mathrm{F}(-p,t)^\mathrm{T} C^{-1} P_\mathrm{L}\Delta^\mathrm{H}(p-k,t)\Big], \end{aligned} \tag{4.10}$$

where we defined the statistical propagators $S^\mathrm{F} \equiv \frac{1}{2}(S^> - S^<)$ and $\Delta^\mathrm{F} \equiv \frac{1}{2}(\Delta^> + \Delta^<)$.

4.3 Tree level propagators

In order to calculate the self-energies further we now introduce the tree level equilibrium approximations for the lepton and Higgs propagators S_ℓ and Δ. We assume that the diagonal elements of the SU(2)-symmetric lepton and Higgs correlators are given, in the Wigner representation, by

$$S^{\mathcal{A}}_{\ell,\mathrm{eq}}(k) = \pi\,\mathrm{sgn}(k^0) P_{\mathrm{L}} \not{k}\, \delta(k^2), \qquad \Delta^{\mathcal{A}}_{\mathrm{eq}}(k) = \pi\,\mathrm{sgn}(k^0)\,\delta(k^2), \tag{4.11a}$$

$$S^{\mathrm{H}}_{\ell,\mathrm{eq}}(k) = P_{\mathrm{L}} \not{k}\ \mathrm{PV}(\tfrac{1}{k^2}), \qquad \Delta^{\mathrm{H}}_{\mathrm{eq}}(k) = \mathrm{PV}(\tfrac{1}{k^2}), \tag{4.11b}$$

$$\mathrm{i}S^{\lessgtr}_{\ell}(k,t) = 2S^{\mathcal{A}}_{\ell,\mathrm{eq}}(k) f_{\mathrm{FD}}(\pm(k^0-\mu_\ell)), \qquad \mathrm{i}\Delta^{\lessgtr}_{\mathrm{eq}}(k) = \pm 2\Delta^{\mathcal{A}}_{\mathrm{eq}}(k) f_{\mathrm{BE}}(\pm k^0), \tag{4.11c}$$

where PV denotes the Cauchy principal value and μ_ℓ is the lepton chemical potential. The $\pm$ sign in equations (4.11c) corresponds to the $\lessgtr$ sign ($+$ for $<$ and $-$ for $>$). The Fermi-Dirac and Bose-Einstein phase space distribution functions are

$$f_{\mathrm{FD}}(k^0) = \frac{1}{\mathrm{e}^{\beta k^0}+1}, \qquad f_{\mathrm{BE}}(k^0) = \frac{1}{\mathrm{e}^{\beta k^0}-1}, \tag{4.12}$$

where $\beta = 1/T$ and we assume a common temperature T for both ℓ and ϕ. Note that the time-dependence of the lepton Wightman functions $S^{<,>}_\ell(k,t)$ in (4.11c) comes solely from the chemical potential $\mu_\ell = \mu_\ell(t)$.

Similarly to the Majorana neutrino correlation function, it is convenient to split the lepton Wightman functions into the equilibrium and non-equilibrium parts,

$$S^{<,>}_\ell(k,t) \equiv S^{<,>}_{\ell,\mathrm{eq}}(k) + \delta S^{<,>}_\ell(k,t), \tag{4.13}$$

where $S^{<,>}_{\ell,\mathrm{eq}}(k)$ is given by equation (4.11c) with $\mu_\ell = 0$ and the non-equilibrium parts satisfy $\delta S^{>}_\ell = -\delta S^{<}_\ell$. It then suffices to consider e.g. $\delta S^{<}_\ell$ only, for which we define the non-equilibrium lepton distribution

$$\delta f^{<}_\ell(k^0) \equiv f_{\mathrm{FD}}(k^0-\mu_\ell) - f_{\mathrm{FD}}(k^0) \simeq -f'_{\mathrm{FD}}(k^0)\mu_\ell. \tag{4.14}$$

Here we also assumed that the lepton chemical potential μ_ℓ remains small during leptogenesis. We can now split the Majorana neutrino self-energies (4.9) and (4.10) using equation (4.13):

$$\Sigma(k,t) = \Sigma_{\mathrm{eq}}(k) + \delta\Sigma(k,t), \tag{4.15}$$

where Σ_{eq} is the thermal equilibrium part with vanishing μ_ℓ, and $\delta\Sigma$ is proportional to δS_ℓ and hence linear in μ_ℓ in the approximation (4.14).

Using equations (4.9)–(4.12), (4.14) and (4.15), together with $\Sigma^{\mathcal{A}} \equiv \frac{\mathrm{i}}{2}(\Sigma^{>} + \Sigma^{<})$, we can calculate all the needed Majorana neutrino self-energies. We parametrise them as

$$\Sigma^{\mathcal{A}}_{\mathrm{eq},ij}(k) = c_{\mathrm{w}}(y_i y_j^* P_{\mathrm{L}} + y_i^* y_j P_{\mathrm{R}}) \not{\mathcal{S}}^{\mathcal{A}}_{\mathrm{eq},\mu}(k), \tag{4.16a}$$

$$\Sigma^{\mathrm{H}(T)}_{\mathrm{eq},ij}(k) = c_{\mathrm{w}}(y_i y_j^* P_{\mathrm{L}} + y_i^* y_j P_{\mathrm{R}}) \not{\mathcal{S}}^{\mathrm{H}(T)}_{\mathrm{eq},\mu}(k), \tag{4.16b}$$

$$\mathrm{i}\delta\Sigma^{<,>}_{ij}(k,t) = c_{\mathrm{w}}(y_i y_j^* P_{\mathrm{L}} - y_i^* y_j P_{\mathrm{R}}) \delta\not{\mathcal{S}}^{<,>}_{\mu}(k)\,\beta\mu_\ell, \tag{4.16c}$$

where the various $\mathfrak{S}_\mu$ functions are calculated explicitly in appendix B. Due to homogeneity and isotropy there are only two independent functions $\mathfrak{S}_0(k) \equiv a(k^0, |\boldsymbol{k}|)$ and $\mathfrak{S}_i(k) \equiv b(k^0, |\boldsymbol{k}|)\hat{k}^i$ (for all $i = 1, 2, 3$) for each Σ. Note that we give only the temperature dependent part $\Sigma^{\mathrm{H}(T)}_{\mathrm{eq}}$ of the dispersive self-energy $\Sigma^{\mathrm{H}}_{\mathrm{eq}}(k)$ in equation (4.16b). The vacuum part $\Sigma^{\mathrm{H(vac)}}_{\mathrm{eq}}$ and its on-shell renormalisation are presented in section 4.8. The renormalisation of the Majorana neutrinos is not trivial because they mix and are unstable. Nevertheless, the relevant outcome for this paper is simple: the renormalised (vacuum part) $\widehat{\Sigma}^{\mathrm{H(vac)}}_{\mathrm{eq}}$ does not contribute to our results in the leading order approximation considered in this work.

4.4 Adiabatic neutrino solutions

Now that we have specified the self-energy, we can calculate the adiabatic solutions (3.7) for the neutrino which are needed in the kinetic equation (3.17). Working to the lowest order approximation we only take the equilibrium part of the neutrino self-energy (4.15) into account:

$$S^p_{\mathrm{ad}}(k, t) = \left[\not{k} - m(t) - \Sigma^p_{\mathrm{eq}}(k)\right]^{-1}, \tag{4.17a}$$

$$S^s_{\mathrm{ad}}(k, t) = S^r_{\mathrm{ad}}(k, t)\Sigma^s_{\mathrm{eq}}(k)S^a_{\mathrm{ad}}(k, t). \tag{4.17b}$$

We are implicitly assuming that all quantities have been renormalised, so the pole self-energy Σ^p_{eq} appearing here is actually the on-shell renormalised pole self-energy $\widehat{\Sigma}^p_{\mathrm{eq}}$ given by equations (4.44) and (4.51). Furthermore, using the KMS relation $\Sigma^>_{\mathrm{eq}}(k) = \mathrm{e}^{\beta k^0}\Sigma^<_{\mathrm{eq}}(k)$ and the exact identity $\mathcal{A} = S^r\Sigma^{\mathcal{A}}S^a$, which holds in direct space as a convolution and as a simple product to zeroth order in gradients in the Wigner representation, we can write the Wightman functions (4.17b) as

$$\mathrm{i}S^<_{\mathrm{ad}}(k, t) = 2\mathcal{A}_{\mathrm{ad}}(k, t)f_{\mathrm{FD}}(k^0), \tag{4.18a}$$

$$\mathrm{i}S^>_{\mathrm{ad}}(k, t) = 2\mathcal{A}_{\mathrm{ad}}(k, t)(1 - f_{\mathrm{FD}}(k^0)). \tag{4.18b}$$

In perturbative expansions it is more convenient to use the form (4.18) than equation (4.17b). For example, a naive coupling constant expansion of the pole propagators in equation (4.17b) would appear to give a $\mathcal{O}(y_i^2)$ result, whereas the right-hand side of equation (4.18) obviously gives the correct $\mathcal{O}(1)$ result. In other words, a consistent expansion of the Wightman function (4.17b) requires resumming the pole propagators, which the identity $\mathcal{A} = S^r\Sigma^{\mathcal{A}}S^a$ implements automatically in equations (4.18).

Given the adiabatic solution, we can now compute the source term $-\partial_t\overline{S}^<_{\mathrm{ad},\boldsymbol{k}}(t, t)$ in equation (3.17). To this end, we employ the inverse Wigner transform

$$F_{\boldsymbol{k}}(t_1, t_2) = \int \frac{\mathrm{d}k^0}{2\pi}\, \mathrm{e}^{-\mathrm{i}k^0(t_1 - t_2)} F\Big(k, \frac{t_1 + t_2}{2}\Big) \tag{4.19}$$

to calculate the two-time representation function $S^<_{\mathrm{ad},\boldsymbol{k}}(t_1, t_2)$ from the Wigner representation (4.18a). Utilising Cauchy's integral theorem to perform the k^0-integral, we can write

the two-time representation as

$$\overline{S}^{<}_{\mathrm{ad},\boldsymbol{k}}(t_1,t_2) = \int \frac{\mathrm{d}k^0}{2\pi}\, \mathrm{e}^{-\mathrm{i}k^0(t_1-t_2)}\mathrm{i}(\overline{S}^{r}_{\mathrm{ad}} - \overline{S}^{a}_{\mathrm{ad}})(k,t) f_{\mathrm{FD}}(k^0)$$
$$\simeq \sum_{p=r,a} \theta(-s_p r^0) \sum_{k^0}^{\text{poles}} \mathrm{e}^{-\mathrm{i}k^0 r^0} f_{\mathrm{FD}}(k^0)\, \mathrm{Res}_{k^0}\big[\overline{S}^{p}_{\mathrm{ad}}(k,t)\big], \tag{4.20}$$

where the k^0-sum is taken over the poles of $S^p_{\mathrm{ad}}(k,t)$, and $s_p = -1, 1$ for $p = r, a$, respectively. We also used the short-hands $r^0 \equiv t_1 - t_2$ and $t \equiv (t_1+t_2)/2$. The corresponding result for $\overline{S}^{>}_{\mathrm{ad},\boldsymbol{k}}$ follows by replacing $f_{\mathrm{FD}}(k^0)$ above with $f_{\mathrm{FD}}(-k^0) = 1 - f_{\mathrm{FD}}(k^0)$. Note that we neglected any branch cuts in equation (4.20) and kept only the residue contributions of the single particle poles, but otherwise the result is general. Also, the poles of $f_{\mathrm{FD}}(k^0)$ at the imaginary axis do not contribute due to the KMS relation.

Leading order approximation. Equation (4.20) is written with a general adiabatic pole function, but it will be eventually sufficient to compute it to lowest order in gradients and in the coupling constants. In this case we can use the free tree-level solution with vacuum dispersion relations for the adiabatic pole propagators $S^p_{\mathrm{ad}}(k,t)$ in equation (4.17a), given by

$$S^{p(0)}_{\mathrm{ad},ij}(k,t) = \frac{\not{k} + m_i(t)}{k^2 - m_i^2(t) - \mathrm{i}s_p\,\mathrm{sgn}(k^0)\varepsilon}\delta_{ij}. \tag{4.21}$$

The small imaginary part with $\varepsilon > 0$ ensures the correct boundary conditions for $p = r, a$. Inserting this solution into equation (4.20), calculating the residues and taking the limit $\varepsilon \to 0^+$ yields the leading order result

$$\overline{S}^{<(0)}_{\mathrm{ad},\boldsymbol{k}ij}(t_1,t_2) = \sum_{s=\pm} \frac{\mathrm{e}^{-\mathrm{i}s(t_1-t_2)\omega_{\boldsymbol{k}i}}}{2s\omega_{\boldsymbol{k}i}} f_{\mathrm{FD}}(s\omega_{\boldsymbol{k}i})(\not{k}_{si} + m_i)\gamma^0\delta_{ij}. \tag{4.22}$$

Here $\not{k}_{si} \equiv s\omega_{\boldsymbol{k}i}\gamma^0 - \boldsymbol{\gamma}\cdot\boldsymbol{k}$ and $\omega_i \equiv \sqrt{|\boldsymbol{k}|^2 + {m_i}^2}$, and the time-dependent masses $m_i(t)$ are evaluated at the average time $t = (t_1+t_2)/2$.[10] Note that the lowest order adiabatic pole and Wightman functions are diagonal in the mass basis in agreement with [63]. We emphasize that in our approach the off-diagonal corrections to the adiabatic propagators are not required to leading order, as we do not need to calculate the homogeneous solution non-dynamically from equation (2.16), as was done in e.g. [62]. Instead, corrections from the full adiabatic pole propagators are already taken into account in the source term of our dynamical equation (3.17) (see also equation (3.4)). More discussion about these corrections is given at the end of section 4.5.

Setting $t_1 = t_2 \equiv t$ in equation (4.22) we then get the equal-time adiabatic function $\overline{S}^{<}_{\mathrm{ad},\boldsymbol{k}}(t,t)$ needed in the kinetic equation (3.17). The result may also be cast into a compact form

$$\overline{S}^{<(0)}_{\mathrm{ad},\boldsymbol{k}ij}(t,t) = \sum_{s=\pm} f_{\mathrm{FD}}(s\omega_{\boldsymbol{k}i}) P^s_{\boldsymbol{k}i}\delta_{ij}, \tag{4.23}$$

[10] The *leading order* result (4.22) can be obtained also by substituting the tree-level spectral function (3.10) directly into the first line of equation (4.20) and performing the integration with the delta function, without resorting to the residue formula. Including a finite width requires using the more general formula however.

where the energy projection matrix $P^s_{\boldsymbol{k}i}$ was defined in equation (3.12). To calculate the time-derivative in order to get the source term $-\partial_t \overline{S}^<_{\mathrm{ad},\boldsymbol{k}ij}(t,t)$ for equation (3.17) is now a simple matter, once the time-dependent masses $m_i(t)$ are specified. Equation (4.23) is also needed to calculate the initial values for the (local) non-equilibrium Wightman function $\delta S^< \equiv S^< - S^<_{\mathrm{ad}}$ once the initial value for the full function $S^<$ has been specified.

4.5 Effective neutrino self-energy

We now calculate the effective self-energy (3.16), which appears in the local kinetic equation (3.17) for Majorana neutrinos. We use the general result for a convolution in terms of the Wigner representation correlation functions:

$$\begin{aligned}(F_{\boldsymbol{k}} * G_{\boldsymbol{k}})(t_1,t_2) &= \int \frac{\mathrm{d}k^0}{2\pi}\, \mathrm{e}^{-\mathrm{i}k^0(t_1-t_2)}\, \mathrm{e}^{-\frac{\mathrm{i}}{2}(\partial_t^F \partial_{k^0}^G - \partial_{k^0}^F \partial_t^G)} F(k,t)G(k,t)\Big|_{t=(t_1+t_2)/2} \\ &= \int \frac{\mathrm{d}k^0}{2\pi}\, \mathrm{e}^{-\mathrm{i}k^0(t_1-t_2)} F_{\mathrm{out}}(k,t)G_{\mathrm{in}}(k,t)\Big|_{t=(t_1+t_2)/2}, \end{aligned} \tag{4.24}$$

where $F_{\mathrm{out}}(k,t)$ and $G_{\mathrm{in}}(k,t)$ were defined below equation (3.9). The first line of equation (4.24) is the inverse Wigner transform of the Moyal product (often denoted by $\lozenge$). When the gradients are small we may further approximate $F_{\mathrm{out}}(k,t) \simeq F(k,t)$ and $G_{\mathrm{in}}(k,t) \simeq G(k,t)$. We will again assume an adiabatic, equilibrium self-energy function and expand to zeroth order in gradients. The general result is then similar to equation (4.20):

$$\overline{\Sigma}^r_{\mathrm{eq,eff},\boldsymbol{k}}(t_1,t_2) = \int \frac{\mathrm{d}k^0}{2\pi}\, \mathrm{e}^{-\mathrm{i}k^0(t_1-t_2)} \overline{\Sigma}^r_{\mathrm{eq}}(k)\mathrm{i}(\overline{S}^r_{\mathrm{ad}} - \overline{S}^a_{\mathrm{ad}})(k,t) \tag{4.25}$$

$$\simeq \sum_{p=r,a} \theta(-s_p r^0) \sum_{k^0}^{\text{poles}} \mathrm{e}^{-\mathrm{i}k^0 r^0} \overline{\Sigma}^r_{\mathrm{eq}}(k)\, \mathrm{Res}_{k^0}\big[\overline{S}^p_{\mathrm{ad}}(k,t)\big]. \tag{4.26}$$

On the last line we again kept only the residue contribution from the poles of the propagator and neglected contributions from possible branch cuts. To calculate the leading tree level approximation we will again use the free pole propagators like in equations (4.22) and (4.23). The calculation proceeds as before and one finds the lowest order coupling constant result

$$\overline{\Sigma}^{r(0)}_{\mathrm{eq,eff},\boldsymbol{k}ij}(t,t) = \sum_{s=\pm} \overline{\Sigma}^r_{\mathrm{eq},ij}(k_{sj}) P^s_{\boldsymbol{k}j}. \tag{4.27}$$

Corrections resulting from resummed pole propagators could be included by using the residue formula (4.26) with complex poles, but as will be argued below, their effect would be formally of higher order ($\sim \mathcal{O}(y_i^4)$) in the coupling constants.

Beyond the leading approximation. To improve on the leading approximation in coupling constants used above, one should solve the complex k^0-poles from the determinant of $S^p_{\mathrm{ad}}(k,t)$, keeping the self-energy corrections and use them to calculate the residues in equations (4.20) and (4.26). This is in principle straightforward, but laborious because the block-wise inversion of equation (4.17a) results in complicated formulae due to the

flavour mixing. We will not implement these corrections in this paper, because we use the weak coupling approximation where these corrections should be small. We give details of the inversion procedure in appendix C for completeness however, and note that a similar analysis was presented in [62], with a non-relativistic approximation for the self-energy. It should also be noted that these higher order corrections to (4.23) and (4.27) remain parametrically small also in the maximally resonant regime where $\Delta m_{21}/m \sim |y|^2$. We have verified this explicitly in a generic power counting expansion of the formula (4.20) where $\Delta m_{21}/m$ and $|y|^2$ are expanded simultaneously, under the assumption that the difference of the full k^0-poles to the corresponding free theory poles is $\mathcal{O}(y^2)$. To get the correct *perturbative* result it is also crucial to start from the resummed form of equation (4.18a).

The self-energy corrections to the pole propagators can be divided into dispersive corrections due to the Hermitian self-energy and dissipative ones due to the antihermitian self-energy part. The main effect of the latter was already discussed qualitatively in section 2.2. While the actual formulae are very complex, it is easy to see that the main qualitative effect of evaluating (4.20) at a complex pole is to introduce complex damping terms $\sim \mathrm{e}^{-\gamma_{ii}|t_1-t_2|}$ into equation (4.22). Such factors represent the dissipation in the relative time coordinate, but eventually do not affect the source term in the local equation (3.17). Indeed, the only effect on the source, and likewise on the self-energy convolutions (4.26) appearing in (3.17), from a finite width then amounts to shifts $\sim y_i^2$ to the energy shells where these terms are evaluated. In the weak coupling limit such corrections should be small, which we have verified numerically.

The dispersive corrections could be more interesting. Including Hermitian self-energy corrections would lead to new real-frequency poles for the adiabatic functions. Combining the vacuum Hamiltonian in equation (3.17) with the effective Hermitian self-energy evaluated at these poles, would give rise to an effective matter Hamiltonian for the quasistates. The effective Hamiltonian would in general be no longer diagonal in the mass basis and the energy difference between the matter eigenstates would be a function of time, similar to the case of mixing light neutrinos in the early universe [3, 4, 7]. Such a dynamical modification of the energy level splitting could be relevant for resonant leptogenesis, although the analysis of ref. [65] (performed in a simplified setup) does not suggest that the effect is quantitatively significant.

4.6 Lepton transport equation

The equation for the lepton asymmetry can be derived from the KB equations (2.5) for the lepton propagator. However, as the lepton is massless and we use the tree-level spectral approximation for its propagator, the lowest order adiabatic source term in equation (3.4) vanishes. To derive the leading source for the lepton asymmetry, it is convenient to use a different but equivalent formulation of the KB equations (see e.g. equations 17 and 18 in [73]). The appropriate form of the equation where the finite width and dispersive contributions have been neglected is

$$(S^{-1}_{\ell,0,\boldsymbol{k}} * S^{\lessgtr}_{\ell,\boldsymbol{k}})(t_1,t_2) = \pm\frac{1}{2}(\Sigma^{>}_{\ell,\boldsymbol{k}} * S^{<}_{\ell,\boldsymbol{k}} - \Sigma^{<}_{\ell,\boldsymbol{k}} * S^{>}_{\ell,\boldsymbol{k}})(t_1,t_2). \tag{4.28}$$

The corresponding local equation for the local correlation function of the lepton can be derived in the same way that we derived equation (3.2). The result is

$$\begin{aligned}\mathrm{i}\partial_t \overline{S}^<_{\ell,\boldsymbol{k}}(t,t) = [\boldsymbol{\alpha}\cdot\boldsymbol{k}, \overline{S}^<_{\ell,\boldsymbol{k}}(t,t)] &- \frac{\mathrm{i}}{2}(\overline{\Sigma}^>_{\ell,\boldsymbol{k}} * \overline{S}^<_{\ell,\boldsymbol{k}} - \overline{\Sigma}^<_{\ell,\boldsymbol{k}} * \overline{S}^>_{\ell,\boldsymbol{k}})(t,t) \\ &- \frac{\mathrm{i}}{2}(\overline{S}^<_{\ell,\boldsymbol{k}} * \overline{\Sigma}^>_{\ell,\boldsymbol{k}} - \overline{S}^>_{\ell,\boldsymbol{k}} * \overline{\Sigma}^<_{\ell,\boldsymbol{k}})(t,t),\end{aligned} \tag{4.29}$$

where $\boldsymbol{\alpha}\cdot\boldsymbol{k}$ is the free Hamiltonian for the massless lepton. We also remind here that equations (4.28) and (4.29) are formulated for the diagonal element S_ℓ of the SU(2)-symmetric lepton correlator (4.2b). This equation could be solved as such, coupled with the local equation for the mixing Majorana states. However, in practice we can make several further approximations, eventually converging to a simple scalar equation for the lepton asymmetry.

Lepton asymmetry. The lepton asymmetry we are interested in this work can be related to the chiral current density of the left-handed leptons, which is defined by

$$j^\mu_\ell(x) \equiv \langle \bar{\ell}_A(x)\gamma^\mu P_\mathrm{L}\ell_A(x)\rangle, \tag{4.30}$$

where an implicit summation over the SU(2)-index is assumed. Since we consider a spatially homogeneous and isotropic system, the current depends only on the time $x^0 = t$ and it can be further related to the local two-time Wightman function. Using definitions (2.2), (2.4) and (4.30), we then get

$$j^\mu_\ell(t) = c_\mathrm{w}\int \frac{\mathrm{d}^3\boldsymbol{k}}{(2\pi)^3}\,\mathrm{tr}\Big[\gamma^\mu P_\mathrm{L}\mathrm{i}S^<_{\ell,\boldsymbol{k}}(t,t)\Big]. \tag{4.31}$$

Because no asymmetry can exist in thermal equilibrium [88], we can define the lepton asymmetry density $n_\ell - \overline{n}_\ell$ as the zeroth component of the non-equilibrium part of the current:

$$n_\ell - \overline{n}_\ell \equiv \delta j^0_\ell(t) = c_\mathrm{w}\int \frac{\mathrm{d}^3\boldsymbol{k}}{(2\pi)^3}\,\mathrm{tr}\Big[P_\mathrm{L}\delta\overline{S}^<_{\ell,\boldsymbol{k}}(t,t)\Big]. \tag{4.32}$$

We can further relate the asymmetry to the chemical potential of the tree-level lepton propagator. Using equations (4.11c), (4.12), (4.13) and (4.19) we calculate the trace on the right-hand side of equation (4.32). The result, written in terms of lepton and anti-lepton phase space distributions, is

$$n_\ell - \overline{n}_\ell = c_\mathrm{w}\int \frac{\mathrm{d}^3\boldsymbol{k}}{(2\pi)^3}\Big(f_\mathrm{FD}(|\boldsymbol{k}| - \mu_\ell) - f_\mathrm{FD}(|\boldsymbol{k}| + \mu_\ell)\Big), \tag{4.33}$$

where $c_\mathrm{w} = 2$ is the weak isospin multiplicity factor. There is no additional spin multiplicity factor because of the chiral projection, i.e. only one spin state couples to the Majorana neutrino and develops an asymmetry in the massless limit. A standard calculation of the integral gives the relation between the asymmetry and the chemical potential:

$$n_\ell - \overline{n}_\ell = \frac{c_\mathrm{w}T^3}{6\pi^2}\left[\pi^2\Big(\frac{\mu_\ell}{T}\Big) + \Big(\frac{\mu_\ell}{T}\Big)^3\right] \simeq \frac{c_\mathrm{w}T^3}{6}\Big(\frac{\mu_\ell}{T}\Big), \tag{4.34}$$

where in the last step we used the linear approximation for μ_ℓ like in equation (4.14).

Lepton asymmetry equation. We can get the equation of motion for the lepton asymmetry (4.32) by using the split (4.13) in equation (4.29), taking the trace over spinor indices and integrating over momentum. The trace of the commutator term vanishes due to the Dirac structure of the tree level propagator, so that we are left with

$$\partial_t(n_\ell - \bar{n}_\ell) = -\frac{c_\mathrm{w}}{2}\int \frac{\mathrm{d}^3\boldsymbol{k}}{(2\pi)^3}\,\mathrm{tr}\Big[(\overline{\Sigma}^{>}_{\ell,\boldsymbol{k}} * \overline{S}^{<}_{\ell,\boldsymbol{k}})(t,t) - (\overline{\Sigma}^{<}_{\ell,\boldsymbol{k}} * \overline{S}^{>}_{\ell,\boldsymbol{k}})(t,t)\Big] + \mathrm{H.c.} \tag{4.35}$$

Substituting the two-time representation of the lepton self-energy (4.8) to the right-hand side then yields

$$\begin{aligned}\partial_t(n_\ell - \bar{n}_\ell) = &-\frac{c_\mathrm{w}}{2}\sum_{i,j} y_i^* y_j \int \frac{\mathrm{d}^3\boldsymbol{k}}{(2\pi)^3}\frac{\mathrm{d}^3\boldsymbol{p}}{(2\pi)^3}\int \mathrm{d}t' \\ &\times \mathrm{tr}\Big[P_\mathrm{R}\mathrm{i}S^{>}_{\boldsymbol{p}ij}(t,t')P_\mathrm{L}\mathrm{i}\Delta^{<}_{\mathrm{eq},\boldsymbol{p}-\boldsymbol{k}}(t',t)\mathrm{i}S^{<}_{\ell,\boldsymbol{k}}(t',t) - (> \leftrightarrow <)\Big] + \mathrm{H.c.}\end{aligned} \tag{4.36}$$

This equation can actually be expressed using the already calculated Majorana neutrino self-energy (4.9). Indeed, because of the trace and the equal time arguments it is just a matter of combining the terms differently in the right-hand side of equation (4.36) to rewrite the integral in terms of the Majorana neutrino correlation function and the chirally projected Majorana self-energy Σ_L, which results in:

$$\partial_t(n_\ell - \bar{n}_\ell) = \frac{1}{2}\int \frac{\mathrm{d}^3\boldsymbol{k}}{(2\pi)^3}\,\mathrm{Tr}\Big[(\overline{\Sigma}^{>}_{\mathrm{L},\boldsymbol{k}} * \overline{S}^{<}_{\boldsymbol{k}})(t,t) - (\overline{\Sigma}^{<}_{\mathrm{L},\boldsymbol{k}} * \overline{S}^{>}_{\boldsymbol{k}})(t,t)\Big] + \mathrm{H.c.} \tag{4.37}$$

One should note that the trace is now taken over both the Majorana neutrino flavours and the Dirac indices and we defined the barred chiral Majorana neutrino self-energy as $\overline{\Sigma}^{<,>}_\mathrm{L} \equiv \gamma^0 P_\mathrm{L}\mathrm{i}\Sigma^{<,>}$. Also note that the lepton doublet multiplicity c_w is now included in the neutrino self-energy.

Results similar to (4.37) are already known in the literature [62], but the novelty of our approach is in the use of the local approximation of section 3 to evaluate the convolution integrals. This is now straightforward because equation (4.37) is written explicitly in terms of the Majorana neutrino propagator. We first use equations (3.3) and (4.15) to split the neutrino Wightman functions and self-energies into the equilibrium and non-equilibrium parts. Then we invoke the local approximation (3.8) to compute convolution integrals with the perturbations $\delta S^{<,>}$, along with the constraint $\delta S^{>}_{\boldsymbol{k}}(t,t) = -\delta S^{<}_{\boldsymbol{k}}(t,t)$, which is imposed by the sum rule. Finally, we write the convolution integrals involving $S^{<,>}_\mathrm{ad}$ in the Wigner representation using equation (4.24) and expand consistently to the leading order in coupling constants and gradients to obtain:

$$\begin{aligned}\partial_t(n_\ell - \bar{n}_\ell) \simeq \int \frac{\mathrm{d}^3\boldsymbol{k}}{(2\pi)^3}\,\mathrm{Tr}\Big[&\overline{\Sigma}^{\mathcal{A}}_{\mathrm{L,eq,eff},\boldsymbol{k}}(t,t)\delta\overline{S}^{<}_{\boldsymbol{k}}(t,t) + \delta\overline{\Sigma}^{\mathcal{A}}_{\mathrm{L,eff},\boldsymbol{k}}(t,t)\delta\overline{S}^{<}_{\boldsymbol{k}}(t,t) \\ &+ \frac{1}{2}\int\frac{\mathrm{d}k^0}{2\pi}\Big(\delta\overline{\Sigma}^{>}_\mathrm{L}(k,t)\overline{S}^{<}_\mathrm{ad}(k,t) - \delta\overline{\Sigma}^{<}_\mathrm{L}(k,t)\overline{S}^{>}_\mathrm{ad}(k,t)\Big)\Big] + \mathrm{H.c.}\end{aligned} \tag{4.38}$$

The first term on the right-hand side of equation (4.38), proportional to $\Sigma^{\mathcal{A}}_\mathrm{eq}$, does not contain the lepton chemical potential μ_ℓ. It is therefore the source term for the lepton asymmetry. The remaining terms, proportional to $\delta\Sigma^\alpha$, are linear in $\mu_\ell \propto n_\ell - \bar{n}_\ell$ (in the approximation (4.14)) and so they contribute to the washout.

4.7 General leptogenesis equations

To summarise, we use the local equation (3.17) with equilibrium self-energies to solve the evolution of the Majorana neutrinos and equation (4.38) to subsequently calculate the lepton asymmetry. Our coupled equations for leptogenesis therefore read

$$\partial_t \delta\overline{S}^<_{\boldsymbol{k}}(t,t) + \mathrm{i}\big[H_{\boldsymbol{k}}(t), \delta\overline{S}^<_{\boldsymbol{k}}(t,t)\big] = -\partial_t \overline{S}^<_{\mathrm{ad},\boldsymbol{k}}(t,t) - \big(\mathrm{i}\overline{\Sigma}^r_{\mathrm{eq,eff},\boldsymbol{k}}(t,t)\delta\overline{S}^<_{\boldsymbol{k}}(t,t) + \mathrm{H.c.}\big), \quad (4.39)$$

$$\partial_t(n_\ell - \overline{n}_\ell) = S_{\mathrm{CP}} + \delta W + W_{\mathrm{ad}}, \quad (4.40)$$

where the CP-violating source term S_{CP} and the washout terms δW and W_{ad} of the lepton equation are given by

$$S_{\mathrm{CP}} = \int \frac{\mathrm{d}^3\boldsymbol{k}}{(2\pi)^3} \mathrm{Tr}\Big[\overline{\Sigma}^{\mathcal{A}}_{\mathrm{L,eq,eff},\boldsymbol{k}}(t,t)\delta\overline{S}^<_{\boldsymbol{k}}(t,t) + \mathrm{H.c.}\Big], \quad (4.41)$$

$$\delta W = \int \frac{\mathrm{d}^3\boldsymbol{k}}{(2\pi)^3} \mathrm{Tr}\Big[\delta\overline{\Sigma}^{\mathcal{A}}_{\mathrm{L,eff},\boldsymbol{k}}(t,t)\delta\overline{S}^<_{\boldsymbol{k}}(t,t) + \mathrm{H.c.}\Big], \quad (4.42)$$

$$W_{\mathrm{ad}} = \int \frac{\mathrm{d}^4k}{(2\pi)^4}\frac{1}{2} \mathrm{Tr}\Big[\delta\overline{\Sigma}^>_{\mathrm{L}}(k,t)\overline{S}^<_{\mathrm{ad}}(k,t) - \delta\overline{\Sigma}^<_{\mathrm{L}}(k,t)\overline{S}^>_{\mathrm{ad}}(k,t) + \mathrm{H.c.}\Big]. \quad (4.43)$$

The washout terms are proportional to the lepton asymmetry $n_\ell - \overline{n}_\ell$ via equation (4.34). The adiabatic source term $-\partial_t\overline{S}^<_{\mathrm{ad},\boldsymbol{k}}(t,t)$ of the neutrino equation (4.39) is calculated from equation (4.23), and the effective self-energy $\overline{\Sigma}^r_{\mathrm{eq,eff},\boldsymbol{k}}(t,t)$ is given by equation (4.27). We expect W_{ad} to be the dominant washout term because it is proportional to the adiabatic functions, as opposed to δW which depends on the non-equilibrium perturbation $\delta S^<$ only.

Equations (4.39)–(4.43) are fully general apart from our using the local ansatz (3.8) to compute the collision terms and the simplifications made in the reduction of the SM sector. The effective self-energies in the lepton source and washout terms (4.41)–(4.43) are all calculated expanding consistently to the leading order in gradients and in the coupling constant expansion (more precisely: they are first order in $|y_i|^2$, $\partial_t m$ and $\partial_t\mu_\ell$ combined). This is the most compact form of the equations relevant for the leptogenesis problem. They correspond to an initial value problem for a set of coupled first order equations which is straightforward to solve numerically by discretising the momentum variable. We shall recast these equations into a set of coupled Boltzmann-like equations for the generalised phase space functions in section 5, after a short discussion of the issue of renormalisation.

4.8 Vacuum on-shell renormalisation

So far we have implicitly assumed that we are working with finite, renormalised quantities. The renormalisation procedure is slightly intricate due to the flavour mixing. For completeness, we perform the one-loop vacuum renormalisation in our model, following the on-shell method of ref. [89]. This is sufficient for our purposes since we do not consider gauge interactions [90, 91]. In this section we denote renormalised quantities by a hat. The renormalised pole self-energies $\widehat{\Sigma}^p_{\mathrm{eq},ij}(k,t)$ can be written in terms of the unrenormalised functions and the counterterms as follows:

$$\begin{aligned}\widehat{\Sigma}^p_{\mathrm{eq},ij}(k,t) = \Sigma^p_{\mathrm{eq},ij}(k) &- (\not{k} - m_i)(P_{\mathrm{L}}\tfrac{1}{2}\delta Z^{\mathrm{L}}_{ij} + P_{\mathrm{R}}\tfrac{1}{2}\delta Z^{\mathrm{R}}_{ij}) \\ &- (P_{\mathrm{L}}\tfrac{1}{2}\delta Z^{\mathrm{R}\,*}_{ji} + P_{\mathrm{R}}\tfrac{1}{2}\delta Z^{\mathrm{L}\,*}_{ji})(\not{k} - m_j) + \delta m_i\delta_{ij}. \end{aligned} \quad (4.44)$$

The complex conjugation is here understood element-wise and not in the matrix sense. The mass counterterms δm_i are diagonal in the vacuum mass basis, but the wave function renormalisation factors $\delta Z_{ij}^{\mathrm{L,R}}$ are in general flavour matrices [89]. Because our neutrinos are Majorana fields, the counterterms for different chiralities are related by

$$\delta Z_{ij}^{L} = \delta Z_{ij}^{\mathrm{R}*}. \tag{4.45}$$

Because of the Hermiticity of the counterterm Lagrangian, only the dispersive part of the self-energy $\Sigma_{\mathrm{eq}}^{p} = \Sigma_{\mathrm{eq}}^{\mathrm{H}} + \mathrm{i}s_p\Sigma_{\mathrm{eq}}^{\mathcal{A}}$ contributes to renormalisation. The absorptive parts are finite as such and can be understood as being computed in terms of renormalised parameters throughout. Also thermal corrections are purely finite and may be split from the vacuum parts according to equations (B.1a) and (B.2) given in appendix B. Renormalisation is then associated only with the vacuum part of the Hermitian self-energy function $\Sigma_{\mathrm{eq}}^{\mathrm{H(vac)}}$.

The on-shell renormalisation conditions which guarantee that there is no mixing in the external legs, that m_i are the renormalised masses and that the residue of the diagonal propagator is unity, are given by [89, 92, 93]

$$\widehat{\Sigma}_{\mathrm{eq},ij}^{\mathrm{H(vac)}}(k)u_j^s(k) \to 0, \quad \text{when } k^2 \to m_j^2, \tag{4.46a}$$

$$\bar{u}_i^s(k)\widehat{\Sigma}_{\mathrm{eq},ij}^{\mathrm{H(vac)}}(k) \to 0, \quad \text{when } k^2 \to m_i^2, \tag{4.46b}$$

$$\frac{1}{\not{k} - m_i}\widehat{\Sigma}_{\mathrm{eq},ii}^{\mathrm{H(vac)}}(k)u_i^s(k) \to 0, \quad \text{when } k^2 \to m_i^2, \tag{4.46c}$$

$$\bar{u}_i^s(k)\widehat{\Sigma}_{\mathrm{eq},ii}^{\mathrm{H(vac)}}(k)\frac{1}{\not{k} - m_i} \to 0, \quad \text{when } k^2 \to m_i^2, \tag{4.46d}$$

where u_i^s satisfies $(\not{k} - m_i)u_i^s(k) = 0$ when $k^2 = m_i^2$. Note that there is no summation over repeated indices here. The dimensionally regularised vacuum self-energy is given by $\Sigma_{\mathrm{eq},ij}^{\mathrm{H(vac)}}(k) = c_{\mathrm{w}}(y_i y_j^* P_{\mathrm{L}} + y_i^* y_j P_{\mathrm{R}})\mathfrak{S}_{\mathrm{eq}}^{\mathrm{H(vac)}}(k)$ with

$$\mathfrak{S}_{\mathrm{eq}}^{\mathrm{H(vac)}}(k) = -\frac{\not{k}}{32\pi^2}\left(\frac{1}{\bar{\varepsilon}} + 2 - \log\left|\frac{k^2}{\mu^2}\right|\right) + \mathcal{O}(\varepsilon), \tag{4.47}$$

where $1/\bar{\varepsilon} \equiv 1/\varepsilon - \gamma_{\mathrm{E}} + \log(4\pi)$, $D = 4 - 2\varepsilon$ is the spacetime dimension, γ_{E} is the Euler-Mascheroni constant and μ is the renormalisation scale parameter. Using these results we find the following counterterms for the Majorana neutrinos:

$$\delta Z_{ij}^{\mathrm{R}} \overset{i\neq j}{=} \frac{c_{\mathrm{w}}}{32\pi^2}\frac{2m_j}{m_i^2 - m_j^2}(m_j\, y_i y_j^* + m_i\, y_i^* y_j)\left[\frac{1}{\bar{\varepsilon}} + 2 - \log\left(\frac{m_j^2}{\mu^2}\right)\right], \tag{4.48a}$$

$$\delta Z_{ii}^{\mathrm{R}} = -\frac{c_{\mathrm{w}}}{32\pi^2}|y_i|^2\left[\frac{1}{\bar{\varepsilon}} - \log\left(\frac{m_i^2}{\mu^2}\right)\right], \tag{4.48b}$$

$$\delta m_i = \frac{c_{\mathrm{w}}}{32\pi^2}m_i|y_i|^2\left[\frac{1}{\bar{\varepsilon}} + 2 - \log\left(\frac{m_i^2}{\mu^2}\right)\right], \tag{4.48c}$$

where $i \neq j$ in the first equation. The corresponding renormalised vacuum self-energy is

$$\begin{aligned}\widehat{\Sigma}_{\mathrm{eq},ij}^{\mathrm{H(vac)}}(k,t) = c_{\mathrm{w}}\Big[&P_{\mathrm{L}}\not{k}(y_i y_j^* c_{ij}^{\mathrm{H}} - y_i^* y_j d_{ij}^{\mathrm{H}}) + P_{\mathrm{L}}(y_i y_j^* m_i - y_i^* y_j m_j)d_{ij}^{\mathrm{H}} \\ &+ P_{\mathrm{R}}\not{k}(y_i^* y_j c_{ij}^{\mathrm{H}} - y_i y_j^* d_{ij}^{\mathrm{H}}) + P_{\mathrm{R}}(y_i^* y_j m_i - y_i y_j^* m_j)d_{ij}^{\mathrm{H}}\Big],\end{aligned} \tag{4.49}$$

with

$$c^{\rm H}_{ij} = \frac{1}{32\pi^2}\log\left|\frac{k^2}{m_i^2}\right| - \frac{m_j}{m_i}d^{\rm H}_{ij}, \qquad d^{\rm H}_{ij} = \frac{1}{32\pi^2}\frac{m_i m_j}{m_i^2 - m_j^2}\log\left(\frac{m_i^2}{m_j^2}\right). \tag{4.50}$$

The full renormalised pole self-energy (4.44) can now be written as

$$\widehat{\Sigma}^{p}_{{\rm eq},ij}(k,t) = \widehat{\Sigma}^{{\rm H(vac)}}_{{\rm eq},ij}(k,t) + \Sigma^{{\rm H}(T)}_{{\rm eq},ij}(k) + {\rm i}s_p\Sigma^{\mathcal{A}}_{{\rm eq},ij}(k). \tag{4.51}$$

Note that the renormalisation procedure associated with the processes relevant for leptogenesis is not affected by the expansion of the universe. Indeed, as long as curvature effects are not relevant for the physical processes involved, renormalisation can be carried out in the local orthonormal coordinate system, which is locally a Minkowski space. We shall introduce the extension of our equations to the expanding Friedman-Robertson-Walker spacetime in section 6.

5 Non-equilibrium distribution functions

The local correlation function $\delta\overline{S}^{<}_{\boldsymbol{k}}(t,t)$ is a matrix in both Dirac and flavour indices and its components have a complicated time dependence involving many different scales. These scales reflect the complicated phase space structure of the underlying Wigner function $\delta\overline{S}^{<}_{\boldsymbol{k}}(k^0,t)$, and they ultimately arise from the different physical phenomena the correlation function describes. In particular, the vast difference between the particle-antiparticle oscillation time $\sim 1/\omega_{\boldsymbol{k}}$ and the flavour oscillation time $\sim 1/\Delta m$ makes equation (4.39) challenging for studying resonant leptogenesis as such. To overcome this problem we will parametrise $\delta\overline{S}^{<}_{\boldsymbol{k}}(t,t)$ in terms of phase space distribution functions $\delta f^{ss'}_{\boldsymbol{k}hij}$, and derive their coupled equations of motion. The benefit of this parametrisation, first introduced in [77], is that each phase space function $\delta f^{ss'}_{\boldsymbol{k}hij}$ describes separate, clearly defined physics with characteristic time-dependence. This allows us to isolate the physics that we are interested in and to write simplified and yet accurate versions of equation (4.39), that are amenable to efficient numerical solution.

5.1 Projection matrix parametrisation

Since we consider a spatially homogeneous and isotropic system, we can construct $\delta\overline{S}^{<}_{\boldsymbol{k}}(t,t)$ using only 8 of the 16 basis elements of the full Dirac algebra. The basis matrices of this subalgebra commute with the momentum representation of the Dirac helicity operator,

$$\hat{h}_{\boldsymbol{k}} \equiv \boldsymbol{\alpha}\cdot\hat{\boldsymbol{k}}\,\gamma^5, \tag{5.1}$$

where $\hat{\boldsymbol{k}} \equiv \boldsymbol{k}/|\boldsymbol{k}|$ is the unit three-momentum vector. As mentioned above, we will use the parametrisation introduced in [77], and which we already used in the spectral solution (3.13):

$$\delta\overline{S}^{<}_{\boldsymbol{k}ij}(t,t) = \sum_{h,s,s'=\pm}\mathcal{P}^{ss'}_{\boldsymbol{k}hij}\,\delta f^{ss'}_{\boldsymbol{k}hij}(t), \tag{5.2a}$$

with

$$\mathcal{P}^{ss'}_{\boldsymbol{k}hij} \equiv N^{ss'}_{\boldsymbol{k}hij}\, P_{\boldsymbol{k}h} P^{s}_{\boldsymbol{k}i} \gamma^0 P^{s'}_{\boldsymbol{k}j}. \tag{5.2b}$$

Here $P_{\boldsymbol{k}h}$ and $P^s_{\boldsymbol{k}i}$ are the helicity and energy projection matrices defined in equation (3.12) and are labelled by helicity $h = \pm 1$, neutrino flavour i, j and the energy sign indices $s, s' = \pm 1$. These matrices obviously satisfy the completeness relations $P_{\boldsymbol{k}+} + P_{\boldsymbol{k}-} = P^+_{\boldsymbol{k}i} + P^-_{\boldsymbol{k}i} = \mathbf{1}$ and it is easy to show that they also satisfy the idempotence and orthogonality relations $P_{\boldsymbol{k}h} P_{\boldsymbol{k}h'} = \delta_{hh'} P_{\boldsymbol{k}h}$ and $P^s_{\boldsymbol{k}i} P^{s'}_{\boldsymbol{k}i} = \delta_{ss'} P^s_{\boldsymbol{k}i}$. It can also be shown that for any given $\boldsymbol{k}, i, j$, the four different matrices $P^s_{\boldsymbol{k}i} \gamma^0 P^{s'}_{\boldsymbol{k}j}$ (with $s, s' = \pm 1$) span the same set as $\{\mathbf{1}, \gamma^0, \boldsymbol{\gamma}\cdot\hat{\boldsymbol{k}}, \boldsymbol{\alpha}\cdot\hat{\boldsymbol{k}}\}$ which commute with the helicity operator $\hat{h}_{\boldsymbol{k}}$. Thus the eight matrices $P_{\boldsymbol{k}h} P^s_{\boldsymbol{k}i} \gamma^0 P^{s'}_{\boldsymbol{k}j}$ (with $h, s, s' = \pm 1$) in equation (5.2) can be used as a basis for the entire homogeneous and isotropic Dirac subalgebra.

The normalisation factors $N^{ss'}_{\boldsymbol{k}hij}$, which in part define the perturbations $\delta f^{ss'}_{\boldsymbol{k}hij}$, can be chosen freely in (5.2). The choice which gives the most symmetric relations between the phase space distribution functions and the correlation function as well as between the different distribution function components, and leads to simplest source terms in the evolution equations is[11]

$$N^{ss'}_{\boldsymbol{k}hij} \equiv \mathrm{tr}\big(P_{\boldsymbol{k}h} P^s_{\boldsymbol{k}i} \gamma^0 P^{s'}_{\boldsymbol{k}j} \gamma^0\big)^{-\frac{1}{2}} = \sqrt{\frac{2\omega_{\boldsymbol{k}i}\omega_{\boldsymbol{k}j}}{\omega_{\boldsymbol{k}i}\omega_{\boldsymbol{k}j} + ss'(m_i m_j - |\boldsymbol{k}|^2)}}. \tag{5.3}$$

With this choice the phase space distributions are also correctly normalised in the thermal limit. Note that despite the fact that the definition (5.3) involves the helicity projector, $N^{ss'}_{\boldsymbol{k}hij}$ does not depend on helicity. It is also symmetric in the energy and flavour indices. We can invert the parametrisation (5.2) to express the phase space distribution functions in terms of the matrix form of the correlation function. Using (5.3) this relation reads simply

$$\delta f^{ss'}_{\boldsymbol{k}hij} = \mathrm{tr}\big[\mathcal{P}^{s's}_{\boldsymbol{k}hji}\, \delta\overline{S}^{<}_{\boldsymbol{k}ij}(t,t)\big]. \tag{5.4}$$

That is, with the normalisation (5.3), $\mathcal{P}^{s's}_{\boldsymbol{k}hji}$ is a "correctly normalised" projection operator in our basis.

The basis spanned by $\mathcal{P}^{s's}_{\boldsymbol{k}hji}$ can be used to define generalised distribution functions for any local correlation function. Below we need the adiabatic distribution functions, which can now be defined analogously to (5.4):

$$f^{ss'}_{\mathrm{ad},\boldsymbol{k}hij} \equiv \mathrm{tr}\big[\mathcal{P}^{s's}_{\boldsymbol{k}hji}\, \overline{S}^{<}_{\mathrm{ad},\boldsymbol{k}ij}(t,t)\big]. \tag{5.5}$$

Substituting here the leading order $\overline{S}^{<}_{\mathrm{ad},\boldsymbol{k}}(t,t)$ given by equation (4.23) (i.e. the free case) we get

$$f^{ss'}_{\mathrm{ad},\boldsymbol{k}hij} \simeq s f_{\mathrm{FD}}(s\omega_{\boldsymbol{k}i})\delta_{ss'}\delta_{ij}. \tag{5.6}$$

This shows that the parametrisation (5.2) with the normalisation (5.3) naturally matches to the Fermi-Dirac distribution in the free theory (up to a sign for negative frequency states).

[11] In the massless limit (5.3) becomes singular. This is a technical problem similar to the one encountered with massless spinors, and it can be avoided by using a different normalisation. Alternatively one can use (5.3) with finite masses, and take the limit $m_i \to 0$ at the end of the calculation when needed.

5.2 Generalised density matrix equation

Using the parametrisation (5.2) with the normalisation (5.3) for $\delta\overline{S}^<_{\boldsymbol{k}}(t,t)$ in equation (4.39) we can derive an equation for the non-equilibrium distribution functions $\delta f^{ss'}_{\boldsymbol{k},hij}(t)$. The calculation is complicated by the fact that also the normalisation factors and the energy projection operators depend on time due to the time dependent masses $m_i(t)$, but the final master equation is structurally very simple:

$$\begin{aligned}\partial_t \delta f^{ss'}_{\boldsymbol{k}hij} = &-\mathrm{i}(s\omega_{\boldsymbol{k}i} - s'\omega_{\boldsymbol{k}j})\delta f^{ss'}_{\boldsymbol{k}hij} - \partial_t f^{ss'}_{\mathrm{ad},\boldsymbol{k}hij} \\ &+ ss'\frac{|\boldsymbol{k}|}{2}\Big(\frac{\dot m_i}{\omega^2_{\boldsymbol{k}i}} f^{-s,s'}_{\boldsymbol{k}hij} + \frac{\dot m_j}{\omega^2_{\boldsymbol{k}j}} f^{s,-s'}_{\boldsymbol{k}hij}\Big) \\ &- \sum_{l,\eta}\Big[C^{s\eta s'}_{\boldsymbol{k}hilj}\delta f^{\eta s'}_{\boldsymbol{k}hlj} + (C^{s'\eta s}_{\boldsymbol{k}hjli})^*\delta f^{s\eta}_{\boldsymbol{k}hil}\Big].\end{aligned} \tag{5.7}$$

Here $\dot m_i \equiv \partial_t m_i$ and we combined $f_{\boldsymbol{k}} = f_{\mathrm{ad},\boldsymbol{k}} + \delta f_{\boldsymbol{k}}$ in the second line, with the adiabatic distribution functions $f_{\mathrm{ad},\boldsymbol{k}}$ defined in equation (5.5), and the collision term is given by

$$C^{s\eta s'}_{\boldsymbol{k}hilj} \equiv \mathrm{i}\,\mathrm{tr}\big[\mathcal{P}^{s's}_{\boldsymbol{k}hji}\,\overline{\Sigma}^r_{\mathrm{eq,eff},\boldsymbol{k}il}(t,t)\,\mathcal{P}^{\eta s'}_{\boldsymbol{k}hlj}\big]. \tag{5.8}$$

Equation (5.7) describes all particle-antiparticle and flavour-coherence effects in the local limit and includes helicity. This universality is reflected in the large number of indices, which may appear overwhelming at first. However, all terms in (5.7) have simple interpretations. For example the first term on the right-hand side corresponds to the Hamiltonian commutator term in equation (4.39). It falls into this simple form because $H_{\boldsymbol{k}i}P^s_{\boldsymbol{k}i} = P^s_{\boldsymbol{k}i}H_{\boldsymbol{k}i} = s\omega_{\boldsymbol{k}i}P^s_{\boldsymbol{k}i}$. The Hamiltonian term causes oscillations in the off-diagonal components and its simple form is pivotal in distinguishing the relevant time scales. For $s = -s'$ the oscillations are very fast. These oscillations are essential e.g. for vacuum particle production, but they can be a problem if one is interested only in flavour oscillations, which correspond to $s = s'$ but $i \neq j$, and usually evolve much more slowly. In the next section we derive an effective equation for flavour oscillations by averaging over the fast oscillations.

The second line in equation (5.7) arises from the time dependence of the basis matrices $\mathcal{P}^{ss'}_{\boldsymbol{k}hij}$ in the parametrisation (5.2). The precise form of these terms depends on the normalisation, and the choice (5.3) turns out to give the most compact form. These terms are again essential for vacuum particle production, but they can be neglected in the leptogenesis application. The source terms $\partial_t f^{ss'}_{\mathrm{ad},\boldsymbol{k}hij}$ result from the projection of the adiabatic matrix source in (4.39). Lastly, the collision terms $C^{s\eta s'}_{\boldsymbol{k}hilj}$ can in general be separated into dispersive and absorptive parts, just by using $\Sigma^r = \Sigma^{\mathrm{H}} - \mathrm{i}\Sigma^{\mathcal{A}}$, and consequently we define

$$C^{s\eta s'}_{\boldsymbol{k}hilj} \equiv C^{\mathrm{H},s\eta s'}_{\boldsymbol{k}hilj} + C^{\mathcal{A},s\eta s'}_{\boldsymbol{k}hilj}. \tag{5.9}$$

The dispersive term $C^{\mathrm{H},s\eta s'}_{\boldsymbol{k}hilj}$ can be broadly characterised as a generalised matter Hamiltonian. It is of course a very general structure, but e.g. in the case of ordinary light neutrino mixing it can be shown [94] to exactly reproduce the neutrino effective potential in matter. It could be interesting for resonant leptogenesis as well, because it would make the energy splitting $\Delta\omega_{\boldsymbol{k}}$ between the neutrinos a dynamical quantity. We will not consider the dispersive corrections numerically in this paper, but also this topic will be pursued elsewhere.

Finally, the absorptive part $C^{\mathcal{A},s\eta s'}_{\boldsymbol{k}hilj}$ of the collision term contains both flavour-diagonal and off-diagonal damping rates, and importantly for leptogenesis, cross couplings between the diagonal and off-diagonal distribution functions. These cross coupling functions together with the CP-violating flavour oscillation are the mechanism which generates the lepton asymmetry.

5.3 Lepton source and washout terms

It is easy to write also the CP-violating source term and the washout terms of the lepton equation using the parametrisation (5.2) and normalisation (5.3) for the Majorana neutrino correlator. For the source term (4.41) and the washout term (4.42) we get, respectively,

$$S_{\mathrm{CP}} = \sum_{h,s,s',i,j} \int \frac{\mathrm{d}^3\boldsymbol{k}}{(2\pi)^3} \operatorname{tr}\Big[\Big(P_{\mathrm{R}}\bar{\Sigma}^{\mathcal{A}}_{\mathrm{eq,eff},\boldsymbol{k}ji} + (\bar{\Sigma}^{\mathcal{A}}_{\mathrm{eq,eff},\boldsymbol{k}ij})^\dagger P_{\mathrm{R}}\Big)\mathcal{P}^{ss'}_{\boldsymbol{k}hij}\Big]\delta f^{ss'}_{\boldsymbol{k}hij}, \tag{5.10}$$

$$\delta W = \sum_{h,s,s',i,j} \int \frac{\mathrm{d}^3\boldsymbol{k}}{(2\pi)^3} \operatorname{tr}\Big[\Big(P_{\mathrm{R}}\delta\bar{\Sigma}^{\mathcal{A}}_{\mathrm{eff},\boldsymbol{k}ji} + (\delta\bar{\Sigma}^{\mathcal{A}}_{\mathrm{eff},\boldsymbol{k}ij})^\dagger P_{\mathrm{R}}\Big)\mathcal{P}^{ss'}_{\boldsymbol{k}hij}\Big]\delta f^{ss'}_{\boldsymbol{k}hij}. \tag{5.11}$$

For the washout term (4.43), we again expand the adiabatic Wightman functions to leading order to get the $\mathcal{O}(y_i^2)$ result

$$W_{\mathrm{ad}} = \sum_{s,i} \int \frac{\mathrm{d}^3\boldsymbol{k}}{(2\pi)^3}\frac{1}{2} \operatorname{tr}\Big[P_{\mathrm{R}}\Big(\{\delta\bar{\Sigma}^{>}_{ii}(k_{si}), f_{\mathrm{FD}}(s\omega_{\boldsymbol{k}i})P^s_{\boldsymbol{k}i}\} - \{\delta\bar{\Sigma}^{<}_{ii}(k_{si}), f_{\mathrm{FD}}(-s\omega_{\boldsymbol{k}i})P^s_{\boldsymbol{k}i}\}\Big)\Big]. \tag{5.12}$$

Expanded forms of equations (5.10)–(5.12) are given in appendix F, where we use the leading order approximation (4.27) for the effective self-energies and perform the traces.

5.4 Mass shell equations

As stated above, the most important benefit of the parametrisation (5.2) is that it allows to separate the physics corresponding to different time scales. In particular we can distinguish the *mass shell* functions corresponding to $s = s'$ (but including the flavour coherences $i \neq j$) from the fast oscillating *coherence shell* functions for which $s \neq s'$.[12] For a graphical illustration see figure 2 in [77]. We denote these functions by

$$\delta f^{m,\pm}_{\boldsymbol{k}} \equiv \delta f^{\pm\pm}_{\boldsymbol{k}}, \tag{5.13}$$

$$\delta f^{c,\pm}_{\boldsymbol{k}} \equiv \delta f^{\pm\mp}_{\boldsymbol{k}}. \tag{5.14}$$

Indeed, from equation (5.7) we see that for $\delta f^{c,\pm}_{\boldsymbol{k}hij}$ the Hamiltonian term is proportional to $\mp\mathrm{i}(\omega_{\boldsymbol{k}i} + \omega_{\boldsymbol{k}j}) = \mp 2\mathrm{i}\bar{\omega}_{\boldsymbol{k}ij}$, corresponding to very fast particle-antiparticle oscillations (zitterbewegung). For the mass shell solutions $\delta f^{m,\pm}_{\boldsymbol{k}hij}$ the Hamiltonian term is proportional to $\mp\mathrm{i}(\omega_{\boldsymbol{k}i} - \omega_{\boldsymbol{k}j}) = \mp\mathrm{i}\Delta\omega_{\boldsymbol{k}ij}$, corresponding to flavour oscillations for $i \neq j$, at a frequency which is suppressed for large $|\boldsymbol{k}|$ or a small mass difference $|m_i - m_j|$. This is the case of interest for resonant leptogenesis.

[12] This naming scheme follows the earlier cQPA notation [77] and the one we already used in (3.13), although in our current treatment the phase space structures are not a priori restricted to a spectral form.

If particle-antiparticle oscillations are much faster than the flavour oscillations, we can drop the coherence functions $\delta f^c_{\boldsymbol{k}}$ in equations (5.7), since their effect on the flavour oscillations averages out.[13] This results in a much simpler coarse-grained master equation for the mass shell functions:

$$\begin{aligned}\partial_t \delta f^{m,s}_{\boldsymbol{k}hij} = & -\mathrm{i}s(\omega_{\boldsymbol{k}i} - \omega_{\boldsymbol{k}j})\delta f^{m,s}_{\boldsymbol{k}hij} - \partial_t f^{m,s}_{\mathrm{ad},\boldsymbol{k}hij} \\ & - \sum_l \Big[C^{sss}_{\boldsymbol{k}hilj}\delta f^{m,s}_{\boldsymbol{k}hlj} + (C^{sss}_{\boldsymbol{k}hjli})^* \delta f^{m,s}_{\boldsymbol{k}hil} \Big]. \end{aligned} \tag{5.15}$$

Equation (5.15) still holds complete information of flavour mixing and the helicity degree of freedom in the local limit. In particular it contains as limiting cases the familiar Boltzmann theory, light neutrino density matrix formalism and the cQPA-formulation of the generic flavour and spin dependent problem. It also agrees with or encompasses a number of other quantum transport approaches in the literature, of which we give a more detailed comparisons in section 9.

Removing the coherence shell solutions greatly facilitates the numerical solution, in particular for quasi-degenerate Majorana neutrinos. In addition, a number of relations hold between different components of $\delta f_{\boldsymbol{k}}$, which further simplify the numerical task; we will give these relations in appendix D. In the following sections we will solve equations (5.15) numerically using the leading order expansion (4.27) for the effective self-energies in the collision terms functions. Detailed expressions for $C^{sss}_{\boldsymbol{k}hilj}$ are given in appendix E.

Hierarchical limit. Let us briefly comment on the validity of our master equations in the hierarchical limit of leptogenesis [20, 42], where $\Delta m/m \sim \mathcal{O}(1)$. The general master equation (5.7) is of course applicable also in this limit. However, the condition $\Delta\omega_{\boldsymbol{k}ij} \ll 2\bar{\omega}_{\boldsymbol{k}ij}$ might hold only to a limited degree (see footnote 13), so that neglecting the coherence shell functions $\delta f^c_{\boldsymbol{k}}$ might not be warranted, possibly reducing the accuracy of the mass-shell equations (5.15). However, using equation (5.7) to model this case would be numerically very challenging, because due to the large hierarchy $H \ll m$, both oscillation time scales are very fast compared to the heavy neutrino decoupling time. Luckily, due to the very same reason, one can in this case work in the decoupling limit (see section 8 below) and derive an effective Boltzmann equation for the lepton asymmetry. To our knowledge the contribution from the coherence shell functions $\delta f^c_{\boldsymbol{k}}$ has never been included, however. This could be done by starting from the master equation (5.7) and it would indeed be interesting to study the size of these corrections.

[13] We can formally justify this as follows. First, generically $\delta f^{c\pm}_{\boldsymbol{k}}(t) = A^{\pm}_{\boldsymbol{k}}(t)\exp(\mp 2\mathrm{i}\bar{\omega}_{\boldsymbol{k}}t)$, where $A^{\pm}_{\boldsymbol{k}}(t)$ are some functions that vary only in the flavour scale. Next, take the convolution of (5.7) with some appropriate normalised weight function W, e.g. the Weierstrass transform with $W(t,t') \sim \exp(-(t-t')^2/2\sigma^2)$, where we can choose $1/\Delta\omega_{\boldsymbol{k}} \gg \sigma \gg 1/2\bar{\omega}_{\boldsymbol{k}}$. This has no effect on the mass-shell contributions, because they do not vary significantly over the time σ. However, the terms involving the coherence solutions behave as

$$\int \mathrm{d}t'\, W(t,t') D^{\pm}_{\boldsymbol{k}}(t')\delta f^{c\pm}_{\boldsymbol{k}}(t') \sim D^{\pm}_{\boldsymbol{k}}(t)\delta f^{c\pm}_{\boldsymbol{k}}(t)\exp\big(-2(\bar{\omega}_{\boldsymbol{k}}\sigma)^2\big),$$

where $D^{\pm}_{\boldsymbol{k}}$ represents whatever term that is multiplying the coherence solution. Because $\bar{\omega}\sigma \gg 1$, these terms are extremely suppressed and completely drop from the averaged mass-shell equations.

6 Expansion of the universe

So far all our equations have been formulated in the flat Minkowski spacetime, but we eventually need to work in the expanding Friedmann-Lemaître-Robertson-Walker (FLRW) background. In this section we show how the generalisation to an expanding universe can be done by a simple reinterpretation of all variables in the comoving frame. We finish this section by rewriting our master equations explicitly in the expanding universe in terms of the scaled inverse temperature.

6.1 Lagrangian in curved spacetime

First we need to generalise the Minkowski Lagrangian (4.1) to curved spacetime:

$$\mathcal{L} = \sqrt{-g}\Big\{ \sum_{i=1}^{2}\Big[\frac{1}{2}\overline{N}_i(\mathrm{i}\gamma^\mu\nabla_\mu - m_i)N_i - y_i^*(\bar{\ell}\widetilde{\phi})P_{\mathrm{R}}N_i - y_i\overline{N}_i P_{\mathrm{L}}(\widetilde{\phi}^\dagger\ell)\Big] + \bar{\ell}\,\mathrm{i}\gamma^\mu\nabla_\mu\ell + (\partial_\mu\phi^\dagger)(\partial^\mu\phi) - \xi R\phi^\dagger\phi\Big\}. \tag{6.1}$$

Here $g \equiv \det(g_{\mu\nu})$ is the determinant of the metric and ∇_μ is the covariant derivative given by the spin connection. We also added the non-minimal coupling of the Higgs field ϕ to the scalar curvature R and the factor $\sqrt{-g}$ originates from the volume form of the curved spacetime action integral. We then assume a spatially flat FLRW metric

$$\mathrm{d}s^2 = g_{\mu\nu}\,\mathrm{d}x^\mu\,\mathrm{d}x^\nu = a(\eta)^2(\mathrm{d}\eta^2 - \mathrm{d}\boldsymbol{x}^2), \tag{6.2}$$

where $a = a(\eta)$ is the dimensionless scale factor and the conformal time η is defined by $\mathrm{d}t = a(\eta)\,\mathrm{d}\eta$. With the metric (6.2) the contracted covariant derivative in equation (6.1) becomes

$$\gamma^\mu\nabla_\mu = \frac{1}{a}\left(\gamma^0\partial_0 + \boldsymbol{\gamma}\cdot\boldsymbol{\nabla} + \frac{3}{2}\frac{a'}{a}\gamma^0\right), \tag{6.3}$$

where $\boldsymbol{\nabla}$ is the usual flat spatial derivative vector, $\partial_0 = \partial/\partial\eta$ and $a' \equiv \partial a/\partial\eta$.

Using equations (6.2) and (6.3) with $\sqrt{-g} = a^4$ and scaling all fermion fields ψ according to $\psi \to a^{-3/2}\psi$ and the Higgs field as $\phi \to a^{-1}\phi$, the Lagrangian (6.1) is transformed to

$$\mathcal{L} = \sum_{i=1}^{2}\left[\frac{1}{2}\overline{N}_i\left(\mathrm{i}\gamma^0\partial_0 + \mathrm{i}\boldsymbol{\gamma}\cdot\boldsymbol{\nabla} - am_i\right)N_i - y_i^*\left(\bar{\ell}\widetilde{\phi}\right)P_{\mathrm{R}}N_i - y_i\overline{N}_i P_{\mathrm{L}}\left(\widetilde{\phi}^\dagger\ell\right)\right] + \bar{\ell}\left(\mathrm{i}\gamma^0\partial_0 + \mathrm{i}\boldsymbol{\gamma}\cdot\boldsymbol{\nabla}\right)\ell + \phi^\dagger\left[-\partial_0^2 + \boldsymbol{\nabla}^2 - a^2\left(\xi R - \frac{a''}{a^3}\right)\right]\phi, \tag{6.4}$$

where the scalar curvature is given by $R = 6a''/a^3$. From the Lagrangian (6.4) we see that the only effects of the expanding universe compared to the Minkowski theory (4.1) are that the time variable is replaced by the conformal time η, spatial coordinates become the comoving ones, neutrino masses are multiplied by the scale factor a and the Higgs field gets a geometric mass term. This mass term vanishes for a conformal coupling $\xi = 1/6$ or when the universe is radiation-dominated: $a(\eta) \propto \eta$, which is the case to a high accuracy in leptogenesis. We shall thus continue to assume that the Higgs field is massless.

The comoving frame. Based on the above, all expressions and equations in the earlier sections given in the Minkowski background remain valid also in the expanding flat spacetime when we make the replacements

$$t \to \eta, \qquad \boldsymbol{k} \to \boldsymbol{k}_{\rm com}, \qquad T \to T_{\rm com}, \qquad m_i(t) \to a(\eta) m_i, \tag{6.5}$$

where $\boldsymbol{k}_{\rm com} \equiv \boldsymbol{k}a$ is the comoving momentum, $T_{\rm com} \equiv Ta$ is the comoving temperature of the relativistic SM heat bath and m_i are the physical constant masses. Note that the phase space distribution functions f are dimensionless scalars and have the same values in both physical and comoving variables.

We assume that the universe is dominated by relativistic SM particles, which are kept in equilibrium by fast gauge interactions, and that the universe expands adiabatically. In the absence of entropy production the physical temperature then scales as $T \propto a^{-1}$, so that $T_{\rm com}$ remains constant. The comoving momentum $\boldsymbol{k}_{\rm com}$ is also constant, as the physical momentum redshifts as $\boldsymbol{k} \propto a^{-1}$. We can also write the Hubble parameter as

$$H(T) = \left(\frac{4\pi^3}{45} g_*\right)^{1/2} \frac{T^2}{m_{\rm Pl}}, \tag{6.6}$$

where $m_{\rm Pl}$ is the Planck mass and g_* is the effective number of relativistic degrees of freedom, which is $g_* = 110.25$ when including all SM fields and two massless Majorana neutrinos. Note that the scale factor can now be written as $a(\eta) = H(T_{\rm com})\eta$. The entropy density is given by $s = 2\pi^2 g_* T^3/45$. Overall, the leptogenesis equations retain the same form they had when formulated with a generic time dependent mass term in the Minkowski background, when using the replacements (6.5) and scaling the equations by appropriate powers of the scale factor a.

6.2 Final master equation in expanding space time

For the numerical implementation it is convenient to formulate the equations using dimensionless variables. The most relevant temperature scale for leptogenesis is around $T = m_1$, where m_1 is the mass of the lightest Majorana neutrino. We thereby use the variables

$$z = \frac{m_1}{T}, \qquad x_i = \frac{m_i}{m_1}, \qquad \kappa = \frac{|\boldsymbol{k}|}{T}, \tag{6.7}$$

with

$$\frac{\mathrm{d}}{\mathrm{d}t} = zH \frac{\mathrm{d}}{\mathrm{d}z} = \frac{H_1}{z} \frac{\mathrm{d}}{\mathrm{d}z}, \tag{6.8}$$

where $H_1 \equiv H(m_1)$ is the Hubble parameter (6.6) evaluated at $T = m_1$. The z-parameter is directly proportional to the scale factor so it serves as the time evolution parameter. Due to the constraints (D.9) there are only four independent mass shell functions for the two mixing Majorana neutrinos. We choose them as follows:

$$\delta f_{\boldsymbol{k}h} \equiv (\delta f^{m,+}_{\boldsymbol{k}h11}, \, \delta f^{m,+}_{\boldsymbol{k}h22}, \, \mathrm{Re}\, \delta f^{m,+}_{\boldsymbol{k}h12}, \, \mathrm{Im}\, \delta f^{m,+}_{\boldsymbol{k}h12}). \tag{6.9}$$

We can now formulate the $\boldsymbol{k}$-dependent neutrino equation (5.15) as a vector equation for the components (6.9). Including also the lepton asymmetry equation (4.40), our final

master equations written using the dimensionless variables are

$$\frac{\mathrm{d}\delta f_{\boldsymbol{k}h}}{\mathrm{d}z} = (\Delta\tilde{\omega}_{\boldsymbol{k}} - \tilde{C}_{\boldsymbol{k}h})\delta f_{\boldsymbol{k}h} - \frac{\mathrm{d}f_{\mathrm{ad},\boldsymbol{k}h}}{\mathrm{d}z}, \tag{6.10}$$

$$\frac{\mathrm{d}Y_L}{\mathrm{d}z} = \tilde{S}_{\mathrm{CP}} + (\delta\tilde{W} + \tilde{W}_{\mathrm{ad}})Y_L, \tag{6.11}$$

where $Y_L \equiv (n_\ell - \bar{n}_\ell)/s$, and we used (4.34) to relate the lepton chemical potential to the asymmetry. The dimensionless tree level oscillation coefficient $\Delta\tilde{\omega}_{\boldsymbol{k}}$ and the collision term coefficient $\tilde{C}_{\boldsymbol{k}h}$ of the neutrino equation, as well as the CP-violating lepton source term $\tilde{S}_{\mathrm{CP}}$ and the washout term coefficients $\tilde{W}$ (with $W = \delta W, W_{\mathrm{ad}}$) are given by

$$\Delta\tilde{\omega}_{\boldsymbol{k}} \equiv \frac{z\,\Delta\omega_{\boldsymbol{k}}}{H_1}, \qquad \tilde{C}_{\boldsymbol{k}h} \equiv \frac{z\,C_{\boldsymbol{k}h}}{H_1}, \tag{6.12}$$

$$\tilde{S}_{\mathrm{CP}} \equiv \frac{z\,S_{\mathrm{CP}}}{sH_1}, \qquad \tilde{W} \equiv \frac{6z\,W}{c_w H_1 \mu_\ell T^2}. \tag{6.13}$$

Equations (6.10) and (6.11) are formally analogous to the momentum dependent Boltzmann equations, which we present in equations (G.5) and (G.6) of appendix G. The difference is that the quantities $\Delta\omega_{\boldsymbol{k}}$ and $C_{\boldsymbol{k}h}$ in equations (6.10) and (6.12) are 4×4 matrices consisting of the coefficients for different components of the column vector $\delta f_{\boldsymbol{k}h}$. To avoid confusion with earlier notation, we denote these components (when needed) with bracketed indices: for example $\delta f_{\boldsymbol{k}h[3]} = \mathrm{Re}\,\delta f^{m,+}_{\boldsymbol{k}h12}$, and $C_{\boldsymbol{k}h[12]}$ is the coefficient of $\delta f_{\boldsymbol{k}h[2]}$ in the equation of $\delta f_{\boldsymbol{k}h[1]}$. The matrix $\Delta\omega_{\boldsymbol{k}}$ corresponds to the tree level flavour oscillation term and its only non-vanishing elements are $\Delta\omega_{\boldsymbol{k}[34]} = -\Delta\omega_{\boldsymbol{k}[43]} = \omega_{\boldsymbol{k}1} - \omega_{\boldsymbol{k}2}$. The collision term coefficient matrix is given by

$$C_{\boldsymbol{k}h} = \begin{pmatrix} 2\,\mathrm{Re}(C^+_{111}) & 0 & 2\,\mathrm{Re}(C^+_{121}) & 2\,\mathrm{Im}(C^+_{121}) \\ 0 & 2\,\mathrm{Re}(C^+_{222}) & 2\,\mathrm{Re}(C^+_{212}) & -2\,\mathrm{Im}(C^+_{212}) \\ \mathrm{Re}(C^+_{211}) & \mathrm{Re}(C^+_{122}) & \mathrm{Re}(C^+_{112} + C^+_{221}) & -\mathrm{Im}(C^+_{112} - C^+_{221}) \\ -\mathrm{Im}(C^+_{211}) & \mathrm{Im}(C^+_{122}) & \mathrm{Im}(C^+_{112} - C^+_{221}) & \mathrm{Re}(C^+_{112} + C^+_{221}) \end{pmatrix}, \tag{6.14}$$

where $C^+_{ilj} \equiv C^{+++}_{\boldsymbol{k}hilj}$ were defined in equation (5.8). Explicit expressions for the collision terms $C^{+++}_{\boldsymbol{k}hilj}$ are given in appendix E, computed using self-energies in the leading order expansion (4.27) and explicitly written in appendix B. Finally, explicit expressions for the lepton source and washout terms can be found in appendix F.

7 Numerical results

In this section we solve numerically the system of equations (6.10) and (6.11) for the Majorana neutrino distribution functions $\delta f_{\boldsymbol{k}h}$ and the (normalised) lepton asymmetry density Y_L in the case of two Majorana neutrinos and one lepton flavour. We start by considering possible initial conditions. Then, before going to the discussion of the final lepton asymmetry and its dependence on model parameters, we establish the time scales relevant for the problem and study the momentum dependent neutrino distribution functions.

7.1 Initial conditions

While we took $t_{\rm in} \to -\infty$ for the CTP to calculate the interactions, we can of course choose any finite time $t = t_0$ (or $z = z_0$) as the starting point of our calculation with arbitrary initial conditions for the correlation functions. In particular, we will consider both vacuum and thermal initial conditions for the Majorana neutrinos, while we assume that the lepton and Higgs distributions stay in local equilibrium in the common SM plasma temperature T. In both cases we assume a vanishing initial lepton asymmetry: $Y_L(t_0) = 0$.

Vacuum initial conditions. Here we assume that at $t = t_0$ the Majorana neutrinos are decoupled and thus effectively in zero temperature (e.g. if only the SM particles get reheated after inflation). The full local neutrino correlator is then given by

$$\overline{S}^<_{\boldsymbol{k}ij}(t_0, t_0) = \overline{S}^<_{\mathrm{ad,vac},\boldsymbol{k}ij}(t_0, t_0) \simeq P^-_{\boldsymbol{k}i}(t_0)\delta_{ij}, \tag{7.1}$$

which is calculated from (4.23) by taking the limit $T \to 0$. For the non-equilibrium part we then get, using equations (3.3) and (7.1),

$$\delta\overline{S}^<_{\boldsymbol{k}}(t_0, t_0) = \overline{S}^<_{\mathrm{ad,vac},\boldsymbol{k}}(t_0, t_0) - \overline{S}^<_{\mathrm{ad},\boldsymbol{k}}(t_0, t_0). \tag{7.2}$$

Note that this perturbation is not necessarily small as it measures the deviation of the full correlator $S^<$ (now initially in vacuum with zero temperature for the Majorana species) from the adiabatic equilibrium correlator $S^<_{\rm ad}$ (with the high temperature T of the SM particle species). For the mass shell functions the initial condition (7.2) with (7.1) becomes

$$\delta f^{m,+}_{\boldsymbol{k}hij}(t_0) = -f^{m,+}_{\mathrm{ad},\boldsymbol{k}hij}(t_0) = -f_{\rm FD}(\omega_{\boldsymbol{k}i})\delta_{ij}, \tag{7.3}$$

$$\delta f^{m,-}_{\boldsymbol{k}hij}(t_0) = -\delta_{ij} - f^{m,-}_{\mathrm{ad},\boldsymbol{k}hij}(t_0) = -f_{\rm FD}(\omega_{\boldsymbol{k}i})\delta_{ij}, \tag{7.4}$$

where we used equations (5.4) and (5.6).

Thermal initial conditions. Here we assume that also the Majorana neutrinos are in local thermal equilibrium with the SM particles at $t = t_0$, corresponding to some high initial temperature $T_0 \gg m_i$. The full local neutrino correlator is then given by

$$\overline{S}^<_{\boldsymbol{k}}(t_0, t_0) = \overline{S}^<_{\mathrm{ad},\boldsymbol{k}}(t_0, t_0) \tag{7.5}$$

which trivially implies that $\delta\overline{S}^<_{\boldsymbol{k}}(t_0, t_0) = 0$ and that all non-equilibrium distribution functions vanish initially: $\delta f^{m,\pm}_{\boldsymbol{k}hij}(t_0) = 0$. Note also that in this case the Majorana neutrinos deviate from equilibrium only due to the dynamical source term $-\partial_t f_{\rm ad}$.

7.2 Physical scales and parameters

The minimal leptogenesis mechanism is mainly controlled by four time scales, corresponding to the expansion rate of the universe H, the Majorana neutrino decay rate Γ, and the oscillation frequencies $\Delta\omega_{\boldsymbol{k}ij}$ and $2\overline{\omega}_{\boldsymbol{k}ij}$. We already discussed the role of the flavour and zitterbewegung oscillations in section 5.4, finding that the latter may be relevant in the hierarchical limit, but can be safely ignored when $\Delta\omega_{\boldsymbol{k}ij} \ll 2\overline{\omega}_{\boldsymbol{k}ij}$. We work in this limit

here, but the question of the relative sizes of the three slow time scales H^{-1}, Γ^{-1} and $\Delta\omega_{\boldsymbol{k}ij}^{-1}$ still remains. The resonant leptogenesis mechanism turns out to be most efficient when all these scales are roughly comparable.

Indeed, if $H \gg \Delta\omega_{\boldsymbol{k}ij}$, there is no time for flavour oscillations to develop, while for $H \ll \Delta\omega_{\boldsymbol{k}ij}$ the source terms $\sim H$ become suppressed. Also, in the very strong washout limit, $\Gamma \gg H$ the asymmetry is suppressed by thermalisation due to interactions, whereas for $\Gamma \ll \Delta\omega_{\boldsymbol{k}ij}$, the magnitude of CP-violation is suppressed, since the source in the asymmetry equation is proportional to the couplings y_i. Additionally, if $\Gamma \gg \Delta\omega_{\boldsymbol{k}ij}$ the flavour oscillations become over-damped [69], analogously to light mixing neutrino systems [3, 4, 7]. This leaves us to seek parameters in the range $\Gamma \sim \Delta\omega_{\boldsymbol{k}ij} \sim H$ for maximal resonant enhancement.

Benchmark parameters. Our simple leptogenesis model has 5 physical input parameters: the magnitudes of the two Yukawa couplings y_1 and y_2, their relative CP-violating phase θ_{12}, the lighter Majorana neutrino mass m_1 and the relative mass-squared difference $\Delta m_{21}^2/m_1^2 \equiv (m_2^2 - m_1^2)/m_1^2$. We define the Yukawa phase as

$$\sin(\theta_{ij}) \equiv \frac{\mathrm{Im}(y_i^* y_j)}{|y_i||y_j|}. \tag{7.6}$$

We use the following set of benchmark values as a baseline:

$$|y_1| = 0.06, \qquad \theta_{12} = \frac{\pi}{4}, \tag{7.7a}$$
$$|y_2| = 0.1,$$
$$m_1 = 10^{13}\,\mathrm{GeV}, \qquad \frac{m_2^2}{m_1^2} = 1 + \frac{|y_1|^2 + |y_2|^2}{16\pi} \approx 1.00027. \tag{7.7b}$$

In addition one has to define the number of effective relativistic degrees of freedom g_* and the initial temperature T_0 where we start the calculation. For these we use $g_* = 110$ and $z_0 = 10^{-2}$. For the benchmark parameters this corresponds to the initial temperature $T_0 = m_1/z_0 = 10^{15}\,\mathrm{GeV}$ and the Hubble expansion rate $H_1 \equiv H(m_1) \approx 1.428 \times 10^8\,\mathrm{GeV}$.

Some more comments are still in order. First, we have chosen a high mass scale $10^{13}\,\mathrm{GeV}$ for the lightest Majorana neutrino, typical for traditional thermal leptogenesis [20]. However, it can be seen that all terms in equations (6.12) and (6.13) scale either as $\sim \Gamma/H_1$ or $\sim \Delta m/H_1$, so that the dynamics does not depend on the mass scale m_1 as long as Γ/H_1 is kept constant (and if $\Delta m \sim \Gamma$). More precisely, the dynamics can be effectively characterised by three parameters: the washout strength parameters

$$K_i \equiv \frac{\Gamma_i^{(0)}}{H_1} \sim \frac{|y_i|^2}{m_1} m_{\mathrm{Pl}} \tag{7.8}$$

and the number of flavour oscillations in a Hubble time: $N_{12} \equiv |\Delta m_{12}|/(2\pi H_1)$. Using $\Gamma_i^{(0)} = |y_i|^2 m_1/(8\pi)$ (see appendix G.1), we find that in the benchmark case $K_i \sim \mathcal{O}(10)$ (corresponding to strong washout) along with $N_{12} \approx 1.5$.

These estimates agree qualitatively with what is previously known from the semiclassical Boltzmann approach, where the CP-asymmetry parameter $\varepsilon_i^{\mathrm{CP}} \propto \sin(2\theta_{12})$ is resonantly

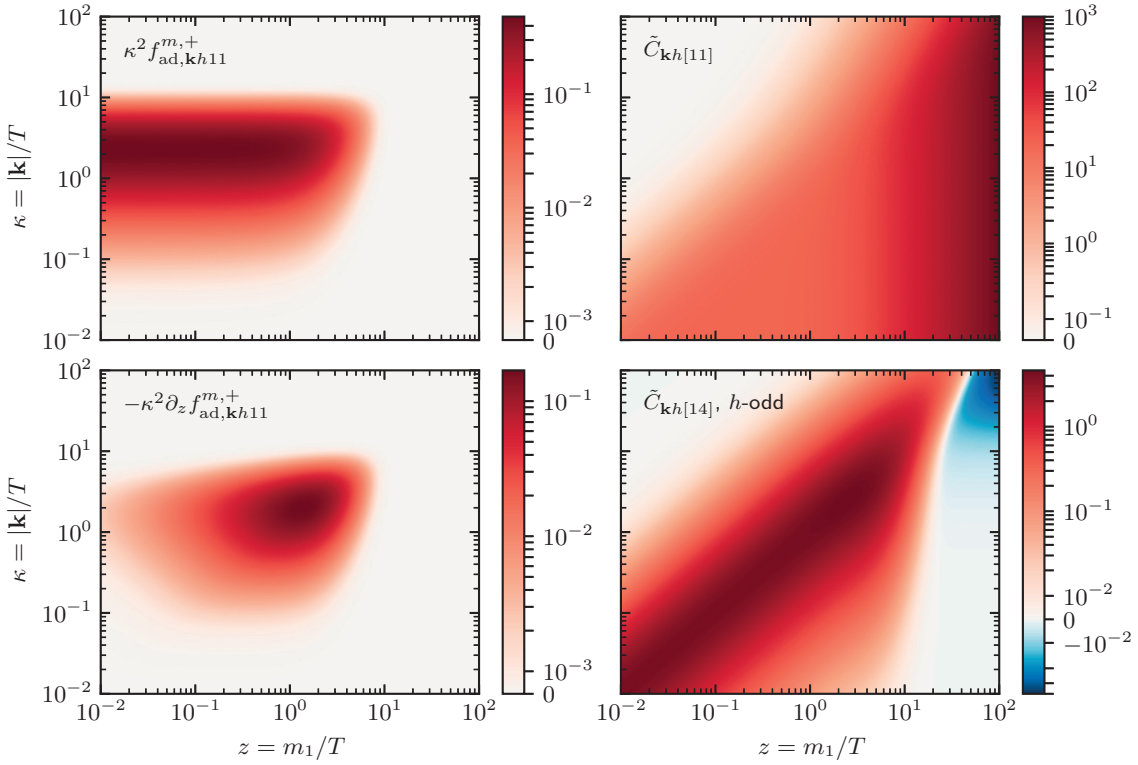

Figure 4. Shown are select intermediate functions of the Majorana neutrino equation (6.10). On the left: the adiabatic distribution function $\kappa^2 f^{m,+}_{\mathrm{ad},\boldsymbol{k}h11} \simeq \kappa^2 f_{\mathrm{FD}}(\omega_{\boldsymbol{k}1})$ (top) and the source term $-\kappa^2\partial_z f^{m,+}_{\mathrm{ad},\boldsymbol{k}h11}$ (bottom). On the right: the collision term coefficient functions $\tilde{C}_{\boldsymbol{k}h[11]}$, which is the same for both helicities (top), and the helicity-odd combination $(\tilde{C}_{\boldsymbol{k},+1[14]} - \tilde{C}_{\boldsymbol{k},-1[14]})/2$ (bottom).

enhanced for $\Delta m \sim \Gamma$. The CP-violating angle θ_{12} was chosen to be maximal in this sense in the benchmark case, but it can be used to adjust the value of the final asymmetry downwards, as it affects the results mainly as an overall scaling factor with only a small impact on the dynamics.

7.3 Neutrino distribution functions

Solving the master equations (6.10) accurately requires of the order of hundred discrete momentum variables. Thousands of collision integrals $C^{+++}_{\boldsymbol{k}hilj}$ are then needed at each time-step, each of which contains a one-dimensional integral. It is clear that these cannot be feasibly computed during the evaluation. Fortunately, to the order we are working, they can be computed and fitted before solving (6.10). Moreover, the source terms in the neutrino equation (6.10) are localised in momenta and temperature, which facilitates the fitting process.

In the left panels of figure 4 we show heat maps of the flavour diagonal adiabatic distribution function (5.6) (top) multiplied by a phase space factor, $\kappa^2 f^{m,+}_{\mathrm{ad},\boldsymbol{k}h11}$, and the corresponding source term (bottom) $-\kappa^2\,\mathrm{d}f^{m,+}_{\mathrm{ad},\boldsymbol{k}h11}/\,\mathrm{d}z$ as a functions of $z = m_1/T$ and $\kappa = |\boldsymbol{k}|/T$. Both functions are indeed localised around $|\boldsymbol{k}| \simeq T$ in momentum and the source term is also localised around $z \simeq 1$, while the distribution function $f_{\mathrm{FD}}(\omega_{\boldsymbol{k}1})$ exhibits

exponential fall off to zero in the same region. Plots for $f^{m,+}_{\mathrm{ad},\boldsymbol{k}h22}$ are qualitatively similar, with the fall off region moving according to the value of m_2.

In the right panels of figure 4 we show heat maps of $\tilde{C}_{\boldsymbol{k}h[11]} = 2\,\mathrm{Re}(C^{+++}_{\boldsymbol{k}h111})\,z/H_1$ and $(\tilde{C}_{\boldsymbol{k},+1[14]} - \tilde{C}_{\boldsymbol{k},-1[14]})/2 = \mathrm{Im}(C^{+++}_{\boldsymbol{k},+1,121} - C^{+++}_{\boldsymbol{k},-1,121})\,z/H_1$, given by equations (6.12) and (6.14). The former is the damping rate for the flavour-diagonal distribution function $\delta f_{\boldsymbol{k}h11}$, and the latter is the helicity-odd part of the function which couples the flavour diagonal distribution to the off-diagonal distribution $\mathrm{Im}(\delta f_{\boldsymbol{k}h12})$. The diagonal damping rate is the same for both helicities in our leading order approximation. Note that the colour bar scales in the figure are logarithmic for both positive and negative directions separately, except for a small region around zero (up to one tick in both directions), where linear scaling is used.

Figure 4 was created using the benchmark resonant leptogenesis parameters given in subsection 7.2. Note that we have dropped the dispersive self-energy Σ^{H} everywhere, as was discussed earlier. All other components of $C^{+++}_{\boldsymbol{k}hilj}$ are qualitatively similar to the ones shown here. In particular, the helicity even parts of the off-diagonal coupling functions $2\,\mathrm{Re}(C^{+++}_{\boldsymbol{k}h121})$ and $2\,\mathrm{Re}(C^{+++}_{\boldsymbol{k}h211})$, which are important for leptogenesis, have similar forms to the diagonal damping rates, and in the quasi-degenerate case $m_1 \simeq m_2$ also their scales are similar. Also, when Σ^{H} is dropped, the diagonal damping rate $C_{\boldsymbol{k}h[ii]}$ is actually just the momentum and temperature dependent decay rate of the Majorana neutrinos. This is because the leading order Majorana neutrino self-energy $\Sigma^{\mathcal{A}}$ used in this work corresponds only to the decay and inverse decay processes.

In figure 5 we show similar heat maps of some non-equilibrium distribution functions $\delta f^{m,+}_{\boldsymbol{k}hij}$, obtained from a numerical solution of equation (6.10), using the same benchmark parameters as in figure 4. In the top row we show the helicity-even parts of the flavour-diagonal and off-diagonal functions: $\kappa^2(\delta f^{m,+}_{\boldsymbol{k},+1,11} + \delta f^{m,+}_{\boldsymbol{k},-1,11})/2$ (left panel) and $\kappa^2\,\mathrm{Im}(\delta f^{m,+}_{\boldsymbol{k},+1,12} + \delta f^{m,+}_{\boldsymbol{k},-1,12})/2$ (right panel). In the bottom row we show the corresponding helicity-odd parts, $\kappa^2(\delta f^{m,+}_{\boldsymbol{k},+1,11} - \delta f^{m,+}_{\boldsymbol{k},-1,11})/2$ (left panel) and $\kappa^2\,\mathrm{Im}(\delta f^{m,+}_{\boldsymbol{k},+1,12} - \delta f^{m,+}_{\boldsymbol{k},-1,12})/2$ (right panel). We will later see that the helicity-even part of $\mathrm{Im}(\delta f^{m,+}_{\boldsymbol{k}h12})$ gives the main contribution to the CP-violating lepton source term. The results show that the off-diagonal components are localised around $z \simeq 1$ and complete approximately one period of flavour oscillation before being exponentially suppressed (the blue colour indicates negative and the red colour positive values). The localisation around $|\boldsymbol{k}| \simeq T$ is due to the phase space factor κ^2 together with the exponential suppression at high momenta. The negative values of the h-even diagonal distribution (top left panel), extending to very small z result from the vacuum initial conditions used here. The other independent components of $\delta f^{m,+}_{\boldsymbol{k}hij}$ are again qualitatively similar to the ones shown here.

7.4 Results on lepton asymmetry

Having now established the scales of the problem and that the numerical solution of the neutrino correlation function is under control, we turn to study the lepton asymmetry evolution. Because of the smallness of the lepton chemical potential μ_ℓ, we can solve the equations (6.10) and (6.11) sequentially. The neutrino equation is solved first and its

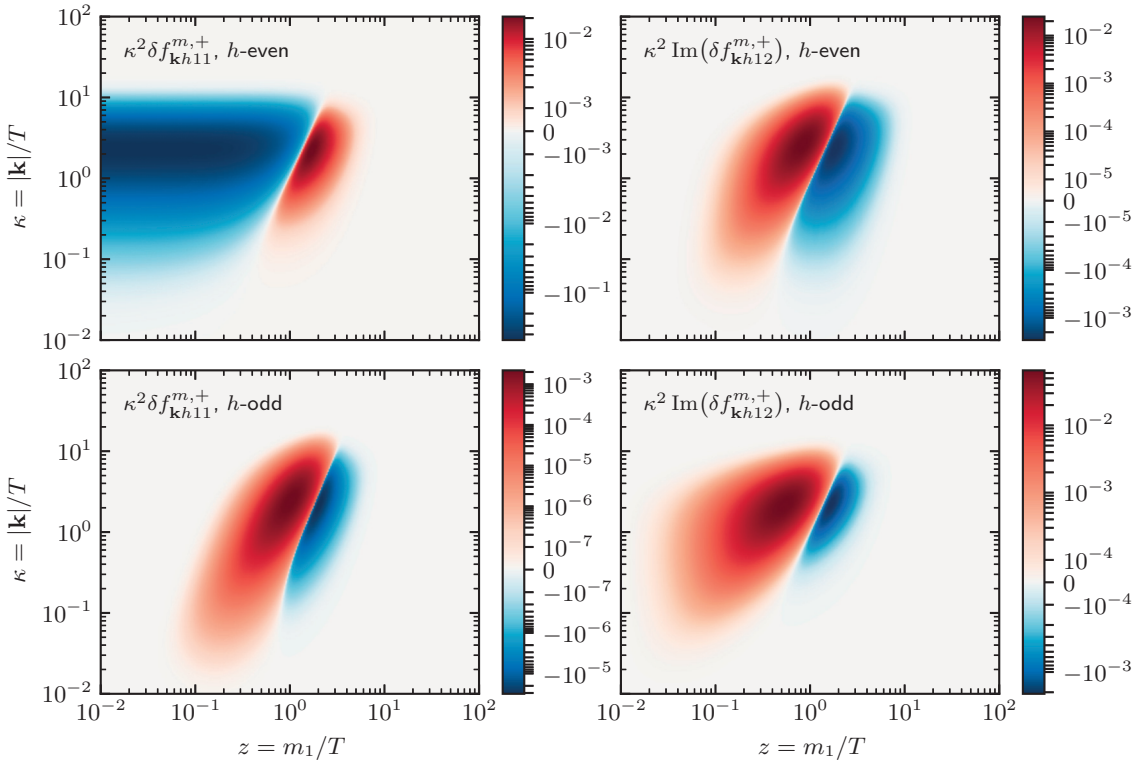

Figure 5. Shown are select components of the numerical solution $\delta f^{m,+}_{\boldsymbol{k},hij}$ of the Majorana neutrino equation (6.10) with vacuum initial conditions. Left and right sides show the flavour-diagonal function $\delta f_{\boldsymbol{k},h11}$ and the off-diagonal function $\mathrm{Im}(\delta f_{\boldsymbol{k},h12})$, respectively. Top row features the helicity-even combination $(\delta f_{\boldsymbol{k},+1} + \delta f_{\boldsymbol{k},-1})/2$ and the bottom row the helicity-odd combination $(\delta f_{\boldsymbol{k},+1} - \delta f_{\boldsymbol{k},-1})/2$ of the corresponding functions. All functions have been scaled by κ^2.

solutions $\delta f_{\boldsymbol{k}h}$ are used to calculate the lepton source term $\tilde{S}_{\mathrm{CP}}$ and the washout term coefficients $\delta\tilde{W}$ and $\tilde{W}_{\mathrm{ad}}$ according to equations (6.13), (F.1a), (F.2a) and (F.3). These are then used to solve the lepton equation (6.11). Note that equation (6.10) does not couple helicities or momenta so we can solve each mode $\delta f_{\boldsymbol{k}h}$ separately. In practice we reformulate the neutrino equations in terms of the helicity-even and helicity-odd combinations $(\delta f_{\boldsymbol{k},+} \pm \delta f_{\boldsymbol{k},-})/2$, which are more convenient for the calculation of S_{CP} and δW, as described in appendix F.

Benchmark case. In section 7.3 we presented some intermediate results for the phase space functions $\delta f_{\boldsymbol{k}h}$ using the vacuum initial condition (7.3) and the benchmark parameter values (7.7). In figure 6 we show the source term $\tilde{S}_{\mathrm{CP}}$ and the washout term coefficients $\tilde{W}_{\mathrm{ad}}$, $\delta\tilde{W}$ of the lepton equation (6.11) as functions of z for the same parameters and initial conditions. We find that dividing the dimensionless momentum $\kappa = |\boldsymbol{k}|/T$ to 100 bins in logarithmic scale between 10^{-2} and 10^4 already ensures that the results are not sensitive to the cutoff or the discretisation. Indeed, one can see from figures 4 and 5 that the largest contributions come from the range $\kappa \in [0.1, 10]$. In figure 6 we also compare the results from our full quantum kinetic equations (QKEs) (6.10) and (6.11) to those following from

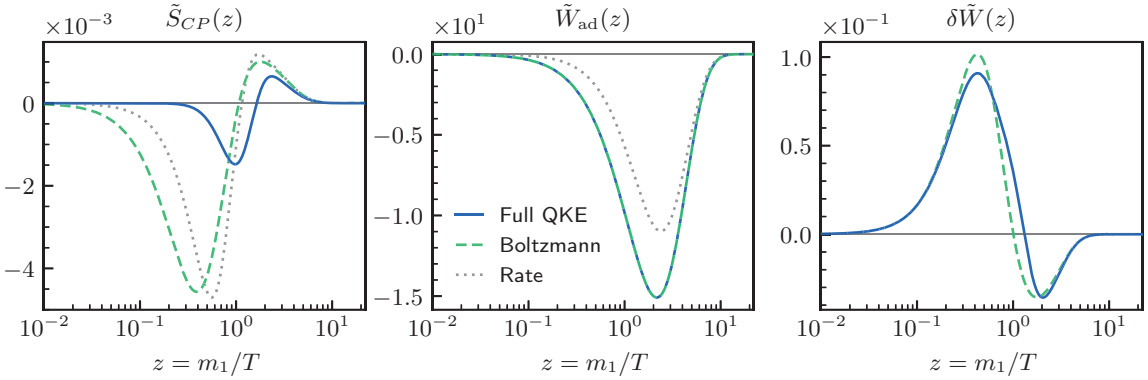

Figure 6. Numerically calculated CP-violating source term $\tilde{S}_{\rm CP}(z)$ and the washout term coefficients $\tilde{W}_{\rm ad}(z)$ and $\delta\tilde{W}(z)$ of our main lepton equation (6.11) (solid line), Boltzmann equation (G.6) (dashed line) and rate equation (G.20) (dotted line). We used the benchmark parameter values (7.7) and vacuum initial conditions.

the traditional semiclassical Boltzmann equations (BEs) given in (G.5) and (G.6) and the corresponding momentum integrated rate equations (REs) (G.19) and (G.20). The latter two sets of equations are well known, but we provided them explicitly for completeness. Also, we wrote all equations using a similar notation, which greatly facilitates the comparisons. Both BEs and REs require an externally provided CP-violating parameter $\varepsilon_i^{\rm CP}$. At this point we are using $\varepsilon_i^{\rm CP}$ corresponding to the "mixed" regulator (G.24) [83, 84] (see also e.g. [95]). Other regulators will be discussed in detail below.

It turns out that both the BEs and the REs significantly overestimate the source term $\tilde{S}_{\rm CP}$ in the relativistic region $z \lesssim 1$. The QKE-source starts to grow and changes the sign later, but all sources start to converge for $z \gtrsim 2$. On the other hand, the washout terms $\tilde{W}_{\rm ad}$ and $\delta\tilde{W}$ have only minor differences. As expected, $\tilde{W}_{\rm ad}$ is by far the dominant of the two. It also appears to be identical in the full QKE and in the BE approach, and indeed it is: this term originates from the flavour-diagonal equilibrium part of the Majorana neutrino distributions, which we have calculated to the zeroth order in gradients in the QKEs. The function $\delta\tilde{W}$, which is proportional to the non-equilibrium perturbation δf, is approximately two orders of magnitude smaller and could be neglected with practically no effect on the final asymmetry. Also, there is no corresponding function $\delta\tilde{W}$ in the leading order rate equations (G.19) and (G.20) because in the Boltzmann approach this part results from the Pauli blocking and stimulated emission factors, which are dropped from the rate equations.

In figure 7 we show the lepton asymmetries Y_L as a function of z in the benchmark case. Left panel corresponds to the vacuum initial conditions used above. The asymmetry behaves as expected from the source term $\tilde{S}_{\rm CP}$ shown in the left panel of figure 6. While the $Y_L(z)$-evolution obtained using the BE or the RE deviate strongly from that found using the full QKE, the final asymmetries differ by less than a factor of 2. In the right panel we show the case with thermal initial conditions for the Majorana neutrinos. The early evolution of the asymmetry is of course very different from the vacuum case, but

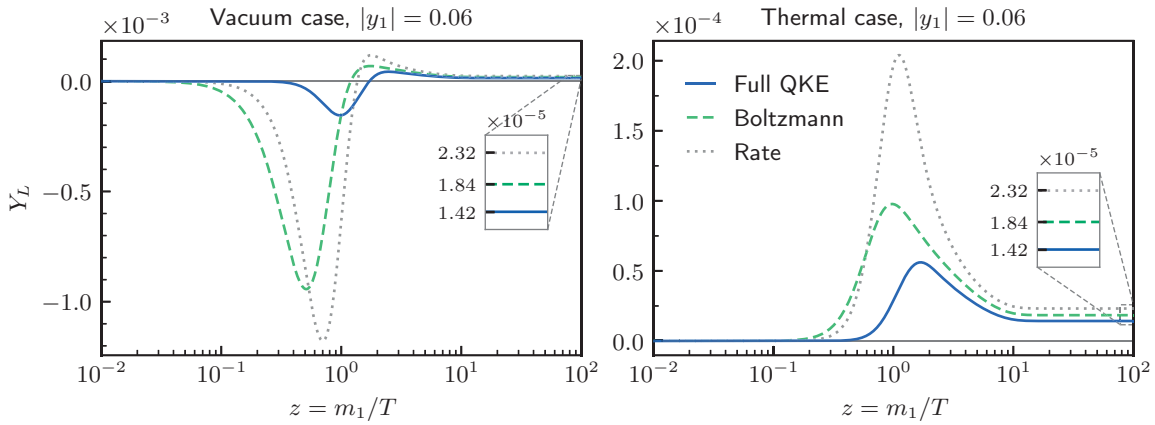

Figure 7. Numerical solutions for the lepton asymmetry $Y_L(z)$ from our main equation (6.11) (solid line), Boltzmann equation (G.6) (dashed line) and rate equation (G.20) (dotted line). We used the benchmark parameter values (7.7). The left (right) panel has vacuum (thermal) initial conditions for the Majorana neutrinos. The final values of the asymmetries are shown as insets.

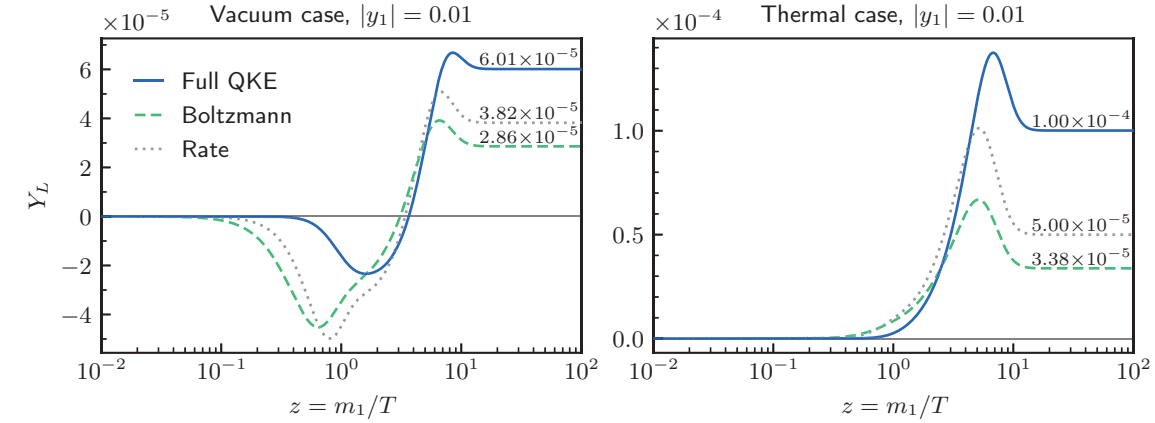

Figure 8. Numerical solutions for the lepton asymmetry $Y_L(z)$, with the same setup and mass difference as figure 7 except $|y_1| = 0.01$. The final values of the asymmetries are indicated on the corresponding graphs.

the final asymmetries are identical with both initial conditions. This behaviour is due to the strong washout assumed in the benchmark case ($K_1 \approx 10.0$ and $K_2 \approx 27.9$), which efficiently erases the early evolution of the lepton asymmetry. The final asymmetry then mostly depends on the source at the very end of the integration range, where the $\tilde{S}_{\mathrm{CP}}$ computed using different methods were found to agree better.

In figure 8 we show for comparison similar plots in the weak washout case, with $|y_1| = 0.01$, corresponding to $K_1 \approx 0.279$. The left panel again corresponds to the vacuum and the right panel to thermal initial conditions. Now the early evolution deviates less in different approaches. Also, as expected, the final asymmetries are no longer the same for vacuum and thermal initial conditions. The differences between the BE and RE predictions and our QKE results for the final asymmetry also remain significant. These results show that the lepton asymmetry evolution and its asymptotic value depend in an essential way on

the model parameters. Also, it is clear that to obtain accurate results, one should use the full QKEs instead of the less accurate BE- or RE-approaches.

Varying mass difference. In the top panels of figure 9 we show the asymptotic lepton asymmetry as a function of $(m_2^2 - m_1^2)/m_1^2 \approx 2\Delta m_{21}/m_1$, keeping other benchmark parameters fixed. We again compare the full QKE results with the BE and RE predictions, now for four different CP-asymmetry parameters $\varepsilon_i^{\mathrm{CP}}$ that have been discussed in the literature [61, 62, 66, 70, 95, 96]. The different choices, which we denote as 'mixed', 'difference', 'sum' and 'effective' vary in how the resonance near $m_1 = m_2$ is regulated. Explicit forms for the $\varepsilon_i^{\mathrm{CP}}$-parameter and the regulators are given in appendix G.3. All approaches give qualitatively similar Δm_{21}-dependence with a single maximum at $\Delta m_{21} \sim \Gamma$. However, a more close look reveals significant quantitative differences between the full QKE results and the BE and RE approximations, as well as between using different regulators in the latter two approaches.

The location of the resonance peak is approximatively given by $\Delta m_{21}^2 = |m_1\Gamma_1^{(0)} \mp m_2\Gamma_2^{(0)}|$ for the difference and sum regulators in the Boltzmann approaches. We have shown these locations in the top-right panel of figure 9, denoting them by $\Delta_{\mathrm{diff.}}^{\mathrm{max}}$ and $\Delta_{\mathrm{sum}}^{\mathrm{max}}$. The BE and RE results using different regulators fall either above or below the correct QKE-result shown by the solid blue line, varying by an almost order of magnitude for $\Delta m_{21} \lesssim \Gamma$. The effective sum regulator given in [70] (see equation (8.13) below) is designed to work in the strong washout case; it is thus not surprising that it works best in our benchmark case. On the other hand, for $\Delta m_{21} > \Gamma$, where we enter the rapid flavour oscillation regime, all results converge. This is expected, since the regulators become irrelevant in the CP-parameter (G.23) and the diagonal elements decouple from the off-diagonals in the QKEs in this limit (we will show this explicitly below). We also observe that the BEs always give a slightly lower final asymmetry than do the REs, as was also observed in [97]. The difference between the BE and RE results is smaller, however, than the difference arising from using different regulators and eventually the correct QKEs. That is, treating the quantum physics part of the problem correctly is more important than the momentum dependence of the phase space distributions.

The situation gets even more interesting when we begin to vary the couplings. In the bottom panels of figure 9 we show the results for hierarchical (left panel) and for almost degenerate (right panel) Yukawa couplings. In the left panel the washout is weaker, $K_1 \approx 0.279$ and $K_2 \approx 27.9$, whereas in the right panel the washout is strong, $K_1 \approx 22.6$. The different CP-asymmetry regulators now lead to even more dispersion in the BE and the RE results when $\Delta m_{21} \lesssim \Gamma$. In the hierarchical case using the mixed regulator leads to two peaks at $\Delta m_{21} \simeq \Gamma_1$ and $\Delta m_{21} \simeq \Gamma_2$, corresponding to the different regulators used for the two Majorana neutrinos in this case. The full QKE result, again shown by the solid blue line, shows no such structure. Also the effective regulator is somewhat less accurate here. In the right panel, with almost degenerate Yukawas, the mixed and sum regulators are in better agreement with the QKEs, but the difference regulator has an extra spurious enhancement because the regulator vanishes and the CP-asymmetry is unbounded in the double limit $m_2 \to m_1$ and $\Gamma_2 \to \Gamma_1$.

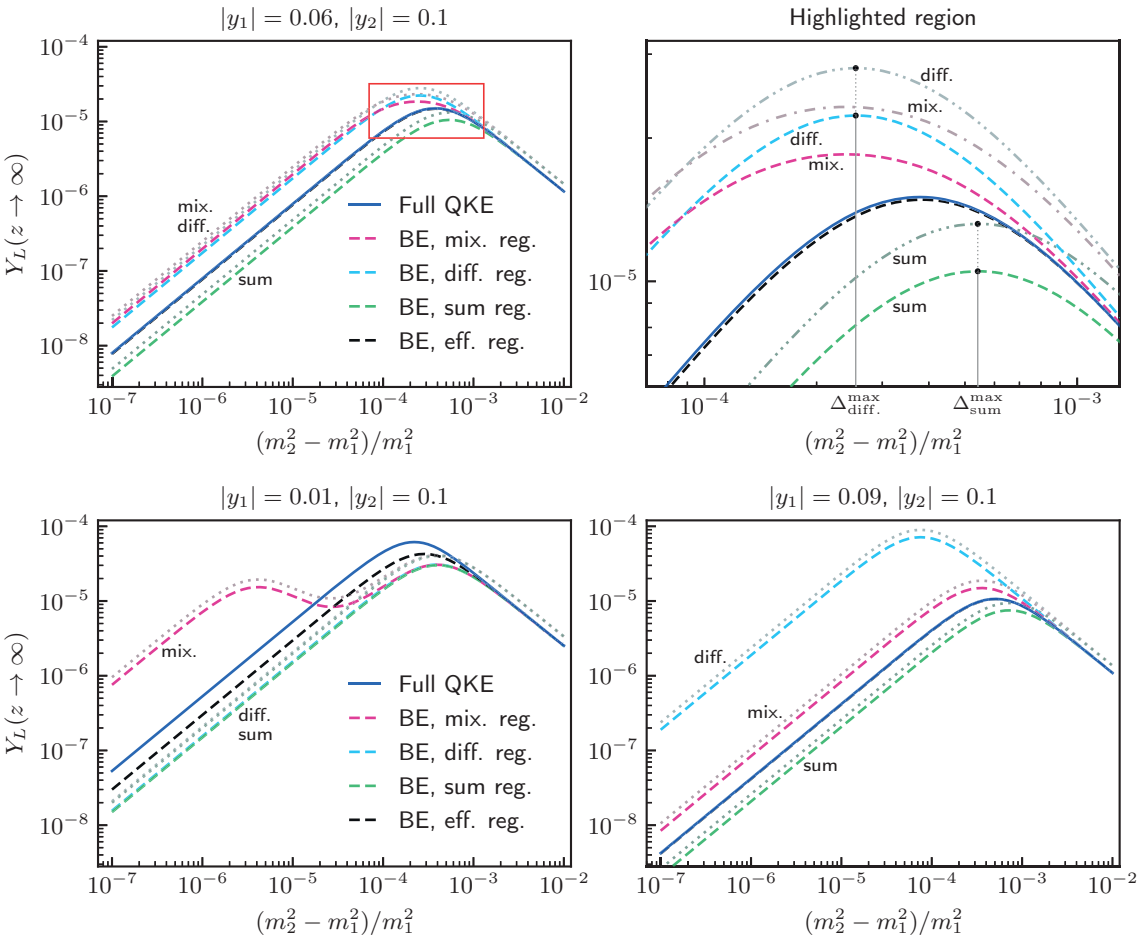

Figure 9. Shown is the asymptotic lepton asymmetry Y_L as a function of the relative mass-squared difference $\Delta m^2_{21}/m^2_1$ for different Yukawa couplings. The Boltzmann equation (BE) results are shown with four different regulators for $\varepsilon_i^{\text{CP}}$. The dotted and dash-dotted lines show the rate equation results for the corresponding BE results. The top-right panel shows the region highlighted in red in the left. The bottom panels have hierarchical (left) and almost degenerate (right) Yukawa couplings. Other parameters have the benchmark values and vacuum initial conditions were used.

The main take-home message from this section is that the Boltzmann equation and the rate equation approaches are inaccurate and strongly sensitive to the choice of the regulator in the resonant and quasidegenerate region $\Delta m_{21} \lesssim \Gamma_i$. The Boltzmann approach reproduces the full QKE results accurately in all cases only in the region $\Delta m_{21} > \Gamma_i$ when the regulator is already negligible and one is approaching the hierarchical mass limit. Also, the most accurate regulator over varying coupling strengths is the sum regulator of [62]. We shall show below how the sum regulator indeed consistently emerges when we reduce the QKEs to BEs in the helicity-symmetric decoupling limit.

Flavour oscillation. Let us look more closely at the role of the flavour oscillations in resonant leptogenesis. In the left panel of figure 10 we show the evolution of the helicity-even part of the off-diagonal Majorana neutrino phase space function $\text{Im}(\delta f^{m,+}_{\boldsymbol{k}h12})$ with

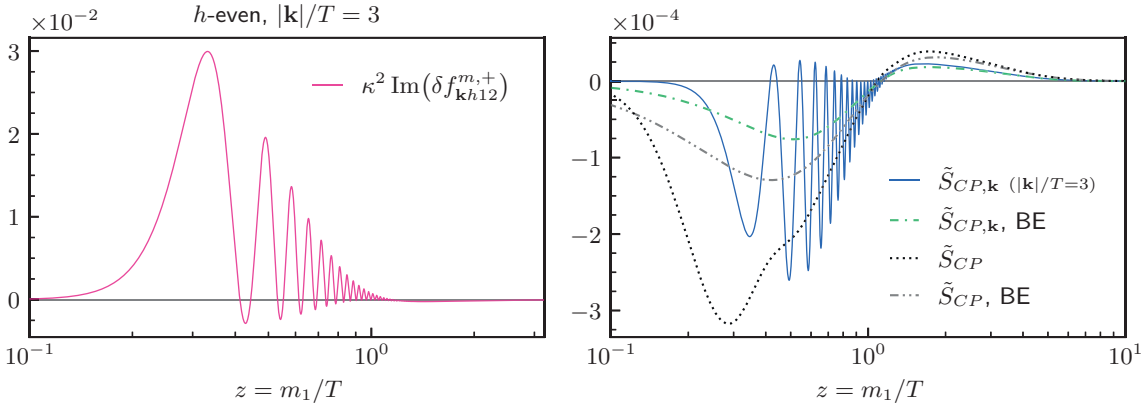

Figure 10. Flavour oscillation of $\mathrm{Im}(\delta f^{m,+}_{\boldsymbol{k},h12})(z)$ (helicity-even component) and $\tilde{S}_{\mathrm{CP},\boldsymbol{k}}(z)$ for a single $\boldsymbol{k}$-mode, with $\Delta m_{21} = 0.01 m_1$. Other parameters have the benchmark values, and vacuum initial conditions were used. On the right we show the single $\boldsymbol{k}$-mode as well as the integrated lepton asymmetry source from the full QKEs and the BEs.

$|\boldsymbol{k}| = 3T$ and $\Delta m_{21} = 0.01 m_1$. This is a case with rapid flavour oscillations corresponding to $N_{12} \approx 110$. The modes of this δf-component in the range $|\boldsymbol{k}|/T \sim 0.1$–$10$ give the dominant contribution to the integrated lepton source term. In the right panel we plot the contribution $\tilde{S}_{\mathrm{CP},\boldsymbol{k}}$ of the same mode to the lepton source term, normalised according to $\tilde{S}_{\mathrm{CP}} \equiv \int \mathrm{d}^3\boldsymbol{k}/(2\pi)^3 \tilde{S}_{\mathrm{CP},\boldsymbol{k}}/T^3$. Both the mode and its contribution to the lepton source display a strong oscillation pattern with a quickly dying amplitude. This decay of the oscillations is precisely the reason for the emergence of the semiclassical limit (shown as the green dash-dotted line) from the QKEs. We will make this explicit in equation (8.8) below. We show also in the right panel the full integrated source term from the QKEs (dotted line) and from the Boltzmann approach with the sum regulator (dash-dot-dotted line). Even in the QKE-result all oscillations are smoothed out in the integrated source, due to the phase differences between different modes.

8 Helicity-symmetric approximation

In this section we will derive a series of approximations to the QKEs (5.15) (or equivalently (6.10)), eventually reducing them to the semiclassical Boltzmann limit. This process also leads to a simplified source term in the asymmetry equation (4.40), which eventually reproduces the CP-asymmetry parameter with the sum regulator.

Looking more closely at equations (4.41) and (F.1a), one can see that the lepton asymmetry is sourced mainly by the helicity-even combination of the imaginary part of the off-diagonal function $\delta f_{\boldsymbol{k}h12}$ in the non-relativistic or mildly relativistic case. Based on this observation, we drop the tracking of the helicity asymmetry in the equations for $\delta f_{\boldsymbol{k}hij}$. We can then write a simpler set of equations for the h-even part, which we denote simply by $\delta f_{\boldsymbol{k}ij}$ henceforth, and a simpler form for the lepton source term S_{CP} including only $\mathrm{Im}(\delta f_{\boldsymbol{k}12})$. We will also work with vacuum dispersion relations, setting $\Sigma^{\mathrm{H}} \equiv 0$. The

resulting *helicity-symmetric* equations are

$$\partial_t \delta f_{\boldsymbol{k}11} = -\Gamma_{\boldsymbol{k}11}\,\delta f_{\boldsymbol{k}11} - \partial_t f^{(0)}_{\mathrm{ad},\boldsymbol{k}11} - \Gamma_{\boldsymbol{k}12}\,\mathrm{Re}(\delta f_{\boldsymbol{k}12}), \tag{8.1}$$

$$\partial_t \delta f_{\boldsymbol{k}22} = -\Gamma_{\boldsymbol{k}22}\,\delta f_{\boldsymbol{k}22} - \partial_t f^{(0)}_{\mathrm{ad},\boldsymbol{k}22} - \Gamma_{\boldsymbol{k}21}\,\mathrm{Re}(\delta f_{\boldsymbol{k}12}), \tag{8.2}$$

$$\partial_t \delta f_{\boldsymbol{k}12} = -\bar{\Gamma}_{\boldsymbol{k}12}\,\delta f_{\boldsymbol{k}12} - \mathrm{i}\Delta\omega_{\boldsymbol{k}12}\,\delta f_{\boldsymbol{k}12} - \frac{1}{2}(\Gamma_{\boldsymbol{k}21}\,\delta f_{\boldsymbol{k}11} + \Gamma_{\boldsymbol{k}12}\,\delta f_{\boldsymbol{k}22}), \tag{8.3}$$

and

$$S_{\mathrm{CP}} = -2\,\frac{\mathrm{Im}(y_1^* y_2)}{\mathrm{Re}(y_1^* y_2)} \int \frac{\mathrm{d}^3\boldsymbol{k}}{(2\pi)^3}(\Gamma_{\boldsymbol{k}21} + \Gamma_{\boldsymbol{k}12})\,\mathrm{Im}(\delta f_{\boldsymbol{k}12}), \tag{8.4}$$

where $\bar{\Gamma}_{\boldsymbol{k}12} \equiv (\Gamma_{\boldsymbol{k}11} + \Gamma_{\boldsymbol{k}22})/2$ and $\Gamma_{\boldsymbol{k}il} \equiv 2\,\mathrm{Re}(C^{+++}_{\boldsymbol{k}hilj})|_{\Sigma^H \to 0}$ with $C^{+++}_{\boldsymbol{k}hilj}$ given by equation (E.1). Note that all $\Gamma_{\boldsymbol{k}il}$ are now real so the diagonal functions $\delta f_{\boldsymbol{k}ii}$ couple directly only to $\mathrm{Re}(\delta f_{\boldsymbol{k}12})$. The diagonal damping rate admits the factorisation $\Gamma_{\boldsymbol{k}ii} = (m_i/\omega_{\boldsymbol{k}i})\Gamma_i^{(0)}\mathcal{X}_{\boldsymbol{k}i}$ where $m_i/\omega_{\boldsymbol{k}i}$ is the time dilation factor, $\Gamma_i^{(0)} = |y_i|^2 m_i/(8\pi)$ is the tree-level vacuum decay width of the Majorana neutrino and $\mathcal{X}_{\boldsymbol{k}i}$ is the thermal quantum statistical correction factor, which obeys $\mathcal{X}_{\boldsymbol{k}i} \to 1$ when $|\boldsymbol{k}|/T \to \infty$ (see equation (G.7)). The damping rate $\bar{\Gamma}_{\boldsymbol{k}12}$ in the off-diagonal equation, given by the average of the diagonal rates, agrees with the flavour coherence damping rate found in the density matrix formalism for mixing neutrinos [3, 4, 7]. This is an expected result, as the two phenomena are of course closely related. Indeed, if we further assume that $\Gamma_{\boldsymbol{k}21} \simeq \Gamma_{\boldsymbol{k}12}$, we can write equations (8.1)–(8.3) in a simple density matrix form:

$$\partial_t \delta f_{\boldsymbol{k}} = -\partial f^{(0)}_{\mathrm{ad},\boldsymbol{k}} - \mathrm{i}[H_{\boldsymbol{k}}, \delta f_{\boldsymbol{k}}] - \frac{1}{2}\{\Gamma_{\boldsymbol{k}}, \delta f_{\boldsymbol{k}}\}, \tag{8.5}$$

where $H_{\boldsymbol{k}} \equiv \mathrm{diag}(\omega_{\boldsymbol{k}1}, \omega_{\boldsymbol{k}2})$. A similar equation has been used earlier to study light neutrino mixing in the early universe [3, 6–8] and in the resonant leptogenesis context it was first derived in [61].[14]

The helicity-symmetric equations (8.1)–(8.4) provide an excellent approximation to the full QKEs with helicity-even initial conditions, as can be seen in figure 11 where we compare the two for our benchmark parameters. This is so because the neutrino source terms are helicity-symmetric and the helicity-asymmetry is only generated by loop effects. Also, it is evident from (F.1a) that the contribution to the source from the helicity-odd $\delta f^m_{\boldsymbol{k}}$-function is thermally suppressed compared to the one coming from helicity-even part. This shows that resonant leptogenesis is dominated by the helicity-independent flavour mixing, although this conclusion partly relies on the fact that the asymmetry is mostly generated in the non-relativistic regime $T \lesssim m_1$. Helicity would play a more important role if the Majorana neutrinos were relativistic when the asymmetry is generated, like in some low scale leptogenesis scenarios [86]. Indeed, equations similar to (8.5), but keeping the helicity degree of freedom, were recently used to study leptogenesis [69, 86, 98]. Our full QKEs (5.7) as well as the mass-shell equations (5.15) are more general than (8.5) and the helicity dependent equations in [86, 98, 99]. Note in particular, that for more than two

[14] In the quasidegenerate limit and restricted to two neutrino flavours, it is easy to generalise equation (8.5) to include helicity as in [61]. We do not write such an equation explicitly here, because it would be but a further special case of our general QKE (5.15) for the flavour mixing problem.

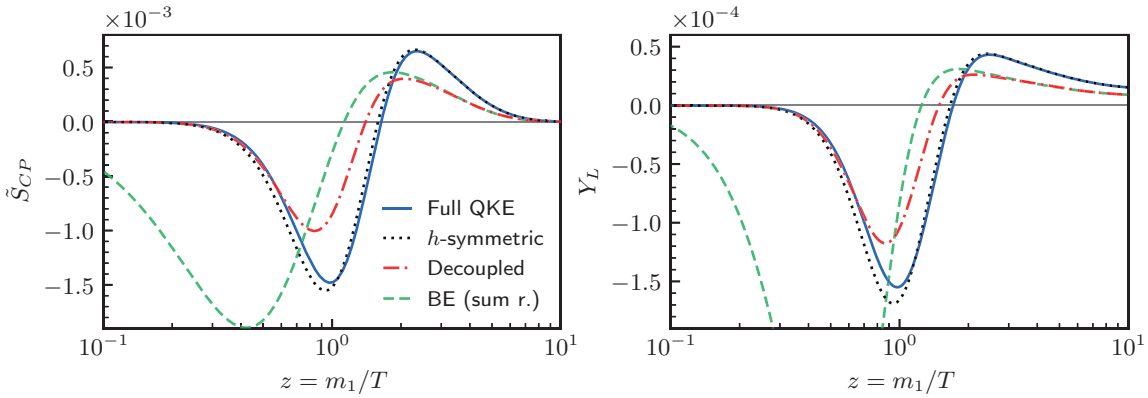

Figure 11. Comparison of the full results (solid line) to the helicity-symmetric approximation (dotted), decoupling limit (dash-dotted) and Boltzmann results with the sum regulator (dashed). We show the results for the lepton asymmetry source term (left) and the lepton asymmetry itself (right) as functions of z. The benchmark parameters with vacuum initial conditions were used.

Majorana neutrino flavours the collision terms in (5.15) cannot in general be reduced to the canonical form for a density matrix equation.

Decoupling limit. Equations (8.1)–(8.4) still incorporate all essential flavour mixing consistent with full resummation of the interaction terms. Now we simplify these equations further in the case where the flavour oscillations are fast ($\Delta m_{21} \gg \Gamma$). We use the same reasoning as in section 5.4 (see footnote 13) to argue for dropping the flavour off-diagonal terms in the diagonal equations (8.1) and (8.2). We call this approximation the *decoupling limit*. The diagonal equations, written with the expansion of the universe, are then identical to the semiclassical Boltzmann equation (G.5). The washout term can also be approximated with the Boltzmann version or even with only the $W_{\rm ad}$ contribution (G.10). Because the flavour-diagonal functions now decouple from the off-diagonal ones, they can be solved independently and their solutions can be treated as external sources to the off-diagonal function $\delta f_{\boldsymbol{k}12}$.

Assuming that initially $\delta f_{\boldsymbol{k}12}(t_0) = 0$ (a non-zero initial value could be easily added as a special solution to the homogeneous equation), the off-diagonal differential equation (8.3) can be integrated to give

$$\delta f_{\boldsymbol{k}12}(t) = -\frac{1}{2}\int_{t_0}^{t} \mathrm{d}u \left(\Gamma_{21}\delta f_{11} + \Gamma_{12}\delta f_{22}\right)_{\boldsymbol{k}}(u) \exp\left[-\int_{u}^{t} \mathrm{d}v \left(\bar{\Gamma}_{12} + \mathrm{i}\Delta\omega_{12}\right)_{\boldsymbol{k}}(v)\right]. \tag{8.6}$$

Substituting this into equation (8.4) we then get a closed formula for $S_{\rm CP}$ which now *defines* the source term in the semiclassical Boltzmann equations; indeed comparing to the Boltzmann formula (G.8), this improved form shows that the combination $\mathrm{Im}(y_1^* y_2)\,\mathrm{Im}(\delta f_{\boldsymbol{k}12})$ acts as an effective dynamical CP-asymmetry parameter.

In the quasidegenerate case $m_1 \simeq m_2$ (i.e. at this point we assume the weakly resonant regime $\Gamma \ll \Delta m_{21} \ll m_1$) we can further approximate $\Gamma_{\boldsymbol{k}ij} \simeq \mathrm{Re}(y_i^* y_j)\Gamma_{\boldsymbol{k}jj}/|y_j|^2$ and $\Gamma_{\boldsymbol{k}11}/|y_1|^2 \simeq \Gamma_{\boldsymbol{k}22}/|y_2|^2$. Then we can write the lepton source term into an even more

suggestive form:

$$S_{\rm CP}(t) \approx \sum_{\substack{i=1,2\\(j\neq i)}} \Gamma_i^{(0)} g_i \int \frac{{\rm d}^3\boldsymbol{k}}{(2\pi)^3} \Big(\frac{m_i}{\omega_{\boldsymbol{k}i}} \mathcal{X}_{\boldsymbol{k}i}\Big) \frac{{\rm Im}\big[(y_1^* y_2)^2\big]}{|y_1|^2 |y_2|^2} \times \frac{1}{4} \int_{t_0}^{t} {\rm d}u \, \big(\Gamma_{jj}(\delta f_{11} + \delta f_{22})\big)_{\boldsymbol{k}}(u) \, {\rm Im} \exp\Big[- \int_u^t {\rm d}v \, \Big(\bar{\Gamma}_{12} + {\rm i}\Delta\omega_{12}\Big)_{\boldsymbol{k}}(v) \Big]. \quad (8.7)$$

This result shows that the lepton asymmetry is cumulatively sourced by the non-equilibrium perturbations in the diagonal mass-shell functions $\delta f_{ii}(u)$, such that past contributions are suppressed by the flavour coherence damping rate $\bar{\Gamma}_{12}$. We show the approximation (8.7) for $S_{\rm CP}$ (with the diagonal solutions δf_{ii} calculated from the ordinary Boltzmann equations) and the resulting lepton asymmetry by the red dash-dotted lines in figure 11. Even though in the figure we used the benchmark parameters where $\Delta m_{21} \simeq \Gamma$, equation (8.7) is still a relatively good approximation to the full QKEs, in particular at early times $z \lesssim 1$. However, when $z \gtrsim 1$ it deviates from the full result, and at late times $z \gg 1$ the asymmetry coincides perfectly with the Boltzmann result (see below) instead, shown by the dashed line in figure 11.

8.1 Boltzmann limit

To get an even closer comparison to the existing literature, we now make stronger approximations to evaluate the time integrals in equation (8.7) analytically. Indeed, if one assumes that the source functions are roughly constant, one can take them outside the u-integral.[15] If one further assumes that $\bar{\Gamma}_{\boldsymbol{k}12}$ and $\Delta\omega_{\boldsymbol{k}12}$ are constants (we take $\mathcal{X}_{\boldsymbol{k}i} \to 1$ in $\Gamma_{\boldsymbol{k}ii}$, assuming $\Gamma_{\boldsymbol{k}ii} \simeq (m_i/\omega_{\boldsymbol{k}i})\Gamma_i^{(0)}$, and neglect the Hubble expansion for the mass and momentum), one can perform the integrals to get

$$\begin{aligned} &{\rm Im} \int_{t_0}^{t} {\rm d}u \, \exp\big[-(\bar{\Gamma}_{12} + {\rm i}\Delta\omega_{12})(t-u)\big] \\ &\simeq \frac{-\Delta\omega_{12}}{(\Delta\omega_{12})^2 + (\bar{\Gamma}_{12})^2} \left[1 - {\rm e}^{-\bar{\Gamma}_{12}(t-t_0)} \left(\cos\big[\Delta\omega_{12}(t-t_0)\big] + \bar{\Gamma}_{12} \frac{\sin\big[\Delta\omega_{12}(t-t_0)\big]}{\Delta\omega_{12}} \right) \right]. \quad (8.8) \end{aligned}$$

A similar expression was also found in [57], but without the exponential damping factor in the oscillating term. This is important, because now we see that taking the limit $t_0 \to -\infty$, the oscillating part is damped to zero.[16] We already saw this effect in figure 10: while the source was there computed using the full QKE, the strongly damped rapid oscillation we observed corresponds to the second term in equation (8.8).

[15] This is consistent if the damping time is much shorter than the time of variation of the diagonal δf_{ii}-functions, which is given by the Hubble time. That is, an approximation of the type of equation (8.9) is valid in the strong damping limit: $\bar{\Gamma}_{12} \gg H$.

[16] Authors of ref. [57] argued that the second term in (8.8) vanishes due to averaging out over oscillations, but this is not the correct explanation; note that (8.8) is valid even in the limit $\Delta\omega_{12} \to 0$. Also, a similar expression and including the damping, albeit with a different damping factor $(\Gamma_{11} - \Gamma_{22})/2$ (giving rise to the 'difference' regulator), was found in [61].

Substituting (8.8) back to equation (8.7) and dropping the damped oscillating term, one finds

$$S_{\rm CP}(t) \approx \sum_{\substack{i=1,2\\(j\neq i)}} \Gamma_i^{(0)} g_i \int \frac{{\rm d}^3\boldsymbol{k}}{(2\pi)^3} \Big(\frac{m_i}{\omega_{\boldsymbol{k}i}} \mathcal{X}_{\boldsymbol{k}i}\Big) \frac{1}{2} (\delta f_{11} + \delta f_{22})_{\boldsymbol{k}}(t) \times \frac{{\rm Im}\big[(y_1^* y_2)^2\big]}{|y_1|^2 |y_2|^2} \frac{1}{2} \bigg[\frac{-\Delta\omega_{12}\Gamma_{jj}}{(\Delta\omega_{12})^2 + (\bar{\Gamma}_{12})^2}\bigg]_{\boldsymbol{k}}. \tag{8.9}$$

This form already greatly resembles the Boltzmann result (G.8) with the constant CP-asymmetry parameter (G.23). It is now also clear that the CP-asymmetry is regulated by the *coherence damping rate* $\bar{\Gamma}_{12}$ in the degenerate limit $m_2 \to m_1$. We also note that dropping the damped oscillating term is the main reason why the BE approach tends to initially overestimate the asymmetry. This effect is clearly visible in figures 6, 7 and 11.

We can go even further and extract the CP-asymmetry parameter by using again the quasidegeneracy $m_2 \simeq m_1$, whereby $\Delta\omega_{\boldsymbol{k}12} \simeq \Delta m_{12}^2/(2\omega_{\boldsymbol{k}i})$, and taking into account the time dilation factor in the damping rate $\Gamma_{\boldsymbol{k}ii} = (m_i/\omega_{\boldsymbol{k}i})\Gamma_i^{(0)}$. The result (8.9) can then be written as

$$S_{\rm CP}(t) \approx \sum_{i=1,2} \Gamma_i^{(0)} g_i \, \varepsilon_{i,{\rm sum}}^{\rm CP} \int \frac{{\rm d}^3\boldsymbol{k}}{(2\pi)^3} \Big(\frac{m_i}{\omega_{\boldsymbol{k}i}} \mathcal{X}_{\boldsymbol{k}i}\Big) \frac{1}{2} (\delta f_{11} + \delta f_{22})_{\boldsymbol{k}}(t), \tag{8.10}$$

where (for $j \neq i$)

$$\varepsilon_{i,{\rm sum}}^{\rm CP} = \frac{{\rm Im}\big[(y_1^* y_2)^2\big]}{|y_1|^2 |y_2|^2} \frac{(m_2^2 - m_1^2) m_i \Gamma_j^{(0)}}{(m_2^2 - m_1^2)^2 + \big(m_1\Gamma_1^{(0)} + m_2\Gamma_2^{(0)}\big)^2}. \tag{8.11}$$

Equation (8.10) is still different from the Boltzmann result (G.8) in its dependence on the flavour-diagonal functions δf_{ii}. But using the quasidegeneracy argument once more to approximate $(m_1/\omega_{\boldsymbol{k}1})\mathcal{X}_{\boldsymbol{k}1} \simeq (m_2/\omega_{\boldsymbol{k}2})\mathcal{X}_{\boldsymbol{k}2}$, it can finally be written exactly in the same form as (G.8).

Strong washout limit. In articles [64, 66, 70] the strong washout limit was considered, where one assumes that the diagonal rate parameters are large separately. In this limit one can find an approximative late-time solution by putting all derivative terms to zero on the left-hand side of equations (8.1)–(8.3). One can then solve all distribution functions algebraically, and eventually the CP-violating source term (8.4) takes the form

$$S_{\rm CP} \approx \frac{{\rm Im}(y_1^* y_2)}{{\rm Re}(y_1^* y_2)} \int \frac{{\rm d}^3\boldsymbol{k}}{(2\pi)^3} (\Gamma_{21} + \Gamma_{12})_{\boldsymbol{k}} (\Gamma_{21}\delta f_{11} + \Gamma_{12}\delta f_{22})_{\boldsymbol{k}} \times \bigg[\frac{-\Delta\omega_{12}}{(\Delta\omega_{12})^2 + (\bar{\Gamma}_{12})^2\Big(1 - \frac{\Gamma_{12}\Gamma_{21}}{\Gamma_{11}\Gamma_{22}}\Big)}\bigg]_{\boldsymbol{k}}. \tag{8.12}$$

No other approximations have yet been made at this point. In the quasidegenerate limit this source then has the same form as (8.9) except that the off-diagonal backreaction to the

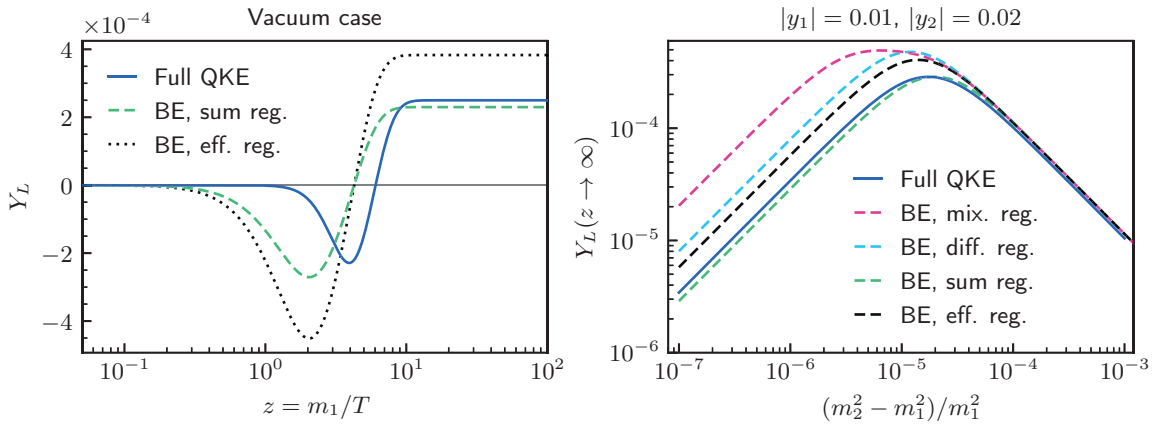

Figure 12. Comparison of the effective sum regulator with the other results in the weak washout case with $|y_1| = 0.01$ and $|y_1| = 0.02$. In the left panel we took $\Delta m_{21}^2/m_1^2 = (0.01^2 + 0.02^2)/(16\pi) \approx 10^{-5}$ near the resonance maximum. We used vacuum initial conditions in both panels, and other parameters have the benchmark values (7.7).

diagonal functions is taken into account by a modification of the regulator term $\bar{\Gamma}_{12}$.[17] This approximation can be again reduced to the Boltzmann equation with yet another effective CP-asymmetry parameter, similar to equation (8.11), but with

$$\left(m_1\Gamma_1^{(0)} + m_2\Gamma_2^{(0)}\right)^2 \quad \longrightarrow \quad \left(m_1\Gamma_1^{(0)} + m_2\Gamma_2^{(0)}\right)^2 \sin^2\theta_{12}. \tag{8.13}$$

Here we used the fact that in the single lepton flavour and quasidegeneracy limit $\Gamma_{\boldsymbol{k}12}\Gamma_{\boldsymbol{k}21} \simeq \cos^2\theta_{12}\,\Gamma_{\boldsymbol{k}11}\Gamma_{\boldsymbol{k}22}$, where the Yukawa phase θ_{12} was defined in equation (7.6). The result (8.13) agrees with the effective sum regulator defined in [70].

We have shown the results using this effective sum regulator in figure 9 as the black dashed line. This is indeed the best approximation in the strong washout limit. On the other hand, this approximation does not work well outside the strong washout case. We show in figure 12 the case where both Yukawa couplings are small, corresponding to the washout strength parameters $K_1 \approx 0.28$ and $K_2 \approx 1.1$. In this case the regulator (8.13) is worse than the simpler sum-regulator we found in the decoupling limit. These examples show that using different approximations one can accommodate the most relevant quantum effects in different parametric regions. However, no approximation remains quantitatively accurate throughout the parameter space.

Summary. We have used a series of controlled approximations to reduce the Majorana neutrino QKEs and the lepton asymmetry source term to the Boltzmann limit. The decoupling limit CP-asymmetry parameter (8.11) corresponds to the sum regulator (G.26) in agreement with [62–64]. The previous work used some extra assumptions about the model

[17] The diagonal distributions in equation (8.12) contain no backreaction from the off-diagonals, and technically they correspond to the late-time approximations $\delta f_{\boldsymbol{k}ii}^{(\mathrm{L})} \equiv -\partial_t f_{\mathrm{ad},\boldsymbol{k}ii}^{(0)}/\Gamma_{\boldsymbol{k}ii}$. However, we have improved this approximation by using here the decoupled diagonal distributions, i.e. the usual diagonal distributions $\delta f_{\boldsymbol{k}ii}$ solved from the Boltzmann equations. This gives the same late-time limit, but a more accurate early time evolution.

parameters however, and their validity in the doubly degenerate limit have been questioned [96]. Our derivation is very different and does not rely on these assumptions. We also find a clear origin and interpretation for the regulator, corresponding to the flavour coherence damping in the neutrino equation. Our numerical work confirmed that the sum-regulator is indeed the most accurate in the Boltzmann approach in the sense that it provided qualitatively best results in all regimes, as can be seen in figures 9 and 12, while the effective sum regulator (8.13) is the most accurate one in the late time limit in the strong washout case. As a byproduct, we demonstrated quantitatively how the quantum oscillations are suppressed and the semiclassical limit arises in the hierarchical strongly damped limit $\Delta m_{21} \gg \bar{\Gamma}_{12} \gg H$. Beyond this case, the BE approach does not provide highly accurate results and QKEs are needed. However, we found that the helicity-symmetric QKEs give a very accurate final asymmetry throughout the resonant leptogenesis parameter range.

9 Comparison to earlier work

Leptogenesis has been studied extensively before [37–71], and many of the results presented here have been found in some form previously. In this section we will provide a more in-depth comparison of our results and other studies based on first-principles CTP methods, which we believe are most closely similar to ours.

In several studies of leptogenesis based on the CTP method (e.g. [46, 62, 65, 68, 100]) the non-equilibrium part of the Majorana propagator is identified with a homogeneous transient, while the inhomogeneous part is taken to be the thermal equilibrium solution. In this approach the only non-equilibrium source is in the initial conditions, as there is no dynamical source for the asymmetry generation. Such approaches have been used to model the lepton asymmetry generation during the initial approach of the Majorana neutrinos to equilibrium [46, 100]. Our formalism contains this effect, which shows up as the initial negative Y_L dip in the left-hand side panels in figures 7 and 8. However, as these figures show, a moderate washout can erase this asymmetry. This restricts the use of pure transient methods to the weak washout case.

A very careful analysis using the transient approach was given in [62]. In particular off-diagonal pole propagators, which are crucial for the evolution of the non-equilibrium initial state in the two-time approach, were calculated in detail. These results are similar to our (4.17a). However, in our approach where the local correlator is evolved dynamically, it is sufficient to compute the pole propagators to a leading order approximation. In [62] it was also found that the sum regulator (G.26) is a reasonable choice for the CP-asymmetry parameter (G.23) in the Boltzmann approach. The Hubble expansion was not included in [62], but the issue was later addressed in [63, 64]. Our derivation is more general, and does not impose restrictions on Yukawa couplings [62, 63] or on the size of the deviation from equilibrium [64]. Our derivation also reveals the physical origin of the sum regulator as corresponding to the flavour coherence damping rate.

The approach in [61] (see also [66, 69]) is similar to ours, but it relies heavily on the Wigner space representation. The neutrino correlator $S^<_{\boldsymbol{k}}$ is also expanded in a different

basis, used earlier in the EWBG context [12, 13] and in the cQPA approach [72–78]. In this basis the division of $S_k^<$ into components with a characteristic time dependence is obscured, making it difficult to separate the particle-antiparticle and flavour coherence effects. Ref. [61] then used several approximations in integrating the particle-antiparticle coherences, in reduction to the spectral shell limit and a restriction to the quasidegenerate case, that we do not need to make. On the balance, the final QKE of [61] agrees with our equation (8.5) in the quasidegenerate limit (and includes the small backreaction to the neutrino equation from the lepton chemical potential, which we omitted.) Overall our derivation is more general and displays a hierarchy of QKEs, which separate the different physical scales. We also provide detailed numerical examples and comparisons, with the Hubble expansion included.

In [67] resonant leptogenesis was studied in the interaction picture method [101], using the double momentum representation, and it was found that the lepton asymmetry source term contains two distinct contributions from mixing and oscillations.[18] These results suggest that the usual Boltzmann approach, which contains only the mixing contribution, potentially captures only half of the actual late time lepton asymmetry. The findings of [67] were supported by an analysis [68] performed in a simplified non-equilibrium setup in the weak-washout regime. Both articles found that the mixing contribution is mainly due to the flavour diagonal functions and the oscillation contribution mainly due to the off-diagonal functions in the Majorana neutrino correlator. Ref. [68] found also another contribution resulting from the interference of the mixing and oscillation terms, which tends to cancel the other contributions in some cases. These results have been further discussed in [55].

Our results do not support these findings. Indeed, our result for the lepton asymmetry converges to the usual Boltzmann result in the weakly resonant case (see figure 9) and a difference by a factor of two should be clearly visible. It is then curious to note that, similarly to refs. [67, 68], our lepton asymmetry source (F.1a) also contains two distinct contributions from the flavour diagonal and off-diagonal phase space functions. However, in our case the flavour-diagonal contribution is helicity suppressed as explained in section 8. This helicity dependence may thus be the source of the discrepancy, especially given that refs. [67, 68] are based on scalar toy models where the effective Majorana states do not have Dirac structure. Also, while the results of [67] were essentially reproduced with true Majorana neutrinos in [96], that analysis was based on a semiclassical approach, which again may not necessarily implement the correct helicity structure.

Finally, flavour coherent equations similar to ones used to study light neutrino mixing in the early universe in [2–8], were used to study leptogenesis in [86, 98, 99]. We showed how these equations arise from our more general formalism. We also showed that a further reduction to even simpler, but very accurate helicity-even equations (8.5) is possible in the resonant leptogenesis case. Our formalism is also self-contained giving explicit expressions for all self-energies involved.

[18] Note that the 'mixing contribution' in [67] contains both of the traditional ε and ε' type CP-violation sources. The oscillation part is an additional contribution. The oscillation contribution is also different from the ARS mechanism [67].

10 Conclusions and outlook

We have developed a general and comprehensive formalism for problems involving quantum coherence effects in spatially homogeneous and isotropic systems with mixing fermions. Our methods are applicable to various problems ranging from vacuum particle production to neutrino physics and resonant leptogenesis, which we used as an example and a platform for the more detailed developments of the method. In particular we concentrated on a benchmark model with two Majorana neutrinos and one lepton flavour including decay and inverse decay interactions.

Our method uses the CTP formalism [30, 31] and the 2PIEA methods [34, 35]. An essential part in our derivation of tractable quantum kinetic equations *including coherence* was finding a closed equation for the *local* correlation function $S^<_{\boldsymbol{k}}(t,t)$. This required a method to evaluate collision integrals which contain the full correlation function $S^<_{\boldsymbol{k}}(t_1,t_2)$. We explained how this can be done when the system has dissipation. Two key elements in the process were the identification of proper adiabatic background solutions and the *ansatz* (3.8) to parametrise the perturbation $\delta S^<_{\boldsymbol{k}}(t_1,t_2)$ in terms of the local correlation function in the collision terms. However, no assumptions were made to restrict the spin or the flavour structure of the local correlator, which makes it well suited for studying dynamical mixing. Another essential element was the use of the projector basis (5.2), which provides a clean separation of physics related to different time scales, e.g. the particle-antiparticle oscillations and the flavour oscillations. Our formalism can be seen as a generalisation of the cQPA method developed in [72–78] and further studied in [79].

Our main results include the quantum kinetic equation (5.7) which contains complete coherence information including particle-antiparticle mixing, and its coarse-grained version (5.15), which completely incorporates the flavour mixing in both particle and antiparticle sectors separately. Note that these QKEs cannot in general be written as a traditional density matrix equation, if there are more than two flavours, due to the complicated flavour structure of the collision term (5.8). For the two-flavour case we derived even more simplified but very accurate helicity-symmetric QKEs (8.1)–(8.4) and further wrote them into a density matrix form (8.5) in the nearly degenerate limit $m_1 \simeq m_2$. Eventually we reduced our QKEs to the diagonal Boltzmann limit, deriving the CP-asymmetry parameter $\varepsilon_i^{\rm CP}$ of leptogenesis with the 'sum'-regulator (8.11) directly from the quantum transport formalism. We also pointed out that the sum-regulator physically corresponds to the coherence damping rate of the Majorana neutrinos in the underlying QKEs.

The question of the correct CP-asymmetry regulator in the semiclassical approach has been under some discussion recently [55, 62, 66, 70]. We performed careful numerical comparisons of our QKEs and the Boltzmann equations endowed with different choices for $\varepsilon_i^{\rm CP}$. We found that the sum-regulator derived here in the decoupling limit, and first found in [62], agrees best qualitatively with the QKEs throughout the parameter range of interest for resonant leptogenesis. We also implemented the integrated Boltzmann rate equations and compared them with the momentum dependent BEs and the QKEs. It turns out that the difference between the REs and BEs was always much smaller than the difference stemming from the choice of different regulators. While the sum-regulator

was generically the best choice for the BE and RE approach, their results can still be wrong by a factor $\sim$ 2–4 for $\Delta m_{21} \lesssim \Gamma$. In the strong washout case the modified sum regulator (8.13) of [66, 70] gives even more accurate late-time results. For high accuracy results throughout the parameter range, QKEs are needed however. We found that the helicity-symmetric QKEs (8.2)–(8.4) give a very accurate approximation to the full flavour QKEs (5.15) for all parameters. Finally, all of these approaches are in good agreement in the weakly resonant case, $m_i \gg \Delta m_{21} \gg \Gamma$, as expected.

Leptogenesis has been studied extensively using the CTP approach [37–71] and many of the results shown here have been found previously. We believe that our treatment stands out in displaying the most complete set of quantum kinetic equations, with a clean separation of different physics and by giving a comprehensive account of the approximations made in deriving them. Based on our results one can easily compute the effective self-energy functions to different levels of approximation in the coupling constant expansion, and including also the coherent propagators in the internal lines. In some accounts we did less than what has been done before. Definitely the phenomenological reach of our results is compromised by our not including the $2 \to 2$ scattering processes or multiple lepton flavours in our equations. We will leave these to a future work.

In this article we mainly concentrated on resonant leptogenesis, but our methods are applicable as such, or easily modifiable to other versions of the leptogenesis mechanism [20, 21]. We already briefly discussed thermal leptogenesis in the hierarchical limit in section 5.4. In this case it would be interesting to compute corrections to the lepton asymmetry source arising from the mixed particle-antiparticle flavour correlation functions ($\delta f^{c,\pm}_{\boldsymbol{k}h12}$ in the notation of section 5.4), starting from the full QKEs (5.7) and working in the decoupling limit. Our equations can also easily accommodate dispersive corrections to the neutrino QKEs. Such corrections would generalise the vacuum Hamiltonian to include the matter effects, similar to the well known case with light neutrinos. This would replace the mass difference Δm_{21} with an effective dynamical quantity and potentially change the quantitative predictions in resonant leptogenesis.

Note added, The Mathematica code package that was used to compute all numerical results in this paper is publicly available at https://doi.org/10.5281/zenodo.5025929.

Acknowledgments

This work was supported by the Academy of Finland grant 318319. HJ was in addition supported by grants from the Väisälä Fund of the Finnish Academy of Science and Letters. We wish to thank Matti Herranen for collaboration during the early stages of this work.

A Resummation of the Schwinger-Dyson equation

Here we present the derivation of the results (2.13) and (2.14), starting from the Schwinger-Dyson equations (2.10). We will shorten the notation explained below equations (2.11) even further, by leaving out the momentum indices and convolution signs: e.g. $S^p_{0,\boldsymbol{k}} * \Sigma^p_{\boldsymbol{k}} * S^p_{\boldsymbol{k}} \to S^p_0 \Sigma^p S^p$. It is also important to note that the inverse free propagator S_0^{-1} contains a

derivative operator, and thus changing the direction of its operation generates additional surface terms.

First, the pole equation (2.10a) for $p = r, a$ can be formally iterated as

$$\begin{aligned} S^p &= S_0^p(\mathbf{1} + \Sigma^p S^p) && \text{(A.1)}\\ &= S_0^p(\mathbf{1} + \Sigma^p S_0^p + \Sigma^p S_0^p \Sigma^p S_0^p + \cdots)\\ &= S_0^p + S_0^p \Sigma^p S_0^p + S_0^p \Sigma^p S_0^p \Sigma^p S_0^p + \cdots && \text{(A.2)}\\ &= (\mathbf{1} + S_0^p \Sigma^p + S_0^p \Sigma^p S_0^p \Sigma^p + \cdots) S_0^p\\ &= (\mathbf{1} + S^p \Sigma^p) S_0^p. && \text{(A.3)} \end{aligned}$$

This is consistent with the Hermiticity properties (2.8) of the pole propagators, which relate equation (A.1) for $p = r$ to equation (A.3) for $p = a$ and vice versa. Equation (2.10b) for $S^<$ (similarly for $S^>$) can now be iterated and rearranged as follows:

$$\begin{aligned} S^< &= S_0^< + S_0^< \Sigma^a S^a + S_0^r \Sigma^< S^a + S_0^r \Sigma^r S^< && \text{(A.4)}\\ &= S_0^< + S_0^< \Sigma^a S^a + S_0^r \Sigma^< S^a\\ &\quad + S_0^r \Sigma^r (S_0^< + S_0^< \Sigma^a S^a + S_0^r \Sigma^< S^a + S_0^r \Sigma^r S^<)\\ &= (\mathbf{1} + S_0^r \Sigma^r)(S_0^< + S_0^< \Sigma^a S^a + S_0^r \Sigma^< S^a)\\ &\quad + S_0^r \Sigma^r S_0^r \Sigma^r (S_0^< + S_0^< \Sigma^a S^a + S_0^r \Sigma^< S^a + S_0^r \Sigma^r S^<)\\ &\;\;\vdots\\ &= (\mathbf{1} + S_0^r \Sigma^r + S_0^r \Sigma^r S_0^r \Sigma^r + \cdots)(S_0^< + S_0^< \Sigma^a S^a + S_0^r \Sigma^< S^a)\\ &= (\mathbf{1} + S^r \Sigma^r)(S_0^< + S_0^< \Sigma^a S^a + S_0^r \Sigma^< S^a)\\ &= (\mathbf{1} + S^r \Sigma^r) S_0^< (\mathbf{1} + \Sigma^a S^a) + S^r \Sigma^< S^a. && \text{(A.5)} \end{aligned}$$

The second and third equalities explicitly show the first and second iteration of the first equation (A.4). In the fourth step this iteration is assumed to continue indefinitely. To get the final two lines we then used equations (A.2) and (A.3). Note that the final line can also be written in the form

$$S^< = (S^r S_0^{-1}) S_0^< (S_0^{-1} S^a) + S^r \Sigma^< S^a. \tag{A.6}$$

This result was derived also in [36] and a similar iterative solution was presented in the double momentum representation in the context of the interaction picture CTP formalism [67].

B Majorana neutrino self-energies

The self-energy functions $\mathfrak{S}_\mu$ defined in equations (4.16) are given by

$$\begin{aligned} \mathfrak{S}^{\mathrm{H}}_{\mathrm{eq}}(k) = \frac{1}{2} \int \frac{\mathrm{d}^4 p}{(2\pi)^4} 2\pi \,\mathrm{sgn}(p^0) \delta(p^2) \,\mathrm{PV}\Big[\frac{1}{(k-p)^2}\Big]\\ \times \Big[(1 + 2 f_{\mathrm{BE}}(p^0))(\not{k} - \not{p}) + (1 - 2 f_{\mathrm{FD}}(p^0)) \not{p}\Big], \end{aligned} \tag{B.1a}$$

$$\not{\mathfrak{S}}^{\mathcal{A}}_{\rm eq}(k) = \frac{1}{2}\int \frac{{\rm d}^4p}{(2\pi)^4}(2\pi)^2\,{\rm sgn}(p^0)\,{\rm sgn}(k^0-p^0)\,\not{p}\,\delta(p^2)\delta((k-p)^2)$$
$$\times\Big[f_{\rm FD}(-p^0)+f_{\rm BE}(k^0-p^0)\Big], \tag{B.1b}$$
$$\delta\not{\mathfrak{S}}^{\lessgtr}(k) = \int \frac{{\rm d}^4p}{(2\pi)^4}(2\pi)^2\,{\rm sgn}(p^0)\,{\rm sgn}(k^0-p^0)\,\not{p}\,\delta(p^2)\delta((k-p)^2)$$
$$\times f_{\rm FD}(p^0)f_{\rm FD}(-p^0)f_{\rm BE}(\pm(k^0-p^0)). \tag{B.1c}$$

Here PV denotes the Cauchy principal value distribution, and $\pm = +,-$ for $\lessgtr = <,>$, respectively. Note that equation (B.1a) contains also the unrenormalised vacuum part of $\mathfrak{S}^{\rm H}_{\rm eq}(k)$, which is UV-divergent. The Yukawa and chirality structure for this part are the same as in equation (4.16b). We split $\mathfrak{S}^{\rm H}_{\rm eq}$ into the vacuum and temperature dependent parts

$$\not{\mathfrak{S}}^{\rm H}_{\rm eq}(k) = \not{\mathfrak{S}}^{\rm H(vac)}_{\rm eq}(k) + \not{\mathfrak{S}}^{\rm H(}_{\rm eq}{}^{T)}(k), \tag{B.2}$$

where the vacuum part was given (using dimensional regularisation) in equation (4.47) and the temperature dependent part is

$$\not{\mathfrak{S}}^{\rm H(}_{\rm eq}{}^{T)}(k) = 2\pi\int\frac{{\rm d}^4p}{(2\pi)^4}\delta(p^2)\,{\rm PV}\left[\frac{1}{(k-p)^2}\right]\Big(f_{\rm BE}|p^0|(\not{k}-\not{p}) - f_{\rm FD}|p^0|\,\not{p}\Big). \tag{B.3}$$

The temperature dependent integral (B.3) has been worked out in [102].

We further parametrise the integrals (B.1b), (B.1c) and (B.3) with

$$\not{\mathfrak{S}}^{\alpha}(k) = a^{\alpha}(k^0,|\boldsymbol{k}|)\gamma^0 + b^{\alpha}(k^0,|\boldsymbol{k}|)\boldsymbol{\gamma}\cdot\hat{\boldsymbol{k}}, \tag{B.4}$$

and

$$a^{\alpha}(k^0,|\boldsymbol{k}|) = T\,\tilde{a}^{\alpha}(k^0/T,|\boldsymbol{k}|/T), \tag{B.5}$$
$$b^{\alpha}(k^0,|\boldsymbol{k}|) = T\,\tilde{b}^{\alpha}(k^0/T,|\boldsymbol{k}|/T), \tag{B.6}$$

where $\tilde{a}^{\alpha},\tilde{b}^{\alpha}$ are dimensionless functions, and $\alpha = \mathcal{A},{\rm H},<,>$ and $\mathfrak{S} = \mathfrak{S}_{\rm eq},\delta\mathfrak{S}$. After some calculation we get the following results (with $\kappa_0\equiv k^0/T$, $\kappa\equiv|\boldsymbol{k}|/T$):

$$\tilde{a}^{\rm H(}_{\rm eq}{}^{T)}(\kappa_0,\kappa) = \frac{1}{16\pi^2\kappa}\int_0^{\infty}{\rm d}x\left\{\left[2x\log\left|\frac{\kappa_+}{\kappa_-}\right| - xL_+(x)\right]\left[\tilde{f}_{\rm FD}(x)+\tilde{f}_{\rm BE}(x)\right]\right.$$
$$\left. - \kappa_0 L_-(x)\tilde{f}_{\rm BE}(x)\right\}, \tag{B.7a}$$
$$\tilde{b}^{\rm H(}_{\rm eq}{}^{T)}(\kappa_0,\kappa) = \frac{1}{16\pi^2\kappa}\int_0^{\infty}{\rm d}x\left\{\left[4x - 2x\frac{\kappa_0}{\kappa}\log\left|\frac{\kappa_+}{\kappa_-}\right| + \frac{\kappa_0^2-\kappa^2}{2\kappa}L_-(x) + \frac{\kappa_0}{\kappa}xL_+(x)\right]\right.$$
$$\left.\times\left[\tilde{f}_{\rm FD}(x)+\tilde{f}_{\rm BE}(x)\right] + \kappa L_-(x)\tilde{f}_{\rm BE}(x)\right\}, \tag{B.7b}$$
$$\tilde{a}^{\mathcal{A}}_{\rm eq}(\kappa_0,\kappa) = \frac{1}{16\pi\kappa}\int_{\kappa_-}^{\kappa_+}{\rm d}x\,x\Big[\tilde{f}_{\rm FD}(-x)+\tilde{f}_{\rm BE}(\kappa_0-x)\Big], \tag{B.7c}$$
$$\tilde{b}^{\mathcal{A}}_{\rm eq}(\kappa_0,\kappa) = \frac{1}{16\pi\kappa}\int_{\kappa_-}^{\kappa_+}{\rm d}x\left(\frac{\kappa_0^2-\kappa^2}{2\kappa} - \frac{\kappa_0}{\kappa}x\right)\Big[\tilde{f}_{\rm FD}(-x)+\tilde{f}_{\rm BE}(\kappa_0-x)\Big], \tag{B.7d}$$

$$\delta\tilde{a}^{\lessgtr}(\kappa_0,\kappa) = \frac{1}{8\pi\kappa}\int_{\kappa_-}^{\kappa_+} \mathrm{d}x\, x \tilde{f}_{\mathrm{FD}}(x)\tilde{f}_{\mathrm{FD}}(-x)\tilde{f}_{\mathrm{BE}}(\pm(\kappa_0 - x)), \tag{B.7e}$$

$$\delta\tilde{b}^{\lessgtr}(\kappa_0,\kappa) = \frac{1}{8\pi\kappa}\int_{\kappa_-}^{\kappa_+} \mathrm{d}x \left(\frac{\kappa_0^2 - \kappa^2}{2\kappa} - \frac{\kappa_0}{\kappa}x\right)\tilde{f}_{\mathrm{FD}}(x)\tilde{f}_{\mathrm{FD}}(-x)\tilde{f}_{\mathrm{BE}}(\pm(\kappa_0 - x)), \tag{B.7f}$$

where

$$L_\pm \equiv \log\Big|\frac{x+\kappa_+}{x+\kappa_-}\Big| \pm \log\Big|\frac{x-\kappa_+}{x-\kappa_-}\Big|, \qquad \kappa_\pm \equiv \frac{1}{2}(\kappa_0 \pm \kappa), \tag{B.8a}$$

and

$$\tilde{f}_{\mathrm{FD}}(x) \equiv \frac{1}{\mathrm{e}^x + 1}, \qquad \tilde{f}_{\mathrm{BE}}(x) \equiv \frac{1}{\mathrm{e}^x - 1}. \tag{B.8b}$$

The integrals given above for $\tilde{a}^{\mathcal{A}}_{\mathrm{eq}}$, $\tilde{b}^{\mathcal{A}}_{\mathrm{eq}}$, $\delta\tilde{a}^{\lessgtr}$ and $\delta\tilde{b}^{\lessgtr}$ may be further calculated in closed form using logarithm and dilogarithm functions (like in [42]). The results given here hold only for $|\kappa_0| > \kappa > 0$ (timelike four-momentum). The corresponding results for $\kappa > |\kappa_0| > 0$ (spacelike four-momentum) are attained by replacing the integral operator above as follows:

$$\int_{\kappa_-}^{\kappa_+} \mathrm{d}x \quad \longrightarrow \quad -\Big(\int_{\kappa_+}^{\infty} + \int_{-\infty}^{\kappa_-}\Big)\mathrm{d}x. \tag{B.9}$$

Also, in the results (B.7) it was assumed that the energy parameter κ_0 is real. If these results are continued to complex values of κ_0 (as required when considering finite widths) then the implicit sign functions in the absolute values must be applied to the real parts only (e.g. $\mathrm{sgn}(\kappa_0)\kappa_0 = |\kappa_0|$ should be replaced by $\mathrm{sgn}(\mathrm{Re}\,\kappa_0)\kappa_0 = \sqrt{\kappa_0{}^2}$).

Finally, the a^α and b^α functions have the following k^0-symmetry properties:

$$a^{\mathrm{H}}_{\mathrm{eq}}(-k^0,|\boldsymbol{k}|) = -a^{\mathrm{H}}_{\mathrm{eq}}(k^0,|\boldsymbol{k}|), \qquad b^{\mathrm{H}}_{\mathrm{eq}}(-k^0,|\boldsymbol{k}|) = b^{\mathrm{H}}_{\mathrm{eq}}(k^0,|\boldsymbol{k}|), \tag{B.10a}$$

$$a^{\mathcal{A}}_{\mathrm{eq}}(-k^0,|\boldsymbol{k}|) = a^{\mathcal{A}}_{\mathrm{eq}}(k^0,|\boldsymbol{k}|), \qquad b^{\mathcal{A}}_{\mathrm{eq}}(-k^0,|\boldsymbol{k}|) = -b^{\mathcal{A}}_{\mathrm{eq}}(k^0,|\boldsymbol{k}|), \tag{B.10b}$$

$$\delta a^{<}(-k^0,|\boldsymbol{k}|) = -\delta a^{>}(k^0,|\boldsymbol{k}|), \qquad \delta b^{<}(-k^0,|\boldsymbol{k}|) = \delta b^{>}(k^0,|\boldsymbol{k}|). \tag{B.10c}$$

C Adiabatic pole propagator inversion

In this paper we have used the leading order spectral approximation for the adiabatic solutions, which indeed is a good approximation in the weak coupling limit. In this appendix we show how to obtain more complete solutions for the adiabatic pole propagators $S^{r,a}_{\mathrm{ad}}(k,t)$. We start by writing equation (4.17a) in an equivalent form and with explicit flavour indices:

$$\sum_{l=1}^{2}\Big([\not{k} - m_i(t)]\delta_{il} - \Sigma^p_{\mathrm{eq},il}(k,t)\Big)S^p_{\mathrm{ad},lj}(k,t) = \delta_{ij}\mathbf{1}. \tag{C.1}$$

Generally, the inverse of a 2×2 block matrix A_{ij}, satisfying $\sum_{l=1}^{2} A_{il}S_{lj} = \delta_{ij}\mathbf{1}$, is given by $S_{ij} = (A_{ji} - A_{jk}A^{-1}_{lk}A_{li})^{-1}$ with $k \neq i$ and $l \neq j$. For given i and j the indices k and l are fixed, because the block dimension is only 2. This block-wise inversion formula can be generalised to larger block matrices, which would indeed be necessary if there were

more flavours. We now solve the flavour components of the pole propagators from (C.1) as follows (equivalent formulae were given in [83]):

$$S^p_{\mathrm{ad},ii}(k,t) = \Big[\not{k} - m_i - \Sigma^p_{\mathrm{eq},ii} - \Sigma^p_{\mathrm{eq},il}(\not{k} - m_l - \Sigma^p_{\mathrm{eq},ll})^{-1}\Sigma^p_{\mathrm{eq},li}\Big]^{-1} \quad (l \neq i), \tag{C.2}$$

$$S^p_{\mathrm{ad},ij}(k,t) = \Big[(\not{k} - m_j - \Sigma^p_{\mathrm{eq},jj})(\Sigma^p_{\mathrm{eq},ij})^{-1}(\not{k} - m_i - \Sigma^p_{\mathrm{eq},ii}) - \Sigma^p_{\mathrm{eq},ji}\Big]^{-1} \quad (i \neq j). \tag{C.3}$$

The inverses here are taken with respect to Dirac indices only and we suppressed the (k,t)-arguments of the self-energies. These solutions can also be obtained formally by expanding the inverse of $\not{k} - m - \Sigma^p_{\mathrm{eq}}$ as a geometric series in powers of the off-diagonal self-energy $\Sigma^p_{\mathrm{eq},ij}$ (with $i \neq j$) and performing a resummation of the series.

The solutions (C.2) and (C.3) are still general. We now use the leading order equilibrium self-energy Σ_{eq} given by equations (4.16a) and (4.16b). We neglect here the vacuum part of $\Sigma^{\mathrm{H}}_{\mathrm{eq}}$ which acquires additional Dirac and flavour structures from the vacuum on-shell renormalisation and would make the resulting formulae below more complicated. However, near the poles the vacuum part should only give small corrections. Hence, we use here the pole self-energies

$$\Sigma^p_{\mathrm{eq},ij}(k) = c_{\mathrm{w}}(y_i y_j^* P_{\mathrm{L}} + y_i^* y_j P_{\mathrm{R}})\gamma^\mu \mathfrak{S}^p_{\mathrm{eq},\mu}(k). \tag{C.4}$$

Using this form, the Dirac matrix inverses in equations (C.2) and (C.3) can be written explicitly as

$$S^p_{\mathrm{ad},ii}(k,t) = \frac{1}{D^p_{il}}\Big[D^p_l(\not{k} + m_i) - \widetilde{D}^p_l\Sigma^p_{\mathrm{eq},ii} - \Sigma^p_{\mathrm{eq},li}(\not{k} - m_l)\Sigma^p_{\mathrm{eq},il}\Big] \quad (l \neq i), \tag{C.5}$$

$$\begin{aligned} S^p_{\mathrm{ad},ij}(k,t) = \frac{1}{D^p_{ij}}\Big[&(\not{k} + m_i)\Sigma^p_{\mathrm{eq},ij}(\not{k} + m_j) - (\not{k} + m_i)\Sigma^p_{\mathrm{eq},ij}\Sigma^p_{\mathrm{eq},jj} \\ &- \Sigma^p_{\mathrm{eq},ii}\Sigma^p_{\mathrm{eq},ij}(\not{k} + m_j)\Big] \quad (i \neq j), \end{aligned} \tag{C.6}$$

with the definitions

$$\begin{aligned} D^p_{ij} \equiv \Delta_i\Delta_j\Big[1 &- 2c_{\mathrm{w}}(k\cdot\mathfrak{S}^p_{\mathrm{eq}})\Big(|y_i|^2\Delta_i^{-1} + |y_j|^2\Delta_j^{-1}\Big) \\ &+ c_{\mathrm{w}}^2(\mathfrak{S}^p_{\mathrm{eq}}\cdot\mathfrak{S}^p_{\mathrm{eq}})\Big(|y_i|^4\Delta_i^{-1} + |y_j|^4\Delta_j^{-1} \\ &+ 2|y_i|^2|y_j|^2(\Delta_i\Delta_j)^{-1}\big(k^2 - \cos(2\theta_{ij})m_i m_j\big)\Big)\Big], \end{aligned} \tag{C.7a}$$

$$D^p_l \equiv \Delta_l - 2c_{\mathrm{w}}|y_l|^2(k\cdot\mathfrak{S}^p_{\mathrm{eq}}) + c_{\mathrm{w}}^2|y_l|^4(\mathfrak{S}^p_{\mathrm{eq}}\cdot\mathfrak{S}^p_{\mathrm{eq}}), \tag{C.7b}$$

$$\widetilde{D}^p_l \equiv \Delta_l - 2c_{\mathrm{w}}|y_l|^2(k\cdot\mathfrak{S}^p_{\mathrm{eq}}), \tag{C.7c}$$

$$\Delta_i \equiv k^2 - m_i^2. \tag{C.7d}$$

Note that since $D^p_{ij} = D^p_{ji}$, the denominator of all flavour components $S^p_{\mathrm{ad},ij}$ is the same, D^p_{12}. Using the formulae presented in this appendix, one can straightforwardly implement more accurate approximations for the adiabatic correlation functions (4.20) and the effective self-energies (4.26).

D Independent components of the neutrino Wightman function

The Hermiticity property (2.8a), the sum rule (2.9) and the Majorana condition (4.4) can be used to derive relations among the components of the neutrino Wightman functions. First, the Majorana condition (4.4) and equation (2.4) imply that $S^{>}_{\boldsymbol{k}}(t_1,t_2) = -CS^{<}_{-\boldsymbol{k}}(t_2,t_1)^{\mathrm{T}}C^{-1}$ in the two-time representation. We can then write the aforementioned three relations as

$$\overline{S}^{<}_{\boldsymbol{k}ij}(t,t) = \overline{S}^{<}_{\boldsymbol{k}ji}(t,t)^{\dagger}, \tag{D.1}$$

$$\overline{S}^{<}_{\boldsymbol{k}ij}(t,t) = \delta_{ij}\mathbf{1} - \overline{S}^{>}_{\boldsymbol{k}ij}(t,t), \tag{D.2}$$

$$\overline{S}^{>}_{\boldsymbol{k}ij}(t,t) = \gamma^0 C\, \overline{S}^{<}_{-\boldsymbol{k},ji}(t,t)^{\mathrm{T}}\, C^{-1}\gamma^0, \tag{D.3}$$

where we also used $2\overline{\mathcal{A}} = \overline{S}^{>} + \overline{S}^{<}$ in the sum rule. These identities hold for the full Majorana Wightman functions $\overline{S}^{<,>}_{\boldsymbol{k}ij}(t,t)$. Assuming that they hold independently for the adiabatic functions $\overline{S}^{<,>}_{\mathrm{ad},\boldsymbol{k}ij}(t,t)$ implies that the non-equilibrium local correlator $\delta\overline{S}^{<}_{\boldsymbol{k}ij}(t,t)$ satisfies the constraints

$$\delta\overline{S}^{<}_{\boldsymbol{k}ij}(t,t) = \delta\overline{S}^{<}_{\boldsymbol{k}ji}(t,t)^{\dagger}, \tag{D.4}$$

$$\delta\overline{S}^{<}_{\boldsymbol{k}ij}(t,t) = -\gamma^0 C\, \delta\overline{S}^{<}_{-\boldsymbol{k},ji}(t,t)^{\mathrm{T}}\, C^{-1}\gamma^0. \tag{D.5}$$

Inserting the parametrisation (5.2) into equations (D.4) and (D.5) and using the identity $\gamma^0 C(\mathcal{P}^{s's}_{-\boldsymbol{k},hji})^{\mathrm{T}}C^{-1}\gamma^0 = -\mathcal{P}^{-s,-s'}_{\boldsymbol{k}hij}$, we get constraints for the phase space functions:

$$\delta f^{ss'}_{\boldsymbol{k}hij} = (\delta f^{s's}_{\boldsymbol{k}hji})^{*} = \delta f^{-s',-s}_{\boldsymbol{k}hji}. \tag{D.6}$$

In terms of the mass and coherence shell functions (5.13) and (5.14) these read

$$\delta f^{m,s}_{\boldsymbol{k}hij} = (\delta f^{m,s}_{\boldsymbol{k}hji})^{*} = \delta f^{m,-s}_{\boldsymbol{k}hji}, \tag{D.7}$$

$$\delta f^{c,s}_{\boldsymbol{k}hij} = (\delta f^{c,-s}_{\boldsymbol{k}hji})^{*} = \delta f^{c,s}_{\boldsymbol{k}hji}. \tag{D.8}$$

In the case of two neutrino flavours ($i,j = 1,2$) these relations imply that for a given helicity h the sixteen different (s,s',i,j) components of $\delta f_{\boldsymbol{k}h}$ can be reduced to only six independent distributions with 10 degrees of freedom, given explicitly by the following equations:

$$\delta f^{m,+}_{\boldsymbol{k}h11} = \delta f^{m,-}_{\boldsymbol{k}h11} \quad \text{(real)}, \tag{D.9a}$$

$$\delta f^{m,+}_{\boldsymbol{k}h22} = \delta f^{m,-}_{\boldsymbol{k}h22} \quad \text{(real)}, \tag{D.9b}$$

$$\delta f^{m,+}_{\boldsymbol{k}h12} = (\delta f^{m,-}_{\boldsymbol{k}h12})^{*} = (\delta f^{m,+}_{\boldsymbol{k}h21})^{*} = \delta f^{m,-}_{\boldsymbol{k}h21} \quad \text{(complex)}, \tag{D.9c}$$

and

$$\delta f^{c,+}_{\boldsymbol{k}h11} = (\delta f^{c,-}_{\boldsymbol{k}h11})^{*} \quad \text{(complex)}, \tag{D.9d}$$

$$\delta f^{c,+}_{\boldsymbol{k}h22} = (\delta f^{c,-}_{\boldsymbol{k}h22})^{*} \quad \text{(complex)}, \tag{D.9e}$$

$$\delta f^{c,+}_{\boldsymbol{k}h12} = (\delta f^{c,-}_{\boldsymbol{k}h12})^{*} = \delta f^{c,+}_{\boldsymbol{k}h21} = (\delta f^{c,-}_{\boldsymbol{k}h21})^{*} \quad \text{(complex)}. \tag{D.9f}$$

Note that these relations are satisfied for perturbations when the sum rule (D.2) is satisfied by the *full* adiabatic solution. This is true e.g. for a full thermal solution and for the free particle solution (4.23). One can still use approximative forms for the adiabatic solutions in various expressions for the sources and collision terms.

E Neutrino collision term traces

Here we give explicit results for the collision term trace functions $C^{sss}_{\boldsymbol{k}hilj}$ which we use in the mass shell equation (5.15) of the Majorana neutrinos. We actually need only the $s = +1$ component $C^{+++}_{\boldsymbol{k}hilj}$ because of the relations (D.9) and because we only solve the positive energy solutions. Using the definition (5.8) and the leading order expansion (4.27) for the effective self-energy, we get first $C^{+++}_{\boldsymbol{k}hilj} = \mathrm{i}\,\mathrm{tr}\big[\mathcal{P}^{++}_{\boldsymbol{k}hji}\overline{\Sigma}^{r}_{\mathrm{eq},il}(k_{+l})\mathcal{P}^{++}_{\boldsymbol{k}hlj}\big]$. Here the self-energy is given in the Wigner representation and evaluated at the four-momentum $(k_{+l})^\mu \equiv (+\omega_{\boldsymbol{k}l}, \boldsymbol{k})$.

Next we observe that in the case with two flavours $(i, l, j = 1, 2)$ $\mathcal{P}^{ss}_{\boldsymbol{k}hlj}\mathcal{P}^{ss}_{\boldsymbol{k}hji} = \mathcal{P}^{ss}_{\boldsymbol{k}hli}$, which implies that $C^{+++}_{\boldsymbol{k}hilj} = \mathrm{i}\,\mathrm{tr}\big[\mathcal{P}^{++}_{\boldsymbol{k}hli}\overline{\Sigma}^{r}_{\mathrm{eq},il}(k_{+l})\big]$. Notably, the collision function is in this specific case independent of the last flavour index j. Using equations (4.16) and (4.51) for the equilibrium Majorana self-energy functions with $\overline{\Sigma}^r = \gamma_0\Sigma^r$ and $\Sigma^r = \Sigma^{\mathrm{H}} - \mathrm{i}\Sigma^{\mathcal{A}}$, and performing the Dirac matrix trace yields the result

$$
\begin{aligned}
C^{+++}_{\boldsymbol{k}hilj} = \frac{c_{\mathrm{w}}N^{m}_{\boldsymbol{k}il}}{2\omega_{\boldsymbol{k}i}\omega_{\boldsymbol{k}l}}\Big[&\mathrm{Re}(y_i^* y_l)(m_i k_{+l} + m_l k_{+i})^\mu - \mathrm{i}h\,\mathrm{Im}(y_i^* y_l)(m_i k^{\perp}_{+l} + m_l k^{\perp}_{+i})^\mu\Big] \\
&\times \Big(\mathfrak{S}^{\mathcal{A}}_{\mathrm{eq}}(k_{+l}) + \mathrm{i}\mathfrak{S}^{\mathrm{H}(T)}_{\mathrm{eq}}(k_{+l})\Big)_\mu .
\end{aligned}
\tag{E.1}
$$

The self-energy four-vector functions $\mathfrak{S}_\mu$ are calculated in appendix B. We also defined $N^m_{\boldsymbol{k}ij} \equiv N^{ss}_{\boldsymbol{k}hij}$ (see equation (5.3)) and $(k^\perp)^\mu \equiv (|\boldsymbol{k}|, k^0\hat{\boldsymbol{k}})$.

F Lepton CP-source and washout terms

Explicit forms for the CP-source and washout terms were given in equations (5.10)–(5.12). We now substitute the self-energy functions defined in (4.16a) and (4.16c) to these expressions and use the symmetry properties (B.10b) and (B.10c). We also use the lowest order result (4.27) for the effective self-energy, adapted for $\overline{\Sigma}^{\mathcal{A}}_{\mathrm{L}} \equiv P_{\mathrm{R}}\overline{\Sigma}^{\mathcal{A}}$ and the constraints (D.9) for the non-equilibrium distribution functions. We keep the coherence shell functions here for completeness, but split the results to separate mass and coherence shell parts, $S_{\mathrm{CP}} = S^m_{\mathrm{CP}} + S^c_{\mathrm{CP}}$ and $\delta W = \delta W^m + \delta W^c$. After performing the traces, we get

$$
\begin{aligned}
S^m_{\mathrm{CP}} = \sum_{i,j}\int \frac{\mathrm{d}^3\boldsymbol{k}}{(2\pi)^3}\frac{c_{\mathrm{w}}N^m_{\boldsymbol{k}ij}}{2\omega_{\boldsymbol{k}i}\omega_{\boldsymbol{k}j}}\Big[&\mathrm{Re}(y_i^* y_j)\textstyle\sum_h h\,\mathrm{Re}(\delta f^{m,+}_{\boldsymbol{k}hij})(m_i k^{\perp}_{+j} + m_j k^{\perp}_{+i})^\mu \\
&- \mathrm{Im}(y_i^* y_j)\textstyle\sum_h \mathrm{Im}(\delta f^{m,+}_{\boldsymbol{k}hij})(m_i k_{+j} + m_j k_{+i})^\mu\Big] \\
&\times \Big(\mathfrak{S}^{\mathcal{A}}_{\mathrm{eq}}(k_{+i}) + \mathfrak{S}^{\mathcal{A}}_{\mathrm{eq}}(k_{+j})\Big)_\mu ,
\end{aligned}
\tag{F.1a}
$$

$$
\begin{aligned}
S^c_{\mathrm{CP}} = \sum_{i,j}\int \frac{\mathrm{d}^3\boldsymbol{k}}{(2\pi)^3}\frac{c_{\mathrm{w}}N^c_{\boldsymbol{k}ij}}{2\omega_{\boldsymbol{k}i}\omega_{\boldsymbol{k}j}}\Big[&-\mathrm{Re}(y_i^* y_j)\textstyle\sum_h h\,\mathrm{Re}(\delta f^{c,+}_{\boldsymbol{k}hij})(m_i k^{\perp}_{+j} + m_j k^{\perp}_{-i})^\mu \\
&- \mathrm{Im}(y_i^* y_j)\textstyle\sum_h \mathrm{Im}(\delta f^{c,+}_{\boldsymbol{k}hij})(m_i k_{+j} + m_j k_{-i})^\mu\Big] \\
&\times \Big(\mathfrak{S}^{\mathcal{A}}_{\mathrm{eq}}(k_{-i}) + \mathfrak{S}^{\mathcal{A}}_{\mathrm{eq}}(k_{+j})\Big)_\mu ,
\end{aligned}
\tag{F.1b}
$$

and

$$\frac{\delta W^m}{\beta\mu_\ell} = \sum_{i,j}\int \frac{\mathrm{d}^3\boldsymbol{k}}{(2\pi)^3}\frac{c_{\rm w}N^m_{\boldsymbol{k}ij}}{2\omega_{\boldsymbol{k}i}\omega_{\boldsymbol{k}j}}\Big[\,\mathrm{Re}(y_i^*y_j)\textstyle\sum_h \mathrm{Re}(\delta f^{m,+}_{\boldsymbol{k}hij})(m_i k_{+j} + m_j k_{+i})^\mu \\ - \,\mathrm{Im}(y_i^*y_j)\textstyle\sum_h h\,\mathrm{Im}(\delta f^{m,+}_{\boldsymbol{k}hij})(m_i k^\perp_{+j} + m_j k^\perp_{+i})^\mu\Big] \\ \times\Big(\delta\mathfrak{S}^{\mathcal{A}}(k_{+i}) + \delta\mathfrak{S}^{\mathcal{A}}(k_{+j})\Big)_\mu, \tag{F.2a}$$

$$\frac{\delta W^c}{\beta\mu_\ell} = \sum_{i,j}\int \frac{\mathrm{d}^3\boldsymbol{k}}{(2\pi)^3}\frac{c_{\rm w}N^c_{\boldsymbol{k}ij}}{2\omega_{\boldsymbol{k}i}\omega_{\boldsymbol{k}j}}\Big[-\mathrm{Re}(y_i^*y_j)\textstyle\sum_h \mathrm{Re}(\delta f^{c,+}_{\boldsymbol{k}hij})(m_i k_{+j} + m_j k_{-i})^\mu \\ - \,\mathrm{Im}(y_i^*y_j)\textstyle\sum_h h\,\mathrm{Im}(\delta f^{c,+}_{\boldsymbol{k}hij})(m_i k^\perp_{+j} + m_j k^\perp_{-i})^\mu\Big] \\ \times\Big(\delta\mathfrak{S}^{\mathcal{A}}(k_{-i}) + \delta\mathfrak{S}^{\mathcal{A}}(k_{+j})\Big)_\mu. \tag{F.2b}$$

Here μ_ℓ is the lepton chemical potential, $\beta = 1/T$, and we further defined $(k^\perp)^\mu \equiv (|\boldsymbol{k}|, k^0\hat{\boldsymbol{k}})$. The self-energy functions $\mathfrak{S}^{\mathcal{A}}_{\mathrm{eq},\mu}$ and $\delta\mathfrak{S}^{\mathcal{A}}_\mu = (\delta\mathfrak{S}^>_\mu + \delta\mathfrak{S}^<_\mu)/2$ are calculated in section B. We also defined here $N^m_{\boldsymbol{k}ij} \equiv N^{ss}_{\boldsymbol{k}hij}$ and $N^c_{\boldsymbol{k}ij} \equiv N^{s,-s}_{\boldsymbol{k}hij}$ using equation (5.3). Finally, the adiabatic washout term $W_{\rm ad}$ can be simplified to

$$\frac{W_{\rm ad}}{\beta\mu_\ell} = c_{\rm w}\sum_i\int\frac{\mathrm{d}^3\boldsymbol{k}}{(2\pi)^3}\frac{2|y_i|^2}{\omega_{\boldsymbol{k}i}}\Big[2f_{\rm FD}(\omega_{\boldsymbol{k}i})\,k_{+i}\cdot\delta\mathfrak{S}^{\mathcal{A}}(k_{+i}) - k_{+i}\cdot\delta\mathfrak{S}^<(k_{+i})\Big]. \tag{F.3}$$

The results (F.1a) and (F.2a) show explicitly how the helicity sums of the non-equilibrium distribution functions $\delta f_{\boldsymbol{k}h}$ enter the leading order CP-source and washout terms. In particular, from equation (F.1a) we see that CP-violation is only sourced by the helicity-odd combinations $\mathrm{Re}(\delta f_{\boldsymbol{k},+1} - \delta f_{\boldsymbol{k},-1})$ of the real parts and helicity-even combinations $\mathrm{Im}(\delta f_{\boldsymbol{k},+1} + \delta f_{\boldsymbol{k},-1})$ of the imaginary parts.

G Semiclassical Boltzmann equations

For comparison with our main quantum kinetic equations, we implement and solve numerically the semiclassical Boltzmann equations (see e.g. [84, 88, 97, 103, 104]) and the momentum integrated rate equations in our model (4.1). We include only the decay and inverse decay contributions supplemented by a RIS-correction term required to cure the problem of spurious equilibrium source [88, 97, 104]. We write the equations first following ref. [103], to establish the notation and to facilitate comparison with the literature. We then present the equations in a more compact form which is directly comparable to our main equations and also more suitable for a numerical implementation.

G.1 Momentum-dependent equations

As in the main text, we assume that SM-fields are in kinetic equilibrium and that Higgs field chemical potential vanishes, $\mu_\phi = 0$. However, we make no assumption about the form of the phase space distribution functions f_i of the Majorana neutrinos $i = 1, 2$, and consider full quantum statistics with Pauli blocking and stimulated emission factors. In

the expanding universe, the Boltzmann equations for f_i and the lepton asymmetry n_L can then be written as

$$\begin{aligned}\frac{\partial f_i}{\partial t} - |\boldsymbol{p}_i| H \frac{\partial f_i}{\partial |\boldsymbol{p}_i|} &= \frac{1}{2\omega_i g_i} \int \mathrm{d}\pi_\ell \, \mathrm{d}\pi_\phi \, (2\pi)^4 \delta(\omega_i - \omega_\ell - \omega_\phi) \delta^{(3)}(\boldsymbol{p}_i - \boldsymbol{p}_\ell - \boldsymbol{p}_\phi) \\ &\quad \times |\mathcal{M}_i|^2 \Big\{ -f_i (1 - f_\ell^+)(1 + f_\phi^{\mathrm{eq}}) + f_\ell^+ f_\phi^{\mathrm{eq}} (1 - f_i) \\ &\qquad + \varepsilon_i^{\mathrm{CP}} f_\ell^- \Big[f_i (1 + f_\phi^{\mathrm{eq}}) - f_\phi^{\mathrm{eq}} (1 - f_i) \Big] \Big\}, \end{aligned} \tag{G.1}$$

$$\begin{aligned}\frac{\mathrm{d}n_L}{\mathrm{d}t} + 3Hn_L &= \sum_i \int \mathrm{d}\pi_i \, \mathrm{d}\pi_\ell \, \mathrm{d}\pi_\phi \, (2\pi)^4 \delta(\omega_i - \omega_\ell - \omega_\phi) \delta^{(3)}(\boldsymbol{p}_i - \boldsymbol{p}_\ell - \boldsymbol{p}_\phi) \\ &\quad \times |\mathcal{M}_i|^2 \Big\{ -f_\ell^- \Big[f_\phi^{\mathrm{eq}} (1 - f_i) + f_i (1 + f_\phi^{\mathrm{eq}}) \Big] \\ &\qquad + \varepsilon_i^{\mathrm{CP}} \Big[-f_\ell^+ f_\phi^{\mathrm{eq}} (1 - f_i) + f_i (1 - f_L^+)(1 + f_\phi^{\mathrm{eq}}) \Big] \Big\}. \end{aligned} \tag{G.2}$$

Here $f_x(\boldsymbol{p}_x, t)$ is the phase space distribution function, $\omega_x \equiv \sqrt{|\boldsymbol{p}_x|^2 + m_x^2}$ is the on-shell energy and $\mathrm{d}\pi_x \equiv \mathrm{d}^3\boldsymbol{p}_x/(2\pi)^3/(2\omega_x)$ is the phase space integration element for particle species $x = i, \ell, \phi$. The RIS-subtraction has been performed as in [88, 97, 104], which ensures that also the term associated with the CP-asymmetry parameter $\varepsilon_i^{\mathrm{CP}}$ in equation (G.2) vanishes in thermal equilibrium. For the number densities and distribution functions we are using the following notations:

$$n_L \equiv n_\ell - \bar{n}_\ell, \qquad n_\ell = c_{\mathrm{w}} \int \frac{\mathrm{d}^3\boldsymbol{p}_\ell}{(2\pi)^3} f_\ell, \qquad \bar{n}_\ell = c_{\mathrm{w}} \int \frac{\mathrm{d}^3\boldsymbol{p}_\ell}{(2\pi)^3} \bar{f}_\ell, \tag{G.3a}$$

$$f_\ell^\pm \equiv (f_\ell \pm \bar{f}_\ell)/2, \qquad f_\ell = f_{\mathrm{FD}}(\omega_\ell - \mu_\ell), \qquad \bar{f}_\ell = f_{\mathrm{FD}}(\omega_\ell + \mu_\ell), \tag{G.3b}$$

$$f_\phi = \bar{f}_\phi = f_\phi^{\mathrm{eq}} = f_{\mathrm{BE}}(\omega_\phi), \tag{G.3c}$$

where f_{FD} and f_{BE} are the Fermi-Dirac and Bose-Einstein distribution functions (4.12). The factor $c_{\mathrm{w}} = 2$ is the SM doublet multiplicity and $g_i = 2$ is the number of spin (or helicity) states of the Majorana neutrino N_i. Finally, the tree level matrix element for the neutrino decay process, summed over the Majorana neutrino spins and the SM doublet multiplicity is:

$$|\mathcal{M}_i|^2 \equiv \big|\mathcal{M}(N_i \to \ell\phi)\big|^2 + \big|\mathcal{M}(N_i \to \bar{\ell}\bar{\phi})\big|^2 = 2c_{\mathrm{w}} |y_i|^2 m_i^2, \tag{G.4}$$

where $m_\ell = m_\phi = 0$ was assumed in the end. The corresponding total decay width is then $\Gamma_i^{(0)} \equiv |\mathcal{M}_i|^2/(16\pi g_i m_i) = |y_i|^2 m_i/(8\pi)$. In the following we use these tree level results for the leading approximation.

We now give equations (G.1) and (G.2) in a more compact dimensionless form similar to (6.10) and (6.11), in terms of the variable $z = m_1/T$. We also omit the lepton back-reaction term (proportional to $\varepsilon_i^{\mathrm{CP}} f_\ell^-$) in equation (G.1), as we did in (6.10). Working consistently to linear order in perturbations we then find

$$\frac{\mathrm{d}\delta f_{\boldsymbol{k}i}}{\mathrm{d}z} = -\tilde{C}_{\boldsymbol{k}i} \, \delta f_{\boldsymbol{k}i} - \frac{\mathrm{d}f_{\boldsymbol{k}i}^{\mathrm{eq}}}{\mathrm{d}z}, \tag{G.5}$$

$$\frac{\mathrm{d}Y_L}{\mathrm{d}z} = \tilde{S}_{\mathrm{CP}} + (\delta\tilde{W} + \tilde{W}_{\mathrm{ad}}) Y_L, \tag{G.6}$$

where $Y_L = n_L/s$, s is the entropy density, $\delta f_{\boldsymbol{k}i} \equiv f_{\boldsymbol{k}i} - f^{\rm eq}_{\boldsymbol{k}i}$ and $f^{\rm eq}_{\boldsymbol{k}i} = f_{\rm FD}(\omega_{\boldsymbol{k}i})$. The dimensionless neutrino collision term coefficient, CP-violating lepton source term and the lepton washout term coefficients are here given by

$$\tilde{C}_{\boldsymbol{k}i} = \frac{z\Gamma_i^{(0)}}{H_1}\Big(\frac{m_i}{\omega_{\boldsymbol{k}i}}\mathcal{X}_{\boldsymbol{k}i}\Big), \tag{G.7}$$

$$\tilde{S}_{\rm CP} = \sum_i \frac{z\Gamma_i^{(0)}}{H_1}\frac{g_i}{s}\,\varepsilon_i^{\rm CP}\int\frac{{\rm d}^3\boldsymbol{k}}{(2\pi)^3}\Big(\frac{m_i}{\omega_{\boldsymbol{k}i}}\mathcal{X}_{\boldsymbol{k}i}\Big)\delta f_{\boldsymbol{k}i}, \tag{G.8}$$

$$\delta\tilde{W} = \sum_i \frac{z\Gamma_i^{(0)}}{H_1}\frac{6g_i}{c_{\rm w}T^3}\int\frac{{\rm d}^3\boldsymbol{k}}{(2\pi)^3}\Big(\frac{m_i}{\omega_{\boldsymbol{k}i}}\mathcal{Y}^{(A)}_{\boldsymbol{k}i}\Big)\delta f_{\boldsymbol{k}i}, \tag{G.9}$$

$$\tilde{W}_{\rm ad} = \sum_i \frac{z\Gamma_i^{(0)}}{H_1}\frac{6g_i}{c_{\rm w}T^3}\int\frac{{\rm d}^3\boldsymbol{k}}{(2\pi)^3}\Big(\frac{m_i}{\omega_{\boldsymbol{k}i}}\mathcal{Y}^{(B)}_{\boldsymbol{k}i}\Big)\,, \tag{G.10}$$

with $H_1 \equiv H(m_1)$ and

$$\mathcal{X}_{\boldsymbol{k}i} = \frac{T}{|\boldsymbol{k}|}\log\Big[\frac{{\rm e}^{(\omega_{\boldsymbol{k}i}+|\boldsymbol{k}|)/T}-1}{{\rm e}^{\omega_{\boldsymbol{k}i}/T}-{\rm e}^{|\boldsymbol{k}|/T}}\Big], \tag{G.11}$$

$$\mathcal{Y}^{(A)}_{\boldsymbol{k}i} = \frac{T}{|\boldsymbol{k}|}\Big[f_{\rm FD}\Big(\frac{\omega_{\boldsymbol{k}i}+|\boldsymbol{k}|}{2}\Big) - f_{\rm FD}\Big(\frac{\omega_{\boldsymbol{k}i}-|\boldsymbol{k}|}{2}\Big)\Big], \tag{G.12}$$

$$\mathcal{Y}^{(B)}_{\boldsymbol{k}i} = f_{\rm FD}(\omega_{\boldsymbol{k}i})(f_{\rm FD}(\omega_{\boldsymbol{k}i})-1)\mathcal{X}_{\boldsymbol{k}i}. \tag{G.13}$$

For the total z-derivative of $f^{\rm eq}_{\boldsymbol{k}i}$ we use ${\rm d}f^{\rm eq}_{\boldsymbol{k}i}/\,{\rm d}z = f^{\rm eq}_{\boldsymbol{k}i}(f^{\rm eq}_{\boldsymbol{k}i}-1)m_i^2/(m_1\omega_{\boldsymbol{k}i})$, assuming that $|\boldsymbol{k}|/T$ is independent of z. Note also that $n_L\tilde{W}_{\rm ad}H_1/z$ is exactly equal to the $W_{\rm ad}$ defined by (F.3), when we use $n_L \approx c_{\rm w}T^2\mu_\ell/6$.

G.2 Rate equations

Simplified rate equations for the number densities can be derived from the Boltzmann equations (G.1) and (G.2) with two additional assumptions: kinetic approximation for the Majorana neutrino distributions and Maxwell-Boltzmann statistics for all particle species. To this end, we use $f_i = (n_i/n_i^{\rm eq})f_i^{\rm eq}$, replace $f_{\rm FD}$ and $f_{\rm BE}$ by $f_{\rm MB}(k^0) \equiv {\rm e}^{-k^0/T}$ and remove all extra terms originating from the Pauli blocking and stimulated emission factors. Integrating equations (G.1) and (G.2) over momenta then gives:

$$\frac{{\rm d}n_i}{{\rm d}t} + 3Hn_i = -\Big(\frac{n_i}{n_i^{\rm eq}}-1\Big)\gamma_i - \frac{n_L}{2n_\ell^{\rm eq}}\varepsilon_i^{\rm CP}\gamma_i, \tag{G.14}$$

$$\frac{{\rm d}n_L}{{\rm d}t} + 3Hn_L = \sum_i\Big[\Big(\frac{n_i}{n_i^{\rm eq}}-1\Big)\varepsilon_i^{\rm CP}\gamma_i - \frac{n_L}{2n_\ell^{\rm eq}}\gamma_i\Big], \tag{G.15}$$

where

$$\gamma_i = g_i\Gamma_i\int\frac{{\rm d}^3\boldsymbol{p}_i}{(2\pi)^3}\frac{m_i}{\omega_i}\,{\rm e}^{-\omega_i/T} = n_i^{\rm eq}\frac{\mathcal{K}_1(m_i/T)}{\mathcal{K}_2(m_i/T)}\Gamma_i, \tag{G.16}$$

$$n_i^{\rm eq} = g_i\int\frac{{\rm d}^3\boldsymbol{p}_i}{(2\pi)^3}\,{\rm e}^{-\omega_i/T} \qquad = \frac{g_i m_i^2 T}{2\pi^2}\mathcal{K}_2(m_i/T), \tag{G.17}$$

$$n_\ell^{\rm eq} = c_{\rm w}\int\frac{{\rm d}^3\boldsymbol{p}_\ell}{(2\pi)^3}\,{\rm e}^{-|\boldsymbol{p}_\ell|/T} \qquad = \frac{c_{\rm w}T^3}{\pi^2}. \tag{G.18}$$

Here $\mathcal{K}_n$ are the modified Bessel functions of the second kind. Here we kept also the lepton backreaction term which is the last term on the right-hand side of equation (G.14).

Again, we can write equations (G.14) and (G.15) in a compact dimensionless form:

$$\frac{\mathrm{d}\delta Y_i}{\mathrm{d}z} = -D_i\,\delta Y_i - \frac{\mathrm{d}Y_i^{\mathrm{eq}}}{\mathrm{d}z} - \frac{Y_i^{\mathrm{eq}}}{2Y_\ell^{\mathrm{eq}}}\varepsilon_i^{\mathrm{CP}} D_i Y_L, \tag{G.19}$$

$$\frac{\mathrm{d}Y_L}{\mathrm{d}z} = \sum_i \left[\varepsilon_i^{\mathrm{CP}} D_i\,\delta Y_i - \frac{Y_i^{\mathrm{eq}}}{2Y_\ell^{\mathrm{eq}}} D_i Y_L\right], \tag{G.20}$$

where $\delta Y_i \equiv Y_i - Y_i^{\mathrm{eq}}$ and

$$Y_x = \frac{n_x}{s}, \qquad z = \frac{m_1}{T}, \qquad D_i = \frac{z\Gamma_i^{(0)}}{H_1}\frac{\mathcal{K}_1(zx_i)}{\mathcal{K}_2(zx_i)}, \qquad x_i = \frac{m_i}{m_1}. \tag{G.21}$$

The lepton source term in these equations is given by $\tilde{S}_{\mathrm{CP}} = \sum_i \varepsilon_i^{\mathrm{CP}} D_i\,\delta Y_i$ and for the washout term $\delta\tilde{W} = 0$ and $\tilde{W}_{\mathrm{ad}} = -\sum_i D_i Y_i^{\mathrm{eq}}/(2Y_\ell^{\mathrm{eq}})$. We used these equations also to check that the lepton backreaction was indeed numerically negligible in all examples (with vanishing initial lepton asymmetry) that we studied.

G.3 CP-asymmetry parameter

The Boltzmann equations (G.1), (G.2), (G.5), (G.6), (G.14), (G.15), (G.19) and (G.20) given above do not depend on the exact form of the CP-asymmetry parameter $\varepsilon_i^{\mathrm{CP}}$. There we used the generic definition (in the unflavoured case)

$$\varepsilon_i^{\mathrm{CP}} = \frac{\Gamma(N_i \to \ell\phi) - \Gamma(N_i \to \bar{\ell}\bar{\phi})}{\Gamma(N_i \to \ell\phi) + \Gamma(N_i \to \bar{\ell}\bar{\phi})}, \tag{G.22}$$

where $\Gamma(N_i \to \ell\phi) + \Gamma(N_i \to \bar{\ell}\bar{\phi}) = \Gamma_i$ is the total (vacuum) decay width of the Majorana neutrino to the lepton and Higgs doublets. The CP-asymmetry parameter vanishes at tree-level and is calculated from the interference of tree level and higher order amplitudes. This is highly nontrivial, as the calculation breaks down when using ordinary perturbation theory in the degenerate limit $m_2 \to m_1$.

We only consider the self-energy contribution (also called indirect or ε-type CP-violation), neglecting the vertex correction (i.e. the direct ε'-type CP-violation), and use the generic form

$$\varepsilon_{i,x}^{\mathrm{CP}} = \frac{\mathrm{Im}[(y_1^* y_2)^2]}{|y_1|^2|y_2|^2}\frac{(m_2^2 - m_1^2)m_i\Gamma_j^{(0)}}{(m_2^2 - m_1^2)^2 + (R_{ij,x})^2}. \qquad (j \neq i) \tag{G.23}$$

This result is specific to the case of two Majorana neutrinos and one lepton flavour. Here $R_{ij,x}$ is the regulator which removes the singularity that would occur when $m_2 \to m_1$. We consider four alternative regulators [62, 70, 83, 84, 105] (the subscript x): the 'mixed' regulator, the 'difference' regulator, the 'sum' regulator and the 'effective' sum regulator

given by

$$R_{ij,\text{mix}} = m_i \Gamma_j^{(0)}, \tag{G.24}$$

$$R_{ij,\text{diff}} = m_i \Gamma_i^{(0)} - m_j \Gamma_j^{(0)}, \tag{G.25}$$

$$R_{ij,\text{sum}} = m_i \Gamma_i^{(0)} + m_j \Gamma_j^{(0)}, \tag{G.26}$$

$$R_{ij,\text{eff}} = (m_i \Gamma_i^{(0)} + m_j \Gamma_j^{(0)}) |\sin \theta_{ij}|. \tag{G.27}$$

The relative phase θ_{ij} of the Yukawa couplings was defined in equation (7.6). Note that $\varepsilon_{i,\text{diff}}^{\text{CP}}$ with the difference regulator is still singular if $|y_1| = |y_2|$. This means that it is unbound and leads to unphysical results when approaching the doubly degenerate limit $|y_2| \to |y_1|$ and $m_2 \to m_1$. For more discussion about the validity of different regulators, see [96].

References

[1] S.M. Bilenky and S.T. Petcov, *Massive Neutrinos and Neutrino Oscillations*, *Rev. Mod. Phys.* **59** (1987) 671 [INSPIRE].

[2] R. Barbieri and A. Dolgov, *Bounds on Sterile-neutrinos from Nucleosynthesis*, *Phys. Lett. B* **237** (1990) 440 [INSPIRE].

[3] K. Enqvist, K. Kainulainen and J. Maalampi, *Refraction and Oscillations of Neutrinos in the Early Universe*, *Nucl. Phys. B* **349** (1991) 754 [INSPIRE].

[4] K. Kainulainen, *Light Singlet Neutrinos and the Primordial Nucleosynthesis*, *Phys. Lett. B* **244** (1990) 191 [INSPIRE].

[5] K. Enqvist, K. Kainulainen and J. Maalampi, *Resonant neutrino transitions and nucleosynthesis*, *Phys. Lett. B* **249** (1990) 531 [INSPIRE].

[6] R. Barbieri and A. Dolgov, *Neutrino oscillations in the early universe*, *Nucl. Phys. B* **349** (1991) 743 [INSPIRE].

[7] K. Enqvist, K. Kainulainen and M.J. Thomson, *Stringent cosmological bounds on inert neutrino mixing*, *Nucl. Phys. B* **373** (1992) 498 [INSPIRE].

[8] G. Sigl and G. Raffelt, *General kinetic description of relativistic mixed neutrinos*, *Nucl. Phys. B* **406** (1993) 423 [INSPIRE].

[9] A. Vlasenko, G.M. Fuller and V. Cirigliano, *Neutrino Quantum Kinetics*, *Phys. Rev. D* **89** (2014) 105004 [arXiv:1309.2628] [INSPIRE].

[10] M. Joyce, T. Prokopec and N. Turok, *Nonlocal electroweak baryogenesis. Part 1: Thin wall regime*, *Phys. Rev. D* **53** (1996) 2930 [hep-ph/9410281] [INSPIRE].

[11] J.M. Cline, M. Joyce and K. Kainulainen, *Supersymmetric electroweak baryogenesis in the WKB approximation*, *Phys. Lett. B* **417** (1998) 79 [*Erratum ibid.* **448** (1999) 321] [hep-ph/9708393] [INSPIRE].

[12] K. Kainulainen, T. Prokopec, M.G. Schmidt and S. Weinstock, *First principle derivation of semiclassical force for electroweak baryogenesis*, *JHEP* **06** (2001) 031 [hep-ph/0105295] [INSPIRE].

[13] K. Kainulainen, T. Prokopec, M.G. Schmidt and S. Weinstock, *Semiclassical force for electroweak baryogenesis: Three-dimensional derivation*, *Phys. Rev. D* **66** (2002) 043502 [hep-ph/0202177] [INSPIRE].

[14] J.M. Cline and K. Kainulainen, *Electroweak baryogenesis at high bubble wall velocities*, *Phys. Rev. D* **101** (2020) 063525 [arXiv:2001.00568] [INSPIRE].

[15] A.E. Nelson, D.B. Kaplan and A.G. Cohen, *Why there is something rather than nothing: Matter from weak interactions*, *Nucl. Phys. B* **373** (1992) 453 [INSPIRE].

[16] P. Huet and A.E. Nelson, *CP violation and electroweak baryogenesis in extensions of the standard model*, *Phys. Lett. B* **355** (1995) 229 [hep-ph/9504427] [INSPIRE].

[17] A. Riotto, *More about electroweak baryogenesis in the minimal supersymmetric standard model*, *Int. J. Mod. Phys. D* **7** (1998) 815 [hep-ph/9709286] [INSPIRE].

[18] M. Postma and J. Van De Vis, *Source terms for electroweak baryogenesis in the vev-insertion approximation beyond leading order*, *JHEP* **02** (2020) 090 [arXiv:1910.11794] [INSPIRE].

[19] M. Fukugita and T. Yanagida, *Baryogenesis Without Grand Unification*, *Phys. Lett. B* **174** (1986) 45 [INSPIRE].

[20] S. Davidson, E. Nardi and Y. Nir, *Leptogenesis*, *Phys. Rept.* **466** (2008) 105 [arXiv:0802.2962] [INSPIRE].

[21] S. Blanchet and P. Di Bari, *The minimal scenario of leptogenesis*, *New J. Phys.* **14** (2012) 125012 [arXiv:1211.0512] [INSPIRE].

[22] D.J.H. Chung, E.W. Kolb, A. Riotto and I.I. Tkachev, *Probing Planckian physics: Resonant production of particles during inflation and features in the primordial power spectrum*, *Phys. Rev. D* **62** (2000) 043508 [hep-ph/9910437] [INSPIRE].

[23] L.A. Kofman and A.D. Linde, *Generation of Density Perturbations in the Inflationary Cosmology*, *Nucl. Phys. B* **282** (1987) 555 [INSPIRE].

[24] M. Fairbairn, K. Kainulainen, T. Markkanen and S. Nurmi, *Despicable Dark Relics: generated by gravity with unconstrained masses*, *JCAP* **04** (2019) 005 [arXiv:1808.08236] [INSPIRE].

[25] V.A. Kuzmin, V.A. Rubakov and M.E. Shaposhnikov, *On the Anomalous Electroweak Baryon Number Nonconservation in the Early Universe*, *Phys. Lett. B* **155** (1985) 36 [INSPIRE].

[26] G. 't Hooft, *Computation of the Quantum Effects Due to a Four-Dimensional Pseudoparticle*, *Phys. Rev. D* **14** (1976) 3432 [*Erratum ibid.* **18** (1978) 2199] [INSPIRE].

[27] F.R. Klinkhamer and N.S. Manton, *A Saddle Point Solution in the Weinberg-Salam Theory*, *Phys. Rev. D* **30** (1984) 2212 [INSPIRE].

[28] P.B. Arnold and L.D. McLerran, *Sphalerons, Small Fluctuations and Baryon Number Violation in Electroweak Theory*, *Phys. Rev. D* **36** (1987) 581 [INSPIRE].

[29] P.B. Arnold and L.D. McLerran, *The Sphaleron Strikes Back*, *Phys. Rev. D* **37** (1988) 1020 [INSPIRE].

[30] J.S. Schwinger, *Brownian motion of a quantum oscillator*, *J. Math. Phys.* **2** (1961) 407 [INSPIRE].

[31] L.V. Keldysh, *Diagram technique for nonequilibrium processes*, *Zh. Eksp. Teor. Fiz.* **47** (1964) 1515 [INSPIRE].

[32] G. Baym and L.P. Kadanoff, *Conservation Laws and Correlation Functions*, *Phys. Rev.* **124** (1961) 287 [INSPIRE].

[33] L.P. Kadanoff and G. Baym, *Quantum Statistical Mechanics*, Benjamin, New York, U.S.A. (1962).

[34] J.M. Cornwall, R. Jackiw and E. Tomboulis, *Effective Action for Composite Operators*, *Phys. Rev. D* **10** (1974) 2428 [INSPIRE].

[35] E. Calzetta and B.L. Hu, *Nonequilibrium Quantum Fields: Closed Time Path Effective Action, Wigner Function and Boltzmann Equation*, *Phys. Rev. D* **37** (1988) 2878 [INSPIRE].

[36] C. Greiner and S. Leupold, *Stochastic interpretation of Kadanoff-Baym equations and their relation to Langevin processes*, *Annals Phys.* **270** (1998) 328 [hep-ph/9802312] [INSPIRE].

[37] W. Buchmüller and S. Fredenhagen, *Quantum mechanics of baryogenesis*, *Phys. Lett. B* **483** (2000) 217 [hep-ph/0004145] [INSPIRE].

[38] A. Hohenegger, A. Kartavtsev and M. Lindner, *Deriving Boltzmann Equations from Kadanoff-Baym Equations in Curved Space-Time*, *Phys. Rev. D* **78** (2008) 085027 [arXiv:0807.4551] [INSPIRE].

[39] A. Anisimov, W. Buchmüller, M. Drewes and S. Mendizabal, *Nonequilibrium Dynamics of Scalar Fields in a Thermal Bath*, *Annals Phys.* **324** (2009) 1234 [arXiv:0812.1934] [INSPIRE].

[40] M. Garny, A. Hohenegger, A. Kartavtsev and M. Lindner, *Systematic approach to leptogenesis in nonequilibrium QFT: Vertex contribution to the CP-violating parameter*, *Phys. Rev. D* **80** (2009) 125027 [arXiv:0909.1559] [INSPIRE].

[41] A. Anisimov, W. Buchmüller, M. Drewes and S. Mendizabal, *Leptogenesis from Quantum Interference in a Thermal Bath*, *Phys. Rev. Lett.* **104** (2010) 121102 [arXiv:1001.3856] [INSPIRE].

[42] M. Beneke, B. Garbrecht, M. Herranen and P. Schwaller, *Finite Number Density Corrections to Leptogenesis*, *Nucl. Phys. B* **838** (2010) 1 [arXiv:1002.1326] [INSPIRE].

[43] M. Garny, A. Hohenegger and A. Kartavtsev, *Quantum corrections to leptogenesis from the gradient expansion*, arXiv:1005.5385 [INSPIRE].

[44] M. Beneke, B. Garbrecht, C. Fidler, M. Herranen and P. Schwaller, *Flavoured Leptogenesis in the CTP Formalism*, *Nucl. Phys. B* **843** (2011) 177 [arXiv:1007.4783] [INSPIRE].

[45] B. Garbrecht, *Leptogenesis: The Other Cuts*, *Nucl. Phys. B* **847** (2011) 350 [arXiv:1011.3122] [INSPIRE].

[46] A. Anisimov, W. Buchmüller, M. Drewes and S. Mendizabal, *Quantum Leptogenesis I*, *Annals Phys.* **326** (2011) 1998 [*Erratum ibid.* **338** (2011) 376] [arXiv:1012.5821] [INSPIRE].

[47] B. Garbrecht, *Leptogenesis from Additional Higgs Doublets*, *Phys. Rev. D* **85** (2012) 123509 [arXiv:1201.5126] [INSPIRE].

[48] M. Drewes and B. Garbrecht, *Leptogenesis from a GeV Seesaw without Mass Degeneracy*, *JHEP* **03** (2013) 096 [arXiv:1206.5537] [INSPIRE].

[49] B. Garbrecht, *Baryogenesis from Mixing of Lepton Doublets*, *Nucl. Phys. B* **868** (2013) 557 [arXiv:1210.0553] [INSPIRE].

[50] T. Frossard, M. Garny, A. Hohenegger, A. Kartavtsev and D. Mitrouskas, *Systematic approach to thermal leptogenesis*, *Phys. Rev. D* **87** (2013) 085009 [arXiv:1211.2140] [INSPIRE].

[51] B. Garbrecht, F. Glowna and M. Herranen, *Right-Handed Neutrino Production at Finite Temperature: Radiative Corrections, Soft and Collinear Divergences*, *JHEP* **04** (2013) 099 [arXiv:1302.0743] [INSPIRE].

[52] B. Garbrecht, F. Glowna and P. Schwaller, *Scattering Rates For Leptogenesis: Damping of Lepton Flavour Coherence and Production of Singlet Neutrinos*, *Nucl. Phys. B* **877** (2013) 1 [arXiv:1303.5498] [INSPIRE].

[53] T. Frossard, A. Kartavtsev and D. Mitrouskas, *Systematic approach to ΔL=1 processes in thermal leptogenesis*, *Phys. Rev. D* **87** (2013) 125006 [arXiv:1304.1719] [INSPIRE].

[54] B. Garbrecht and M.J. Ramsey-Musolf, *Cuts, Cancellations and the Closed Time Path: The Soft Leptogenesis Example*, *Nucl. Phys. B* **882** (2014) 145 [arXiv:1307.0524] [INSPIRE].

[55] P.S.B. Dev, P. Di Bari, B. Garbrecht, S. Lavignac, P. Millington and D. Teresi, *Flavor effects in leptogenesis*, *Int. J. Mod. Phys. A* **33** (2018) 1842001 [arXiv:1711.02861] [INSPIRE].

[56] B. Garbrecht, P. Klose and C. Tamarit, *Relativistic and spectator effects in leptogenesis with heavy sterile neutrinos*, *JHEP* **02** (2020) 117 [arXiv:1904.09956] [INSPIRE].

[57] A. De Simone and A. Riotto, *Quantum Boltzmann Equations and Leptogenesis*, *JCAP* **08** (2007) 002 [hep-ph/0703175] [INSPIRE].

[58] A. De Simone and A. Riotto, *On Resonant Leptogenesis*, *JCAP* **08** (2007) 013 [arXiv:0705.2183] [INSPIRE].

[59] V. Cirigliano, A. De Simone, G. Isidori, I. Masina and A. Riotto, *Quantum Resonant Leptogenesis and Minimal Lepton Flavour Violation*, *JCAP* **01** (2008) 004 [arXiv:0711.0778] [INSPIRE].

[60] M. Garny, A. Hohenegger, A. Kartavtsev and M. Lindner, *Systematic approach to leptogenesis in nonequilibrium QFT: Self-energy contribution to the CP-violating parameter*, *Phys. Rev. D* **81** (2010) 085027 [arXiv:0911.4122] [INSPIRE].

[61] B. Garbrecht and M. Herranen, *Effective Theory of Resonant Leptogenesis in the Closed-Time-Path Approach*, *Nucl. Phys. B* **861** (2012) 17 [arXiv:1112.5954] [INSPIRE].

[62] M. Garny, A. Kartavtsev and A. Hohenegger, *Leptogenesis from first principles in the resonant regime*, *Annals Phys.* **328** (2013) 26 [arXiv:1112.6428] [INSPIRE].

[63] S. Iso, K. Shimada and M. Yamanaka, *Kadanoff-Baym approach to the thermal resonant leptogenesis*, *JHEP* **04** (2014) 062 [arXiv:1312.7680] [INSPIRE].

[64] S. Iso and K. Shimada, *Coherent Flavour Oscillation and CP-violating Parameter in Thermal Resonant Leptogenesis*, *JHEP* **08** (2014) 043 [arXiv:1404.4816] [INSPIRE].

[65] A. Hohenegger and A. Kartavtsev, *Leptogenesis in crossing and runaway regimes*, *JHEP* **07** (2014) 130 [arXiv:1404.5309] [INSPIRE].

[66] B. Garbrecht, F. Gautier and J. Klarić, *Strong Washout Approximation to Resonant Leptogenesis*, *JCAP* **09** (2014) 033 [arXiv:1406.4190] [INSPIRE].

[67] P.S. Bhupal Dev, P. Millington, A. Pilaftsis and D. Teresi, *Kadanoff-Baym approach to flavour mixing and oscillations in resonant leptogenesis*, *Nucl. Phys. B* **891** (2015) 128 [arXiv:1410.6434] [INSPIRE].

[68] A. Kartavtsev, P. Millington and H. Vogel, *Lepton asymmetry from mixing and oscillations*, *JHEP* **06** (2016) 066 [arXiv:1601.03086] [INSPIRE].

[69] M. Drewes, B. Garbrecht, D. Gueter and J. Klarić, *Leptogenesis from Oscillations of Heavy Neutrinos with Large Mixing Angles*, *JHEP* **12** (2016) 150 [arXiv:1606.06690] [INSPIRE].

[70] B. Dev, M. Garny, J. Klarić, P. Millington and D. Teresi, *Resonant enhancement in leptogenesis*, *Int. J. Mod. Phys. A* **33** (2018) 1842003 [arXiv:1711.02863] [INSPIRE].

[71] B. Garbrecht, *Why is there more matter than antimatter? Calculational methods for leptogenesis and electroweak baryogenesis*, *Prog. Part. Nucl. Phys.* **110** (2020) 103727 [arXiv:1812.02651] [INSPIRE].

[72] M. Herranen, K. Kainulainen and P.M. Rahkila, *Towards a kinetic theory for fermions with quantum coherence*, *Nucl. Phys. B* **810** (2009) 389 [arXiv:0807.1415] [INSPIRE].

[73] M. Herranen, K. Kainulainen and P.M. Rahkila, *Quantum kinetic theory for fermions in temporally varying backgrounds*, *JHEP* **09** (2008) 032 [arXiv:0807.1435] [INSPIRE].

[74] M. Herranen, K. Kainulainen and P.M. Rahkila, *Kinetic transport theory with quantum coherence*, *Nucl. Phys. A* **820** (2009) 203C [arXiv:0811.0936] [INSPIRE].

[75] M. Herranen, K. Kainulainen and P.M. Rahkila, *Kinetic theory for scalar fields with nonlocal quantum coherence*, *JHEP* **05** (2009) 119 [arXiv:0812.4029] [INSPIRE].

[76] M. Herranen, K. Kainulainen and P.M. Rahkila, *Coherent quantum Boltzmann equations from cQPA*, *JHEP* **12** (2010) 072 [arXiv:1006.1929] [INSPIRE].

[77] C. Fidler, M. Herranen, K. Kainulainen and P.M. Rahkila, *Flavoured quantum Boltzmann equations from cQPA*, *JHEP* **02** (2012) 065 [arXiv:1108.2309] [INSPIRE].

[78] M. Herranen, K. Kainulainen and P.M. Rahkila, *Flavour-coherent propagators and Feynman rules: Covariant cQPA formulation*, *JHEP* **02** (2012) 080 [arXiv:1108.2371] [INSPIRE].

[79] H. Jukkala, K. Kainulainen and O. Koskivaara, *Quantum transport and the phase space structure of the Wightman functions*, *JHEP* **01** (2020) 012 [arXiv:1910.10979] [INSPIRE].

[80] J. Berges, *Introduction to nonequilibrium quantum field theory*, *AIP Conf. Proc.* **739** (2004) 3 [hep-ph/0409233] [INSPIRE].

[81] M. Garny and U. Reinosa, *Renormalization out of equilibrium in a superrenormalizable theory*, *Phys. Rev. D* **94** (2016) 045012 [arXiv:1504.06643] [INSPIRE].

[82] G. Mahan, *Quantum transport equation for electric and magnetic fields*, *Phys. Rept.* **145** (1987) 251.

[83] A. Pilaftsis, *CP violation and baryogenesis due to heavy Majorana neutrinos*, *Phys. Rev. D* **56** (1997) 5431 [hep-ph/9707235] [INSPIRE].

[84] A. Pilaftsis and T.E.J. Underwood, *Resonant leptogenesis*, *Nucl. Phys. B* **692** (2004) 303 [hep-ph/0309342] [INSPIRE].

[85] E.K. Akhmedov, V.A. Rubakov and A.Y. Smirnov, *Baryogenesis via neutrino oscillations*, *Phys. Rev. Lett.* **81** (1998) 1359 [hep-ph/9803255] [INSPIRE].

[86] J. Klarić, M. Shaposhnikov and I. Timiryasov, *Uniting Low-Scale Leptogenesis Mechanisms*, *Phys. Rev. Lett.* **127** (2021) 111802 [arXiv:2008.13771] [INSPIRE].

[87] A. Granelli, K. Moffat and S.T. Petcov, *Flavoured Resonant Leptogenesis at Sub-TeV Scales*, arXiv:2009.03166 [INSPIRE].

[88] E.W. Kolb and S. Wolfram, *Baryon Number Generation in the Early Universe*, *Nucl. Phys. B* **172** (1980) 224.

[89] B.A. Kniehl and A. Pilaftsis, *Mixing renormalization in Majorana neutrino theories*, *Nucl. Phys. B* **474** (1996) 286 [hep-ph/9601390] [INSPIRE].

[90] B.A. Kniehl, *All-order renormalization of propagator matrix for unstable Dirac fermions*, *Phys. Rev. D* **89** (2014) 096005 [INSPIRE].

[91] E. Fuchs and G. Weiglein, *Breit-Wigner approximation for propagators of mixed unstable states*, *JHEP* **09** (2017) 079 [arXiv:1610.06193] [INSPIRE].

[92] K.I. Aoki, Z. Hioki, M. Konuma, R. Kawabe and T. Muta, *Electroweak Theory. Framework of On-Shell Renormalization and Study of Higher Order Effects*, *Prog. Theor. Phys. Suppl.* **73** (1982) 1 [INSPIRE].

[93] D. Espriu and J. Manzano, *CP violation and family mixing in the effective electroweak Lagrangian*, *Phys. Rev. D* **63** (2001) 073008 [hep-ph/0011036] [INSPIRE].

[94] H. Jukkala, K. Kainulainen and H. Parkkinen, work in progress.

[95] A. Anisimov, A. Broncano and M. Plümacher, *The CP-asymmetry in resonant leptogenesis*, *Nucl. Phys. B* **737** (2006) 176 [hep-ph/0511248] [INSPIRE].

[96] P.S. Bhupal Dev, P. Millington, A. Pilaftsis and D. Teresi, *Flavour Covariant Transport Equations: an Application to Resonant Leptogenesis*, *Nucl. Phys. B* **886** (2014) 569 [arXiv:1404.1003] [INSPIRE].

[97] A. Basboll and S. Hannestad, *Decay of heavy Majorana neutrinos using the full Boltzmann equation including its implications for leptogenesis*, *JCAP* **01** (2007) 003 [hep-ph/0609025] [INSPIRE].

[98] S. Eijima, M. Shaposhnikov and I. Timiryasov, *Freeze-in generation of lepton asymmetries after baryogenesis in the νMSM*, arXiv:2011.12637 [INSPIRE].

[99] J. Klarić, M. Shaposhnikov and I. Timiryasov, *Reconciling resonant leptogenesis and baryogenesis via neutrino oscillations*, *Phys. Rev. D* **104** (2021) 055010 [arXiv:2103.16545] [INSPIRE].

[100] P.F. Depta, A. Halsch, J. Hütig, S. Mendizabal and O. Philipsen, *Complete leading-order standard model corrections to quantum leptogenesis*, *JHEP* **09** (2020) 036 [arXiv:2005.01728] [INSPIRE].

[101] P. Millington and A. Pilaftsis, *Perturbative nonequilibrium thermal field theory*, *Phys. Rev. D* **88** (2013) 085009 [arXiv:1211.3152] [INSPIRE].

[102] H.A. Weldon, *Effective Fermion Masses of Order gT in High Temperature Gauge Theories with Exact Chiral Invariance*, *Phys. Rev. D* **26** (1982) 2789 [INSPIRE].

[103] M.A. Luty, *Baryogenesis via leptogenesis*, *Phys. Rev. D* **45** (1992) 455 [INSPIRE].

[104] G.F. Giudice, A. Notari, M. Raidal, A. Riotto and A. Strumia, *Towards a complete theory of thermal leptogenesis in the SM and MSSM*, *Nucl. Phys. B* **685** (2004) 89 [hep-ph/0310123] [INSPIRE].

[105] W. Buchmüller and M. Plümacher, *CP asymmetry in Majorana neutrino decays*, *Phys. Lett. B* **431** (1998) 354 [hep-ph/9710460] [INSPIRE].